

AD-783 393

FLIGHT TEST OF A HINGELESS FLEXBEAM
ROTOR SYSTEM

Charles W. Hughes, et al

Bell Helicopter Company

Prepared for:

Army Air Mobility Research and Development
Laboratory

June 1974

DISTRIBUTED BY:

NTIS

National Technical Information Service
U. S. DEPARTMENT OF COMMERCE
5285 Port Royal Road, Springfield Va. 22151

Unclassified

SECURITY CLASSIFICATION OF THIS PAGE (When Data Entered)

REPORT DOCUMENTATION PAGE		READ INSTRUCTIONS BEFORE COMPLETING FORM
1. REPORT NUMBER USAAMRDL-TR-74-38	2. GOVT ACCESSION NO.	3. RECIPIENT'S CATALOG NUMBER
4. TITLE (and Subtitle) FLIGHT TEST OF A HINGELESS FLEXBEAM ROTOR SYSTEM		5. TYPE OF REPORT & PERIOD COVERED Final report
		6. PERFORMING ORG. REPORT NUMBER 299-099-575
7. AUTHOR(s) Charles W. Hughes Rodney K. Wernicke		8. CONTRACT OR GRANT NUMBER(s) Contract DAAJ02-72-C-0036
		10. PROGRAM ELEMENT, PROJECT, TASK AREA & WORK UNIT NUMBERS Task 1F263211D15711
9. PERFORMING ORGANIZATION NAME AND ADDRESS Bell Helicopter Company, Fort Worth, Texas 76101		12. REPORT DATE June 1974
11. CONTROLLING OFFICE NAME AND ADDRESS Eustis Directorate U. S. Army Air Mobility R&D Lab Fort Eustis, Virginia 23604		13. NUMBER OF PAGES 199 214
		15. SECURITY CLASS. (of this report) Unclassified
14. MONITORING AGENCY NAME & ADDRESS (if different from Controlling Office)		15a. DECLASSIFICATION/DOWNGRADING SCHEDULE
16. DISTRIBUTION STATEMENT (of this Report) Approved for public release; distribution unlimited.		
17. DISTRIBUTION STATEMENT (of the abstract entered in Block 20, if different from Report)		
18. SUPPLEMENTARY NOTES		
19. KEY WORDS (Continue on reverse side if necessary and identify by block number) Fatigue Helicopters Reproduced by Maneuvers Rigidity NATIONAL TECHNICAL Struts Vibration INFORMATION SERVICE Helicopter rotors U S Department of Commerce Springfield VA 22151		
20. ABSTRACT (Continue on reverse side if necessary and identify by block number) This report presents the results of flight tests of a stiff- in-plane flexbeam hingeless four-bladed main rotor, hereafter referred to as the Model 609. The tests were conducted on a modified UH-1 at gross weights from 10,000 to 14,000 pounds and at level-flight speeds up to 150 knots to evaluate performance, handling qualities, maneuverability, and load levels. The		

DD FORM 1 JAN 73 1473

EDITION OF 1 NOV 65 IS OBSOLETE

Unclassified

SECURITY CLASSIFICATION OF THIS PAGE (When Data Entered)

Unclassified

SECURITY CLASSIFICATION OF THIS PAGE(When Data Entered)

20. Continued.

tests also evaluated a focused pylon system designed for isolating rotor vibrations.

The overall handling qualities of the test helicopter were good to excellent, with all forward flight modes statically and dynamically stable. The basic control was too sensitive at high speeds, but was manageable with the aid of an adjustable force-feel system. The handling qualities in hover were judged to be excellent.

The rotor structural loads in level flight were within endurance limits. In maneuvers, the oscillatory loads in the blades and yoke were limiting, with handling qualities and vibration levels remaining acceptable. One-per-rev Coriolis forces generated a large portion of the rotor loads observed in maneuvers.

Flight test results were correlated with analytical computer predictions using the C-81 computer program. Correlation of loads was good in level flight, but poor in maneuvers. Performance correlation was good in forward flight, but poor for hover.

The focused pylon evaluation established the focus point and spring rate which would allow the lowest fuselage vibration without compromising handling characteristics. The effects of changes in focus point and spring rate on rotor loads were negligible. The predominant vibration of the rotor was a low-amplitude four-per-rev. The vibration environment in the aircraft was comfortable.

A blade out-of-track condition encountered at high advancing blade tip Mach numbers (approximately 0.92) caused large one-per-rev vibrations which precluded the evaluation of the rotor at higher tip Mach numbers. No other pylon or rotor instabilities were observed during the flight evaluation.

ii.

Unclassified

SECURITY CLASSIFICATION OF THIS PAGE(When Data Entered)

PREFACE

The work reported here was performed by Bell Helicopter Company for the U. S. Army Air Mobility Research and Development Laboratory under Contract DAAJ02-72-C-0036 (DA Task 1F263211D15711).

Technical program direction was provided by Mr. D. Arents of USAAMRDL. Principal Bell Helicopter personnel associated with the program were Messrs. S. Blackman, K. Builta, D. Cannon, L. Dooley, D. Greenlee, L. Hartwig, C. Hughes, T. McLarty, V. Shami, W. Spivey, J. Van Gaasbeek, H. Vela, R. Wernicke, and W. Wilson.

A complete compilation of measured data is contained in Bell Helicopter Company Report 299-099-572, Flight Test Data Report. The computer flight simulation approach is discussed in Bell Helicopter Company Report 299-099-573, Computer Program Report. Both of these reports are on file at USAAMRDL.

TABLE OF CONTENTS

	<u>Page</u>
PREFACE	iii
LIST OF ILLUSTRATIONS	vii
LIST OF TABLES	xiv
INTRODUCTION	1
BACKGROUND	2
CONFIGURATION	4
METHODS	7
PILOT'S OBSERVATIONS AND QUALITATIVE ASSESSMENTS . . .	9
PERFORMANCE - RESULTS AND DISCUSSION	12
FORWARD FLIGHT PERFORMANCE	12
HOVER PERFORMANCE	16
CALCULATED BLADE STALL LIMITS	16
HANDLING QUALITIES - RESULTS AND DISCUSSION	21
HOVER	21
TRANSITION	24
SIDEWARD AND REARWARD FLIGHT	24
AUTOROTATION	28
CONTROL RESPONSE AND AIRCRAFT STABILITY	28
FORCE-FEEL SYSTEM	52
STABILITY AND CONTROL AUGMENTATION SYSTEM (SCAS) .	52
ROTOR LOADS IN LEVEL FLIGHT AND MANEUVERS - RESULTS AND DISCUSSION	54
LEVEL-FLIGHT AND MANEUVER ENVELOPE	54
LEVEL FLIGHT	54
MANEUVER FLIGHT	54
CORRELATION OF COMPUTED AND MEASURED ROTOR LOADS .	64

TABLE OF CONTENTS - Continued

	<u>Page</u>
LOAD LEVEL SURVEY AND FATIGUE LIFE ANALYSIS - RESULTS AND DISCUSSION	
FLIGHT SPECTRUM AND FREQUENCY OF OCCURRENCE . . .	85
CALCULATED FATIGUE LIVES OF COMPONENTS	85
ANALYSIS OF RESULTS	91
FUSELAGE VIBRATION - RESULTS AND DISCUSSION	95
FLIGHT TEST RESULTS	95
COMPUTED HUB MOTIONS	101
NASTRAN ANALYSIS AND MODEL CORRELATION	101
NASTRAN MODE SHAPE SIMULATION	103
FOCUSED PYLON EVALUATION	107
SUMMARY OF TECHNICAL PROBLEM AREAS	120
MAIN ROTOR CLAMP SET	120
LOAD DIFFERENCES BETWEEN UPPER AND LOWER BLADE PAIRS	120
POPPING OUT OF TRACK	121
PERMANENT DEFORMATIONS IN BLADE CONTOURS	126
BLADE TRACKING	126
CONCLUSIONS	133
PERFORMANCE	133
HANDLING QUALITIES	133
FUSELAGE VIBRATIONS	133
ROTOR LOADS IN LEVEL FLIGHT AND MANEUVERS	134
FATIGUE LIFE ANALYSIS	135
REFERENCES	136
APPENDIXES	
I. TEST VEHICLE AND ROTOR	138
II. WIND-TUNNEL DATA	153
III. FATIGUE LIFE ANALYSIS	157
LIST OF SYMBOLS	197

LIST OF ILLUSTRATIONS

<u>Figure</u>		<u>Page</u>
1	Test Vehicle	5
2	Three-View Sketch of Test Vehicle	6
3	Forward Flight Performance	13
4	Measured and Computed Main Rotor Horsepower in Forward Flight at Two Gross Weights	14
5	Measured and Computed Nondimensional Thrust Parameter in Forward Flight at Two Gross Weights	15
6	Measured and Computed Nondimensional OGE Hover Performance	17
7	Computed C-81 Rotor Lift and Drag at Constant Collective Pitch Settings	18
8	Measured and Computed Maximum Steady-State Rotor Lifting Capability	19
9	Longitudinal Cyclic Step in IGE Hover, Flight Test Data, 12,000 Pounds GW, Aft CG	22
10	Lateral Cyclic Pulse in IGE Hover, Flight Test Data, 12,000 Pounds GW, Aft CG	22
11	Collective Step in IGE Hover, Flight Test Data, 12,000 Pounds GW, Aft CG	23
12	Sideward Flight Characteristics, Flight Test Data, 10,500 Pounds and 14,000 Pounds GW	25
13	Sideward Flight Characteristics, Flight Test Data, 12,000 Pounds GW	26
14	Rearward Flight Characteristics, Flight Test Data	27
15	Autorotation Entry and Subsequent Descent, Flight Test Data, 12,000 Pounds GW, Forward CG	29
16	Measured and Computed Forward Flight Trim Values, 12,000 Pounds GW	31

LIST OF ILLUSTRATIONS - Continued

<u>Figure</u>		<u>Page</u>
17	Measured and Computed Forward Flight Trim Values, 10,500 Pounds and 14,000 Pounds GW ..	32
18	Apparent Speed Stability in Autorotation and Climb, Flight Test Data	33
19	Static Longitudinal Stability, Flight Test Data	34
20	Measured and Computed Level Flight Static Longitudinal Stability	35
21	Static Lateral-Directional Control Gradients, Flight Test Data	37
22	Forward Cyclic Pulse at 100 Knots, Flight Test Data, 12,000 Pounds GW, Aft CG	38
23	Lateral Cyclic Pulse at 130 Knots, Flight Test Data, 12,000 Pounds GW, Aft CG	40
24	Pedal Step at 130 Knots, Flight Test Data, 12,000 Pounds GW, Aft CG	41
25	Longitudinal Cyclic Pulse at 100 Knots, Flight Test Data, 12,000 Pounds GW, Aft CG	42
26	Longitudinal Cyclic Step at 100 Knots, Flight Test Data, 12,000 Pounds GW, Aft CG	44
27	Lateral Cyclic Step at 100 Knots, Flight Test Data, 12,000 Pounds GW, Aft CG	45
28	Measured and Computed Longitudinal Cyclic Control Characteristics	46
29	Measured and Computed Lateral Cyclic Control Characteristics	47
30	Longitudinal Cyclic Stick Position Variation With Normal Acceleration, Flight Test Data, 12,000 Pounds GW	50
31	Symmetric Pullup and Pushover, Flight Test Data, 12,000 Pounds GW, Aft CG	51

LIST OF ILLUSTRATIONS - Continued

<u>Figure</u>		<u>Page</u>
32	Measured and Computed Maneuver Comparison 12,000 Pounds GW, Aft CG	53
33	Maneuver Investigation Dimensional Envelope, Flight Test Data	55
34	Nondimensional Maneuver Envelope, Flight Test Data	56
35	Constant Chordwise Moments Versus C_T/σ and μ , Flight Test Data	57
36	Comparison Between Maneuver and Level Flight Loads, Flight Test Data	58
37	Maximum Nondimensional Lift (at a Constant Oscillatory Blade Moment) Versus Advance Ratio and Collective Pitch	60
38	Main Rotor Overspeed Characteristics in Maneuvers, Flight Test Data	62
39	Rapid Roll Reversal Characteristics, Flight Test Data	63
40	Flapping and Coriolis 1/Rev Limitation	65
41	1/Rev Hub Moments and Flapping Amplitudes in Level Flight, Flight Test Data	66
42	Flapping as a Function of Thrust During Maneuvers, Flight Test Data	67
43	Flapping Contribution to Loads During a Maneuver at 14,000 Pounds GW, Flight Test Data	68
44	Measured and Computed Oscillatory Beam Bending Moment (Station 7) in Forward Flight at Three Gross Weights	70
45	Measured and Computed Harmonic Analysis of Oscillatory Beam Bending Moment (Station 7) for Three Airspeeds	71

LIST OF ILLUSTRATIONS - Continued

<u>Figure</u>		<u>Page</u>
46	Measured and Computed Oscillatory Chord Bending Moment (Station 7) in Forward Flight at Three Gross Weights	73
47	Measured and Computed Harmonic Analysis of Oscillatory Chord Bending Moment (Station 7) for Three Airspeeds	74
48	Measured and Computed Oscillatory Beam and Chord Bending Moments (Station 94) in Forward Flight	75
49	Measured and Computed Oscillatory Pitch Link Load in Forward Flight	76
50	Measured and Computed Oscillatory Beam Bending Moment (Station 7) in Hover	78
51	Measured and Computed Oscillatory Chord Bending Moment (Station 7) in Hover	78
52	Harmonic Analysis of Oscillatory Chord Bending Moment (Station 7) in Hover	79
53	Measured and Computed Oscillatory Beam and Chord Bending Moments (Station 94) in Hover .	80
54	Measured and Computed Oscillatory Pitch Link Load in Hover	81
55	Time Histories of Measured and Computed Blade Loads (Station 7) for Symmetric Pullup	82
56	Time Histories of Measured and Computed Blade Loads (Station 94) for Symmetric Pullup	83
57	Main Rotor Yoke Stresses for Each Condition in the Flight Spectrum (Data from Table XIII, Appendix III)	93
58	Effect of Maneuvering Restrictions on Rotor Yoke Fatigue Life	94
59	Summary of 4/Rev Vibration Versus Gross Weight, Flight Test Data	96

LIST OF ILLUSTRATIONS - Continued

<u>Figure</u>		<u>Page</u>
60	Summary of 4/Rev Vibration Versus Center-of-Gravity Location, Flight Test Data	97
61	Summary of 4/Rev Vibration Versus Rotor Speed, Flight Test Data	93
62	Summary of Vibration Versus Main Rotor Harmonic, Flight Test Data	99
63	Correlation of 4/Rev Vibrations in the Fuselage With Rotor System Loads and Vibrations, Flight Test Data	100
64	Comparison of Computed and Measured Hub Vibrations, 12,000 Pounds GW, Neutral CG	102
65	NASTRAN Finite Element Model	104
66	NASTRAN and Vibration Test Mode Shape Correlation	105
67	NASTRAN 4/Rev Mode Shape Correlation With Flight Test Data	106
68	Rigid Body Analysis Model	108
69	Test Configurations Compared to Theoretical 4/Rev Minimum Fuselage Response Locus	109
70	Pylon Fore and Aft 4/Rev Mode Shapes, Focused at WL 36, Flight Test Data	112
71	Computed and Measured Pylon Fore and Aft 4/Rev Mode Shapes, Focused at WL 36	113
72	Typical 4/Rev Hub Vibration Displacement and Response in the Fixed System, Flight Test Data	114
73	Pylon Lateral 4/Rev Mode Shapes, Focused at WL 36, Flight Test Data	116
74	Computed and Measured Lateral 4/Rev Mode Shapes, Focused at WL 36	117

LIST OF ILLUSTRATIONS - Continued

<u>Figure</u>		<u>Page</u>
75	Effect of Pylon Focal Point Location and Spring Rate on Pilot and Copilot Seat Vertical Response at 120 Knots Airspeed, Flight Test Data	118
76	"Popping-Out-Of-Track" Boundary, Flight Test Data	122
77	Lines of Constant Angle of Attack	123
78	Mach Drag Divergence for Various M_{Adv} Tip ...	124
79	Measured Blade Torsional Moments and Pilot Vertical Acceleration	125
80	609 Main Rotor System	145
81	609 Yoke and Mast Mounting Details	146
82	609 Blade Assembly	147
83	Stabilizer and Trim Angle Versus Longitudinal Stick Position	148
84	Pylon and 609 Main Rotor Assembly	149
85	Pylon Base and Lateral Restraint Link	150
86	Measured Stick Gradients as a Function of Airspeed and Switch Position	151
87	Stick Gradients due to Pitch Rate	152
88	Cyclic Stick Trim Rates Versus Airspeed	152
89	Lift Versus Drag Coefficients for Advance Ratio of .36	154
90	Lift Versus Drag Coefficients for Advance Ratio of .40	155
91	Lift Versus Drag Coefficients for Advance Ratio of .51	156
92	Modified Goodman Diagram for 2024-T4 and/or 2024-T42 Aluminum Alloy	158

LIST OF ILLUSTRATIONS - Concluded

<u>Figure</u>		<u>Page</u>
93	Main Rotor Yoke, Part No. 609-010-102-1	160
94	Main Rotor Spindle, Part No. 609-010-140-1 ..	167
95	Oscillatory Stress Versus Cycles for the 204-011-102-17 Main Rotor Yoke Used To Substantiate the 609-010-140-1 Spindle	168
96	Main Rotor Blade Retention Fitting, Part No. 609-010-105-3	175
97	Swashplate Outer Ring, Part No. 609-010-401-3	182
98	Oscillatory Stress Versus Cycles for the 540-011-478-1 Swashplate Outer Ring Pin Used To Substantiate the 609-010-419-5 Slider Lug Bolt	190

LIST OF TABLES

<u>Table</u>		<u>Page</u>
I	Measured and Predicted Trim Parameters in Autorotation	28
II	Measured and Predicted Phugoid Characteristics . .	39
III	Model 609 Spectrum Frequency of Occurrence	86
IV	Gross Weight and Center-of-Gravity Variations Flown for the Fatigue Life Analysis	88
V	Description of Conditions Flown in the Load Level Survey	89
VI	Summary of Calculated Fatigue Lives for Model 609 Hingeless Flexbeam Rotor System	90
VII	Shake Test Correlation	103
VIII	Flight Test Pylon Configurations	110
IX	Summary of Technical Problems Encountered During the 609 Flexbeam Rotor Program	128
X	Dimensional Data	141
XI	Flight Control Systems	143
XII	Component Speed Ratios	144
XIII	Fatigue Life Determination of 609 M/R Yoke, Part No. 609-010-102-1	162
XIV	Fatigue Life Determination of 609 M/R Spindle, Part No. 609-010-140-1	169
XV	Fatigue Life Determination of 609 M/R Blade, Part No. 609-010-200-1	177
XVI	Fatigue Life Determination of 609 Swashplate Outer Ring, Part No. 609-010-401-3	184
XVII	Fatigue Life Determination of 609 Slider Lug Bolt, Part No. 609-010-419-5	191

INTRODUCTION

The class of helicopter rotors referred to as "rigid" rotors may be defined as that group of rotors in which the blades are not hinged or pinned to the hub or mast in such a way as to allow the blade to flap or lag freely. "Hingeless" is a better adjective to use in describing these rotors, since their blades are clamped to the mast, and move with respect to the mast only as the flexibility of the rotor structure allows. In early rotors, the high structural loads inherent in such a design were discouraging. In the past fifteen years, the science of materials has developed to the point where such a rotor has approached practicality.

The Model 609 hingeless flexbeam rotor is part of a continuing development of hingeless rotors started at Bell Helicopter in 1957. The rotor uses a direct control system without any gyro-stabilized inputs. It was designed for use with a stronger, shorter mast, and an upgraded transmission without the limitations of the standard UH-1 mast and power train designed for a two-bladed teetering rotor system. The rotor is mounted on the focused pylon vibration isolation system.

The purpose of this program was to obtain flight test data and perform analyses on the Model 609 in the areas of rotor structural loads, performance, handling qualities, maneuverability, and the focused pylon as an isolation mount for the transmission-rotor system. The analyses also included the determination of fatigue life, rotor-fuselage dynamic response, and stability and control. Flight test results were compared with theoretical predictions obtained from the C-81 computer program to validate the accuracy of this analysis for helicopters with hingeless rotors. Pilot observations were correlated with test records. The results of this test program are presented in this report.

BACKGROUND

Bell Helicopter Company has been building and flight-testing experimental stiff in-plane hingeless rotors since 1957. The first designs were small three-bladed rotors which were flown on the Model 47 light helicopter. One, the Model 504, was flexible in flapping. It doubled the cg range of the helicopter and quadrupled the control power, but the resulting stress levels in the mast were unacceptable, even during modest flight maneuvers.

Another hingeless rotor had high flapwise as well as in-plane stiffness and was mounted on a tilting pylon. This configuration also gave the helicopter a greater allowable cg range than did the equivalent semirigid rotor, as well as better stability, faster response to cyclic control, and more precise maneuverability. It also subjected the mast to unacceptable stresses. Development continued, going to a more elaborate three-bladed hingeless rotor for the Model 47, then to a larger three-bladed hingeless rotor for the heavier UH-1B. This rotor, the Model 533, was flight-tested in two configurations before giving way to the first Bell four-bladed hingeless rotor, the Model 8065, in 1964. Five versions of the Model 8065 were tested on various UH-1 airframes (including the high performance compound helicopter). Results were promising, particularly with respect to vibrations, cg range, and maneuverability, but the value of the tests was limited by the shortcomings of the rotor mast, constrained in diameter by the transmission and hence in strength and rigidity. The testing of the Model 8065 hingeless rotor on the compound HPH is reported in Reference 1.

In 1969, the development of the Model 609 series of hingeless rotors began. The basic Model 609 rotor has a forged titanium hub for strength and fatigue resistance, and has some flapwise freedom because of the flexibility of the hub at shallow sections inboard of the pitch-change bearings. The test vehicle has a transmission able to take a mast of increased diameter, strength, and stiffness, and uses the T55-L-7B/C engine. The development and preliminary testing of the rotor and modifications of the test helicopter proceeded under IR&D funding.

The Model 609 rotor was first flown in 1971, which revealed some problems with the rotor and test vehicle. The vehicle experienced "tail wag" in hover and forward flight. The tail wag was alleviated by installing a stronger and stiffer tail boom as well as adding an enlarged fairing that enclosed the swashplate, thereby reducing the turbulence of the air impinging on the vertical fin.

During maneuvers, the chord loads in the rotor were much larger than expected, with the lowest strength area being the spindle and blade bolt hole. The original titanium spindles were replaced with increased diameter steel spindles, and the blades were strengthened by modifying the bolt hole area and adding doublers from the inboard end out to midspan. Also during the flights in 1971, an out-of-track condition was encountered. The swept tip portion of the blades was cut off and 10-pound leading edge tip weights were added to improve the mass balance of the blades. In 1972, Army Contract DAAJ02-72-C-0036 was awarded which extended flight testing of the Model 609 rotor. The program was concluded with a brief Government flight evaluation.

The benefits to be derived from hingeless rotors include simplicity and reliability by reducing the need for bearings. Multibladed rotors offer reductions in noise, vibrations, and control loads.

CONFIGURATION

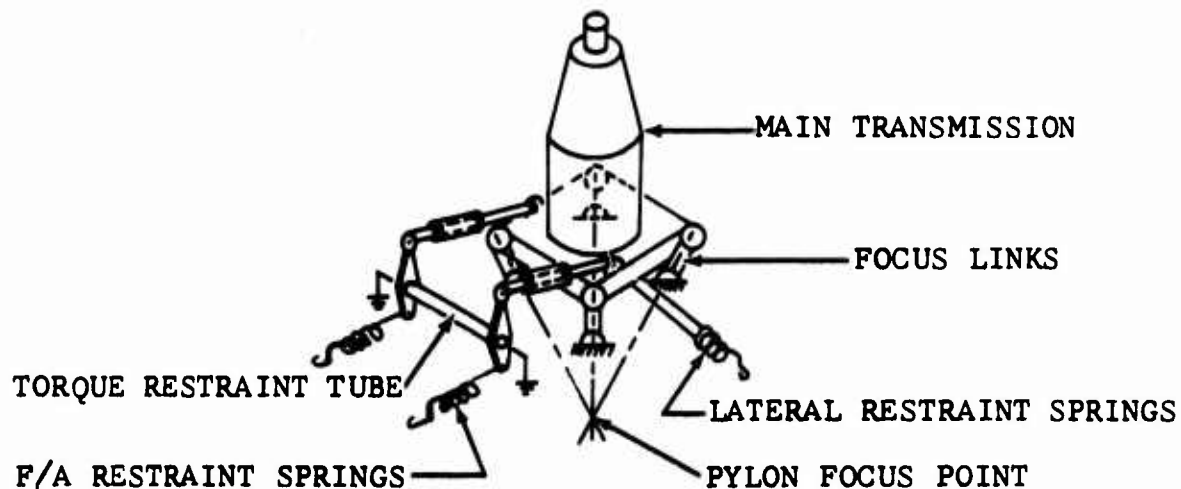
MAIN ROTOR

The main rotor is a four-bladed, hingeless, flexbeam, stiff-in-plane rotor designated Bell Model 609. The rotor diameter is 48.3 feet, and the blades have a chord length of 21 inches. A detailed description of the rotor with all pertinent dimensional data is given in Appendix I.

TEST VEHICLE

The test vehicle is a Bell Model 204B helicopter modified for greater strength and performance, using a 2000-shp main transmission and a T55-L-7B/7C engine. The fuselage structure, the landing gear, and the antitorque system are upgraded accordingly. Figure 1 is a photograph of the test vehicle in flight, and Figure 2 is a three-view sketch with notations of the salient features.

The test vehicle is equipped with a "focused pylon." This is a kinematic passive vibration isolation system shown schematically below.



A detailed description of the test vehicle is given in Appendix I, and a discussion of the focused pylon is given in the "Fuselage Vibration" section.

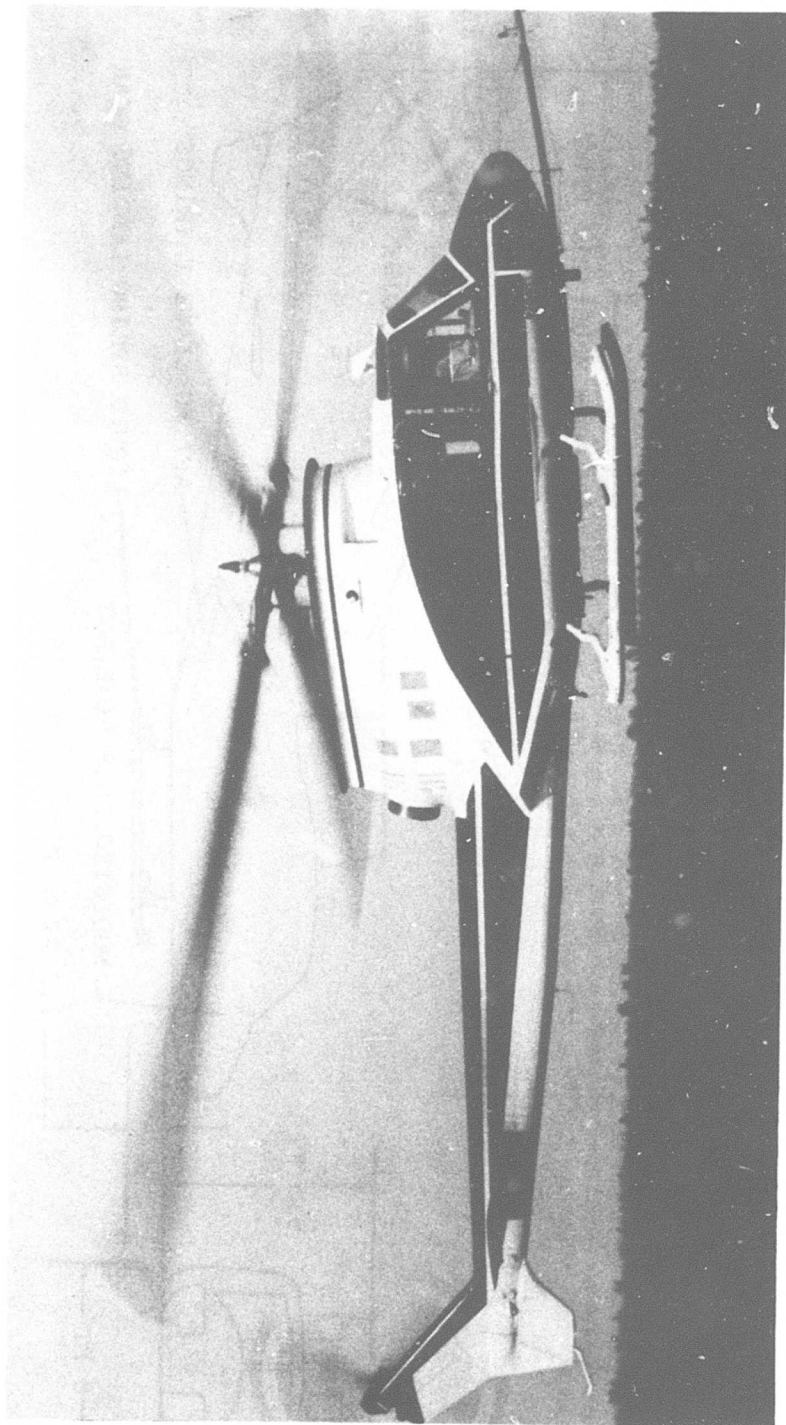


Figure 1. Test Vehicle.

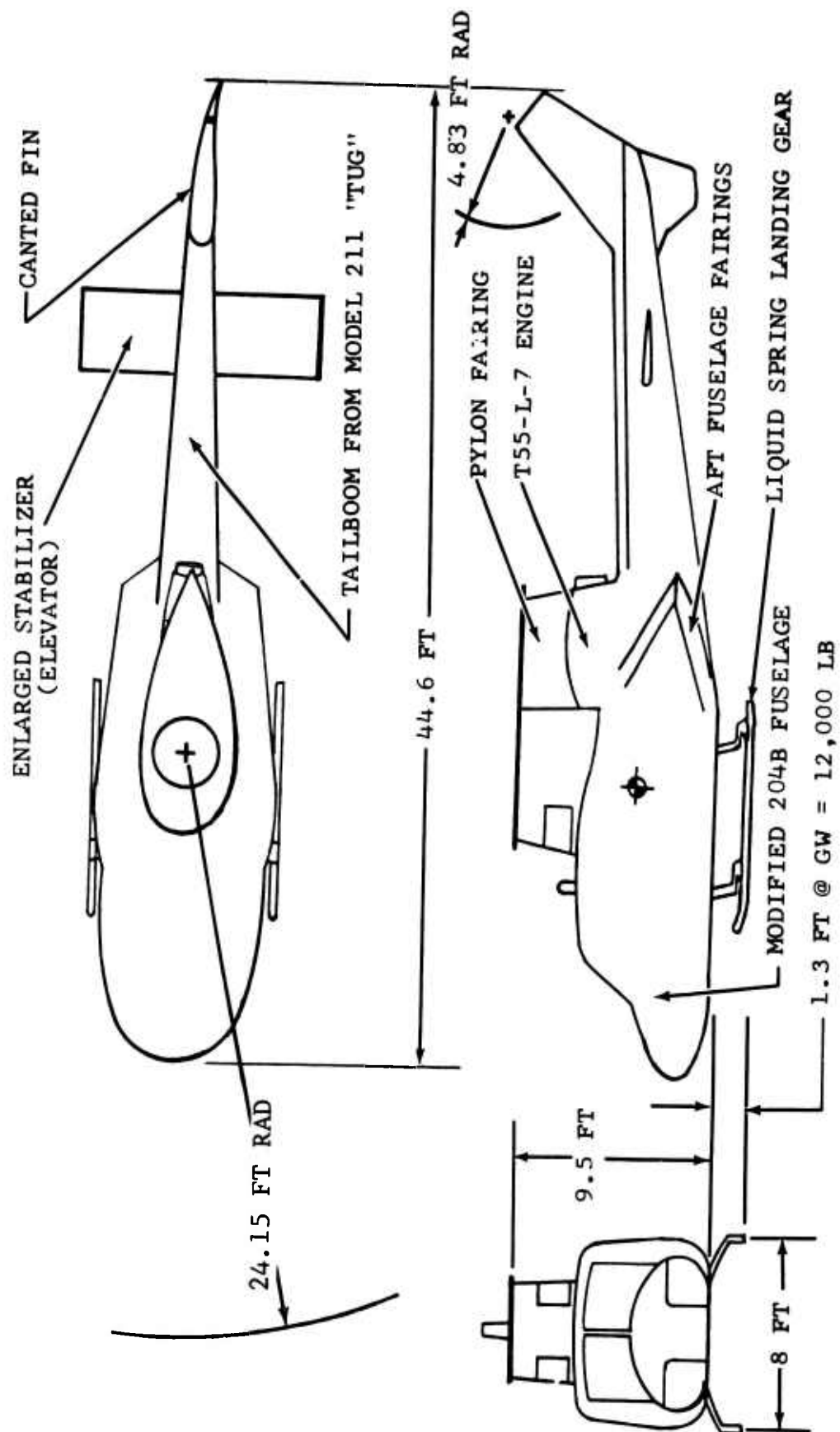


Figure 2. Three-View Sketch of Test Vehicle.

METHODS

FLIGHT TEST PROGRAM AND DATA ACQUISITION

The specific tasks to be accomplished by this program were:

1. Focused pylon evaluation
2. Rotor systems and airframe load level survey
3. Helicopter performance measurements
4. Helicopter handling qualities
5. Limit maneuver evaluation

The data acquisition system, which is also described in detail in Reference 1, consists of an airborne magnetic tape system, special pilot panel indicators, a photo panel, and air-to-ground telemetry. The magnetic tape system uses frequency multiplexing to record up to 104 channels. Thirteen of the channels recorded on the magnetic tape were also telemetered to a ground data center to permit real time assessment of the more critical parameters. The telemetry system assisted in rapid flight envelope expansion and contributed to safety of flight.

Several options are available for the reduction of data recorded on magnetic tape. These include analog stripouts, analog analysis using an x-y plotter, digitized tape compatible with BHC's IBM 360 computer, and several digital "quick-look" programs for an immediate analysis on an IBM 1800 computer. All of these methods were used to obtain the data presentations shown in this report. The quick-look routine was used extensively during the program to augment the telemetry information.

COMPUTER SIMULATION

The purpose of the computer simulation was to establish the accuracy of the C-81 analysis (Reference 2) for predicting the aeroelastic and aerodynamic behavior of a hingeless rotor helicopter. The program simulates helicopter flight, and it can be used to analyze single-rotor, compound, tandem, or side-by-side helicopter configurations in hover, transition, cruise, or high-speed flight. The analysis, with a uniform level of complexity for its different phases, can calculate performance, stability and control, or rotor loads. Its inputs are organized to make the program easy to use, and the output format facilitates comparison of computed results with flight and tunnel test data.

Three major parts of the analysis are a mathematical model of an elastic rotor, rotor aerodynamics, and rigid-vehicle flight mechanics. The program is used in support of three phases of rotor system design and evaluation: wind tunnel simulation, steady-state flight simulation, and transient or maneuvering flight simulation.

The stability and control section calculates trim positions (including control positions), gradients, and stick margins--in level, climbing, diving, turning, or accelerated flight. It uses linear analysis to compute response characteristics and the locations of stability roots for coupled flight modes. It can also use fully coupled nonlinear equations to calculate and plot variables against time. Disturbances like gusts, sinusoidal control motions, and weapon recoil can be simulated.

The program includes a fully coupled, time-variant aeroelastic analysis of the rotor blades. This portion uses modal equations to calculate beam, chord, and torsional loads during either steady or maneuver flight, and prints out the results.

A detailed description of the methods and sources for preparing the C-81 input data for this project is given in Reference 3. The approach was to use the best initial estimates of the required input data and then adjust them to obtain level flight performance correlation. This procedure also produced satisfactory rotor loads agreement in level flight. In maneuvering flight, additional input parameter adjustments were required for correlation with measured blade loads. The rationale for this is given in the section entitled "Rotor Loads in Level Flight and Maneuvers - Results and Discussion."

PILOT'S OBSERVATIONS AND QUALITATIVE ASSESSMENTS

Many of the specific or understood goals of any rotor development program have to do with the pilot--how easy or difficult it is for him to make the helicopter do what it must to carry out a mission, how long he can fly it without being worn down by excessive demands on his skills, and how much vibration he has to endure at his flight station. Therefore, it is appropriate to include a summary of the test pilot's observations about the test helicopter and the Model 609 rotor. Bell's Chief Experimental Test Pilot, with over 6,000 hours of helicopter flight time, flew all the test flights for this program. His comments will aid the reader in a better interpretation of the measured data.

In general, the pilot was pleased with the flight characteristics. Vibration levels at the pilot's seat were acceptable. High control response, sensitivity, and damping gave the helicopter excellent handling characteristics in hover, but the control sensitivity at high speed was excessive. The helicopter was equipped with an electric-hydraulic force-feel and trim system which increased the cyclic force-feel gradient with air-speed. This overcame the problem of high control sensitivity at high speeds. The pilot could also use this system to adjust the lateral and longitudinal stick-force gradient while airborne. Also, the stick position trim rate decreased with air-speed to help compensate for increasing control sensitivity.

The hingeless rotor hub generates high control moments per degree cyclic control. At high forward speeds, it is easy to get high pitching and rolling accelerations at the low and medium gross weights with acceptable blade loads. In high-speed maneuvers at high gross weight, however, the pilot could easily overstress the rotor by making too large a cyclic control input. The pilot had a critical-load meter (blade chord load at station 94) on the instrument panel, and his use of it helped to define the limit maneuver envelope. The pilot also received some warning from the buildup in fuselage vibration during high stress maneuvers, but vibration was not a reliable indication of excessive rotor stresses.

The range of center-of-gravity station locations from 122.0 to 136.0 inches was the widest range that allowed a good ride and the most reasonable rotor loads for maneuvering throughout the speed range. Controllability was satisfactory at the extremes.

Symmetrical pullups could exceed 2 G's at the low and medium gross weights tested without overstressing the rotor. Pushovers following symmetrical pullups resulted in accelerations as low

as 0.1 G. Neither high- nor low-G maneuvers generated significant roll tendencies (previous rigid rotor configurations always had an excessive amount of roll coupling with G's).

The directional axis had the weakest stability in both power-on and power-off flight. A ventral fin, added to improve the directional stability, did improve it considerably, but it was still considered to be weak. The ventral fin was canted to help counteract main rotor torque; in autorotation, it was too effective: it took almost full right pedal to hold heading during autorotation. The tail rotor control power required for maneuvering with power on prevented a change in tail rotor rigging to increase the right pedal margin.

An undesirable control coupling occurred during transition from hover to forward flight. The helicopter would roll right (page 24) as it went through the 15- to 20-knot speed range, and it took about 25 percent of left cyclic to correct the roll. After passing through 30 knots, the helicopter would rapidly roll back to level trim. Previous rigid rotors have exhibited this same rolling characteristic. The amount and rate of roll are influenced by the rate of acceleration through transition, with a slow acceleration through this range resulting in the largest migration of the cyclic stick to the left. Deceleration back to a hover from forward flight resulted in very little cyclic trim change in the roll axis. The use of the stability and control augmentation system (SCAS) during takeoff greatly reduced the roll tendency.

The SCAS was also effective in attenuating gust response. With stability augmentation off, the gust response was considered to be excessive at all speeds, including hover.

The helicopter could develop moderately high forward accelerations in the 0- to 30-knot speed range. The pilot developed an ability to use the load meter to anticipate how much control he could use without causing fatigue damage in the rotor. On the ground, motions of the helicopter on the skid gear were an adequate indication of high oscillatory rotor loads.

Landings in full autorotation also caused high rotor loads, but these loads occurred for only 2 to 3 rotor revolutions. The landings seemed normal, with no indication that loads were high.

At the highest gross weight tested, the maximum level-flight speed (limited by the transmission takeoff power limit) was 150 knots. The maximum dive speed was 160 knots. This was limited by a "popping-out-of-track" phenomenon which occurred at high advancing tip Mach numbers. The onset of the out-of-track could be observed visually, and was accompanied by a

buildup in one-per-rev vibration. The problem is believed to be associated with changes in the shape of the hollow thin-wall blade section near the tip of the blade caused by changes in the chordwise pressure distribution at high Mach numbers.

Other hardware problems also affected vibration levels. It was impossible to keep the one per rev out of the rotor because of a relatively soft clampup between the upper and lower blade sets which necessitated frequent retorquing of the clamping bolts.

Vibrations at higher frequencies were very low until midway in the evaluation, when there was a sudden increase in the four-per-rev level. The bearing staking in one of the pylon focus links had become loose. The link was replaced, greatly reducing the four per rev, but the level of this vibration was never as low as on the previous flights.

PERFORMANCE - RESULTS AND DISCUSSION

Performance was measured in both hover and stabilized level flight. The power required was based on main rotor mast torque and rpm measurements.

For C-81 computer correlation, the aerodynamic characteristics of the fuselage had to be extrapolated from full-scale wind-tunnel tests of a standard UH-1 helicopter (Reference 4). The equivalent fuselage flat plate drag area was increased over the initial estimates to match flight test performance. The main rotor blade airfoil section tapers linearly from an NACA 64X18 Mod inboard to an NACA 0008 Drooped Mod at the tip. The average blade airfoil section characteristics were obtained by interpolation of section data from wind-tunnel tests of the inboard and tip airfoil (Reference 5). These average aerodynamic values were used in C-81 which was limited to the use of one set of aerodynamic section characteristics to represent all blade stations. The estimated aerodynamic characteristics (drag coefficient and drag divergence Mach number) were then modified to match flight test performance results.

FORWARD FLIGHT PERFORMANCE

Level flight performance measurements were obtained for three gross weights: 10,500 pounds, 12,000 pounds, and 14,000 pounds. At 12,000 pounds, measurements were obtained at two referred rotor speeds ($N_R/\sqrt{\theta}$) to isolate Mach number effects from advance ratio (μ) effects. These results are shown in Figure 3, and good correlation with computed values is apparent.

The measurements at 10,500 pounds and 14,000 pounds were obtained at only one rotor speed and were used primarily in conjunction with rotor loads correlation, but they were obtained in sufficiently smooth air to yield valid performance data. These performance data are shown in Figure 4, and are presented as main rotor horsepower versus advance ratio (μ) and true airspeed. Again, good correlation with computed values is apparent.

Data from these two flights were also used to compare measured and computed rotor thrust levels. Although the resultant force of the main rotor could not be measured directly in flight, the sum of the gross weight and the elevator download can be measured and is approximately equal to the rotor lift. The lift derived in this way is shown in Figure 5, and reasonable correlation with computed values is indicated.

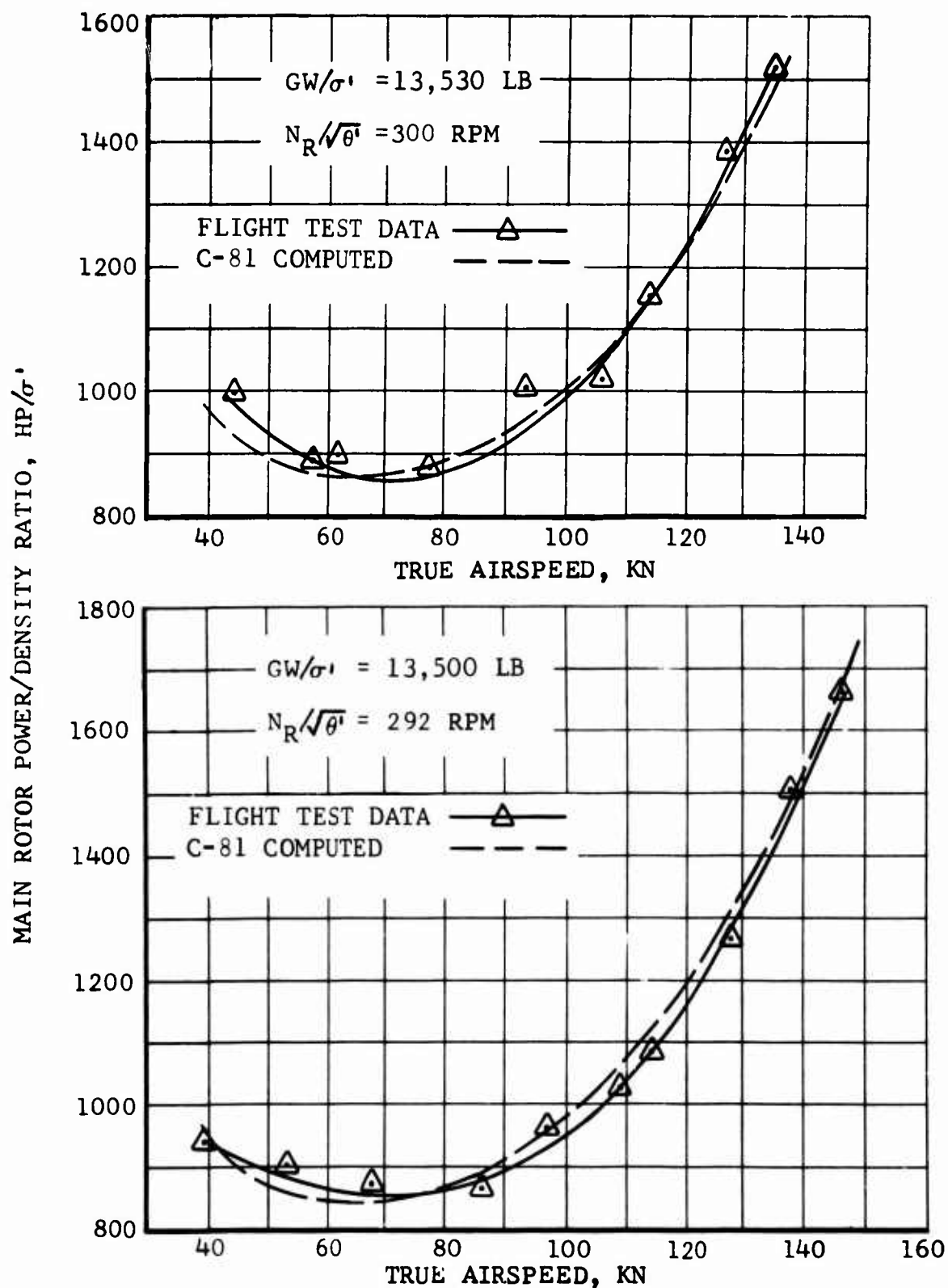


Figure 3. Forward Flight Performance.

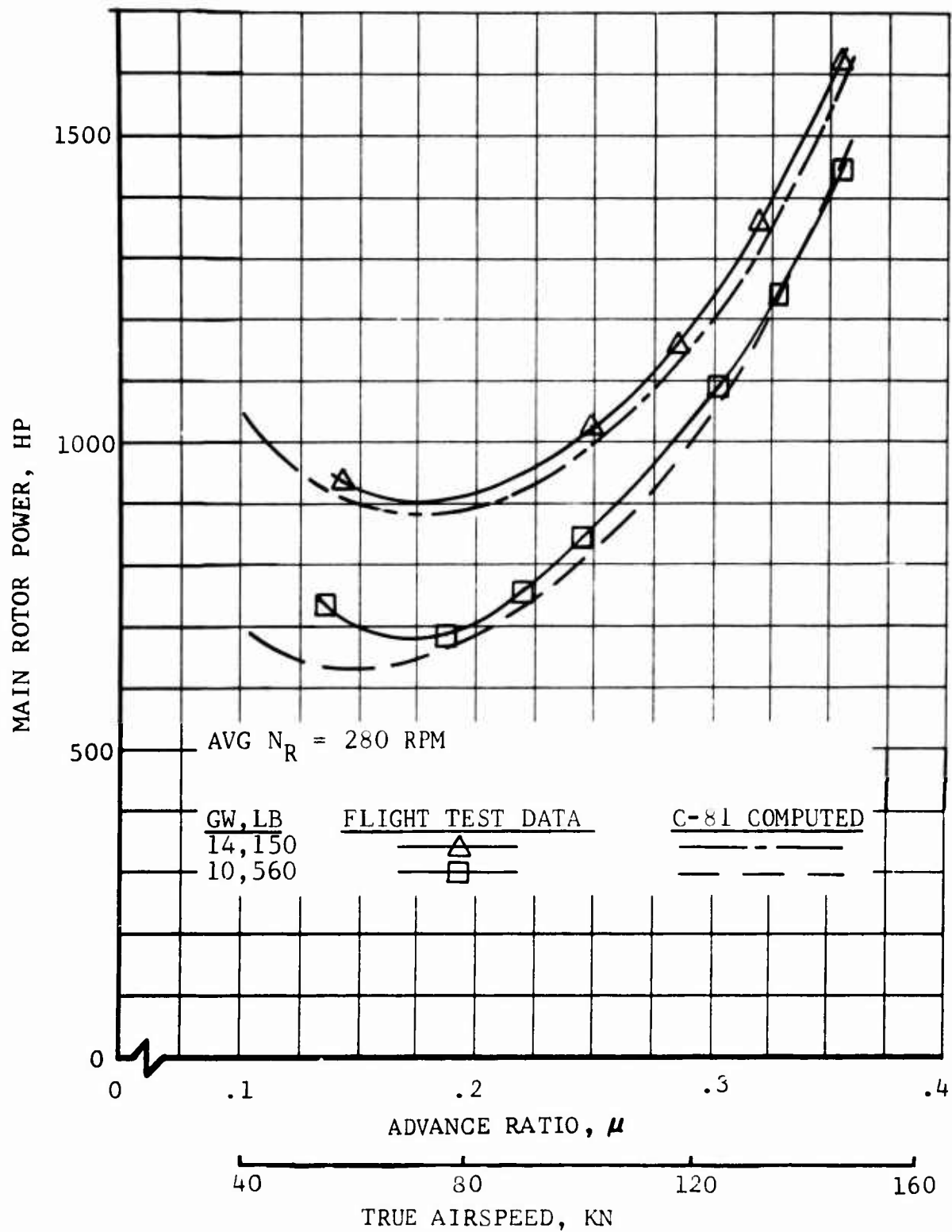


Figure 4. Measured and Computed Main Rotor Horsepower in Forward Flight at Two Gross Weights.

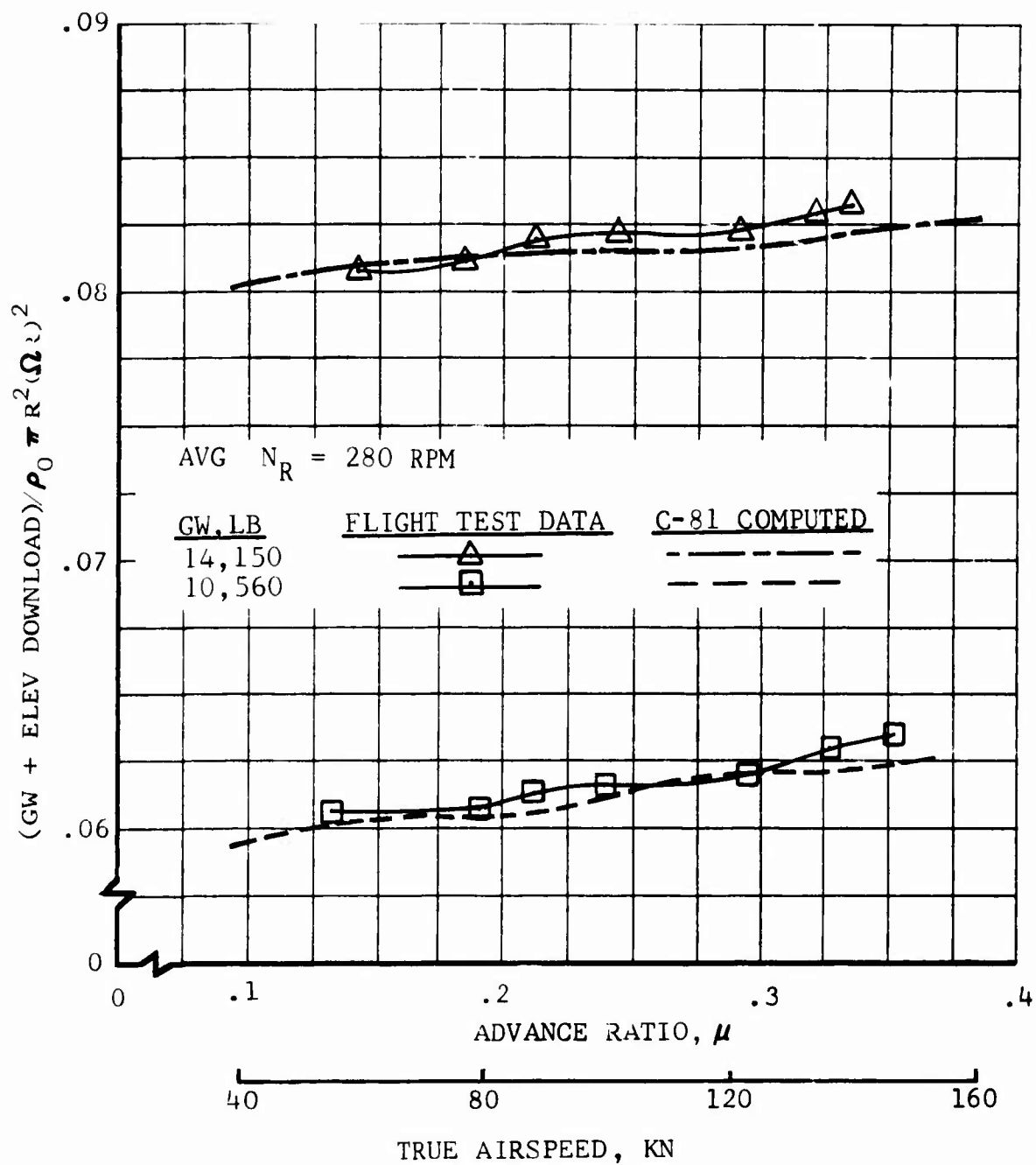


Figure 5. Measured and Computed Nondimensional Thrust Parameter in Forward Flight at Two Gross Weights.

In all the above computer correlation work, an average minimum blade profile drag coefficient C_{d0} of 0.009 was used, and a value of 22 square feet was used for the equivalent (flat plate) drag area of the fuselage at zero angle of attack.

HOVER PERFORMANCE

Hover performance OGE was obtained at one loading condition and four rotor speeds. These data are presented nondimensionally in Figure 6 together with computed values. Using the "level flight" C_{d0} value of 0.009, correlation is poor. To indicate the magnitude of this difference, a change in C_{d0} of over 40 percent ($C_{d0} = 0.013$) would be required to match test results.

This discrepancy between "hover" and "level flight" values of C_{d0} probably results from two factors. One is aerodynamic interference, an effect which causes power required as calculated by blade-element methods to be increasingly optimistic as the number of blades increases. The other factor -- substantiated by mean yoke-beam bending data -- could be a difference in thrust produced by the upper and lower blade pairs possibly reducing rotor efficiency.

CALCULATED BLADE STALL LIMITS

Performance calculations were made to determine the steady-state rotor thrust limits. For these calculations, the C-81 computer program was used in the "wind-tunnel" mode, in which the fuselage and tail rotor are deleted from the computations. (C-81 correlation with all the complexities of a total flight simulation are presented in a later section.) Lift, propulsive force, and horsepower were calculated as if the rotor were operated in a wind tunnel at various blade collective pitch settings and shaft angles from 50 degrees forward to 30 degrees aft, with cyclic blade feathering manipulated to zero-out flapping. These calculations were made using steady aerodynamics and a rigid blade pinned at the root.

Figure 7 shows the calculated rotor lift and drag for constant collective pitch angles at airspeeds of 80 and 160 knots. The maximum lift obtainable before encountering deep stall is indicated on the figure by the "STALL" line. This figure also shows that the collective setting establishes the rotor propulsive force.

These computed values of maximum steady-state rotor lift are also presented on Figure 8 in terms of lift coefficients versus advance ratio for three values of fuselage equivalent drag area, f , of +25, 0 and -25 square feet. The first value of drag is representative of the test vehicle drag. The latter two values

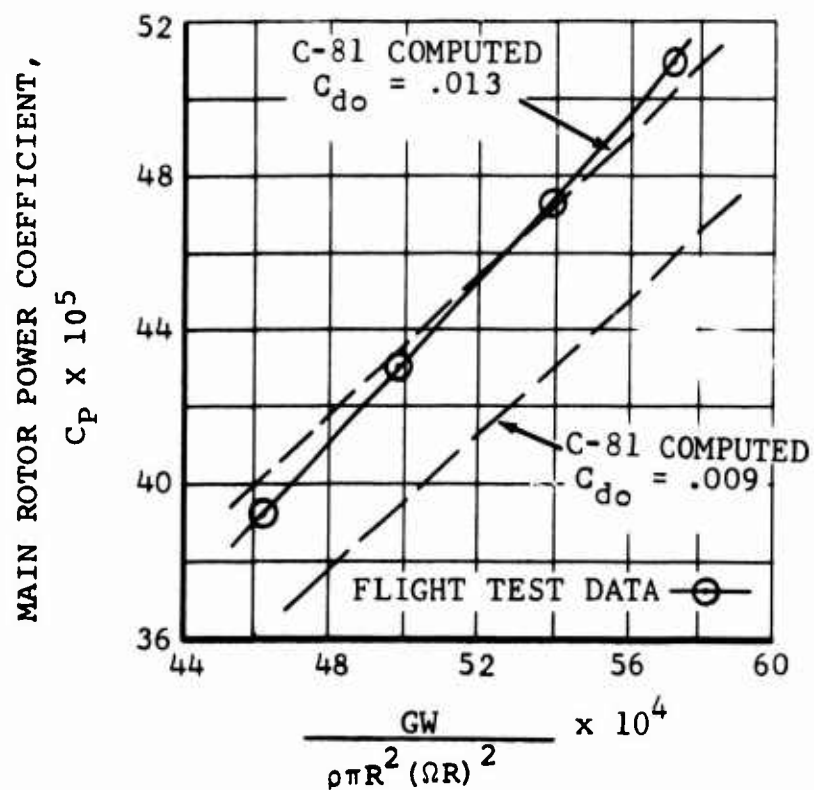


Figure 6. Measured and Computed Nondimensional OGE Hover Performance.

COLLECTIVE PITCH ANGLE, DEG

NOTE: C-81 RIGID BLADE ANALYSIS
STEADY AERODYNAMICS

θ_0	θ_0
8	0.75
12	1.25
16	4.25
20	9.25
24	13.25
	17.25

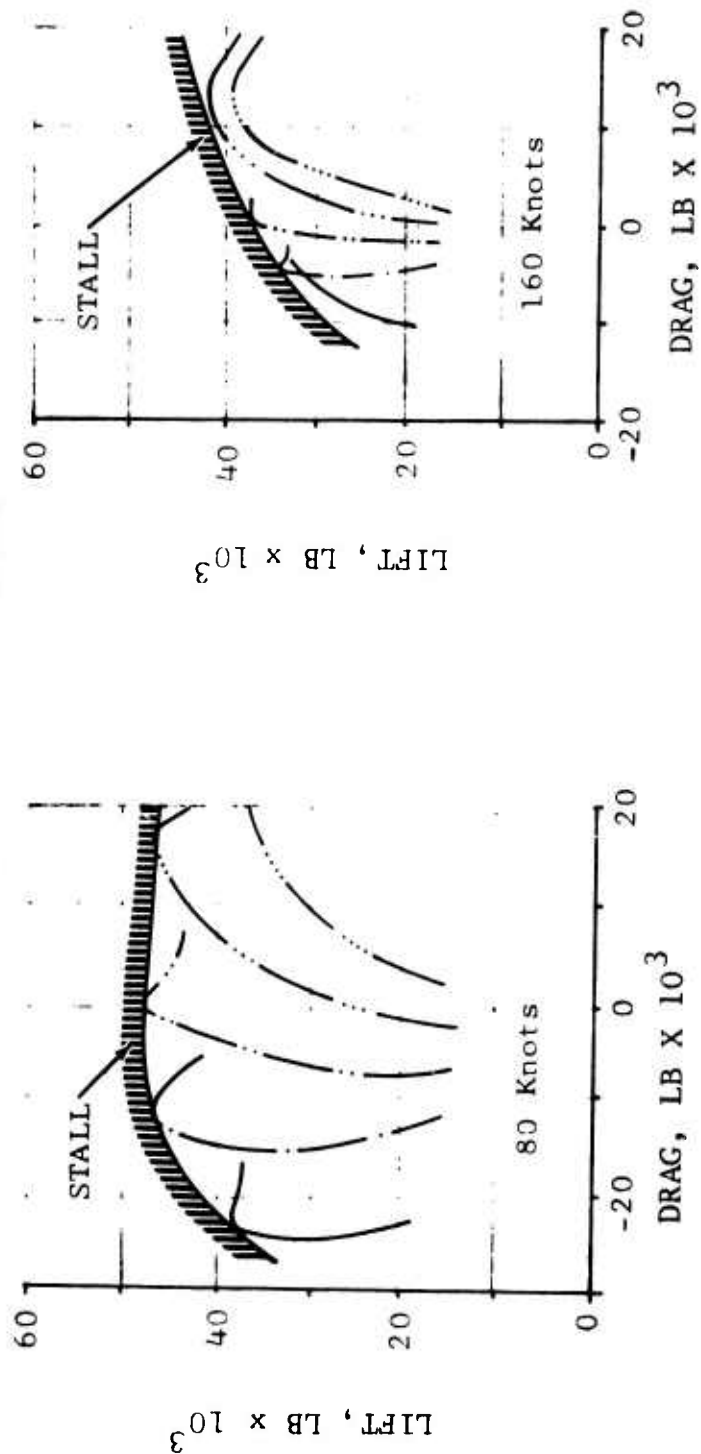


Figure 7. Computed C-81 Rotor Lift and Drag at Constant Collective Pitch Settings.

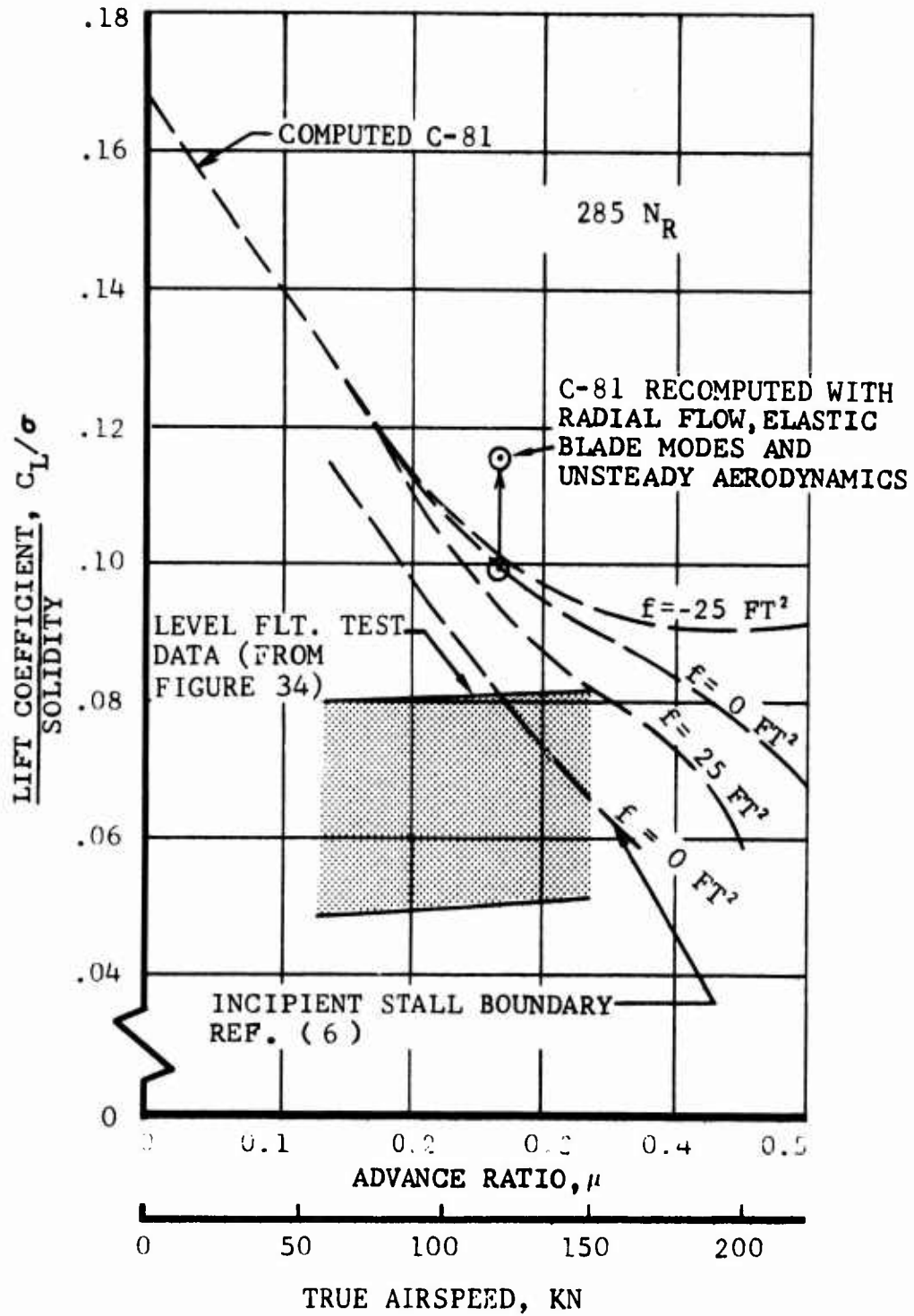


Figure 8. Measured and Computed Maximum Steady-State Rotor Lifting Capability.

are arbitrary choices which could be achieved with a compound helicopter, or may be considered quasi-static simulations of conditions encountered during maneuvers. An incipient stall boundary from Reference 6 calculated at $f = 0$ is shown for comparison. An envelope of the measured level flight data is also shown and reaches the calculated thrust limit. The maximum thrust was then recalculated for a selected point of $f = 0$, velocity = 120 knots, using elastic blade modes, unsteady aerodynamics, and allowing large radial flow angles. This recalculated value is included in Figure 8 and is believed to be more nearly representative of the true lift limit.

HANDLING QUALITIES - RESULTS AND DISCUSSION

This section contains a discussion of stability and control characteristics of the helicopter in various flight regimes. The discussion covers flight records, pilot interpretations, and computations. The method of computation is discussed in Reference 3.

The helicopter exhibits handling qualities peculiar to hingeless rotors and this particular configuration. In general, they are judged acceptable in all flight test conditions.

The control positions in this section are presented from 0 to 100 percent. The sign conventions at 100 percent are as follows:

F/A cyclic stick position - full forward

Lat cyclic stick position - full right

Pedal position - full right

Collective stick position - full up

Positive angular rates are determined as follows: pitch - nose-up; roll - right; and yaw - nose right.

For this section of the report, the following cg locations were tested: forward - 122.6; mid - 128.9; and aft - 136.0.

HOVER

The high control response, sensitivity, and damping of this rotor system give the pilot precise control in hovering flight. Figure 9 shows the pitch rate and response of the helicopter to a step input of forward cyclic. The small amount of lateral cyclic and pedal input required to stabilize rates about the roll and yaw axes shows that there is little control coupling.

Figure 10 shows how the helicopter responds to a right lateral cyclic pulse input. The response is stable, and all rates are well damped with no short-period divergent tendencies.

The flexbeam rotor with its high hub moment per degree flapping contributes to excessive gust sensitivity in hover, as well as at all other flight speeds. The Stability and Control Augmentation System (SCAS) reduces this gust sensitivity to an acceptable level.

Collective step inputs were performed both in- and out-of-ground effect. Figure 11, the record of a typical case, shows an

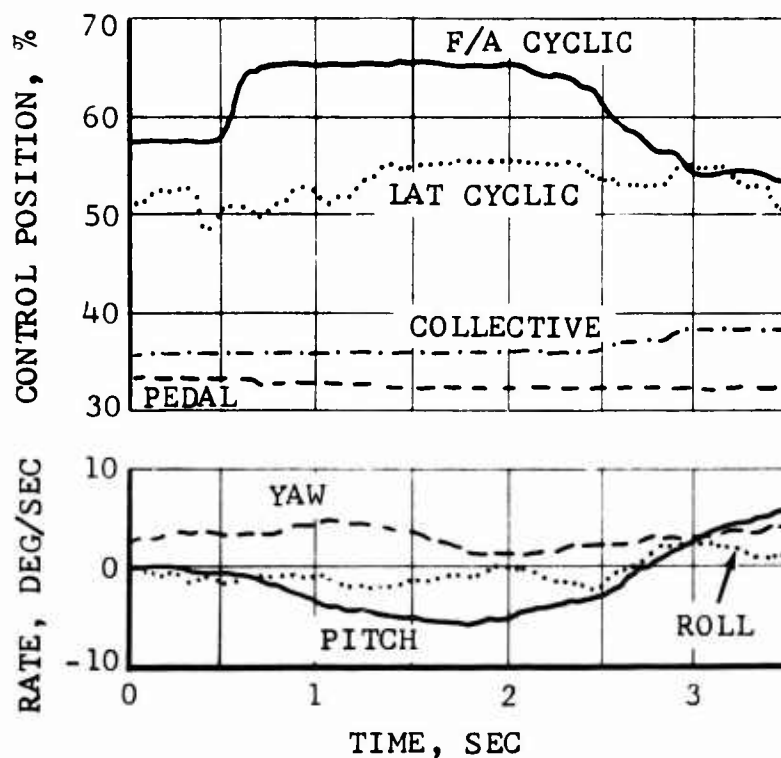


Figure 9. Longitudinal Cyclic Step in IGE Hover, Flight Test Data, 12,000 Pounds GW, Aft CG.

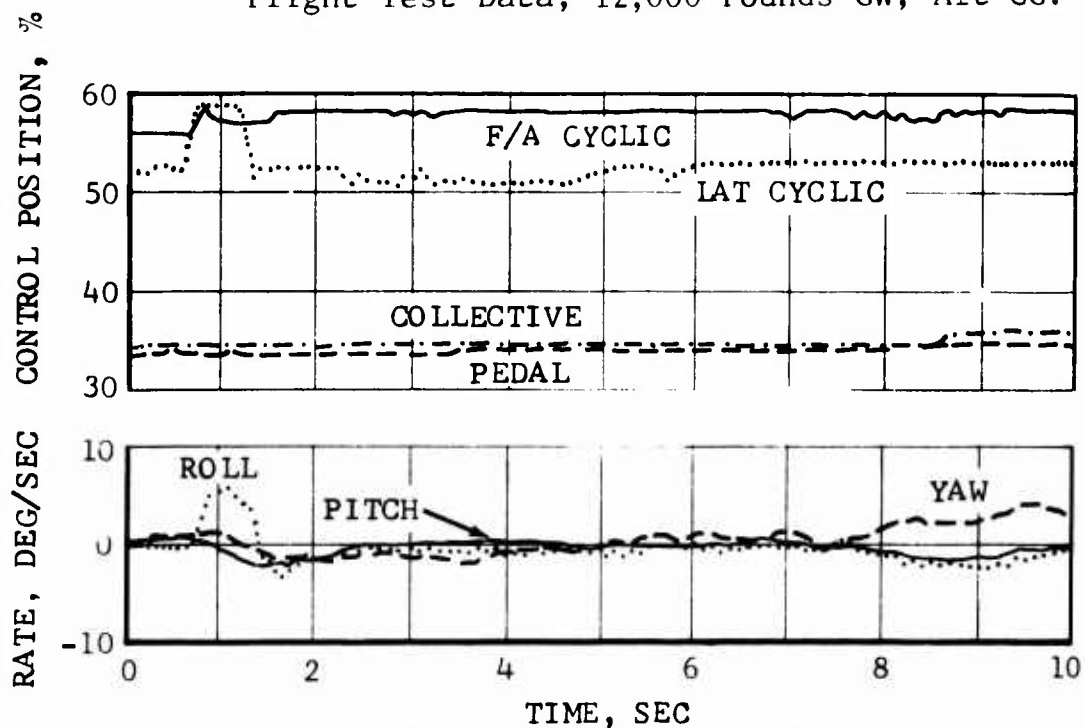


Figure 10. Lateral Cyclic Pulse in IGE Hover, Flight Test Data, 12,000 Pounds GW, Aft CG.

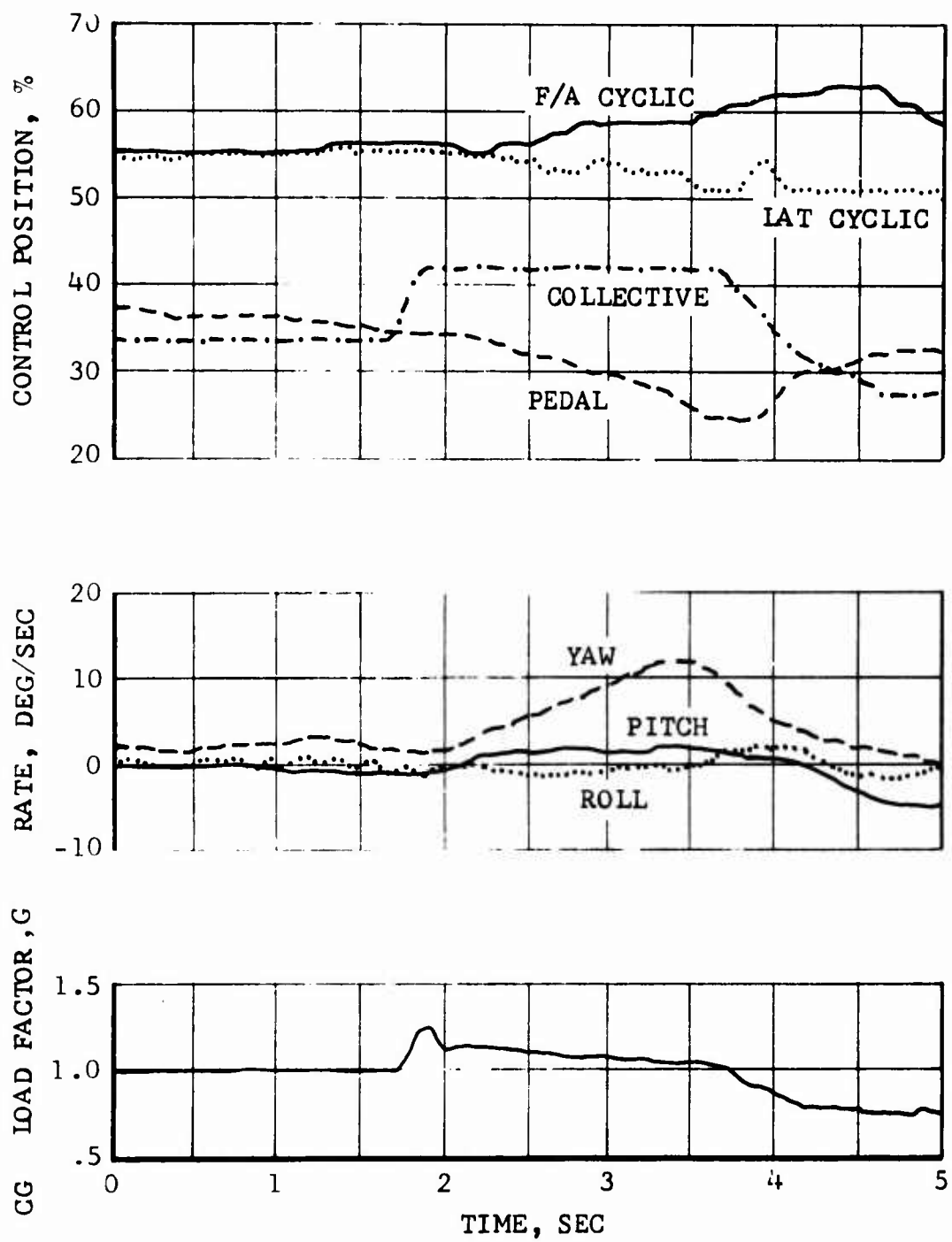


Figure 11. Collective Step in IGE Hover, Flight Test Data, 12,000 Pounds GW, Aft CG.

immediate (delay less than 0.05 second) normal acceleration in response to the collective input, with the acceleration peaking as the full step is reached. The normal acceleration has a damped oscillation.

TRANSITION

During transition from hover to forward flight, the helicopter rolls right in the 15- to 30-knot speed range. A variation in induced velocity over the main rotor disk combines with rotor coning to give the blades a higher blade angle of attack at the forward azimuth than the aft azimuth. The resulting right rotor flapping rolls the fuselage to the right. (This characteristic has been noted in other rigid rotor configurations tested at BHC previously.) The high control power was not reduced throughout the transitional flight regime, as cyclic stick inputs still resulted in high pitch and roll accelerations in the 0- to 30-knot speed range.

No unusual control inputs were required for the transition from forward flight to hover. There was no roll comparable to that in the transition from hover to forward flight.

SIDEWARD AND REARWARD FLIGHT

Sideward and rearward flight was investigated for four combinations of gross weight and center-of-gravity location, and no unusual characteristics were noted. In sideward flight, variations in control positions and fuselage attitude with velocity are smooth (Figures 12 and 13) at speeds up to 30 knots. In sideward flight to the left, there is a sharp increase in the right pedal at 30 knots. This is probably a result of the tail rotor going into the vortex ring state at this speed (induced velocity for the tail rotor is about 30 knots to the left in the hover).

Figure 14 presents attitudes and control positions during rearward flight. The control positions vary consistently for the different gross weights and cg's, but the pitch attitude variation with airspeed is different for the 12,000-pound, aft cg case. The elevator download was examined for these areas. Due to the large moment arm of the elevator (22 feet), small variations of download can cause measurable differences in pitch attitude. The elevator download for the 20-knot flight cases was less than 50 pounds except for the 12,000-pound, aft cg flight which had a download of approximately 100 pounds, causing the higher noseup pitch attitude.

The lack of fuselage data ruled out any attempt at the simulation of sideward or rearward flight with the C-81 computer program.

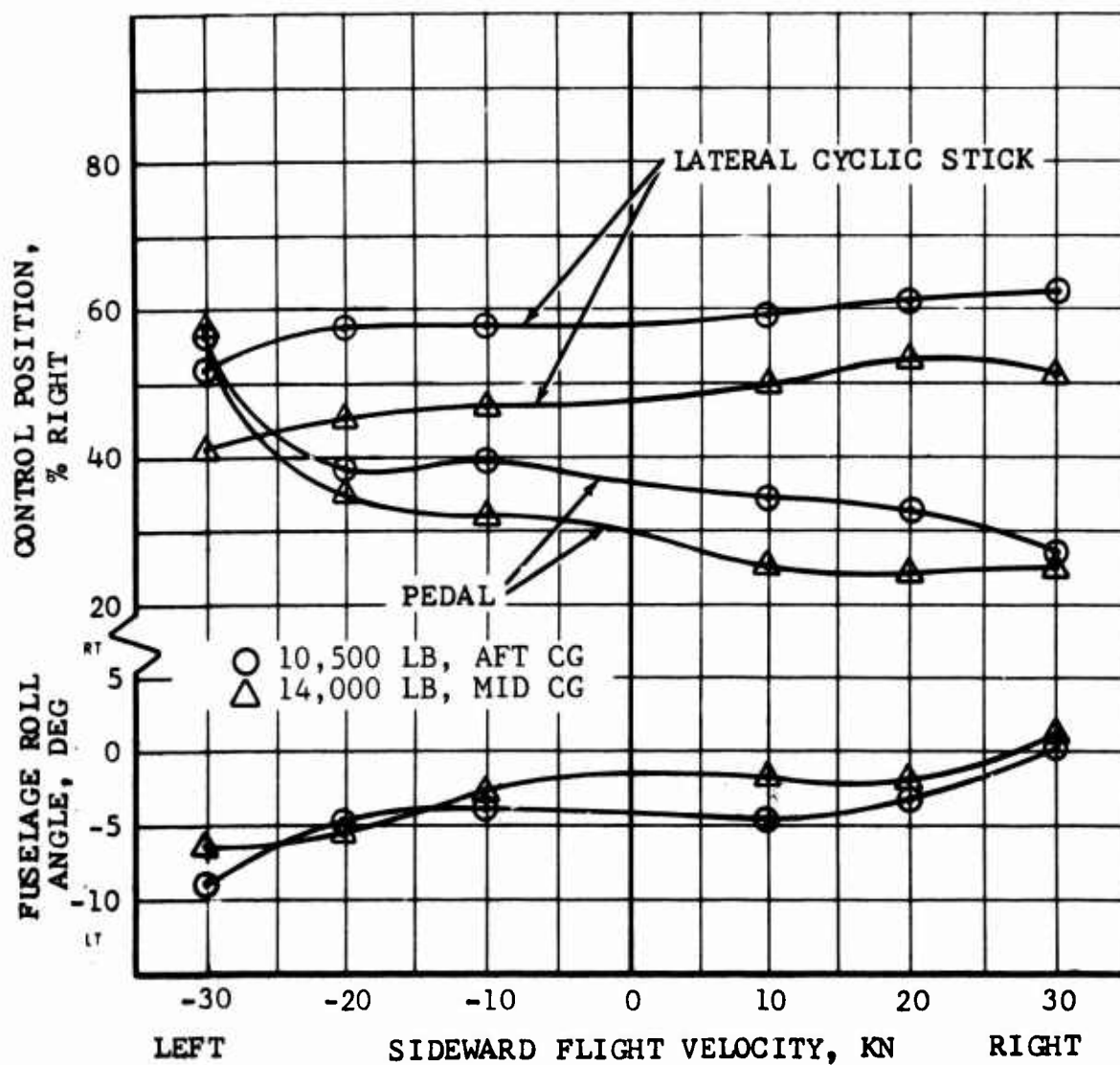


Figure 12. Sideward Flight Characteristics, Flight Test Data, 10,500 Pounds and 14,000 Pounds GW.

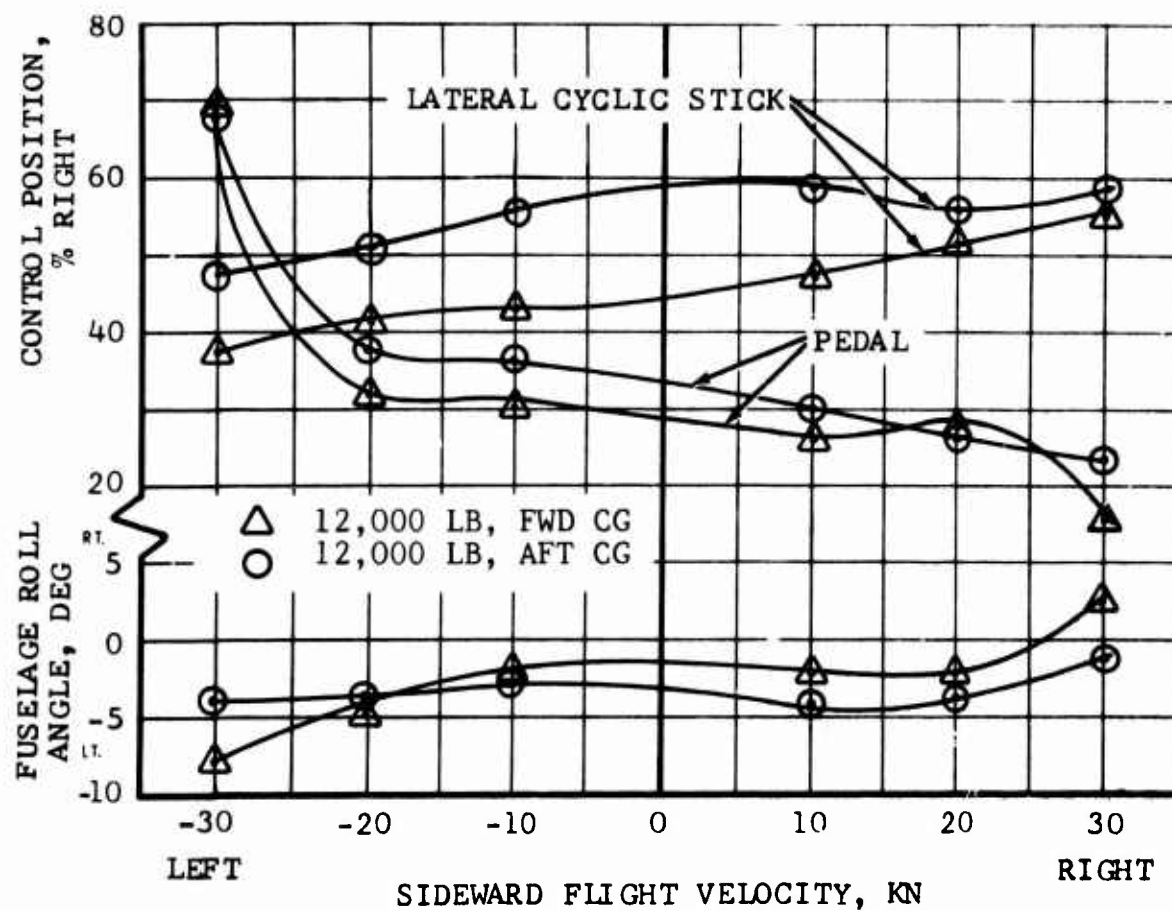
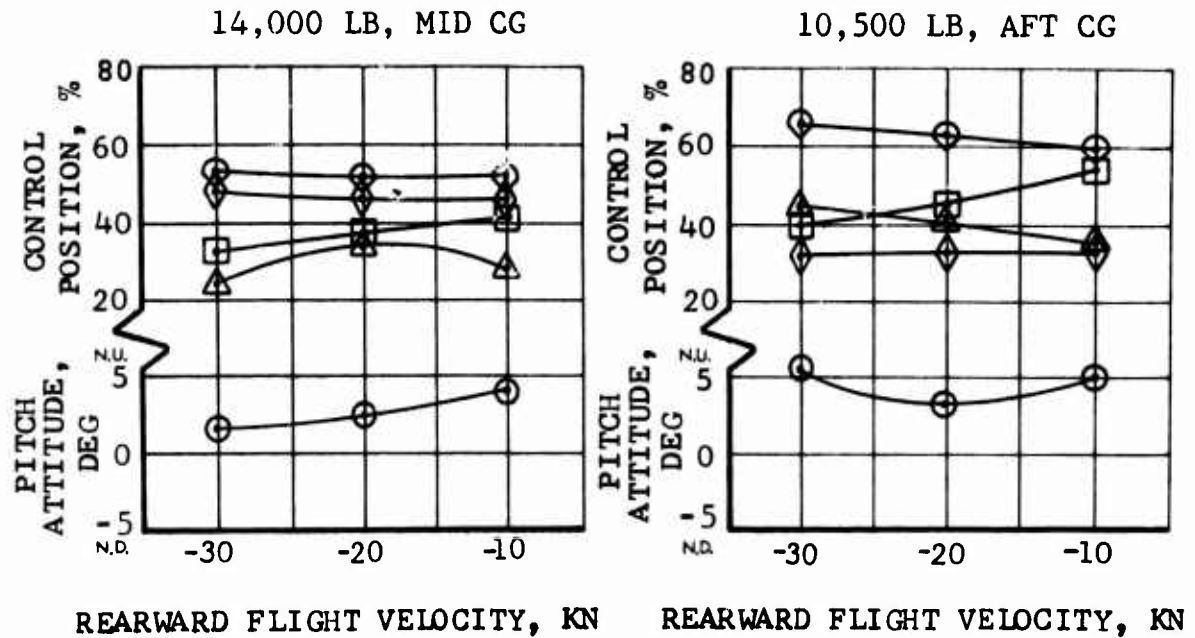


Figure 13. Sideward Flight Characteristics, Flight Test Data, 12,000 Pounds GW.



□ F/A CYCLIC STICK ◇ COLLECTIVE STICK
 ○ LATERAL CYCLIC STICK △ PEDAL ○ PITCH ATTITUDE

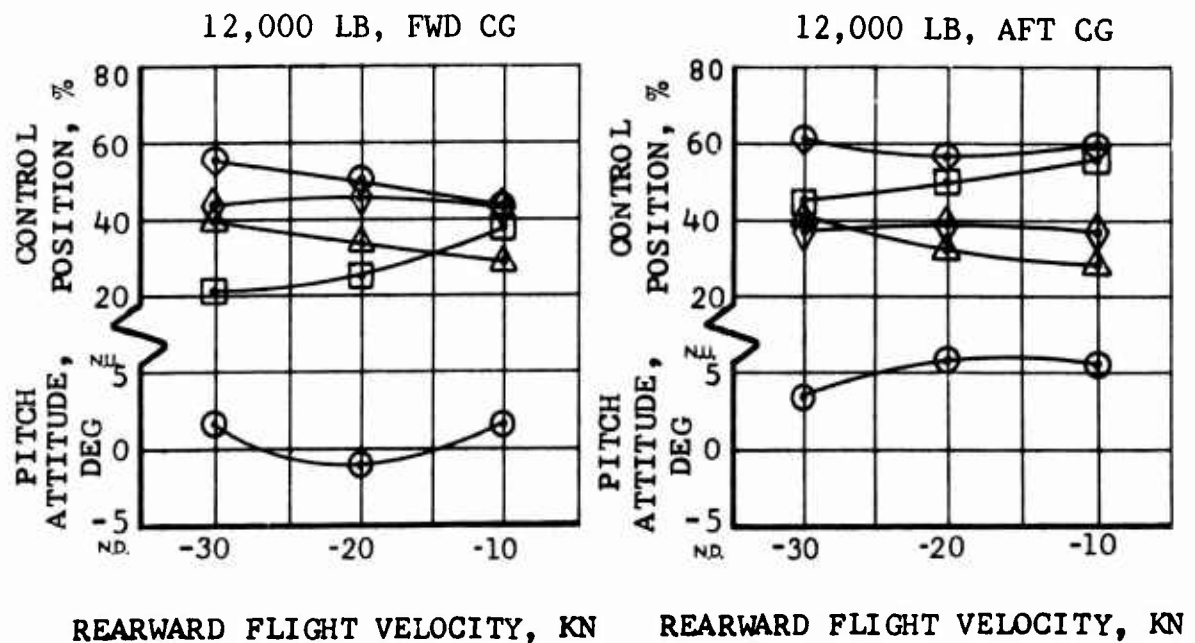


Figure 14. Rearward Flight Characteristics, Flight Test Data.

AUTOROTATION

The helicopter entered autorotation easily at all speeds and loading conditions tested. A large amount of right pedal was needed to balance the effect of the canted ventral fin, which was very effective with the fuselage at the positive angles of attack of autorotation. A record of an autorotational entry and subsequent descent is presented in Figure 15. The variations in roll attitude represent turns the pilot made during the descent.

Table I compares measured and C-81 computed characteristics. The flight test data were obtained in steady-state autorotations and are not comparable to the entry conditions shown in Figure 15.

TABLE I. MEASURED AND PREDICTED TRIM PARAMETERS IN AUTOROTATION				
	Forward cg		Aft cg	
	Flight Test	C-81 Com- puted	Flight Test	C-81 Com- puted
F/A Cyclic Stick Position	42%	41%	59%	53%
Lat Cyclic Stick Position	44%	51%	48%	59%
Pedal Position	98%	89%	90%	88%
Fuselage Pitch Attitude	-1.3 deg	-3.5 deg	-	-1.6 deg
Elevator Lift (+ Up)	-100 lb	+160 lb	+254 lb	+260 lb
Gross weight:	12,000 lb	Airspeed:	100 kn	

This comparison shows roughly the same trend as that for level flight at the same speed--good agreement for fore-and-aft stick position at forward cg, but a higher predicted elevator upload. The fuselage pitch attitude, however, does not agree as well as in the level flight case.

CONTROL RESPONSE AND AIRCRAFT STABILITY

A large number of test records were taken to define the flight dynamic characteristics of the aircraft. The results are presented below.

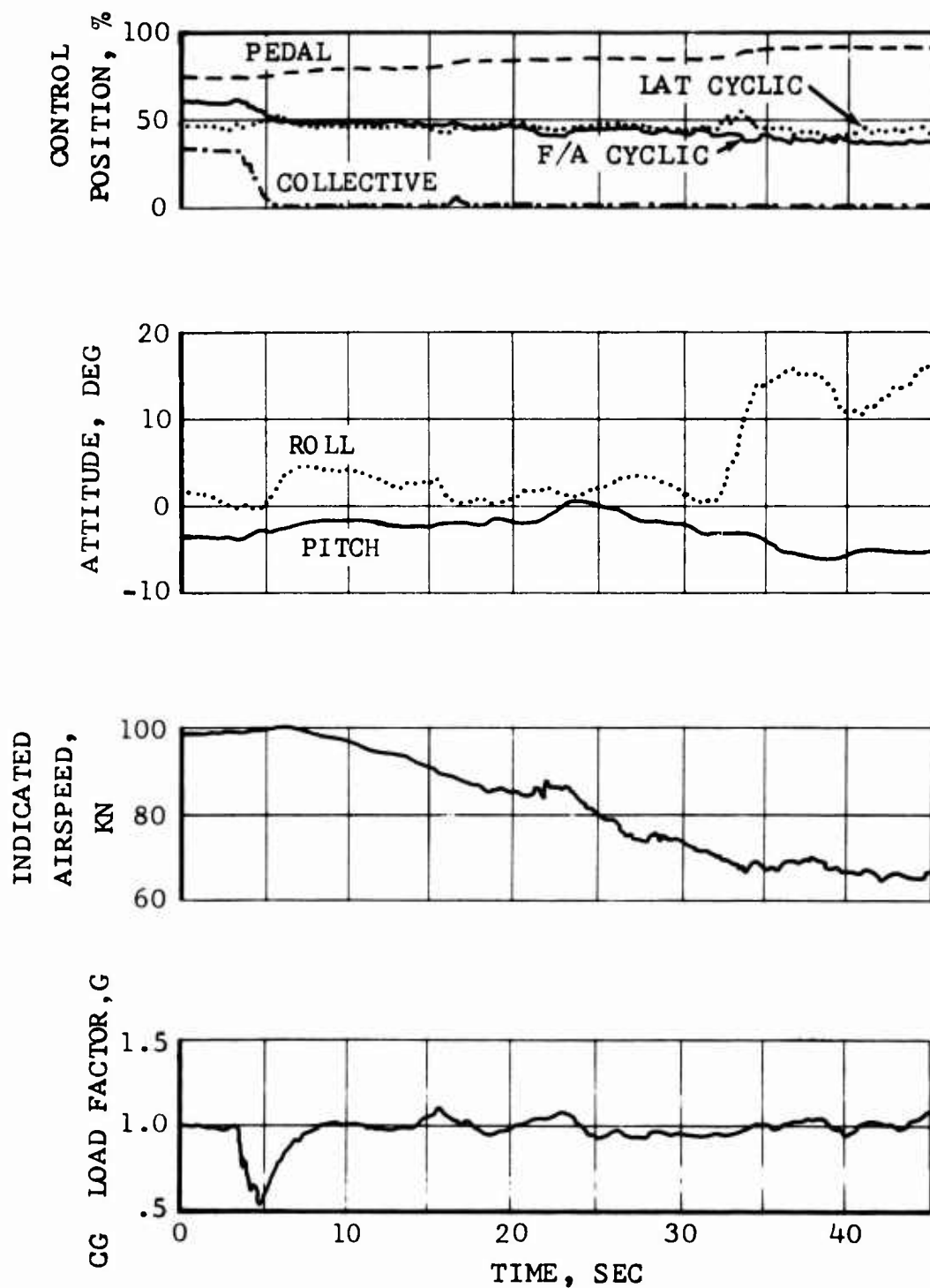


Figure 15. Autorotation Entry and Subsequent Descent, Flight Test Data, 12,000 Pounds GW, Forward CG.

Apparent Speed Stability

The helicopter has positive apparent speed stability and adequate control margin in level flight, climb, and autorotation for all combinations of gross weight, center of gravity, and main rotor speed tested. Positive apparent speed stability is defined as increasing fore and aft cyclic stick position with increasing airspeed, and the collective stick position is allowed to vary. The flight test data and computed values in Figures 16 and 17 verify the accuracy of the computer simulation over a range of level flight conditions. Figure 18 shows stick position versus airspeed for climb and autorotative flight conditions.

At forward and mid center-of-gravity test conditions and at low speed, the predicted fuselage pitch attitude is more noseup than measured in flight test. The computer simulation shows the elevator angle of attack at 60 knots for these loadings to be very near the stall, making it difficult to predict lift accurately in this speed range. With an aft center of gravity, the elevator is not near stall and the predicted fuselage attitude agrees more closely with flight test.

Static Longitudinal Stability

The helicopter has positive static longitudinal stability between 70 and 140 knots at 12,000 pounds gross weight with the center of gravity forward. Positive static longitudinal stability is defined as increasing fore and aft cyclic stick position with increasing airspeed and the collective stick held fixed. With the center of gravity aft, the longitudinal cyclic stick gradient was slightly negative (-1 percent in 20 knots) at 140 knots and positive for all speeds less than 140 knots. The gradient was positive for the same speed with a forward center of gravity. Stability was positive in climb and autorotation at 100 knots. The flight test data are presented in Figure 19.

Analysis predicted the decrease in static longitudinal stability at high speed and aft center of gravity. The increasing noseup attitude of the elevator with increasing speed generates adequate control margin but decreases speed stability (pitching moment change with speed). The rigid hub also reduces angle-of-attack stability. The combination of these two effects tends to reduce the longitudinal cyclic stick gradient with speed. A comparison of predicted and measured values of this gradient is presented in Figure 20.

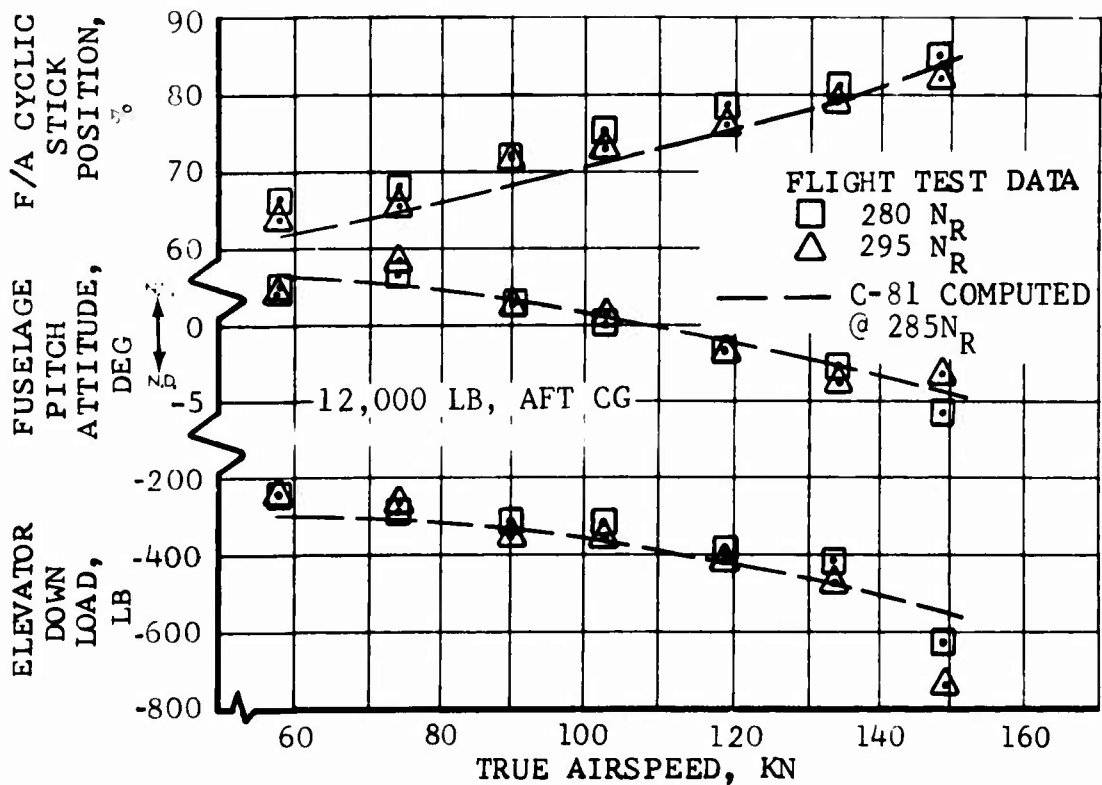
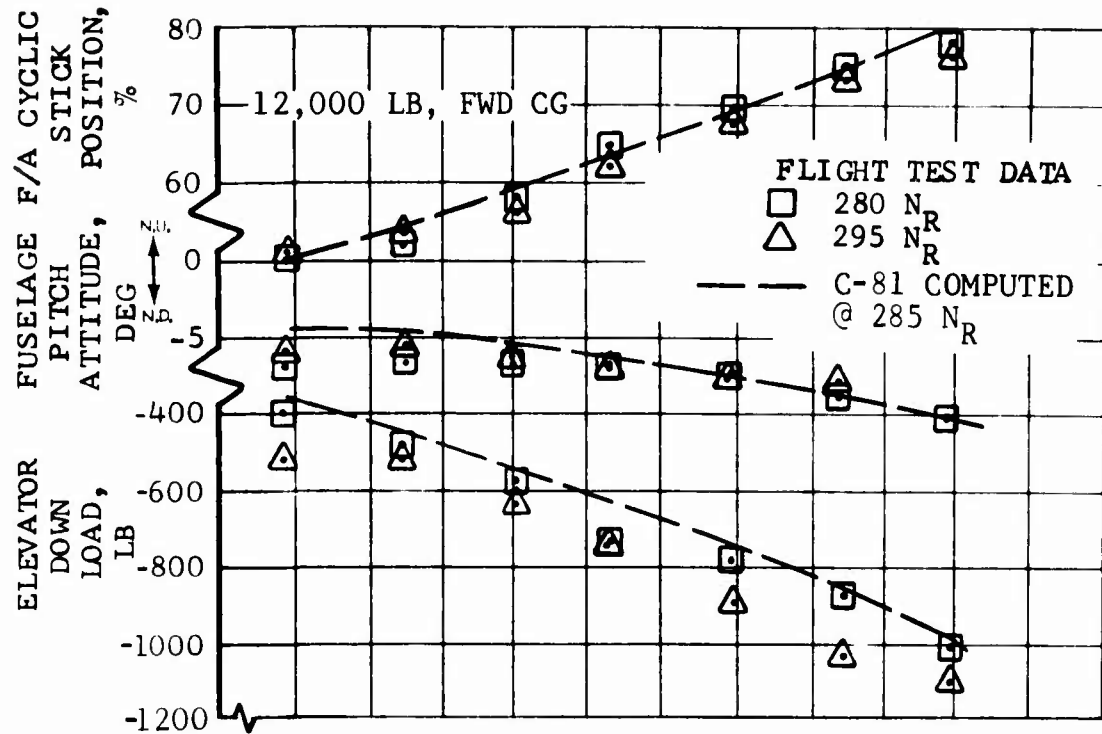


Figure 16. Measured and Computed Forward Flight Trim Values, 12,000 Pounds GW.

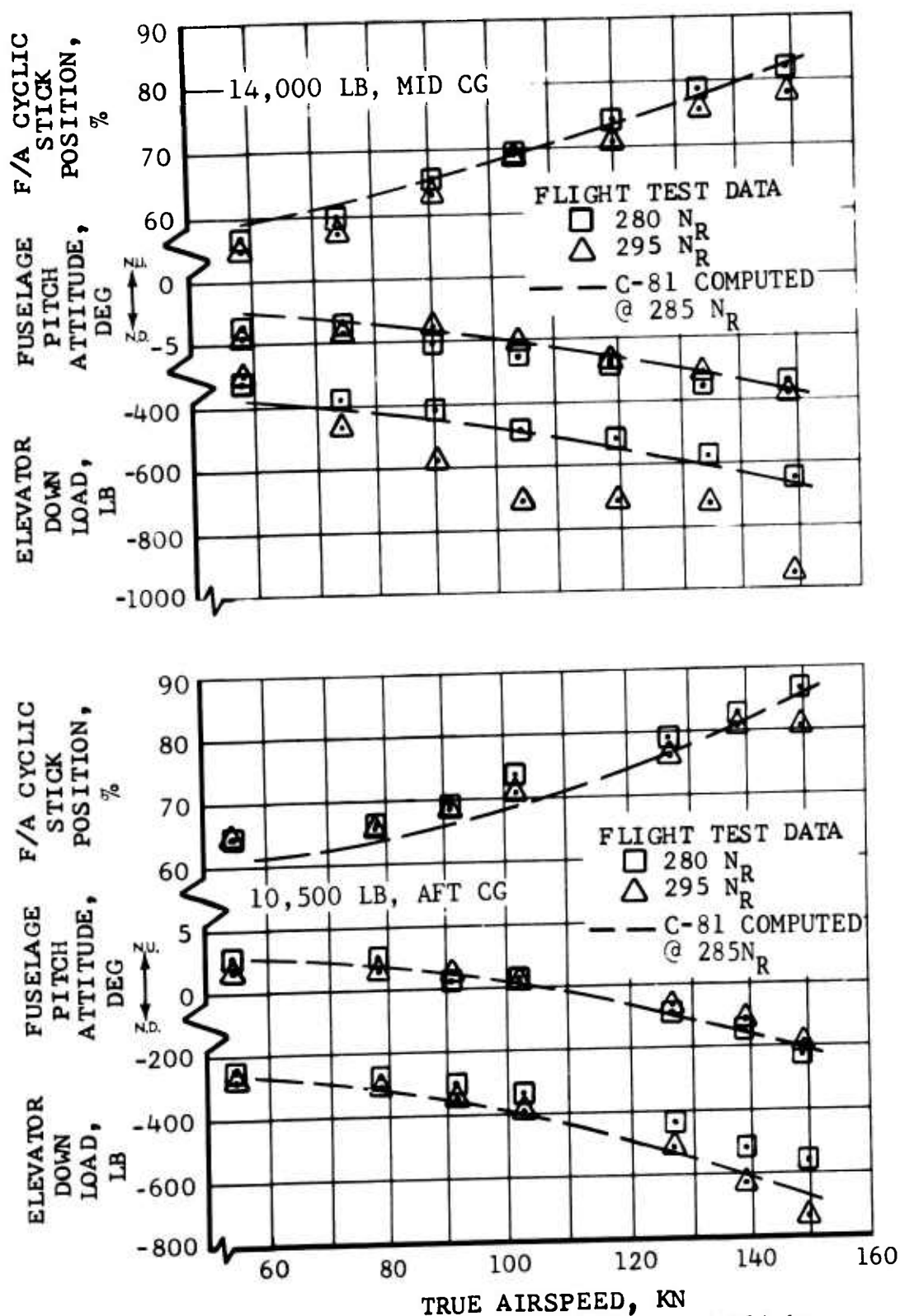


Figure 17. Measured and Computed Forward Flight Trim Values, 10,500 Pounds and 14,000 Pounds GW.

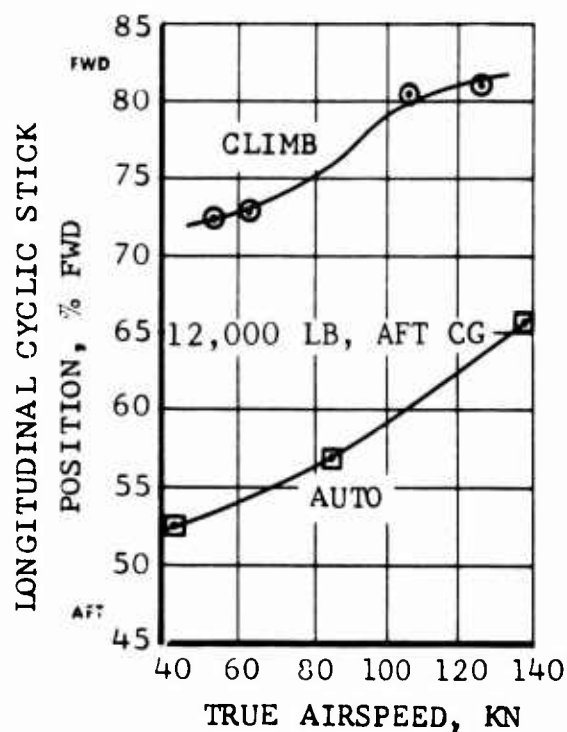
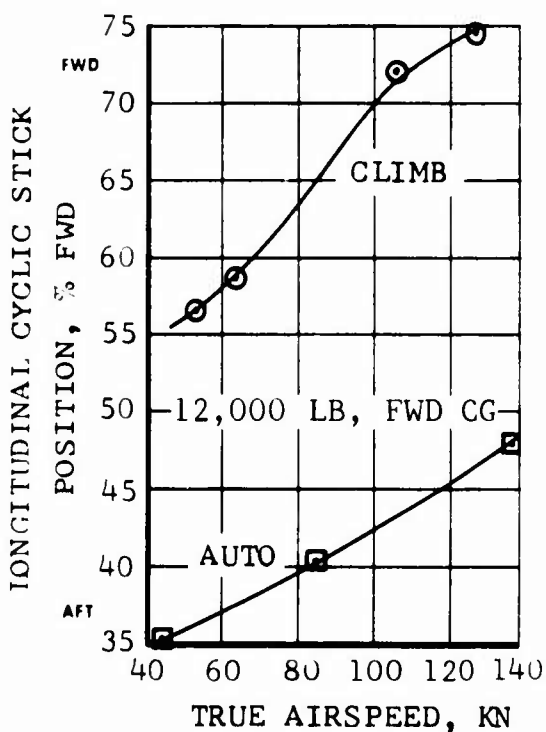
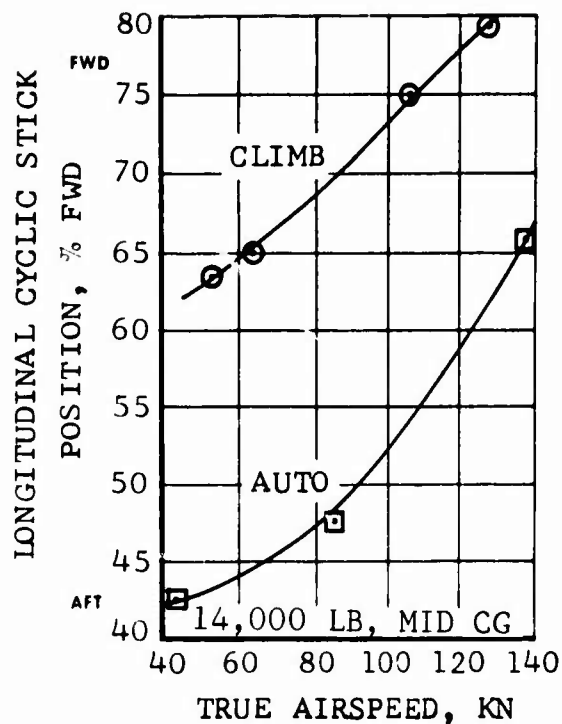
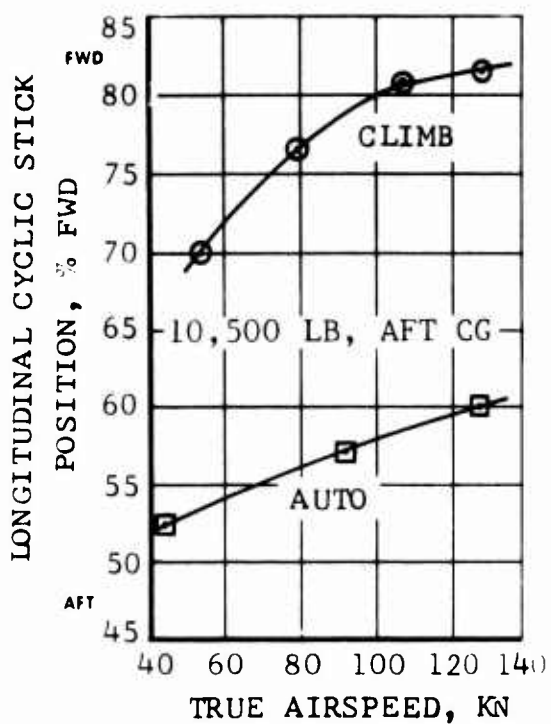


Figure 18. Apparent Speed Stability in Autorotation and Climb, Flight Test Data.

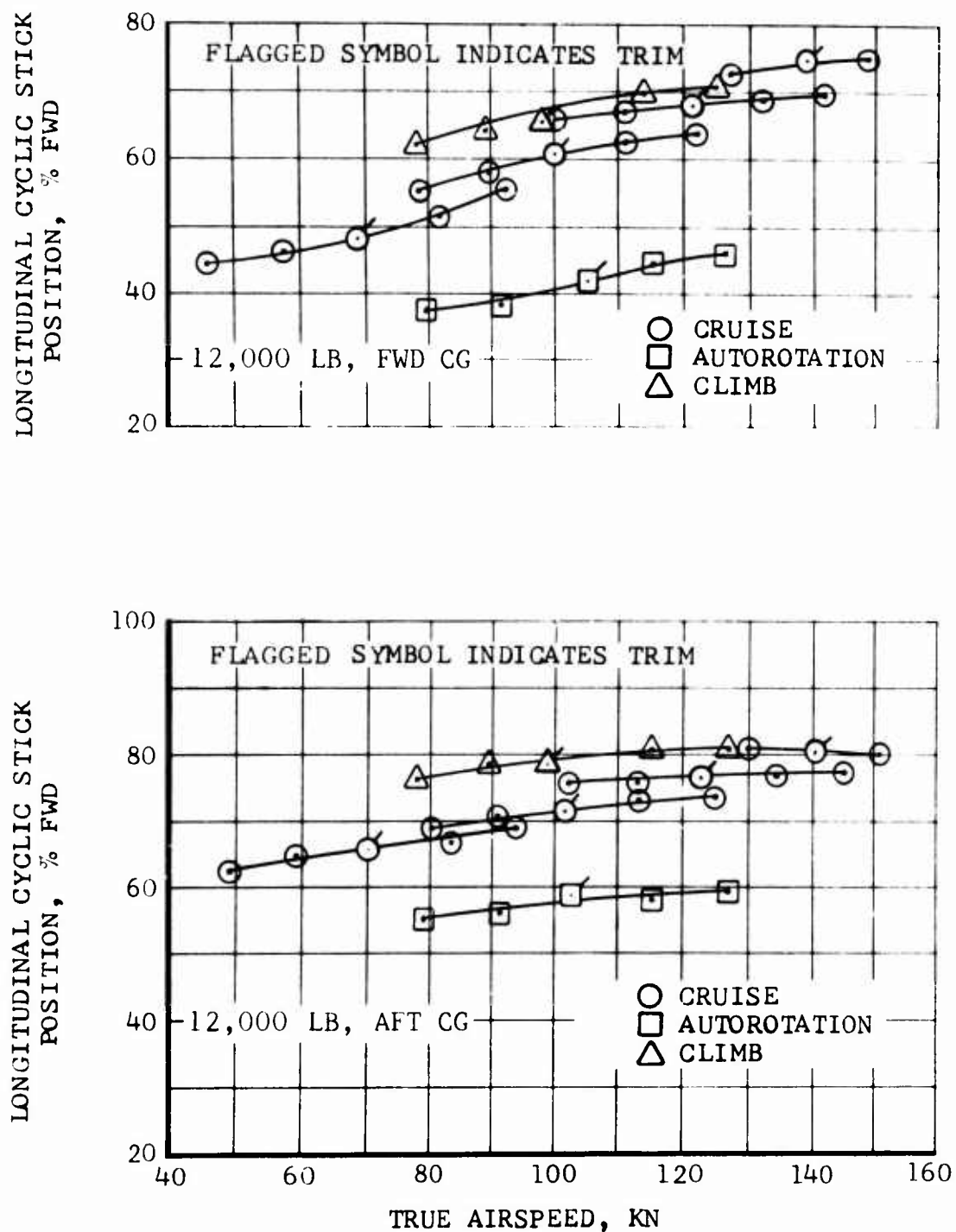


Figure 19. Static Longitudinal Stability, Flight Test Data.

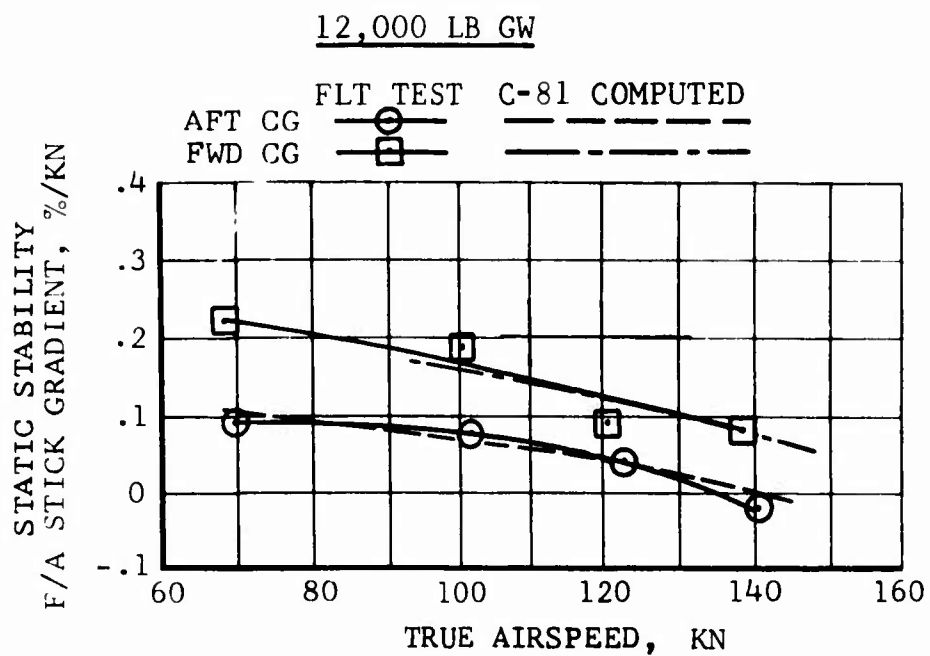


Figure 20. Measured and Computed Level Flight Static Longitudinal Stability.

Static Lateral-Directional Stability

The helicopter has positive static directional stability and dihedral effect for all conditions tested. Dihedral effect, indicated by the change of the lateral cyclic stick position with sideslip angle, is positive for all flight conditions and increases with forward speed (Figure 21).

Static directional stability is positive but varies with flight conditions and with airspeed. The directional stability of the fuselage and fin changes with fuselage angle of attack. Negative angles of attack (forward flight and climb) reduce the sweepback of the fin and make it more effective. At positive angles of attack (autorotation), tailboom interference and the increase in fin sweepback reduce directional stability. This appears in Figure 21 as a more negative gradient of the pedal with sideslip angle as power increases. At high speed, the angle of attack changes less between level flight and climb than it does at low speed, and the pedal gradients for these two flight conditions approach each other.

The contribution of the vertical stabilizer to yawing moment due to sideslip increases with forward speed. Yawing moment produced by a unit pedal deflection increases with forward speed, but it does not increase as much as the vertical stabilizer contribution. These factors combine to increase pedal gradient linearly with freestream dynamic pressure, as shown in Figure 21.

Dynamic Stability

The dynamic stability of the helicopter at a gross weight of 12,000 pounds was investigated with the center of gravity at both forward and aft locations. Longitudinal modes were excited with cyclic stick pulses and lateral-directional modes with cyclic stick or pedal inputs. All modes exhibited coupling between longitudinal and lateral-directional parameters.

The longitudinal short period mode is characterized by a pitch rate oscillation which is shown in Figure 22. This mode has a period of 2 to 4 seconds, and damps after no more than 1-1/2 cycles. The presence of a roll and yaw oscillation indicates lateral-directional coupling. Computer analysis agrees with the test predicting a period between 2 and 4 seconds, a damping ratio between 0.35 and 0.7, and strong coupling between longitudinal and lateral-directional motion.

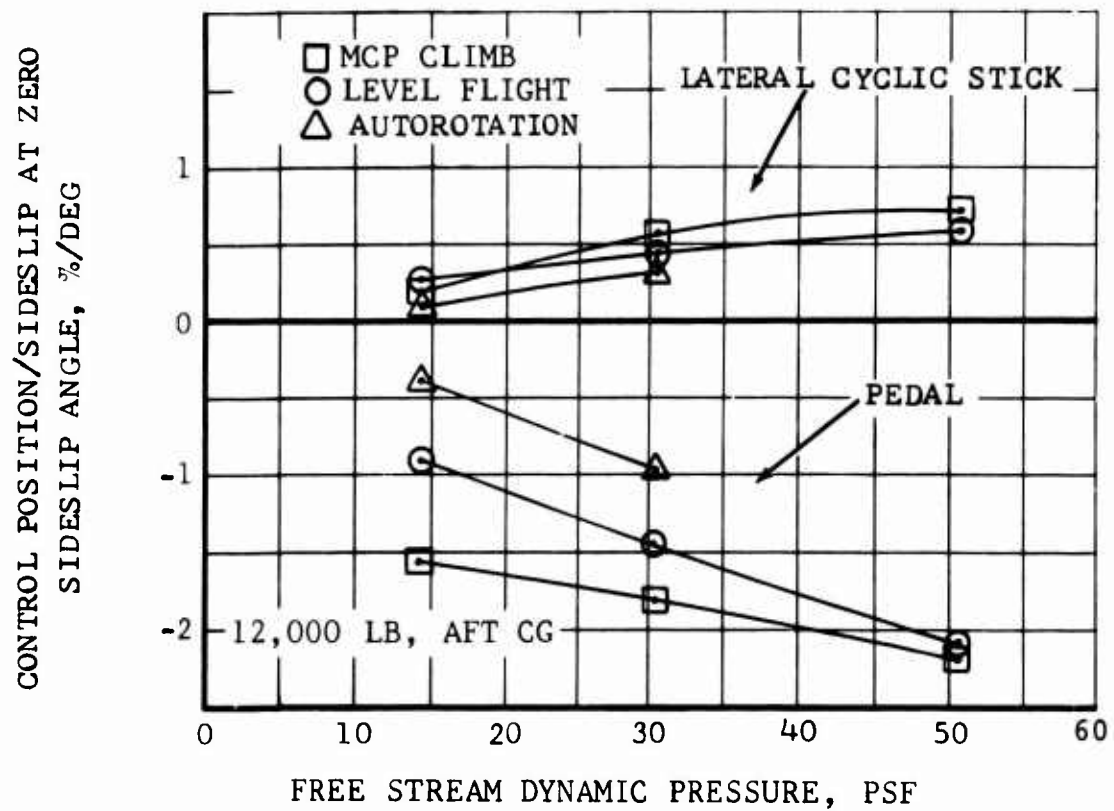


Figure 21. Static Lateral-Directional Control Gradients, Flight Test Data.

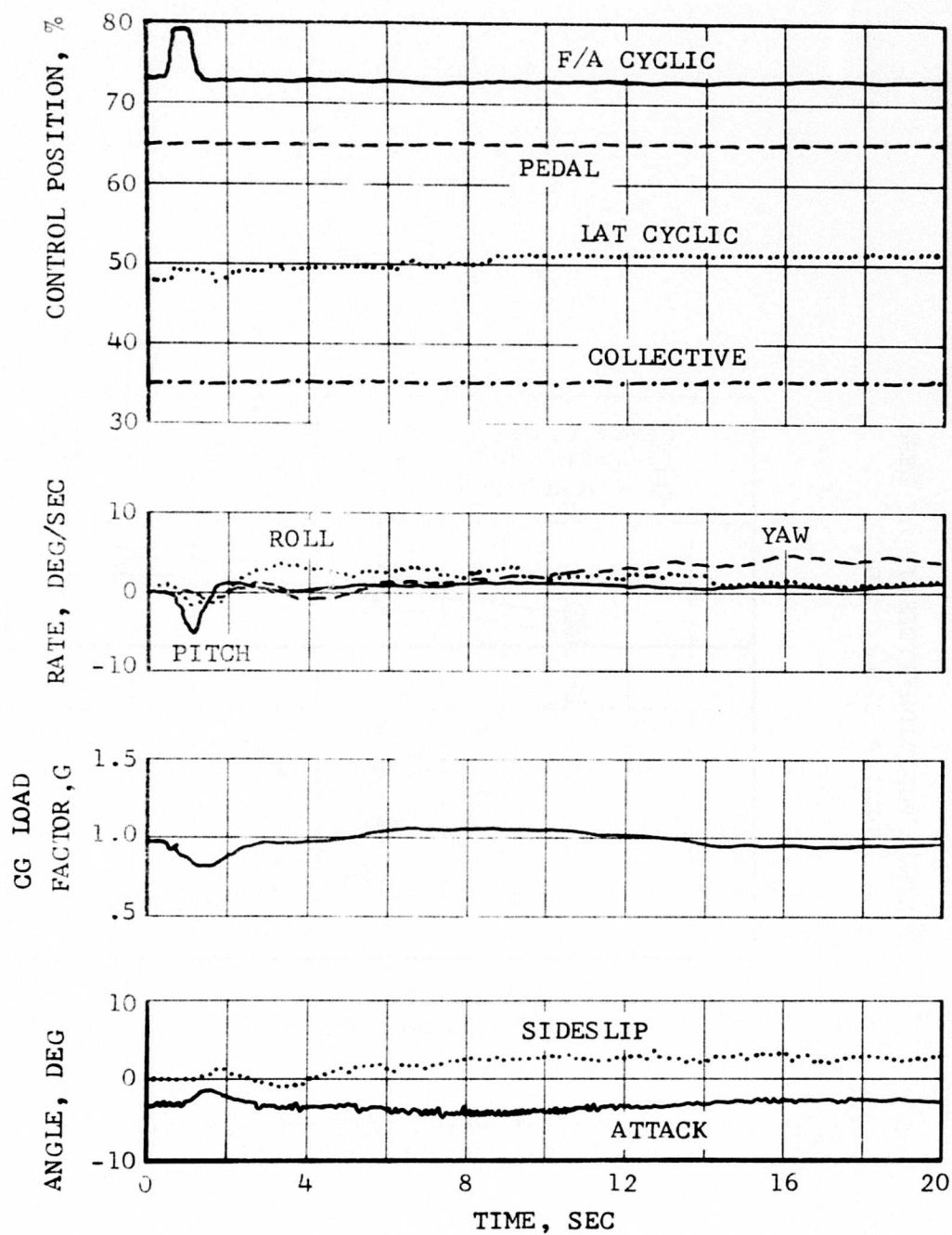


Figure 22. Forward Cyclic Pulse at 100 Knots, Flight Test Data, 12,000 Pounds GW, Aft CG.

Dutch roll motion can be induced with a lateral cyclic stick pulse, as is shown in Figure 23, or with a pedal step as shown in Figure 24. The period of this mode is between 2 and 3 seconds and damps in less than 2 cycles. Coupling is apparent in that the pitch rate is almost half the magnitude of roll and yaw rates, which are approximately equal.

Computed dutch roll period and damping agree with test data. The predicted magnitude of the pitch to yaw rate is similar to flight test results, but the roll rate is one-half the yaw rate.

The long-period longitudinal response (phugoid), shown in Figure 25, has a pitch attitude oscillation with a period of 25 seconds and neutral to slightly negative damping. Some roll coupling is present which induces a right roll, which was left uncorrected and caused a gradual right turn.

Table II shows the measured and computed phugoid mode characteristics. The predicted periods agree well, but the damping is overestimated.

TABLE II. MEASURED AND PREDICTED PHUGOID CHARACTERISTICS				
True Airspeed (kn)	Flight Test		Calculated	
	Period (sec)	Damping Ratio	Period (sec)	Damping Ratio
70	25	~ 0	22	.008
99	25	~ 0	27	.031
145	43	~ 0	49	.096
150	-	-	90	.046
Gross weight: 12,000 lb cg aft				

Although the spiral mode is computed to be stable, with a time-to-half amplitude between 6 and 8 seconds, the flight tests showed it to be nearly neutral. Right and left banked turns at 130 knots with controls fixed had a time-to-double of 30 seconds for the bank angle, after which the bank angle started to return slowly toward zero. This difference between computed and flight-test results is probably due either to a high estimate of dihedral stability or a low estimate of directional stability. Since few

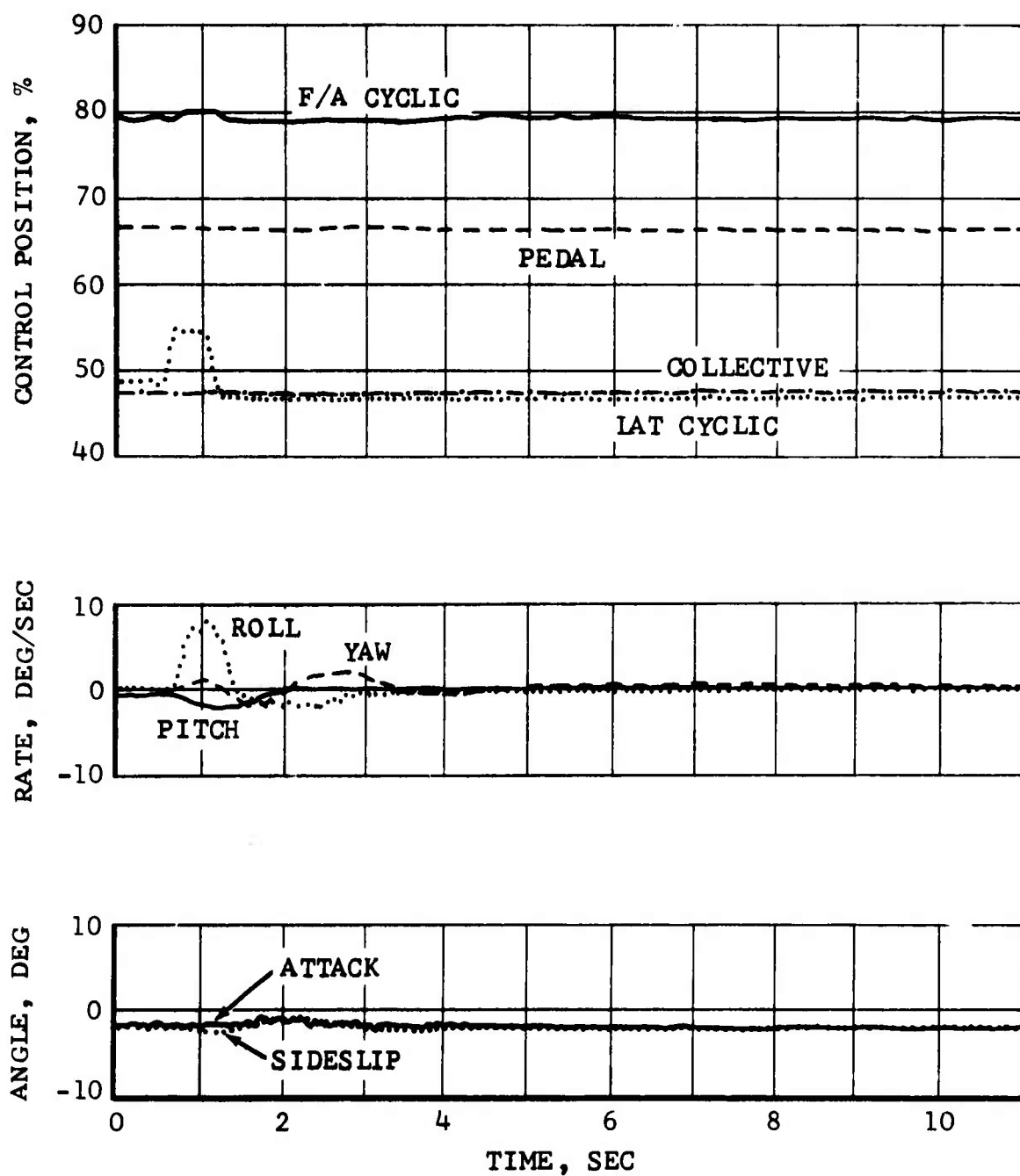


Figure 23. Lateral Cyclic Pulse at 130 Knots, Flight Test Data, 12,000 Pounds GW, Aft CG.

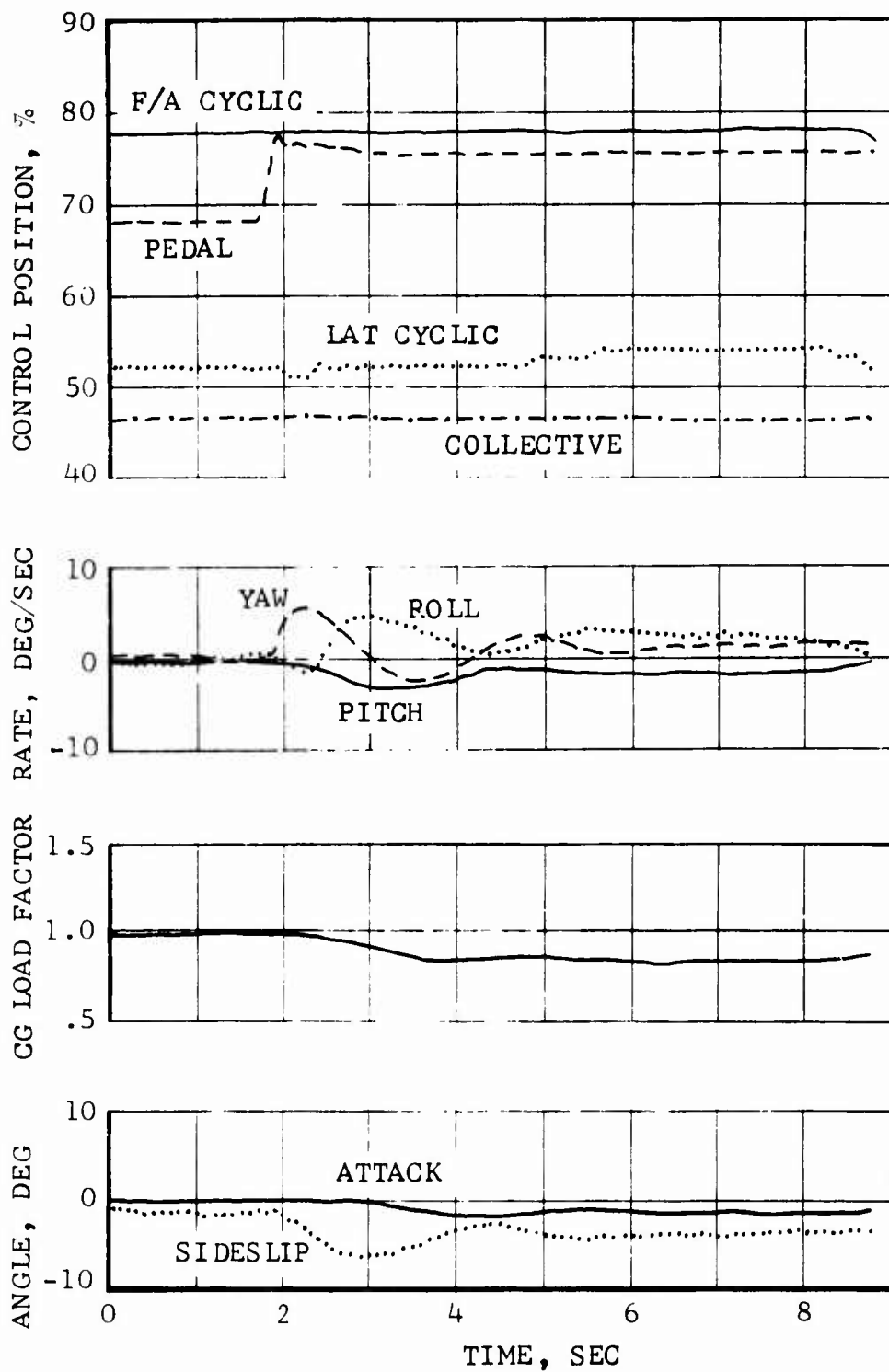


Figure 24. Pedal Step at 130 Knots, Flight Test Data, 12,000 Pounds GW, Aft CG.

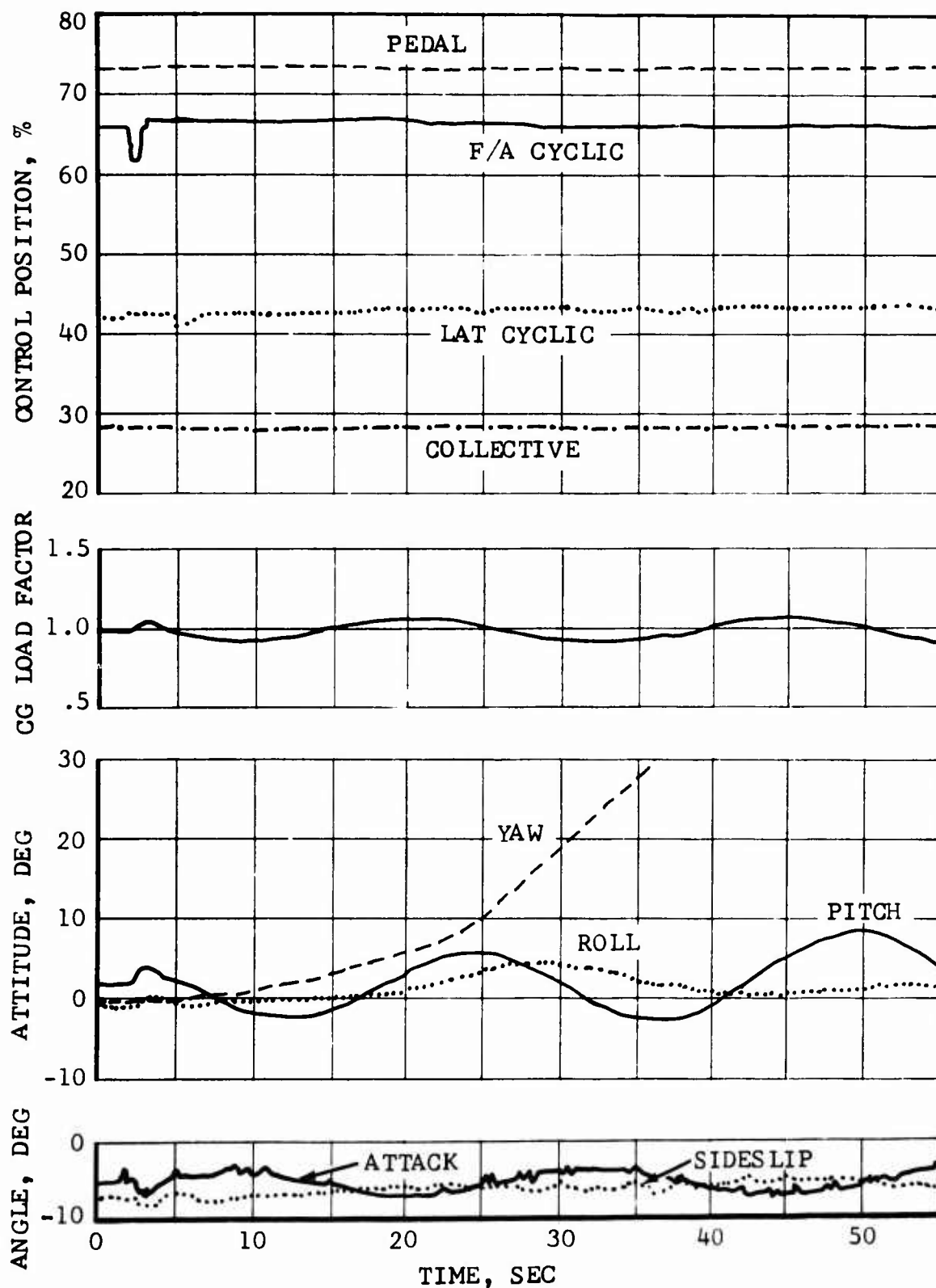


Figure 25. Longitudinal Cyclic Pulse at 100 Knots, Flight Test Data, 12,000 Pounds GW, Aft CG.

wind-tunnel data were available for fuselage sideslip derivatives, the exact cause could not be determined.

Forward Flight Control Response and Sensitivity

A series of control steps in the longitudinal and lateral directions were performed at 12,000 pounds gross weight and forward and aft center-of-gravity locations. Control response and sensitivity were measured from records of the resulting pitch and roll rates and normalized for 1-inch control displacements. Because the control inputs were small, it was not possible to check the linearity of control response. Sample records are shown in Figures 26 and 27, and a summary of all test data is presented in Figures 28 and 29.

The near-zero lag between the insertion of the full step cyclic input and the peak angular acceleration shows the rotor responsiveness to the cyclic controls. Since angular accelerations are measured from the slope of the angular rate plot, the time of peak angular accelerations was difficult to determine (in general, the peak acceleration occurred less than 0.1 second after the control motion stopped).

Some difficulty was encountered in measuring the control inputs used in these tests of response and sensitivity. The pilot's cyclic stick used for the step input was instrumented for displacement measurements, but the fixture which acted as a positive stop was on the copilot's stick. Deflections between these two sticks and the swash-plate washed out some of the control input. The control inputs were restricted to 1/2 inch or less above 100 knots; therefore, a small amount of lost motion was a significant percentage of the step size and consequently of control response and sensitivity. As much as 25 percent of the stick input has been lost in some measured cases.

1. Lateral Control

At high speed, the test helicopter has higher lateral sensitivity for left steps than for right steps, as shown in Figure 29. A left step causes the rotor to tilt aft (indicated by the initial noseup pitch rate in Figure 27), increasing the rotor angle of attack. This produces an increase in rotor thrust and thus an increased rolling moment. A right step produces the opposite effect (Figure 23), reducing thrust and thus reducing the right rolling moment. The rotor thrust versus angle-of-attack gradient increases with speed, and

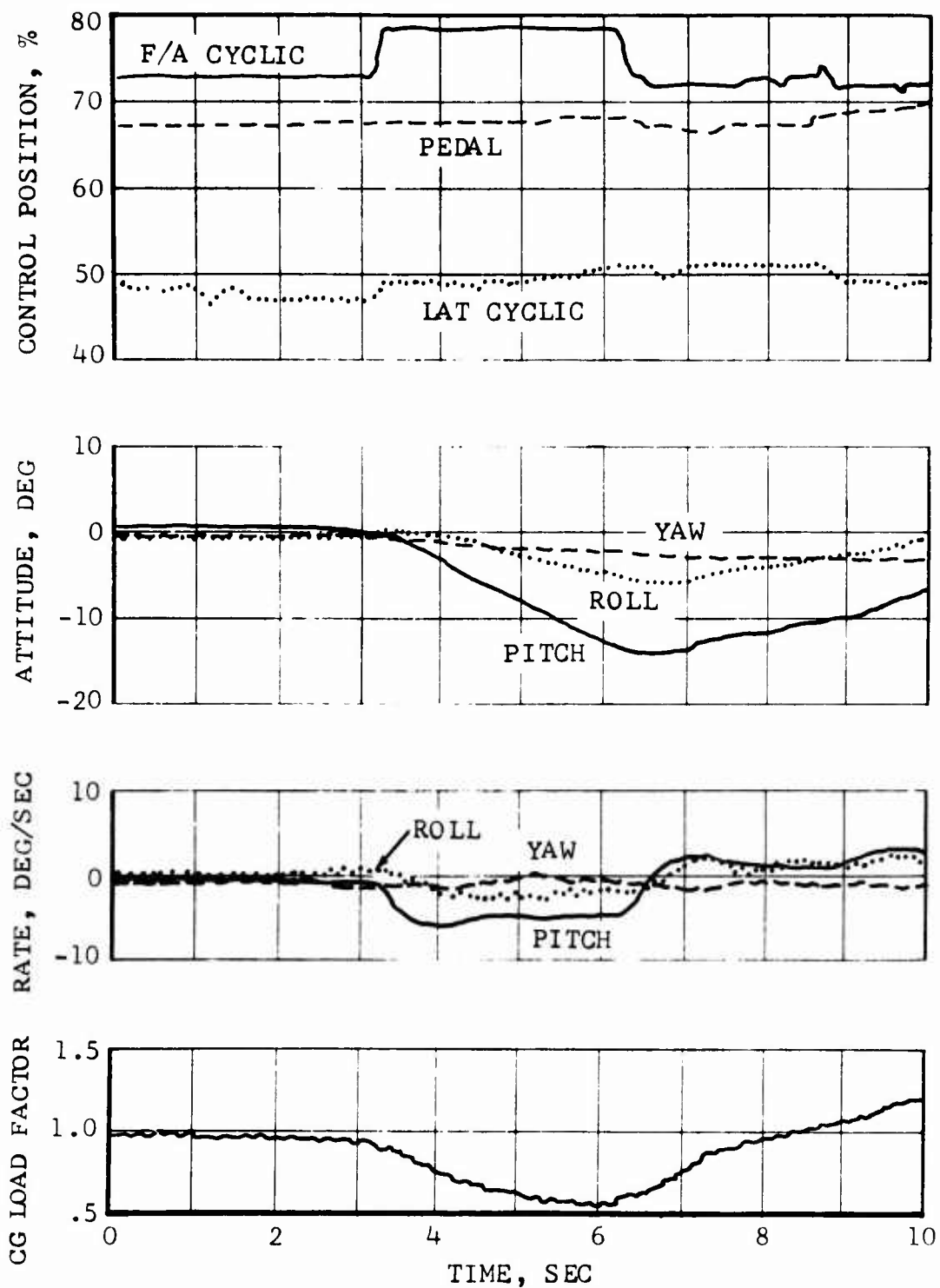


Figure 26. Longitudinal Cyclic Step at 100 Knots, Flight Test Data, 12,000 Pounds GW, Aft CG.

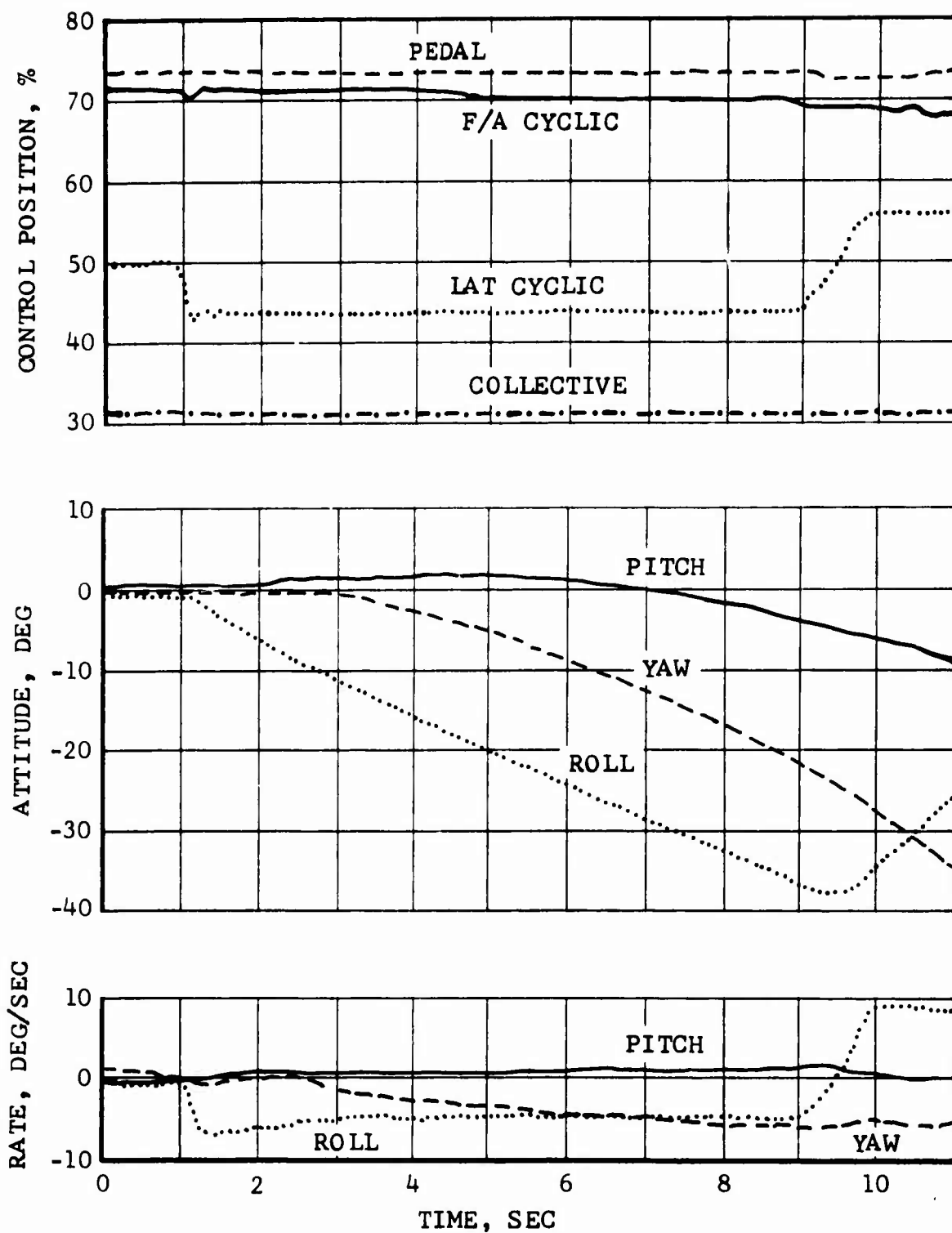


Figure 27. Lateral Cyclic Step at 100 Knots, Flight Test Data, 12,000 Pounds GW, Aft CG.

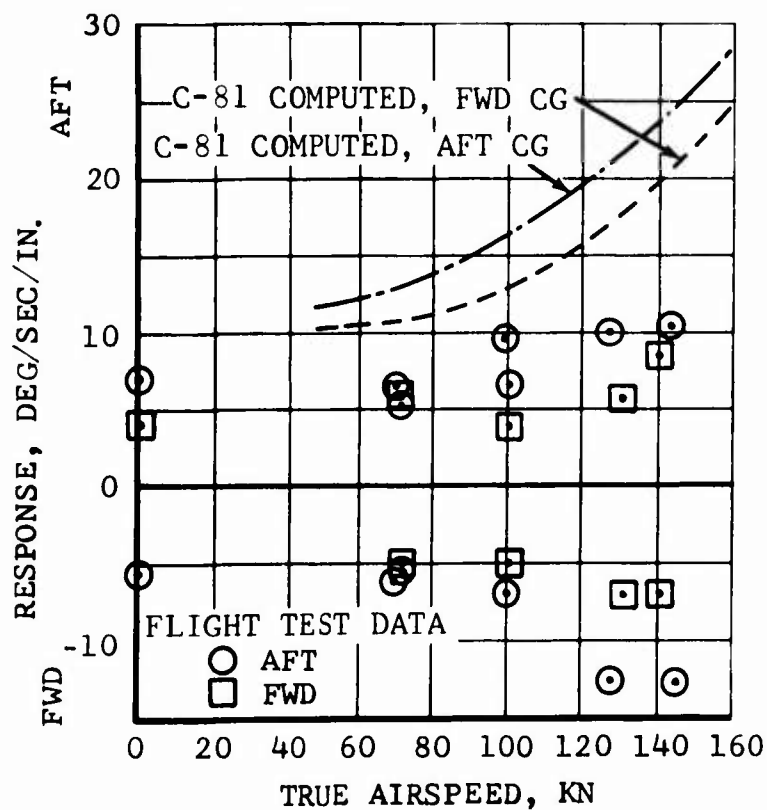
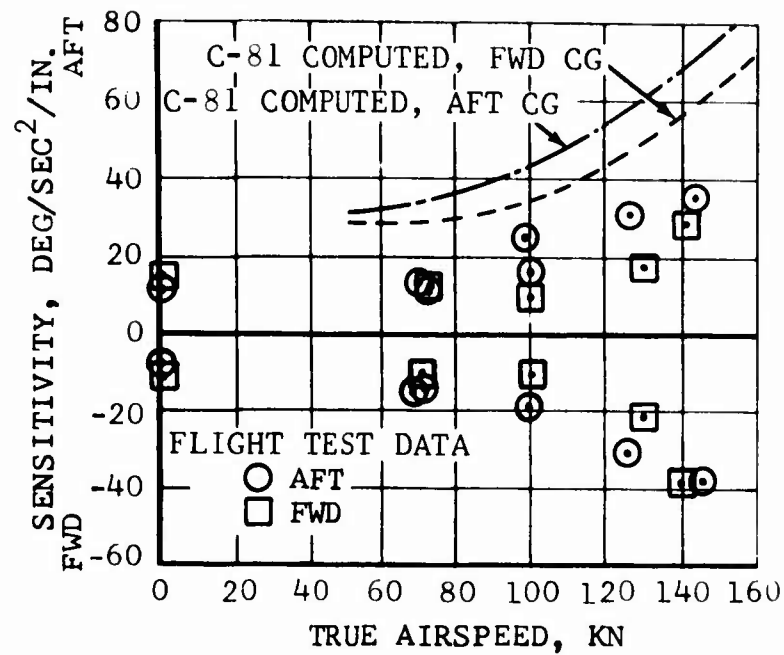


Figure 28. Measured and Computed Longitudinal Cyclic Control Characteristics.

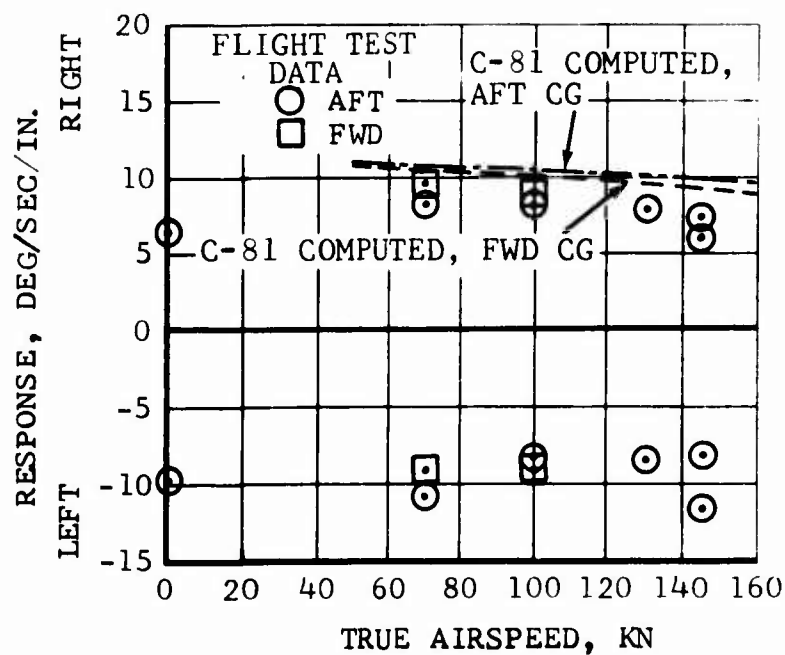
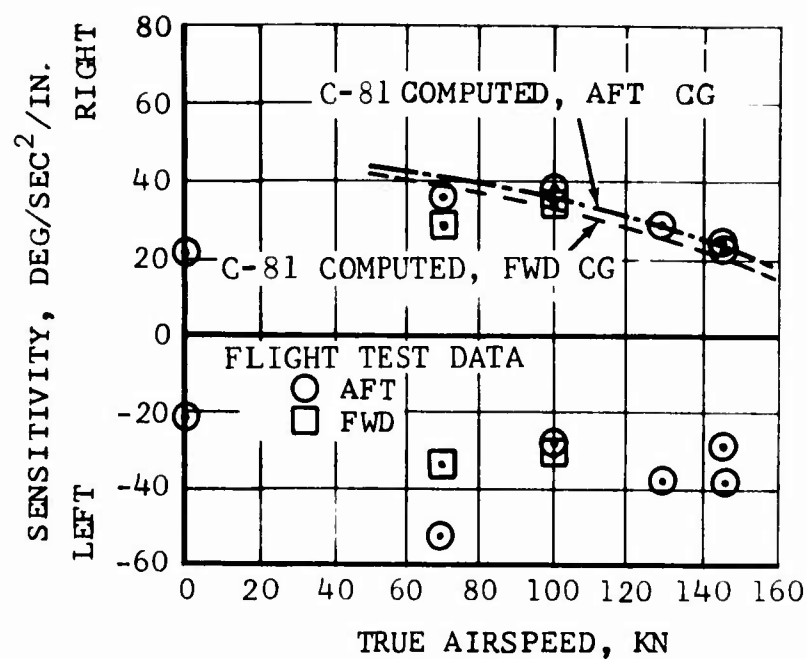


Figure 29. Measured and Computed Lateral Cyclic Control Characteristics.

therefore, the difference between the response to a left step and that to a right step is greatest at high speed.

This effect also applies to longitudinal steps and generates left roll with forward steps (Figure 26) and right roll with aft steps. Motions in this plane, however, have no mechanism similar to the rotor angle-of-attack change described above to magnify this effect.

2. Longitudinal Control

Control sensitivity in the test helicopter increases with airspeed, and at 150 knots it is approximately four times its value at hover. This increase is primarily due to the horizontal stabilizer, which is geared to move with the longitudinal cyclic stick as shown in Figure 83. This gearing provides adequate control margins and reduces rotor flapping loads in maneuvers. At high speed, the stick is forward--in the region where elevator incidence changes significantly with stick displacement. This, combined with the high dynamic pressure, acts to markedly increase the pitching moment contribution of the elevator. This acts with the increased moment response of the rigid hub with speed to produce the high control sensitivity seen in the flight test data. At high forward speeds, step inputs had to be limited to one-quarter inch.

The force feel system (described in Appendix I) increases the cyclic force-feel gradient with airspeed, thereby avoiding excessive control responses at high speed. Longitudinal cyclic stick inputs were normally applied by means of the beeper trim system at high forward speeds, giving a slower trim rate.

Longitudinal control response also increases with speed, as does pitch damping. The latter tendency is countered by increasing pitch control sensitivity to make the response at high speed approximately twice that in the hover.

Control Sensitivity and Response Estimation

Longitudinal and lateral control sensitivity and response predictions agree with flight-test trends, although the magnitudes of longitudinal response and sensitivity are

overestimated (Figure 28). The washout of control inputs noted previously is not modeled in the computer; therefore, the computer predicts higher control sensitivities than were actually measured. This difference is accentuated when both rotor and elevator contribute to the response and sensitivity about the pitch axis.

Maneuverability

Maneuverability was investigated for the test helicopter at a gross weight of 12,000 pounds with the center of gravity in the forward and aft locations, and at a gross weight of 14,000 pounds with the center of gravity at its mid location. The purpose of these tests was primarily to define the maximum maneuverability of the helicopter for these loading conditions throughout the forward flight speed range.

A series of left and right turns was performed at constant airspeed to define the variations of normal acceleration with longitudinal cyclic stick position. The results are shown in Figure 30 for two airspeeds and two center-of-gravity locations. Aft stick motion is required for increasing load factor at all conditions tested, but the gradient is lower when the center of gravity is aft.

The pilot reported a tendency for the main rotor to "dig in" (the load factor increases when the cyclic stick is held fixed after a step input) during maneuvers at positive load factors with the center of gravity aft. This tendency was not present when the center of gravity was forward. High-speed flight with the center of gravity aft produces a low gradient of stick position with load factor. This combines with high longitudinal control power to make the helicopter very sensitive in pitch. Although the "digging in" phenomenon did not show up on flight records, the high pitch sensitivity could give the pilot cues which would convince him that the phenomenon was present. This condition did not receive a thorough computer investigation because it was not possible to model the helicopter precisely under these maneuvering conditions.

Figure 31 shows the record of a symmetrical pullup and pushover flown during the flight tests. Entry speed was 148 knots, with the aircraft at a gross weight of 12,000 pounds and its center of gravity aft. At this speed, small control inputs resulted in over 1.7G. A right roll tendency was countered with a small amount of left cyclic stick to hold a level roll attitude. (Rotor load variation will be considered later.)

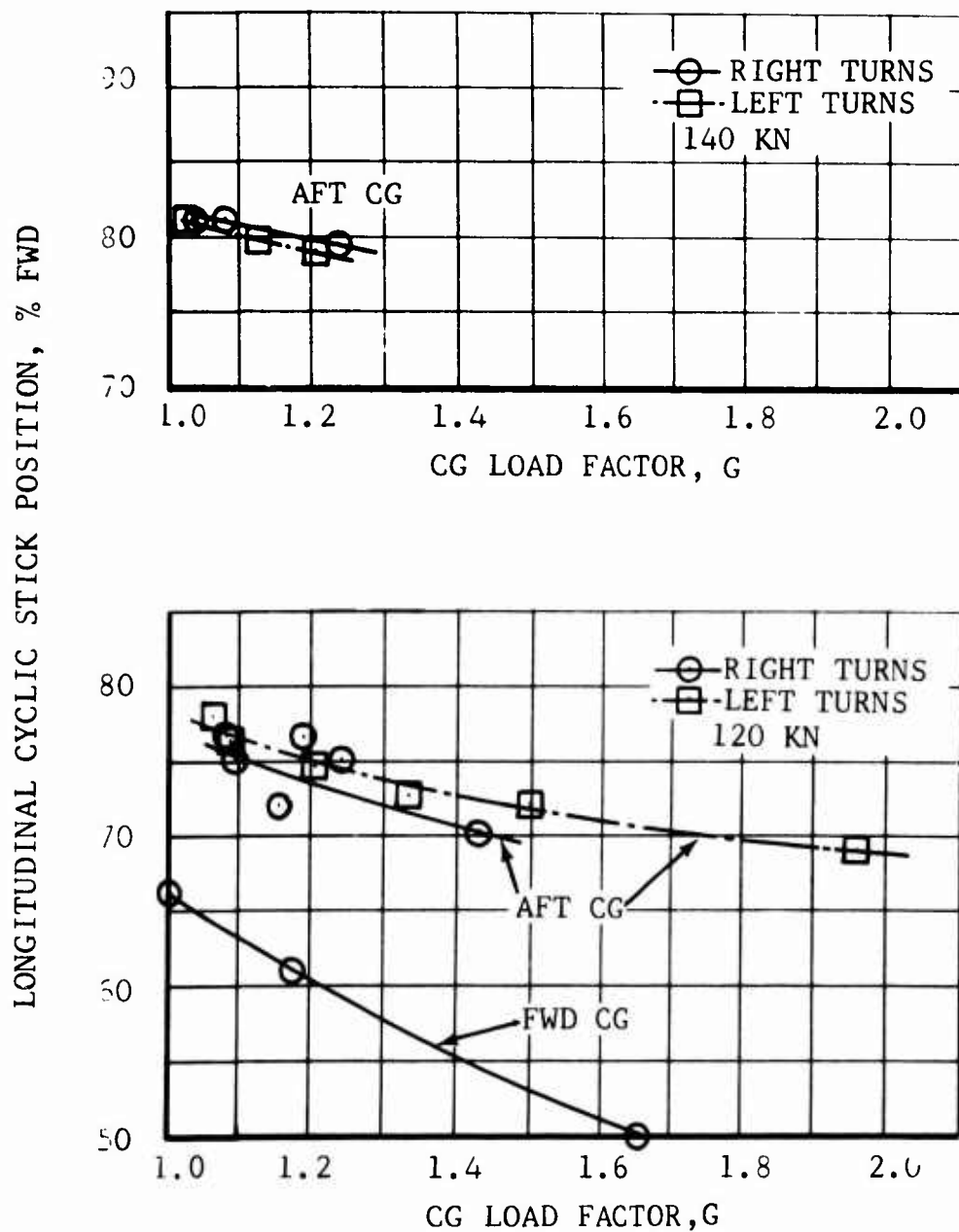


Figure 30. Longitudinal Cyclic Stick Position Variation With Normal Acceleration, Flight Test Data, 12,000 Pounds GW.

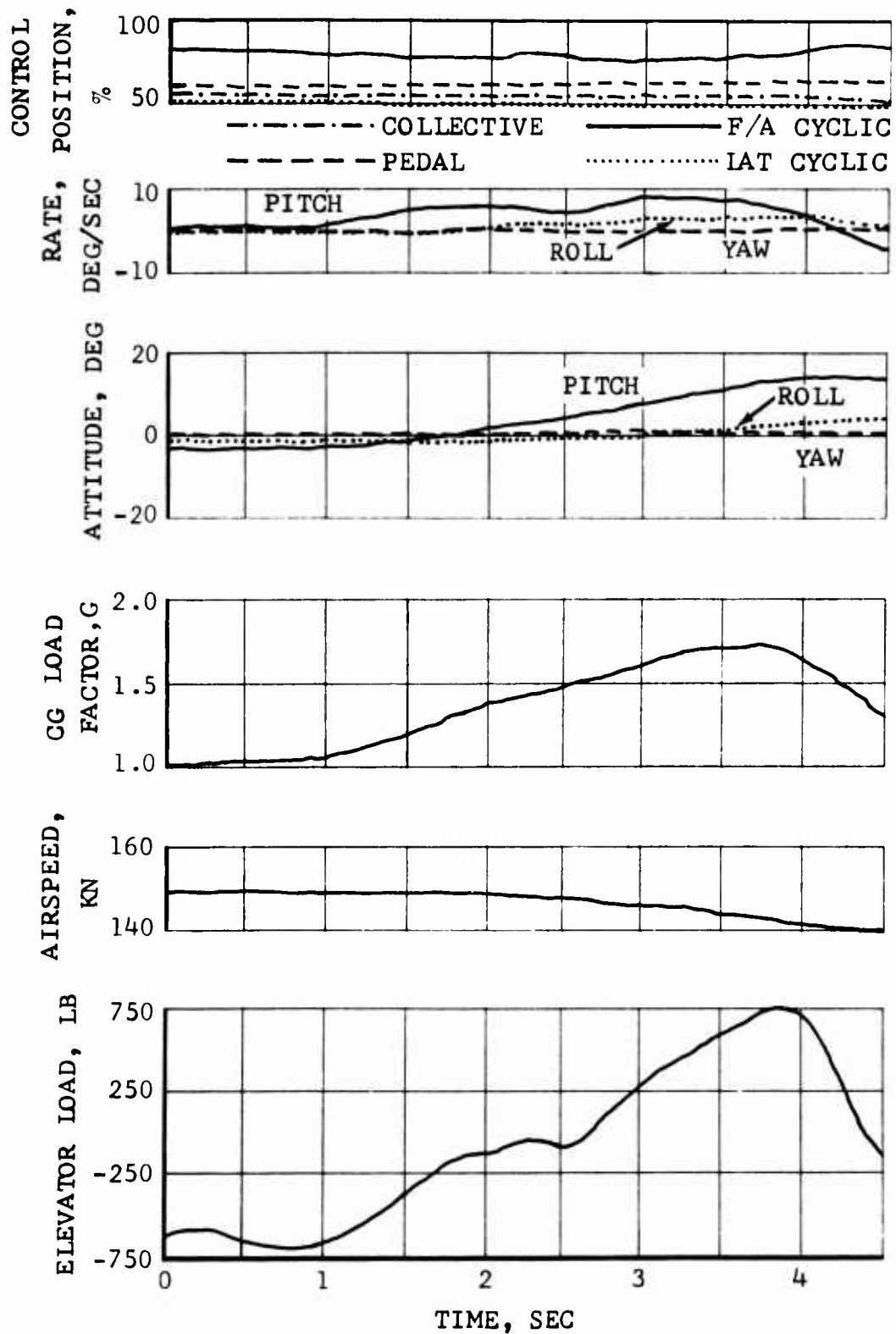


Figure 31. Symmetric Pullup and Pushover, Flight Test Data, 12,000 Pounds GW, Aft CG.

This maneuver was simulated on the computer for comparison with flight test results. A series of control inputs devised for the simulation matched normal load factor and fuselage attitudes. This simulation is compared with the test results in Figure 32. Control motions required to duplicate this maneuver were smaller than those recorded in flight. This is attributed primarily to control washout mentioned earlier in the discussion of control response.

FORCE-FEEL SYSTEM

The test helicopter had a force-feel system which incorporated a trim feature. The system furnished longitudinal and lateral cyclic stick force gradients which increased with forward airspeed. The force gradient counteracted the increasing sensitivity of the cyclic controls with increasing speed. It was variable between 1-1/2 and 7 pounds per inch longitudinally and between 1/2 and 4-1/2 pounds per inch laterally. The pilot could select different gradients as shown in Figure 86, Appendix I.

The cyclic stick trim rate varied automatically with airspeed--from 1.2 inches per second in hover to 0.2 inch per second at high speed. This gives the pilot fast control response for precise hovering and protection against overcontrolling at high speeds. The pilot used this trim to perform normal flight tasks, such as turns and changes in airspeed or altitude.

The flight tests also included a limited evaluation of a longitudinal stick force gradient which increased with pitch rate. Increased gradient due to pitch rate was detectable in forward flight, but the force applied at the stick was limited to a maximum of 10 pounds, and this proved to be too low to warn the pilot of potentially dangerous maneuvering loads. The system would probably be a useful warning device if the stick forces developed were higher.

STABILITY AND CONTROL AUGMENTATION SYSTEM (SCAS)

Although the basic test helicopter was not considered excessively hard to fly, the gust sensitivity and control power of the hingeless main rotor demanded a relatively high level of pilot proficiency and attention. The SCAS reduced pilot work load, and was especially helpful during IGE maneuvering and cruise flight in rough air. It was also helpful in alleviating the right rolling tendency noted in transition from hover to forward flight. (Approximately 75 percent of the required left cyclic stick correction was applied by the SCAS unit.) The three-axis SCAS installed in the test vehicle had been used previously with other two- and four-bladed experimental main rotors and was found to work well during the Model 609 rotor program without modification.

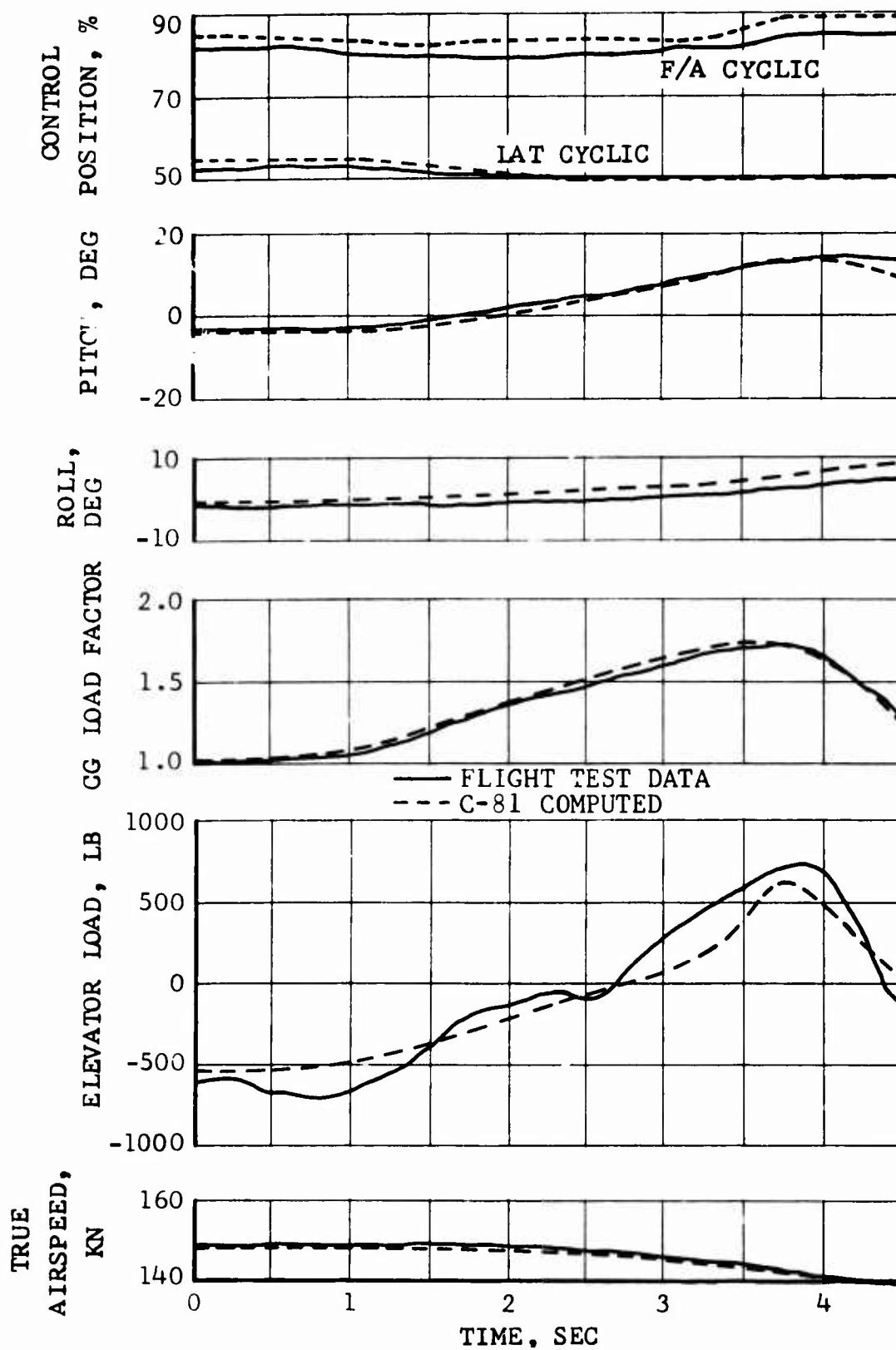


Figure 32. Measured and Computed Maneuver Comparison, 12,000 Pounds GW, Aft CG.

ROTOR LOADS IN LEVEL FLIGHT AND MANEUVERS - RESULTS AND DISCUSSION

LEVEL-FLIGHT AND MANEUVER ENVELOPE

The maneuver envelope investigated during the evaluation is presented in Figure 33. This figure presents load factors and delineates the types of maneuvers flown at each gross weight. The level-flight and maneuver envelope is presented nondimensionally in terms of rotor thrust coefficients in Figure 34. The high-speed, high "G" maneuvers were used to define the maneuver envelope in Figure 34. The maneuver rotor thrust coefficients are calculated from the measured airspeed and main rotor rpm at the instant of maximum or minimum G. Also shown for comparison are the maximum maneuver thrust coefficients achieved in an earlier investigation of two- and four-bladed rotors on the Bell High Performance Helicopter (HPH).

LEVEL FLIGHT

Measured level-flight rotor loads are functions of thrust coefficient and advance ratio. For example, the lines of constant chordwise oscillatory moments shown in Figure 35 for the critical blade station (94.0) plot in an orderly manner. This map was constructed from 280-rpm level-flight data for the three gross weights flown (inset Figure 35).

MANEUVER FLIGHT

The orderly plots of loads generated during level flight suggest that simple extrapolation would predict loads during maneuvers, but a comparison (Figure 36) of peak loads encountered during maneuvers with the level-flight loads shown in Figure 35 makes it apparent that simple extrapolation will not work. Consistency even seems to be lacking within the maneuver data themselves. For example, in the level V_L turn at the 14,000-pound gross weight, loads were much higher than at comparable rotor lift coefficients in other maneuvers.

Since most maneuvers were transient, the nondimensional maneuver data in Figure 36 are based on the actual rpm's and airspeeds occurring when the maximum vertical load factors were developed. Maneuvers were entered at 285 rpm. Rotor speed in maneuvers did not exceed 295 rpm significantly. The figure includes level-flight data obtained at 295 rpm to show that the differences between maneuver and level-flight loads cannot be explained simply by rpm overspeeding.

The maneuver data are analyzed to quantify those factors having first-order effects on loads generated during maneuvers. Factors which can increase maneuver loads significantly in any type of rotor are (see Reference 7):

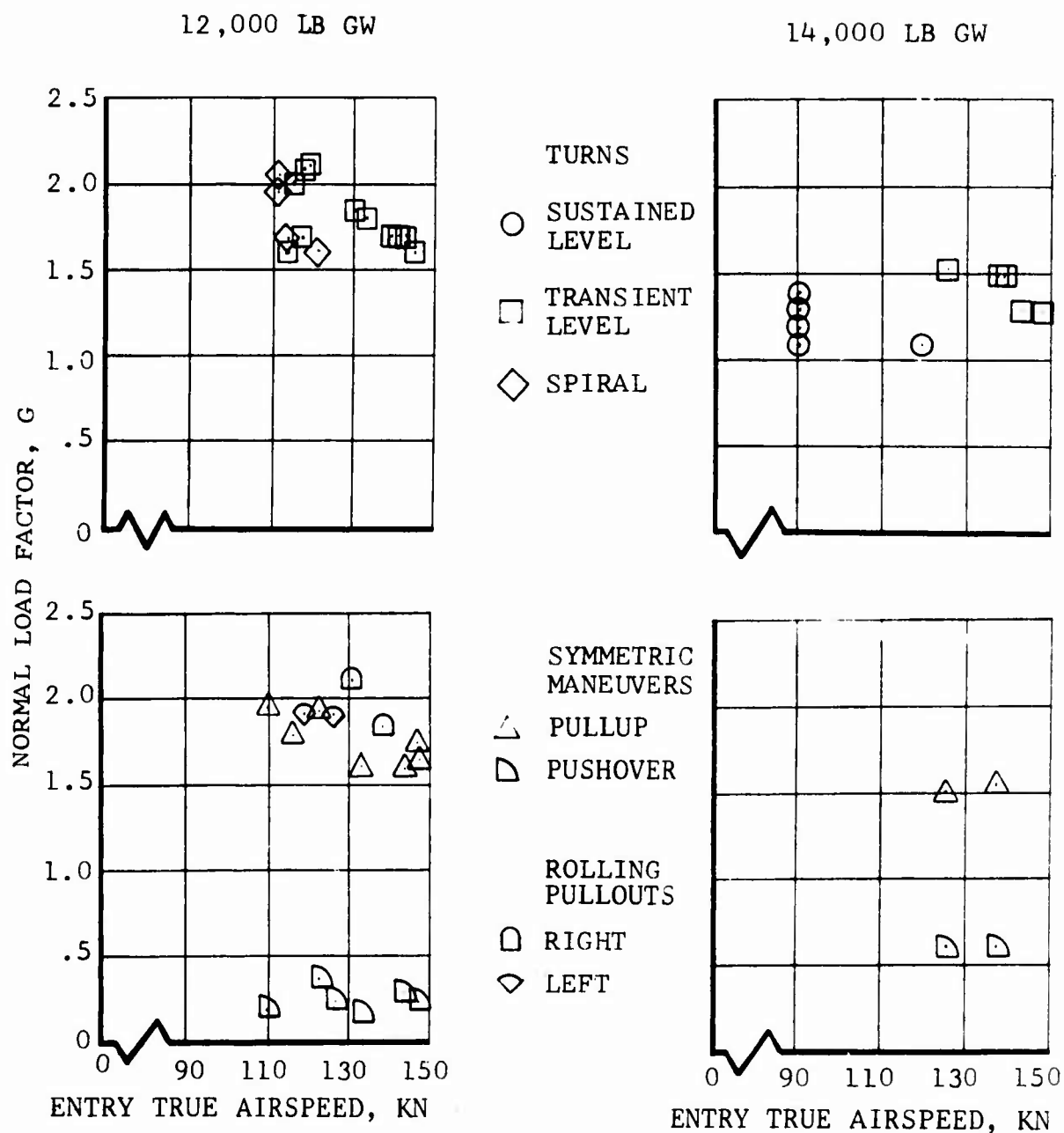


Figure 33. Maneuver Investigation Dimensional Envelope, Flight Test Data.

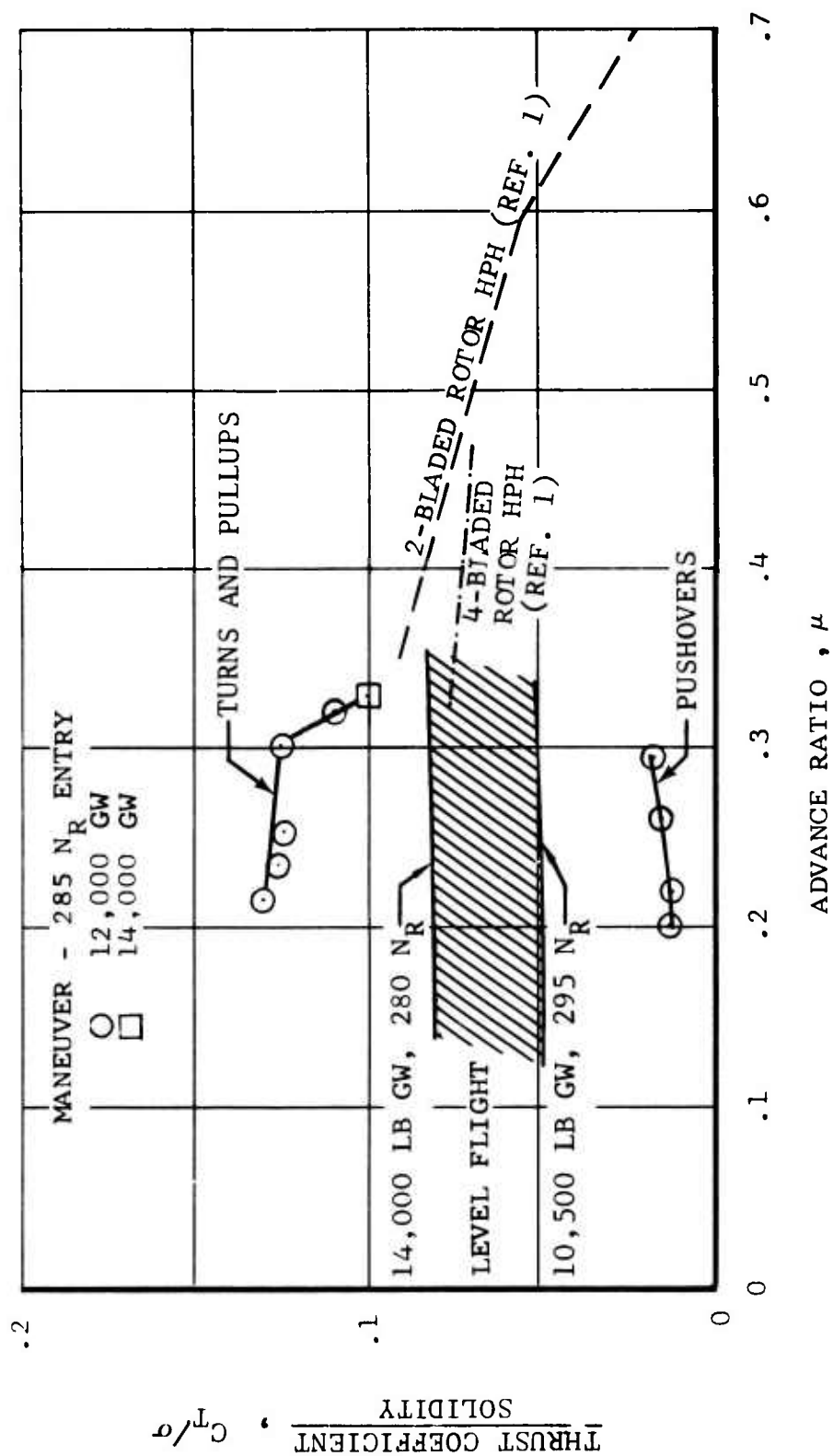


Figure 34. Nondimensional Maneuver Envelope,
Fig. Test Da'

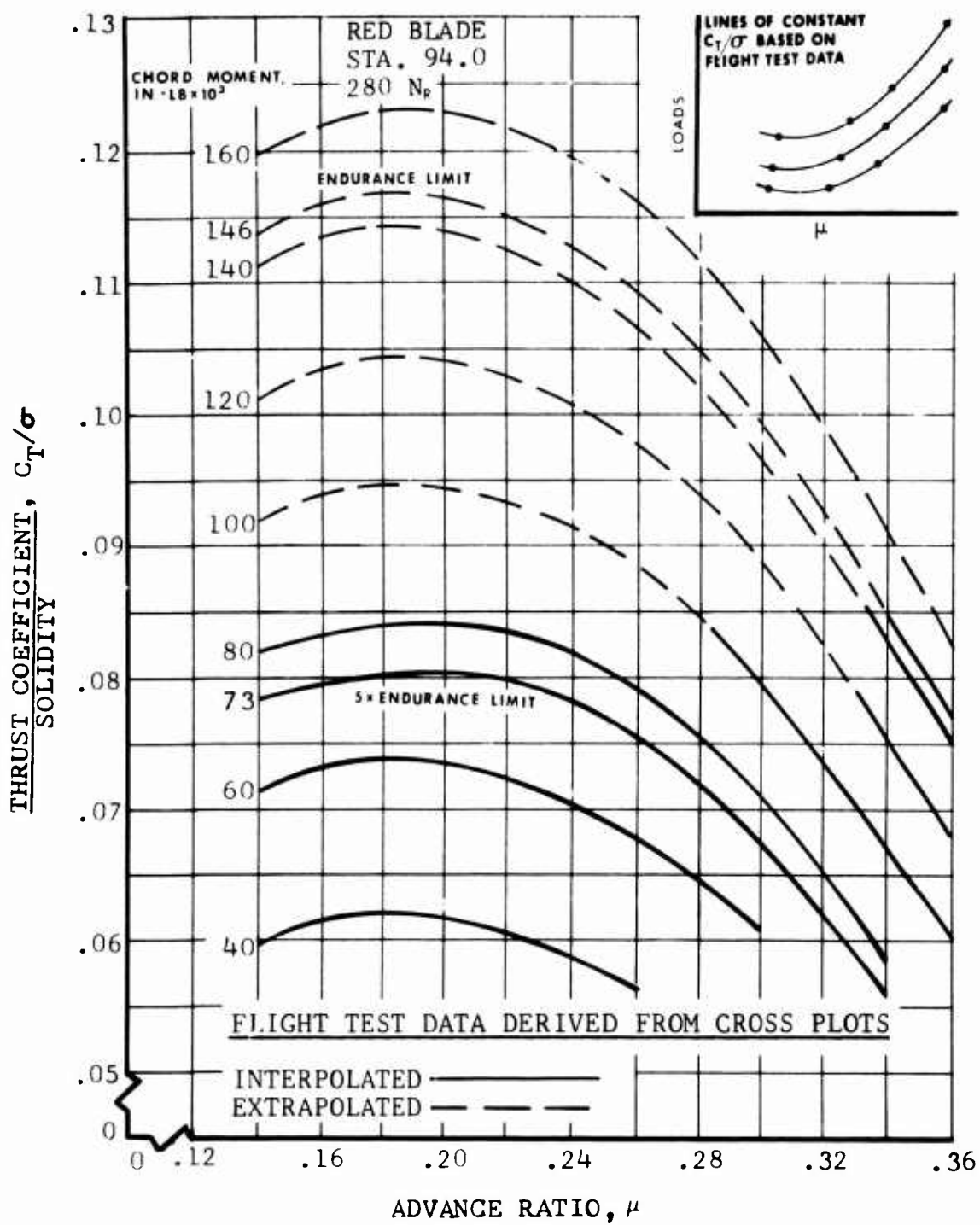


Figure 35. Constant Chordwise Moments Versus C_T/σ and μ , Flight Test Data.

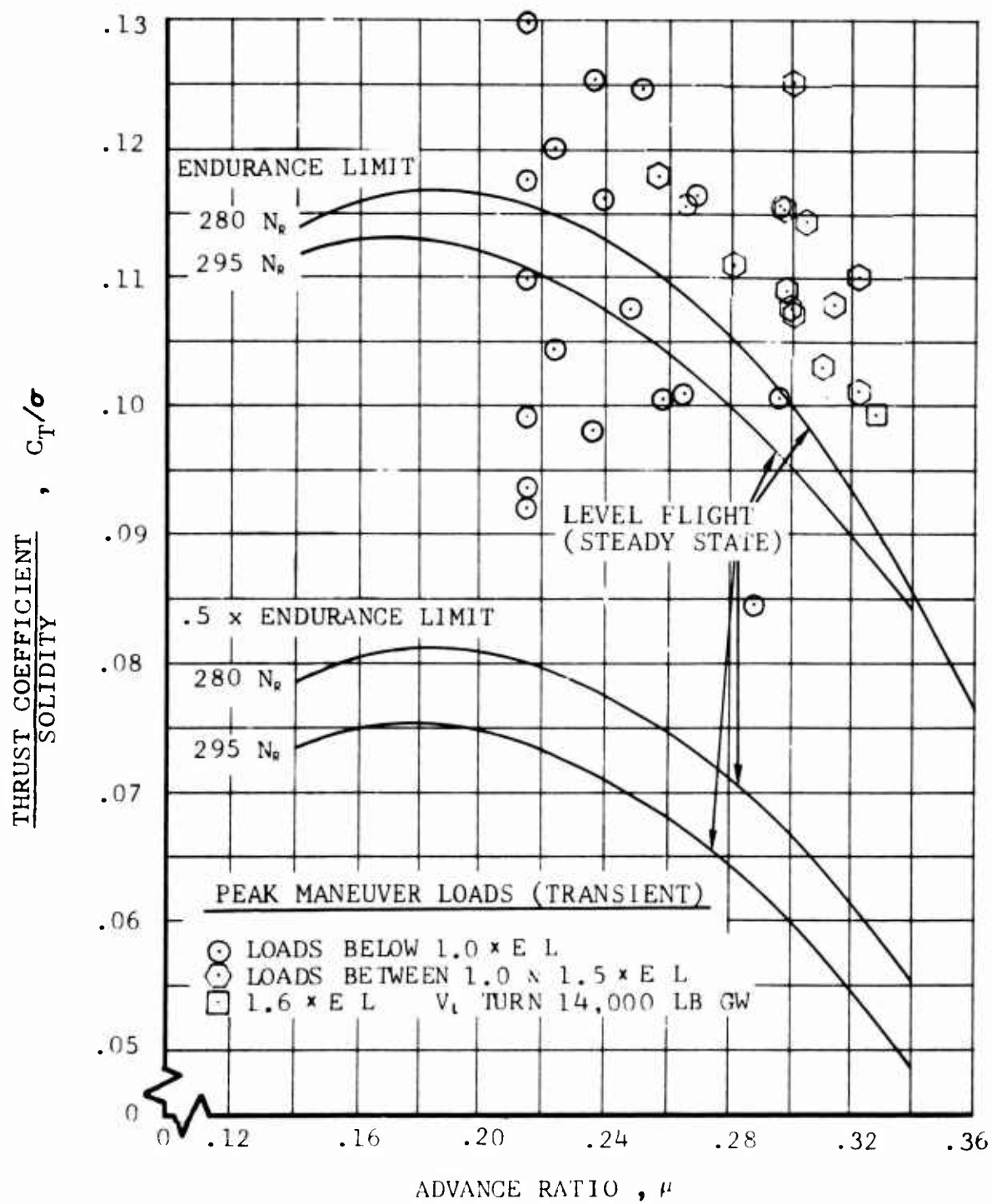


Figure 36. Comparison Between Maneuver and Level Flight Loads, Flight Test Data.

- Retreating blade stall (thrust coefficient and advance ratio)
- Rotor propulsive force
- Collective pitch (entry power)
- Rotor speed changes during maneuvers
- Pitch and roll velocities
- Rotor flapping (hub restraint)

In a hingeless rotor, flapping amplitude has a particularly strong influence on both beamwise and chordwise loads.

Collective Pitch and Advance Ratio

The aerodynamic effects of collective pitch settings at various advance ratios have been discussed in the section entitled "Performance". It was shown that the collective pitch controls the propulsive force and the rotor stall conditions. As can be seen from Figure 7, higher lifts can be obtained at the lower collective pitch angles before stall is encountered. Since oscillatory rotor loads in maneuvers are primarily stall induced, higher load factors can be achieved at similar rotor structural loads when lower collective pitch values are used for the maneuver.

Flight test values of collective blade pitch at the 0.75 radius during maneuvers are plotted in Figure 37. All maneuvers were performed with collective fixed (the rotor also had zero pitch cone coupling). The lower collective settings were for either low gross weights, low-speed entries, low-power diving pullouts, or combinations thereof. Values are plotted for the instant at which the oscillatory chord moment at Station 94 reached or passed through the endurance limit of $\pm 146,000$ inch-pounds. The plot shows the trend toward higher obtainable thrust coefficients with lower collective angles for a given oscillatory load level.

Blade loads data from wind-tunnel tests of a full-scale two-bladed semirigid rotor (previously published in part in Reference 1) are also presented in Figure 37 to show that this trend also exists in a different kind of rotor system and at higher advance ratios. This figure is a plot of the loci of rotor lift coefficients for a selected oscillatory chordwise blade moment and shows clearly the increase in lift at a given load level when lower collective settings were used. (See also Appendix II.)

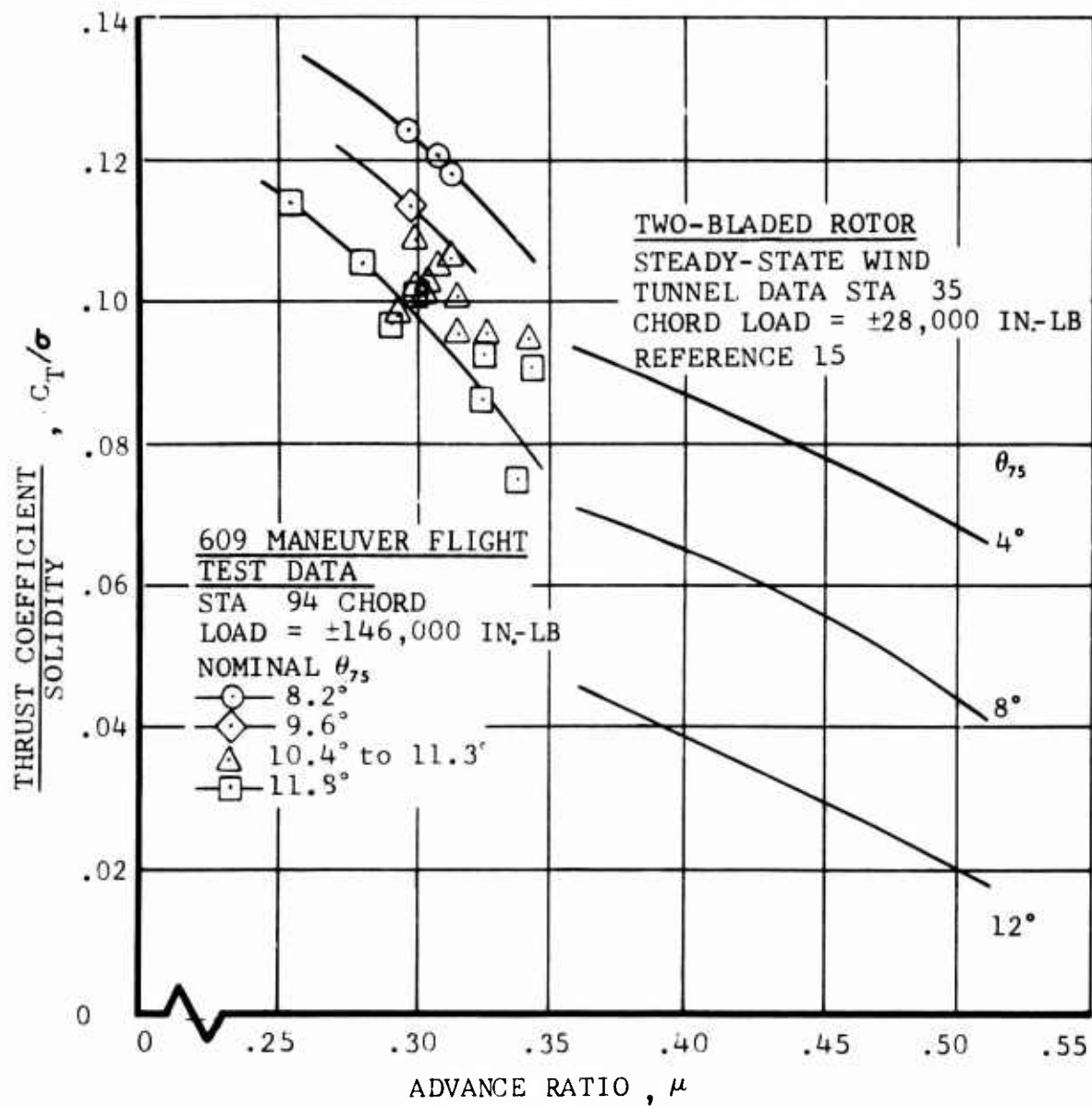


Figure 37. Maximum Nondimensional Lift (at a Constant Oscillatory Blade Moment) Versus Advance Ratio and Collective Pitch.

The collective pitch setting at entry into a maneuver is a measure of the entry power, and the severity of load generated during a maneuver can be related to this power. As shown in the "Performance - Results and Discussion" section, the collective setting also established the variation in rotor propulsive force (drag coefficient) as a function of rotor lift. Consequently, propulsive force was not examined as an independent factor.

Rotor Speed Changes During Maneuvers

The overspeed and decay characteristics of the main rotor during maneuvers are a function of the type of maneuver, how it is flown, and the response characteristics of the engine governor. Reference 8 reported significant increases in the speed of a hingeless rotor on the XH-51A during maneuvers, with the rotor frequently going into autorotation. Maneuvers with the 609 rotor were performed with the collective fixed in the middle of the pitch range. Consequently, changes in rpm were functions of only the changing rotor torque requirements and the response of the power turbine governor.

During maneuvers, the main rotor speed stayed fairly constant and never increased by more than 12 rpm. The maneuvers that generated the highest blade loads (because of stall effects) were at high speed and were either pullups where peak G occurred soon after the control inputs were made or steady turns with a sustained G level. For both these types of maneuver, the largest increase in rotor speed was only 4 rpm. Figure 38 presents the increase in rpm (normalized by the peak load factor) versus entry airspeed for the maneuvers investigated.

Pitch and Roll Velocity

Rapid roll reversals were performed to demonstrate the performance of the rotor in this type of maneuver and to determine the effects of roll accelerations and velocities on rotor loads. Measured quantities plotted in Figure 39 are for the maximum maneuver that the pilot could perform comfortably at each airspeed. High accelerations and rates were developed without exceeding the endurance limit at Blade Station 94, the critical station. In turns and rolling pullouts, rolling accelerations and velocities are of little consequence, since rolling velocities and accelerations in those maneuvers were only a fraction of those developed in the rapid roll reversals.

Pitch rates developed in maneuvers entered at high speeds were on the order of 9 to 12 degrees per second. The

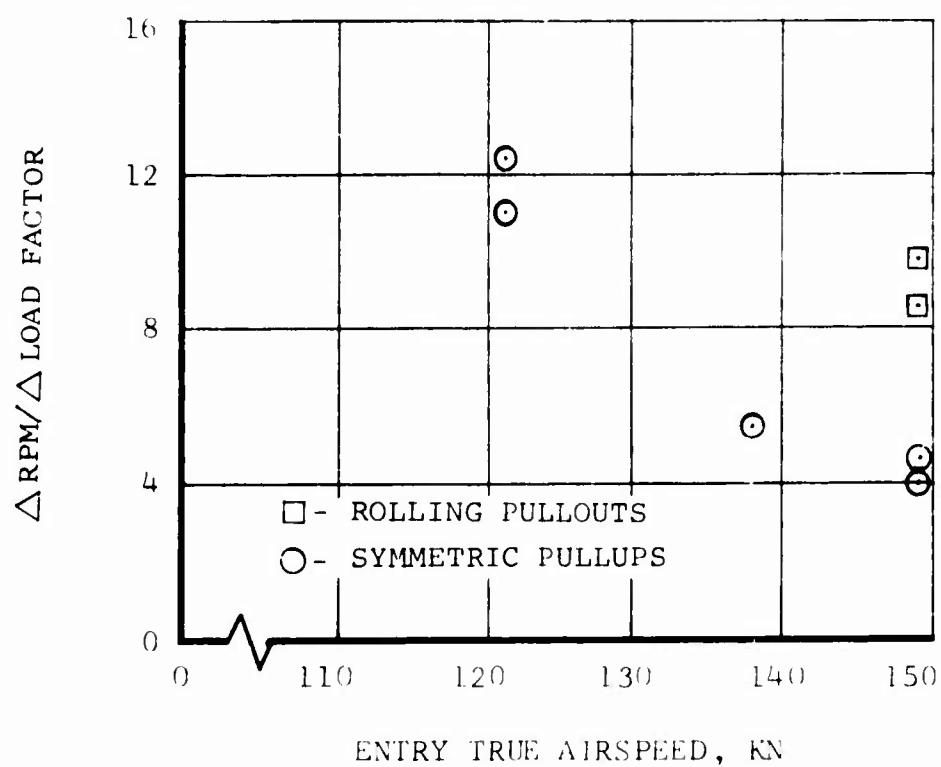
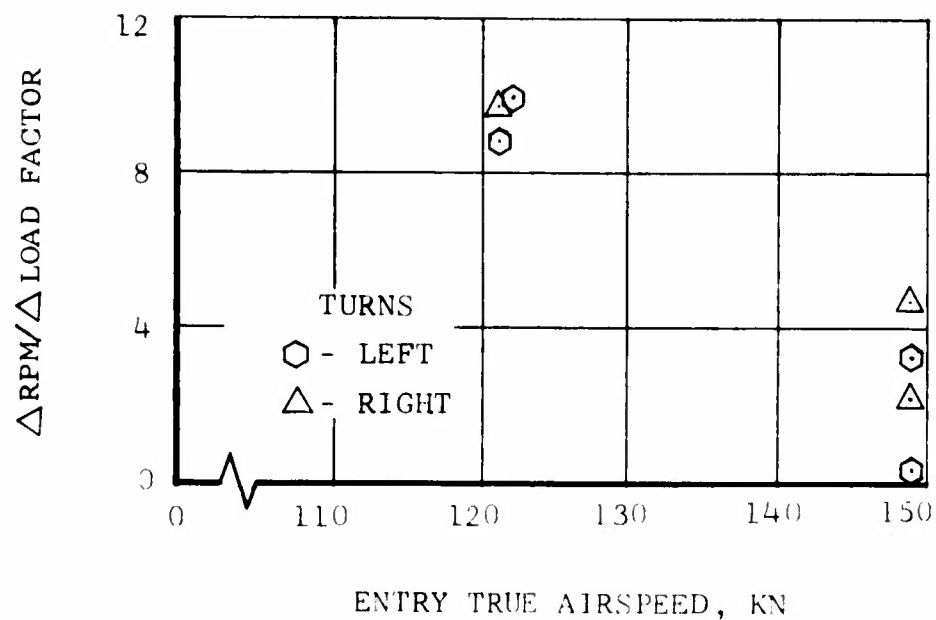


Figure 38. Main Rotor Overspeed Characteristics in Maneuvers, Flight Test Data.

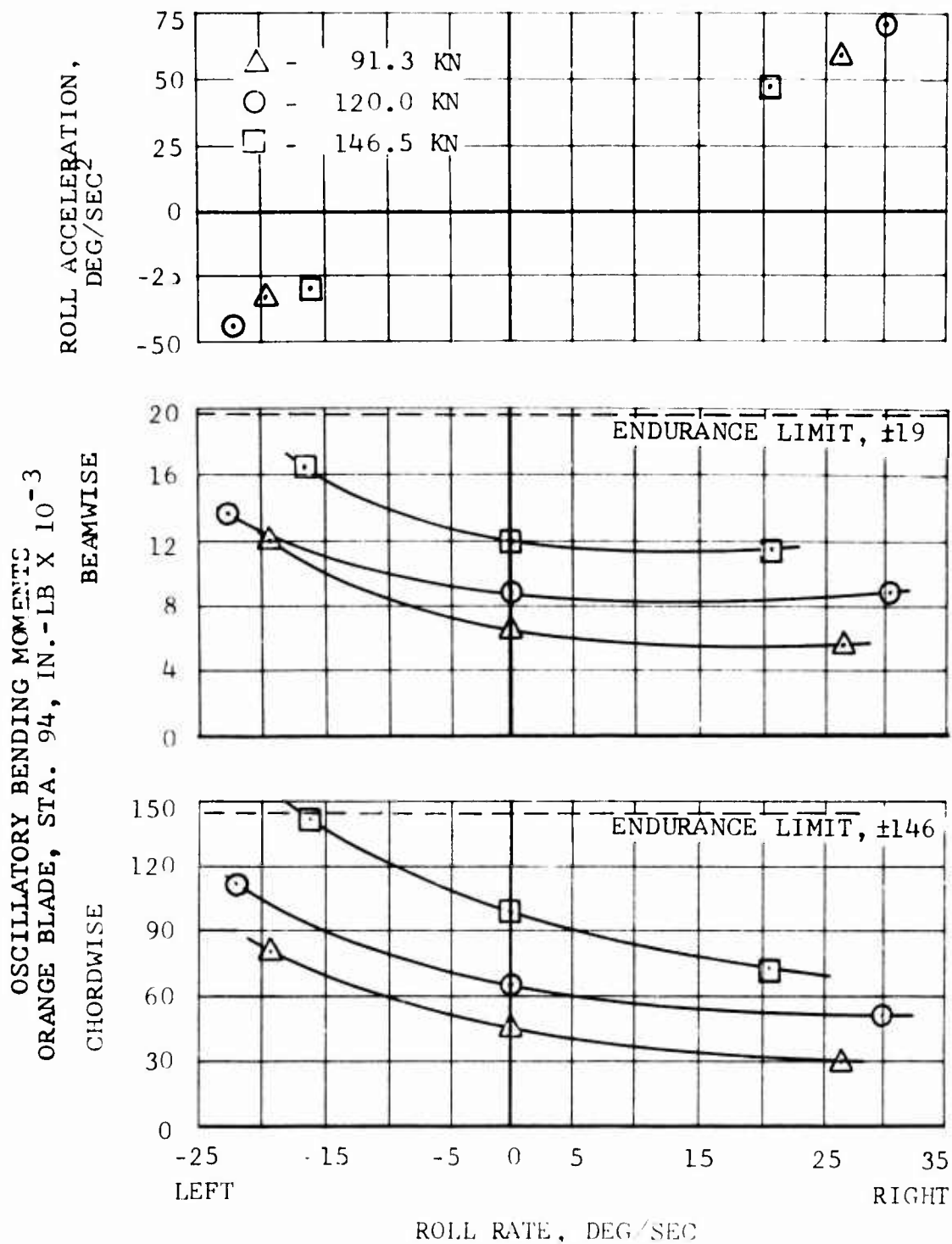


Figure 39. Rapid Roll Reversal Characteristics, Flight Test Data.

limit maneuver investigation was not designed to permit identification of pitching rate effects; therefore, these effects are not discussed here.

Rotor Flapping in Maneuvers

One-per-rev beamwise moments develop in the hub flexure in proportion to rotor flapping. (The magnitudes of beamwise moments at higher harmonics were insignificant from a stress standpoint.) One-per-rev chordwise moments develop in the blade and flexure in response to air loads and in proportion to Coriolis forces generated by rotor flapping and coning. Coning varies as a function of rotor thrust. Figure 40 presents the maximum allowable rotor flapping and thrust (coning) before the rotor endurance limits are reached (no aerodynamic excitations and assuming that no high harmonics are present). A 21,300 inch-pound moment is indicative of one degree of rotor flapping at the 3/4 blade radius station. The rotor flapping limits were determined from this flapping "spring rate."

The elevator control system was designed to minimize fore-and-aft rotor flapping in level flight, and a plot of one-per-rev beamwise moments (Figure 41) shows that the flapping was low in forward flight. In Figure 41, the measured moments have been resolved into lateral and fore-and-aft flapping components. This shows that most of the flapping was to the left, implying that the elevator control was very effective in minimizing fore-and-aft flapping.

Figure 42 shows how flapping varied in maneuvers entered at high speed. Flapping approaches the structural limits of the rotor at 12,000 pounds for the forward center-of-gravity cases and, at 14,000 pounds, for the neutral center-of-gravity case.

The highest loads encountered during the evaluation were in a 1.3-G left turn at 14,000 pounds. This maneuver was therefore selected for closer examination. The flapping contribution to loads is shown in Figure 43. This figure indicates that the elimination of flapping in maneuvers would increase maneuverability at forward and neutral centers-of-gravity. Feedback of the flapping moments to the elevator control system could be used to alleviate the flapping.

CORRELATION OF COMPUTED AND MEASURED ROTOR LOADS

Blade loads on the Model 609 rotor have been computed for comparison with loads measured in flight. The computation used

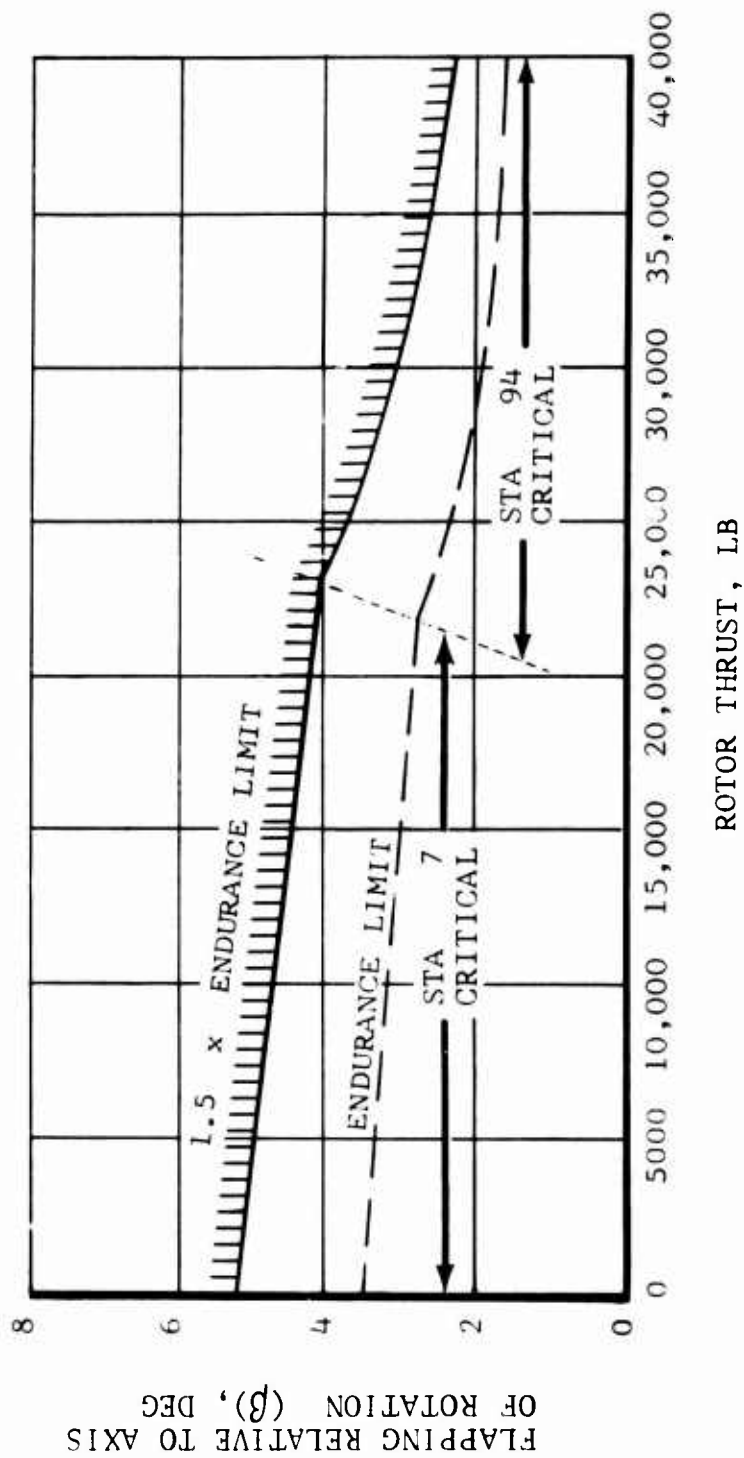


Figure 40. Flapping and Coriolis 1/Rev Limitation.

M/R RED YOKE BEAM BEND. MOM.,
STA 7.0 1/REV, IN.-LB X 10³

LATERAL FLAPPING,
DEG

F/A FLAPPING,
DEG

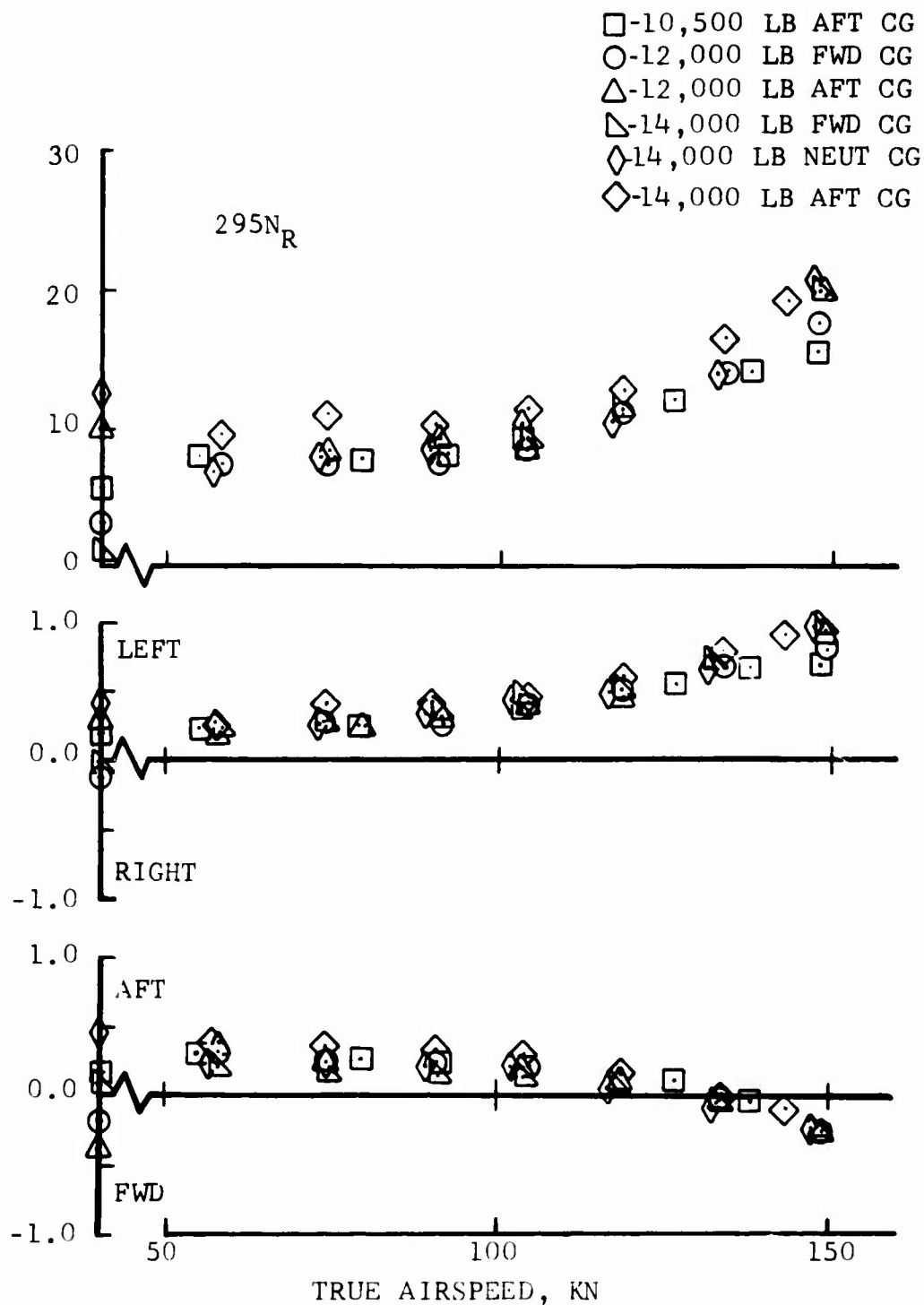


Figure 41. 1/Rev Hub Moments and Flapping Amplitudes in Level Flight, Flight Test Data.

12,000 LB AFT CG
 14,000 LB NEUTRAL CG
 12,000 LB FORWARD CG

OPEN SYMBOLS - ENTRY: FLAGGED - PEAK G

NOSE UP

6

4

ROTOR FLAPPING, DEG

2

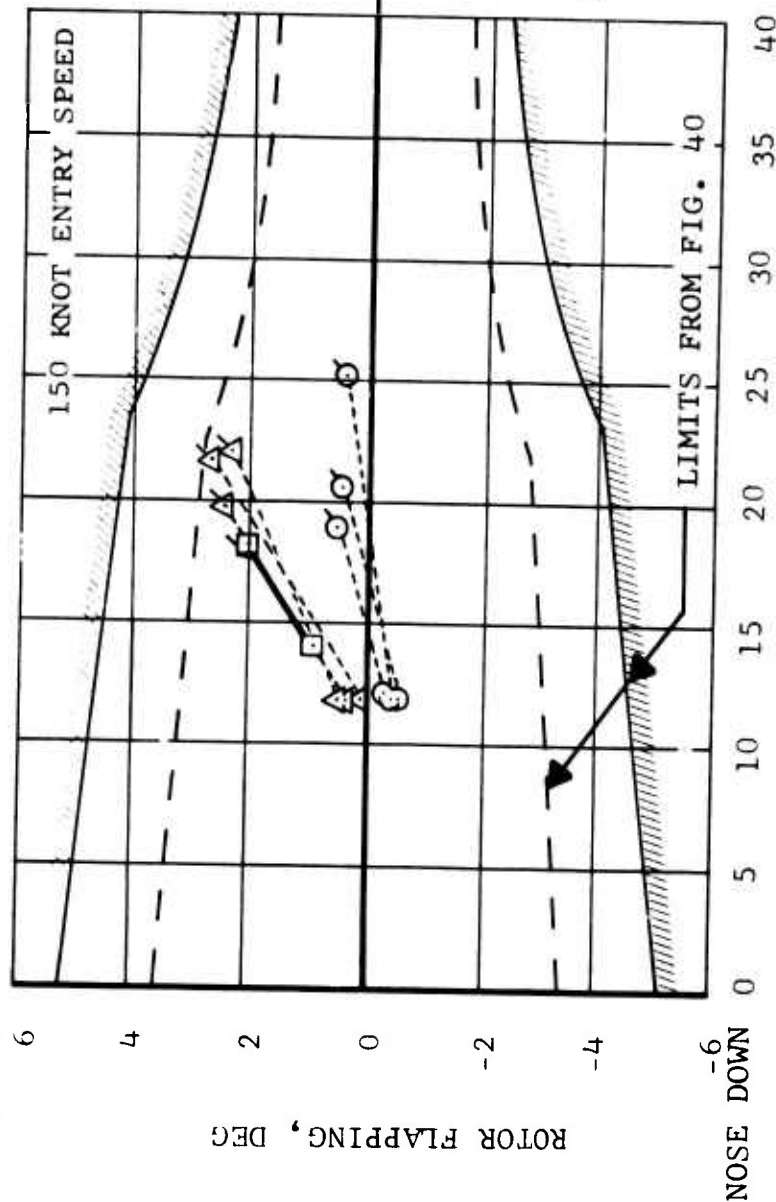
0

-2

-4

-6

NOSE DOWN



ROTOR THRUST, LB
1000

Figure 42. Flapping as a Function of Thrust During Maneuvers, Flight Test Data.

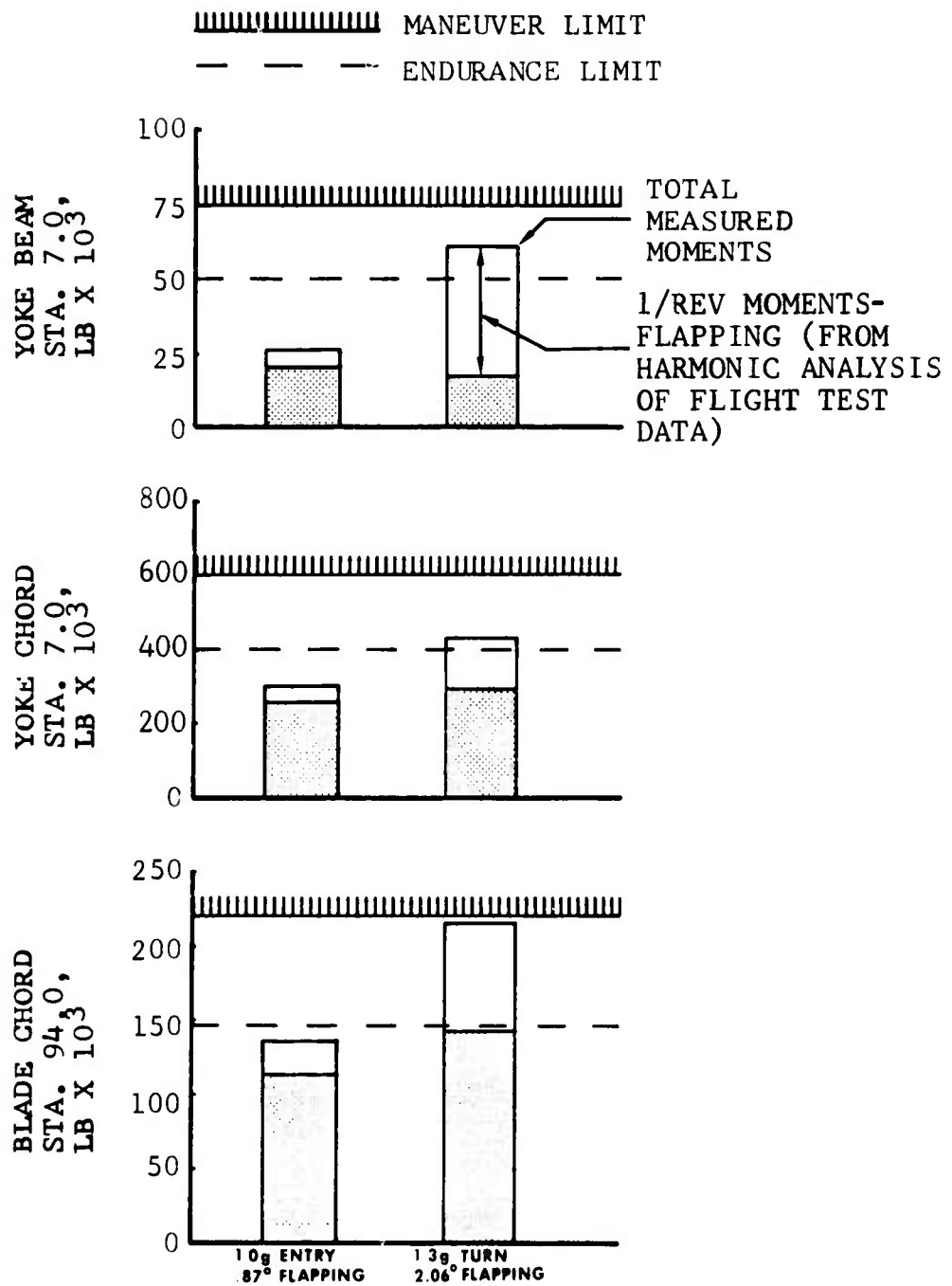


Figure 43. Flapping Contribution to Loads During a Maneuver at 14,000 Pounds GW, Flight Test Data.

the time-variant aeroelastic analysis of computer program C-81, with inputs as given in Reference 3.

Level Flight Simulation

Blade response is a function of parameters such as the control plane angle of attack, rotor resultant force, and rotor power. If computations are to predict the rotor loads accurately, these parameters must be matched in the analysis. The performance and handling qualities sections have already shown that helicopter power, thrust, pitch attitude, and control positions have been reasonably matched by the C-81 mathematical model for three gross weight level flight conditions. For these three flight conditions, the oscillatory beam bending moments at Blade Station 7 are shown in Figure 44. At airspeeds above 60 knots, the differences between measured and computed beam bending moments are primarily due to differences between calculated flapping angles and those obtained in flight. The largest discrepancies between beam moments at speeds above 60 knots could be accounted for by only 1/2 degree of flapping. The small mismatch in flapping arises from a small deviation of the trim pitch attitude due to uncertainties in the location of the fuselage aerodynamic center. In addition, the nonlinear elevator coupling with fore and aft stick could not be matched exactly, so small variations in the elevator download occurred which contributed to the pitch attitude discrepancy.

The 12,000-pound gross weight flight was a performance flight, and the speed points were very well stabilized; selected data points were harmonically analyzed. Figure 45 presents the harmonic analysis of the beam loads. At 44.7 knots, C-81 and flight test are in reasonably good agreement. At 86.9 knots, the one-per-rev component of the computed load is larger than that in flight. At 144.8 knots, the harmonic distribution of the flight test data has shifted, whereas the C-81 distribution is proportionally the same as at lower speeds. The one-per-rev discrepancy could be explained by a flapping error of only 1/2 degree, as discussed above, or a fore-and-aft cyclic stick position error of 0.37 inch. (The mismatch between measured and computed stick position has been discussed on page 43.)

At low speeds (below 60 knots), the discrepancies between the computed and measured moments in Figure 44 are due to the modeling of the induced velocity and the modeling of the elevator stall. The computed beam bending moment for the 12,000-pound flight at low speed decreases sharply due to a change in flapping induced by the representation of

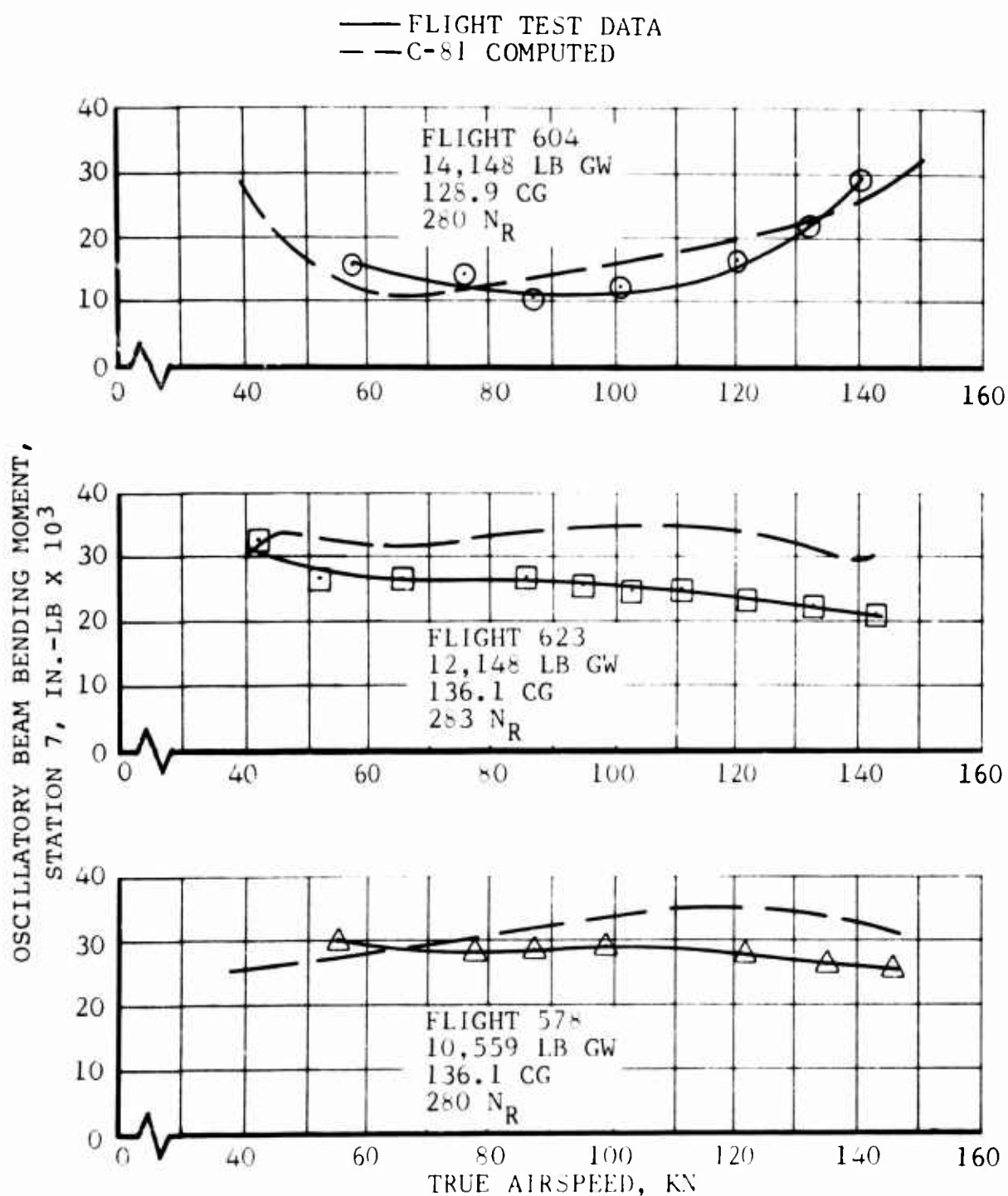


Figure 44. Measured and Computed Oscillatory Beam Bending Moment (Station 7) in Forward Flight at Three Gross Weights.

FLIGHT 623
12,148 LB GW
136.1 CG
283 N_R

○ FLIGHT TEST DATA
□ C-81 COMPUTED

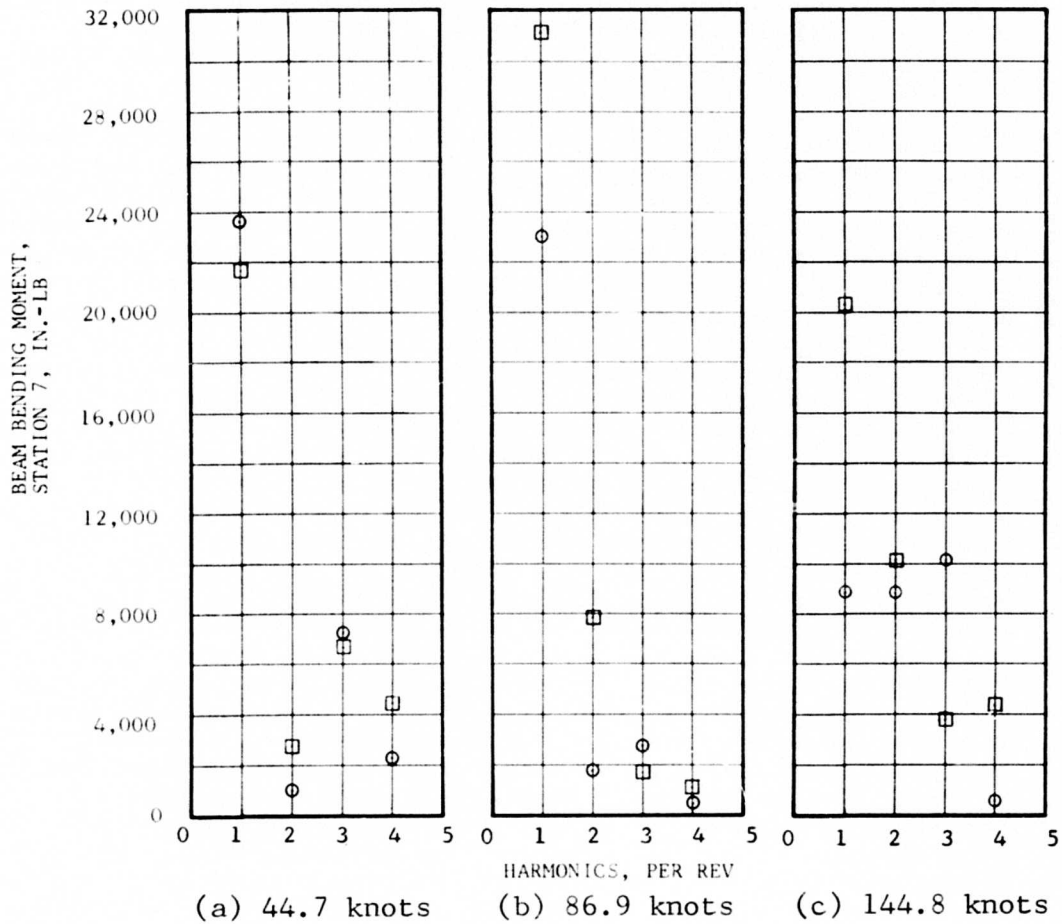


Figure 45. Measured and Computed Harmonic Analysis of Oscillatory Beam Bending Moment (Station 7) for Three Airspeeds.

elevator stall in C-81. Also, the elevator model in the program has a very sharp stall, while stall of the actual elevator is probably much less severe. An analysis of measured elevator bending moments indicates that stall occurs between 45 and 70 knots, depending upon the center of gravity and gross weight, and this is the speed range in question. The steep slope of the computed bending moment trace for the high gross weight case at 45 knots is caused by the pronounced nonlinear nature of the induced velocity model at that speed. This model, which accounts for the tip vortex and wake effects, is described in detail in Reference 9. Since the 14,000-pound gross weight flight is at neutral center of gravity (128.9), the elevator stall effects are not predominant.

A comparison of the chordwise bending moments for the three gross weights is shown in Figure 46. The measured and computed data agree quite well for the 10,500- and 12,000-pound gross weight flights. Correlation with the high gross weight case is not as good. At higher gross weights, the rotor is operating closer to stall. The differences between the measured and computed loads indicate that the airfoil model has a higher stall angle than the actual airfoil. Further support for this assumption is the fact that the helicopter operates at a lower collective pitch in C-81 than in flight. The chord moment data from the 12,000-pound flight was also harmonically analyzed and is presented in Figure 47. The overall oscillatory chordwise bending moment at Station 7 (Figure 46) shows excellent correlation between C-81 and flight test, but the harmonic contents indicate some discrepancies. The differences between the computed and measured chord loads at lower airspeeds are due to the wake and tip vortex model, as discussed in Reference 9.

The beam and chord bending moments at Blade Station 94 are given in Figure 48 for the 12,000-pound gross weight case. The correlation between computed and measured values is good, although the computed beam bending moments increase a little faster at the higher airspeed. This is due to the small flapping difference which causes the computed beam bending moment at Station 7 to be high again. The difference in the chord loads at the lower airspeeds is due to the tip vortex model (Reference 9).

Main rotor pitch link loads are shown in Figure 49. These have traditionally been difficult to predict; the C-81 results show the proper trend. The differences between the measured and calculated loads are due in part to the simplified modeling of the torsional properties of the blade and the control system. The differences are also due, in part, to the in-flight tip airfoil deformation problem (see

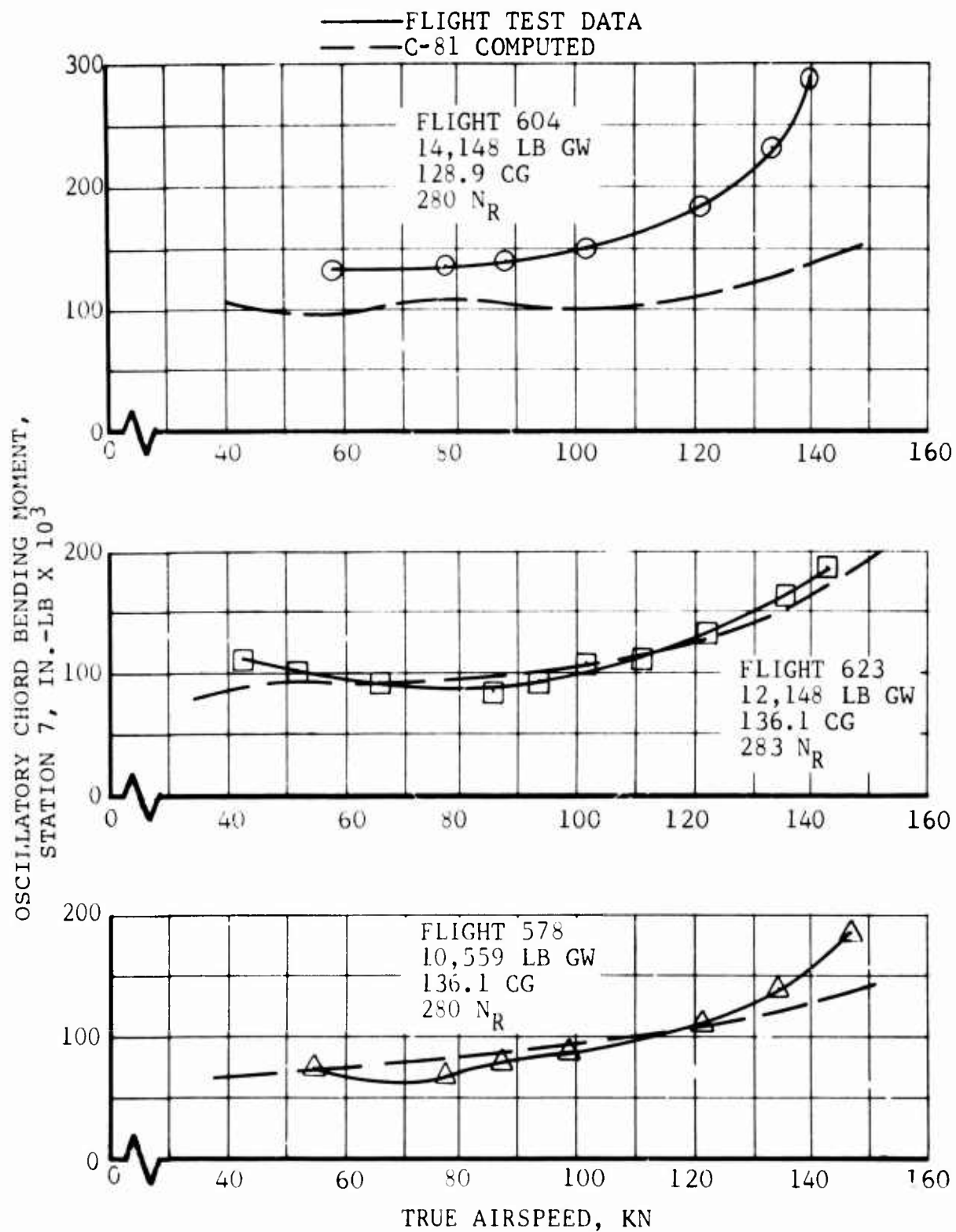


Figure 46. Measured and Computed Oscillatory Chord Bending Moment (Station 7) in Forward Flight at Three Gross Weights.

FLIGHT 623
12,148 LB GW
136.1 CG
283 N_R

○ FLIGHT TEST DATA
□ C-81 COMPUTED

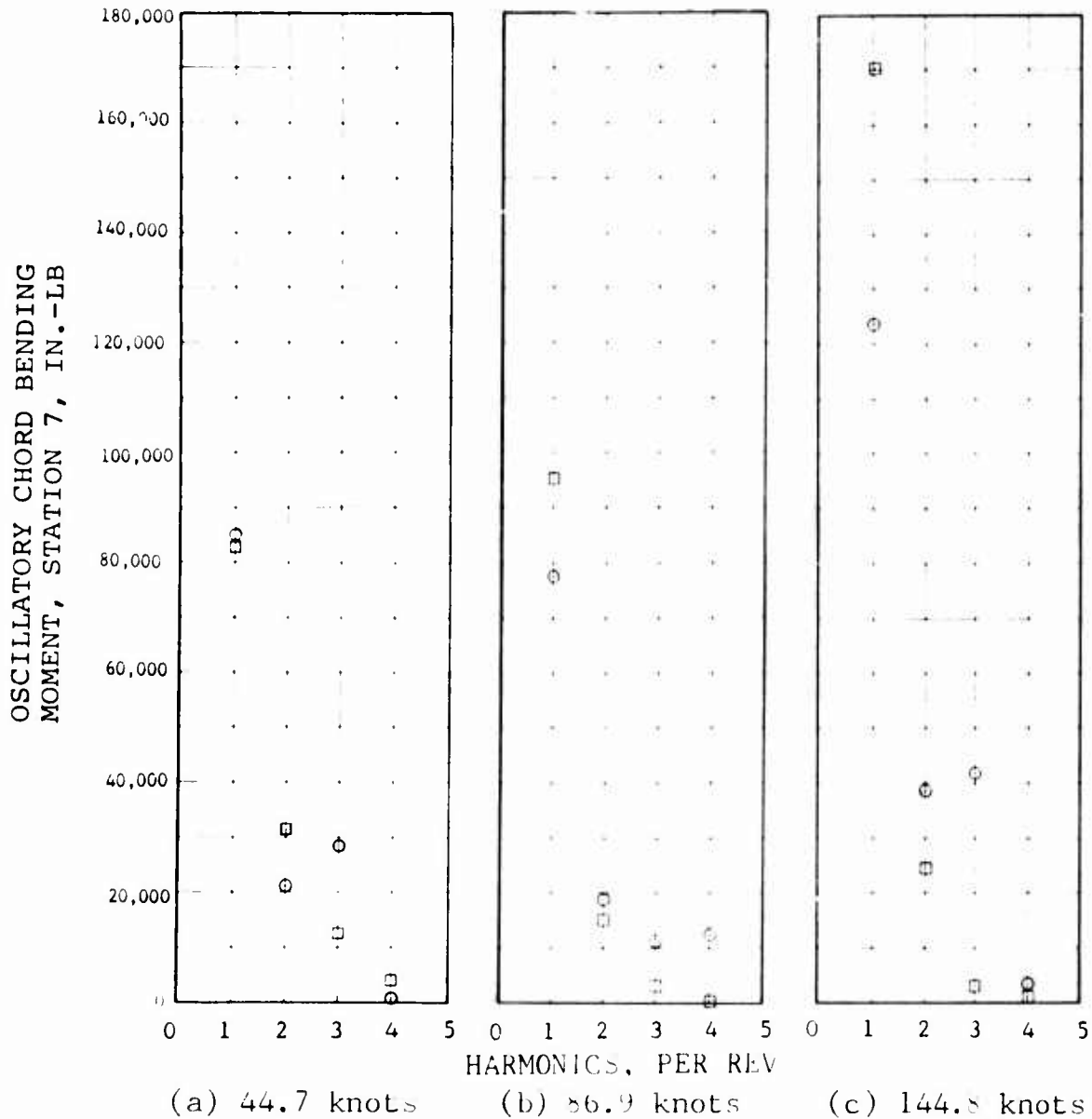
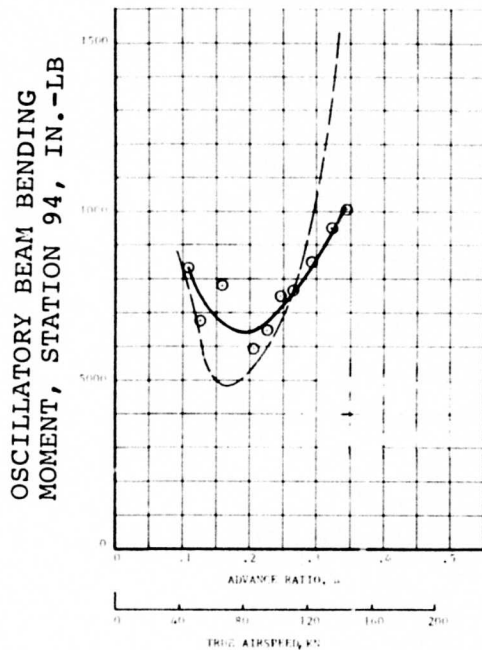


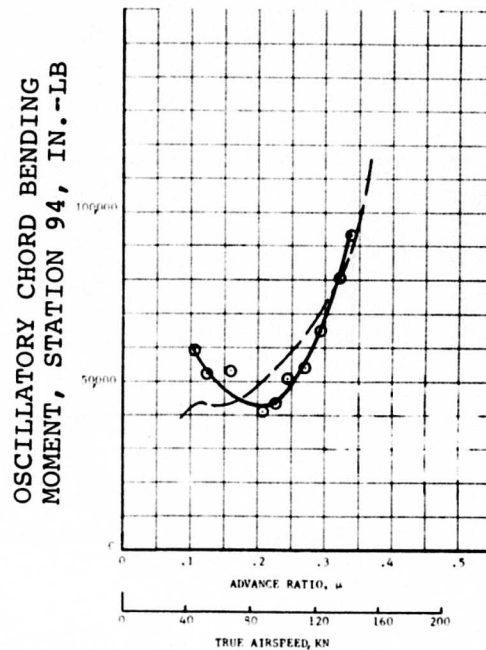
Figure 47. Measured and Computed Harmonic Analysis of Oscillatory Chord Bending Moment (Station 7) for Three Airspeeds.

FLIGHT 623
12,143 LB GW
136.1 CG
283 N_R

—○— FLIGHT TEST DATA
— — C-81 COMPUTED



a) Oscillatory Beam Bending Moment



b) Oscillatory Chord Bending Moment

Figure 48. Measured and Computed Oscillatory Beam and Chord Bending Moments (Station 94) in Forward Flight.

FLIGHT 623
 12,148 LB GW
 136.1 CG
 283 N_R

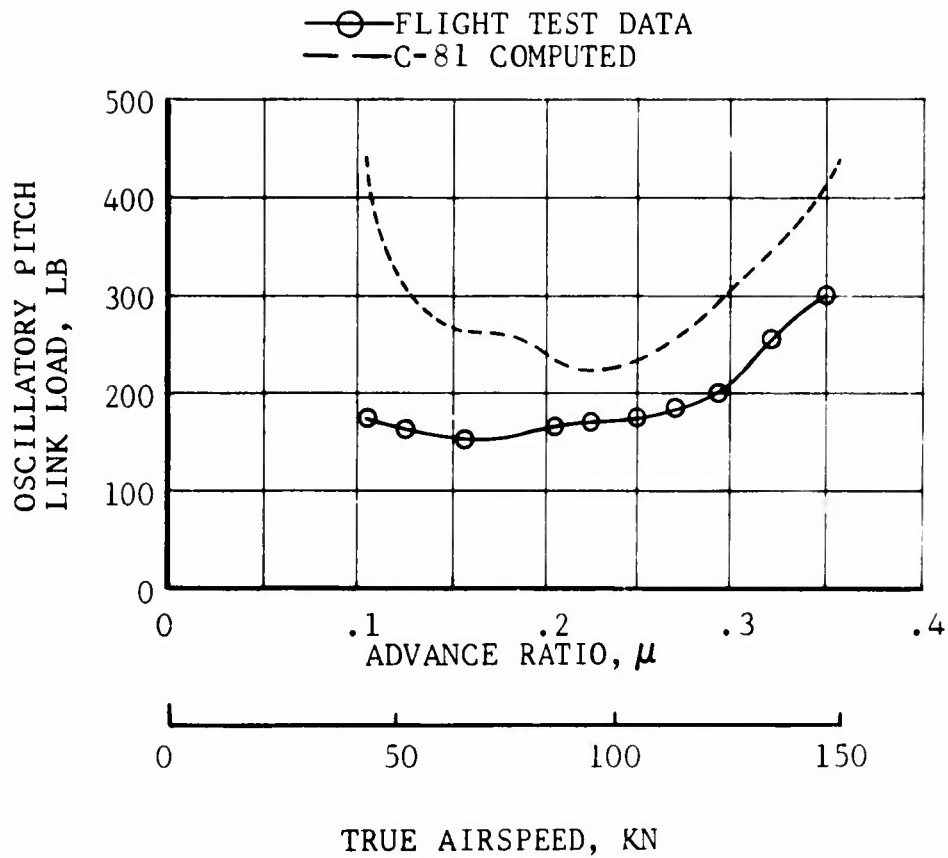


Figure 49. Measured and Computed Oscillatory Pitch Link Load in Forward Flight.

summary of technical problems) as the blade element pitching moment developed in flight would not equal the moment computed for the theoretical cross section.

Hover

Blade loads during out-of-ground effect hover were computed in C-81 using new blade mode shapes for each rpm. The results of this analysis are given in Figures 50 through 54. The Station 7 beam bending moment correlation is excellent (Figure 50), except for the test point at 280 rpm. This point may be in error, since it does not agree with the trend established by the other three test points. The correlation of the other three points implies that the flapping has been matched almost exactly. The Station 7 chord bending moment data show the correct trend, but do not increase as fast with rpm as the measured data (Figure 51). The harmonic analysis (Figure 52) shows that much of this discrepancy is the one-per-rev load and probably indicates a slight error in the calculated first chord natural frequency. Although lower than the loads measured in flight, the bending moments computed for Station 94 (Figure 53) show the correct trend with rpm. The computed oscillatory pitch link loads (Figure 54) are somewhat low, probably because of the simplified torsional model or the uncertainties in the blade element aerodynamics due to the possible airfoil contour deformations discussed previously.

Maneuver

Maneuvering loads were computed with C-81 using the input parameters developed during the level flight simulation. The flight path of the 1.75-G symmetric maneuver was matched (G level, pitch rate, and pitch attitude) for the four-second duration by guessing a control input, calculating the response, and modifying the control input. The calculated maneuver rotor loads are shown by dashed lines in Figures 55 and 56. Since the initial correlation of the C-81 maneuver loads with flight test was not considered satisfactory, the reasons for the discrepancies were briefly investigated.

During the level flight simulation, it was deduced that the airfoil as represented in C-81 stalled at higher angles of attack than the actual airfoil. Therefore, the input blade element aerodynamic data were altered in order to get stall effects into the simulation. The major alterations were designed to lower the lift coefficient at a given angle of attack. The lift coefficient is computed as the sum of the static lift coefficient for the angle of attack plus a ΔC_L due to unsteady aerodynamic effects. The static

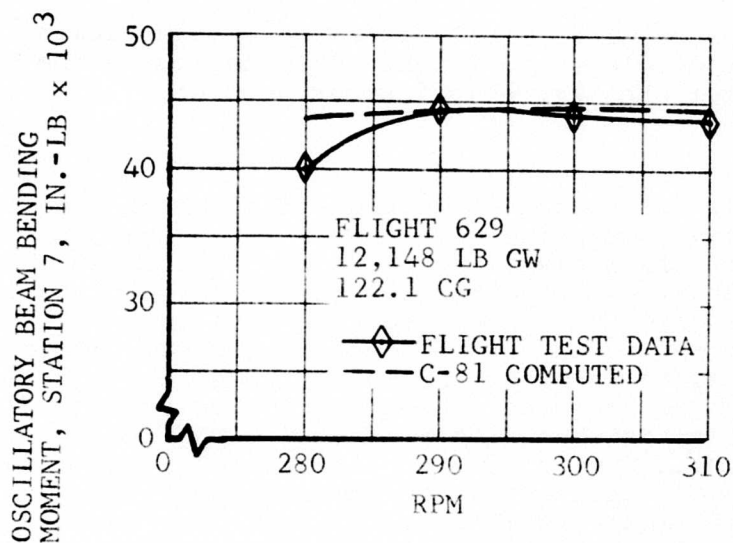


Figure 50. Measured and Computed Oscillatory Beam Bending Moment (Station 7) in Hover.

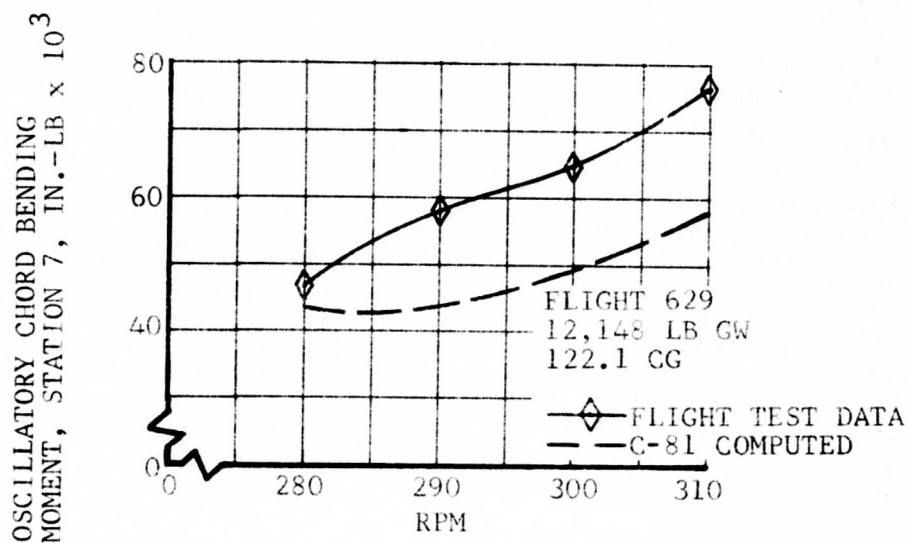
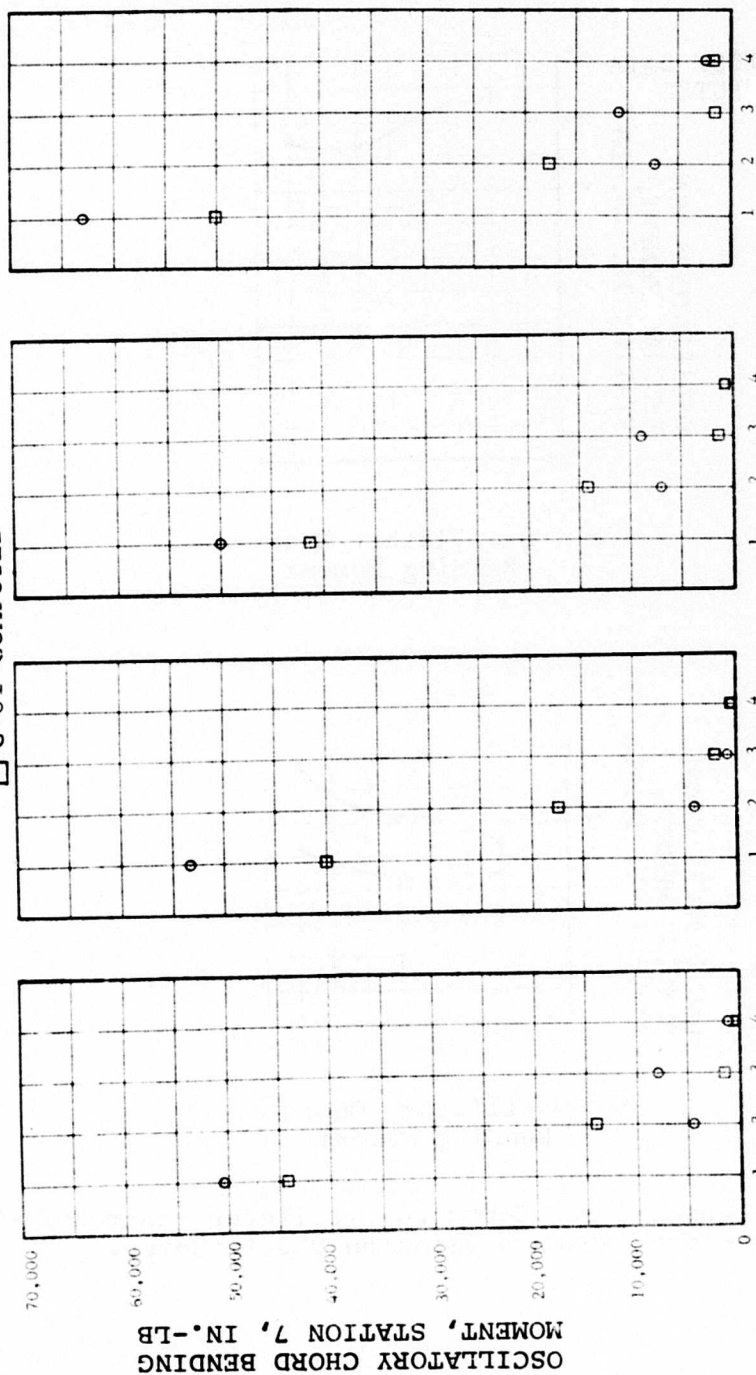


Figure 51. Measured and Computed Oscillatory Chord Bending Moment (Station 7) in Hover.

FLIGHT 629
12,148 LB GW
122.1 CG

○ FLIGHT TEST DATA
□ C-81 COMPUTED

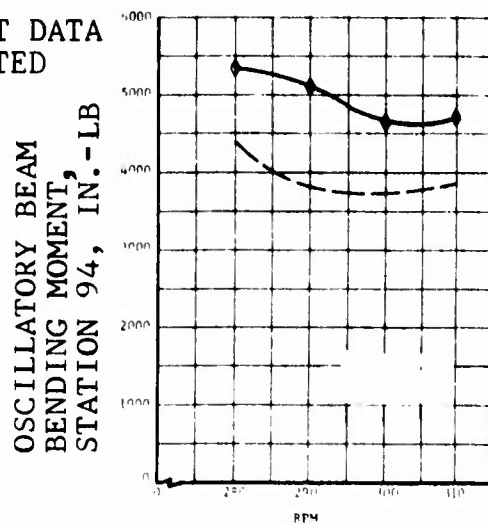


(a) 280 RPM
HARMONICS, PER REV
(b) 290 RPM
(c) 300 RPM
(d) 310 RPM
Harmonic Analysis of Oscillatory Chord Bending Moment (Station 7) in Hover.

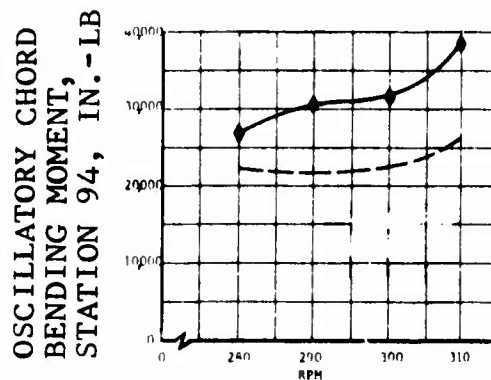
Figure 52.

FLIGHT 629
12,148 LB GW
122.6 CG

—◇— FLIGHT TEST DATA
— — — C-81 COMPUTED



a) Oscillatory Beam Bending Moment



b) Oscillatory Chord Bending Moment

Figure 53. Measured and Computed Oscillatory Beam and Chord Bending Moments (Station 94) in Hover.

FLIGHT 629
12,148 LB GW
122.1 CG

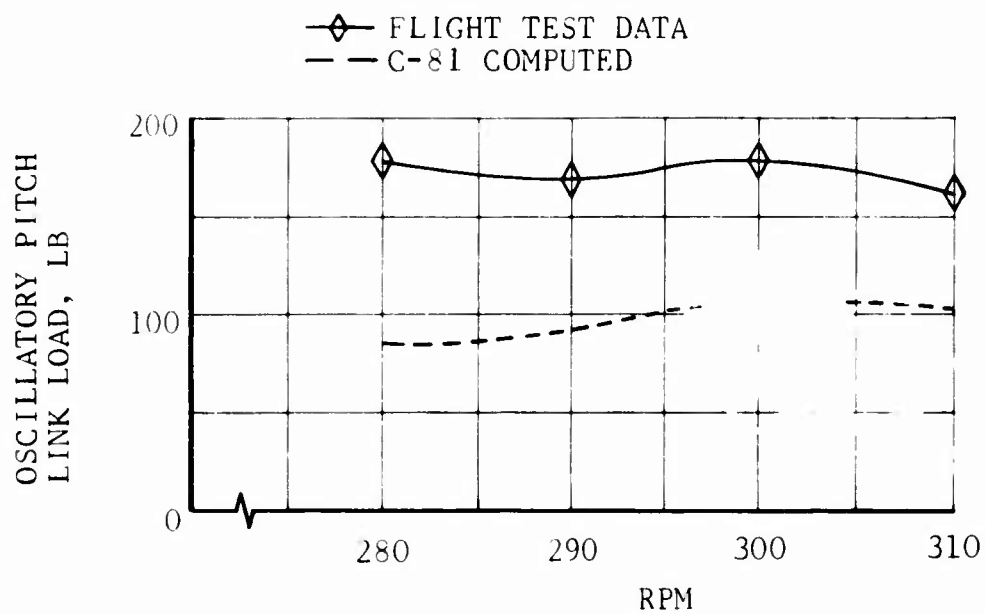


Figure 54. Measured and Computed Oscillatory Pitch Link Load in Hover.

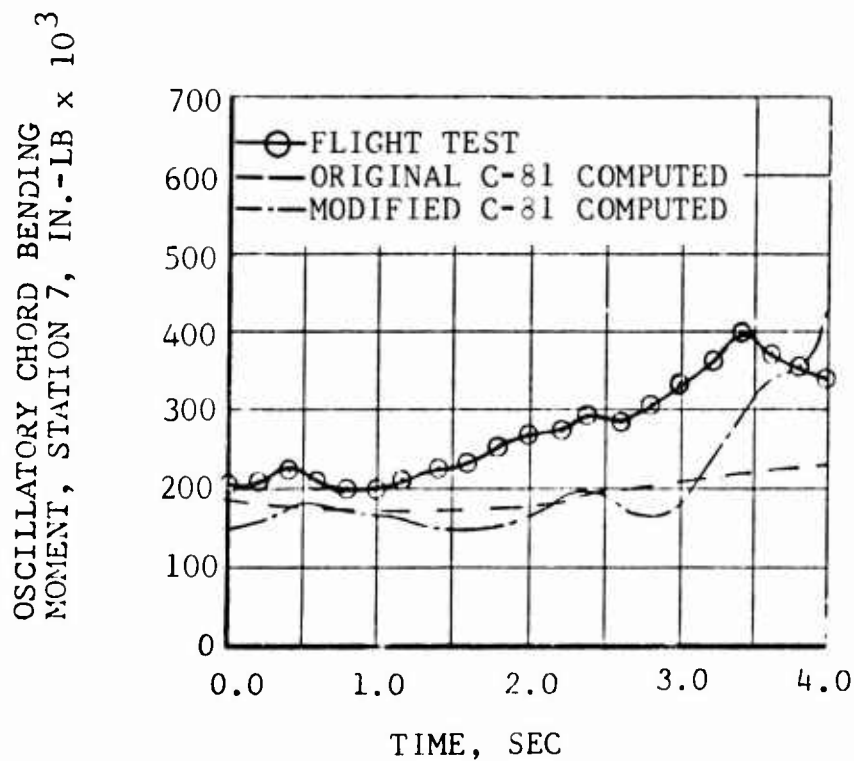
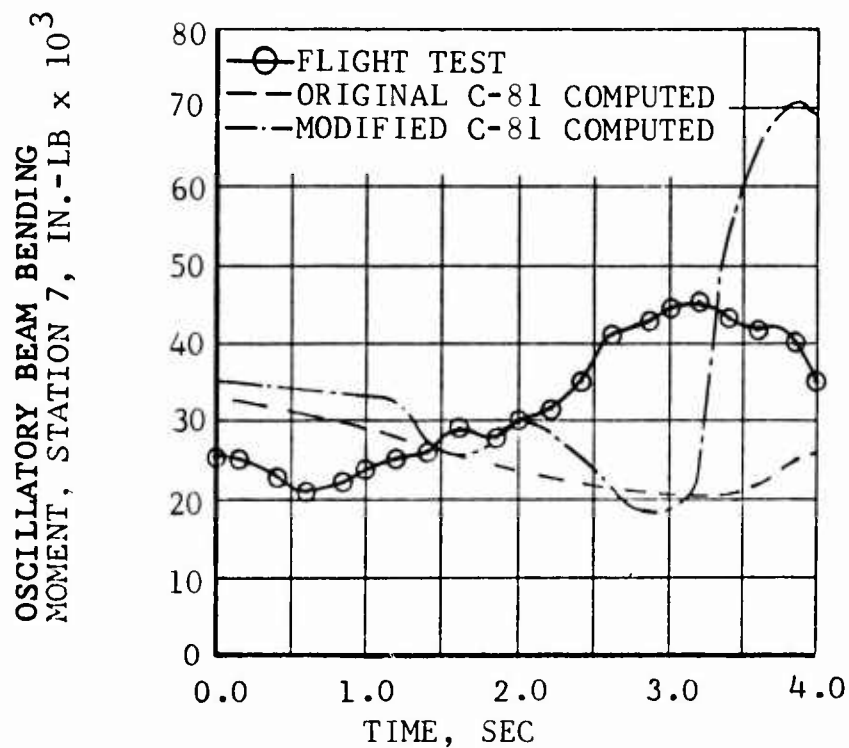
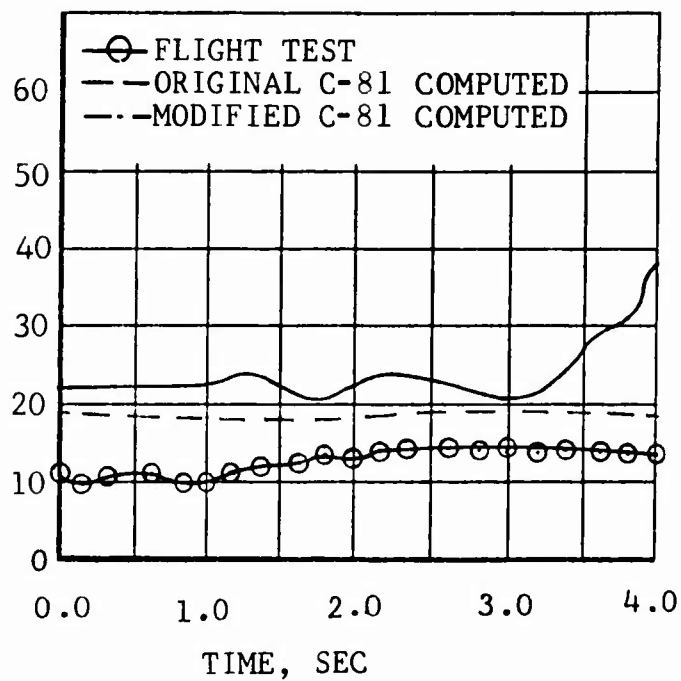


Figure 55. Time Histories of Measured and Computed Blade Loads (Station 7) for Symmetric Pullup.

OSCILLATORY BEAM BENDING MOMENT,
STATION 94, IN.-LB $\times 10^3$



OSCILLATORY CHORD BENDING MOMENT,
STATION 94, IN.-LB $\times 10^3$

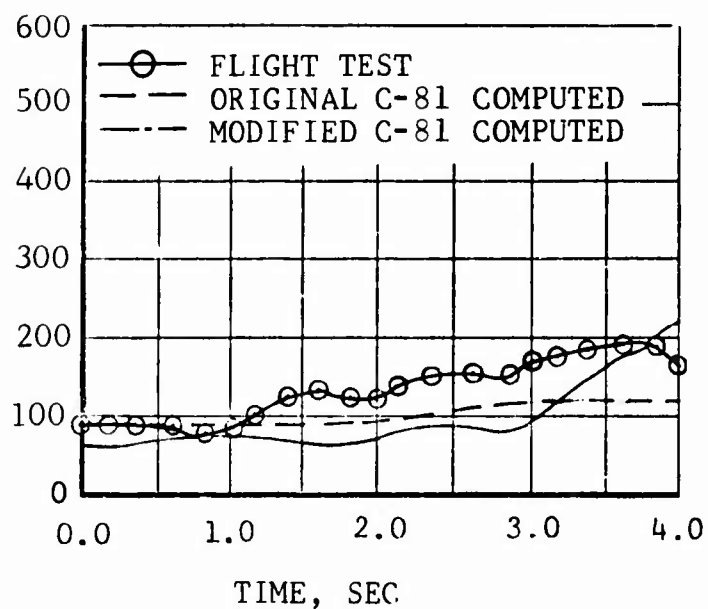


Figure 56. Time Histories of Measured and Computed Blade Loads (Station 94) for Symmetric Pullup.

$C_{L_{max}}$ was lowered, and the torsional component was removed from the blade mode shapes, as the elastic pitching velocity is the major source of the C_L terms. Higher blade element drag coefficients resulted for a given rotor thrust level because the blade elements had to operate at higher angles of attack to get the same lift coefficients and because the drag divergence Mach number was decreased. These modifications improved the correlation, as shown in Figures 55 and 56.

LOAD LEVEL SURVEY AND FATIGUE LIFE ANALYSIS - RESULTS AND DISCUSSION

The loads that the rotor and control system encountered during flight in a utility helicopter flight spectrum were measured. Fatigue lives were then calculated from the flight measurements and frequency-of-occurrence spectrum (Table III).

FLIGHT SPECTRUM AND FREQUENCY OF OCCURRENCE

The frequency-of-occurrence spectrum is similar to the utility helicopter spectrum of Reference 10. It differs from that spectrum in that times spent at low speeds have been reduced to allow the assignments of periods for maneuvers without affecting other areas of the spectrum.

Each condition in the flight spectrum was flown at several combinations of gross weight and cg, as shown in Table IV. The percentage of time assumed spent at each gross weight is also indicated in Table IV. (Time was not distributed on the basis of cg location.) The highest load measured at each gross weight (irrespective of cg) was used in the fatigue life analysis. Table V lists the flight conditions for each increment of the load level survey.

CALCULATED FATIGUE LIVES OF COMPONENTS

Fatigue life calculations are based on a comparison between stresses encountered in the flight spectrum and the endurance-limit stress for the component being analyzed. Fatigue tests of Model 609 rotor blade sections established the shape of the S-N curve (stress versus cycles) and the endurance limit. Endurance limits and S-N curve shapes for other components were established from one of the following:

- Published fatigue data for the material
- Fatigue test data for a similar component
- Fatigue test data for material specimens

Calculations using data from these sources make allowances for steady stress and stress concentrations. Details of the fatigue life analysis are included in Appendix III for each component analyzed.

The calculated fatigue lives for rotor and control system components are summarized in Table VI. The most critical station for each rotor component has been analyzed. Loads from the instrumented (red) blade and hub segment in the upper half of the rotor were used in the life analysis. Loads in the lower

TABLE III. MODEL 609 SPECTRUM -- FREQUENCY OF OCCURRENCE

N ₁	CONDITION	TIME	RPM
1	I. GROUND CONDITIONS		
1	A. NORMAL START	0.5000	295.0
2	B. NORMAL SHUTDOWN	0.5000	295.0
3	II. POWER-ON IGE		
3	A. HOVERING		
3	1. STEADY		
3	(A) 280 RPM	3.4720	280.0
4	(H) 295 RPM	3.4720	295.0
5	2. LEFT TURN	1.1110	285.0
6	3. RIGHT TURN	1.1110	285.0
7	4. CONTROL REVERSAL		
7	(A) LONGITUDINAL	0.2780	285.0
8	(R) LATERAL	0.2780	285.0
9	(C) RUDDER	0.2780	285.0
10	B. MANEUVERS		
10	1. SIDEWARD FLIGHT		
10	(A) TO THE RIGHT	0.5000	285.0
11	(B) TO THE LEFT	0.5000	285.0
12	2. REARWARD FLIGHT	0.5070	285.0
13	3. NORMAL TAKE-OFF	0.8890	285.0
14	4. NORMAL LANDING	2.0830	285.0
15	III. POWER-ON IGE		
15	A. LEVEL FLIGHT		
15	% VL RPM		
15	1. 40 280	0.9330	280.0
16	295	0.9330	295.0
17	2. 50 280	2.4585	280.0
18	295	2.4585	295.0
19	3. 60 280	3.9190	280.0
20	295	3.9190	295.0
21	4. 70 280	5.0000	280.0
22	295	5.0000	295.0
23	5. 80 280	7.5000	280.0
24	295	7.5000	295.0
25	6. 90 280	8.6670	280.0
26	295	8.6670	295.0
27	7. 100 280	4.9190	280.0
28	295	4.9190	295.0
29	8. VNE 280	1.7500	280.0
30	295	1.7500	295.0
31	B. MANEUVERS		
31	1. CLIMB 0-50 KNOTS		
31	(A) M.C. POWER	3.0000	285.0
32	(B) T.O. POWER	1.0000	285.0

TABLE III. Concluded

NO.	CONDITION	TIME	RPM
33	2. CYCLIC PULL-UP		
33	(A) 50 KNOTS	0.1620	285.0
34	(B) 100 KNOTS	0.1620	285.0
35	(C) VL	0.1620	285.0
36	3. LEFT TURN		
36	(A) 50 KNOTS	1.0000	285.0
37	(B) 100 KNOTS	1.0000	285.0
38	(C) VL	0.5000	285.0
39	4. RIGHT TURN		
39	(A) 50 KNOTS	1.0000	285.0
40	(B) 100 KNOTS	1.0000	285.0
41	(C) VL	0.5000	285.0
42	5. CONTROL REVERSAL		
42	(A) LONGITUDINAL	0.2220	285.0
43	(B) LATERAL	0.2220	285.0
44	(C) RUDDER	0.2220	285.0
45	IV. POWER TRANSITIONS		
45	A. POWER TO AUTO		
45	1. 40 KNOTS	0.0110	285.0
46	2. VL	0.0110	285.0
47	B. AUTO TO POWER	0.0560	285.0
48	V. AUTOROTATION		
48	A. STABILIZED FLIGHT		
48	1. 40 KNOTS	0.2890	285.0
49	2. 80 KNOTS	0.3880	285.0
50	3. MAX AUTO A/S	0.1890	285.0
51	B. TURNS. (NORMAL		
51	AUTO A/S)		
51	1. TO THE LEFT	0.2000	285.0
52	2. TO THE RIGHT	0.2000	285.0
53	C. CONTROL REVERSAL		
53	1. LONGITUDINAL	0.1000	285.0
54	2. LATERAL	0.1000	285.0
55	3. RUDDER	0.1000	285.0
56	D. CYCLIC PULL-UP		
56	(NORMAL AUTO A/S)	0.0560	285.0
57	E. PART PWR DSNT, 80KT	2.0830	285.0
58	F. FULL AUTO LANDING	0.3000	285.0
TOTAL TIME = 100.0000 PERCENT			

TABLE IV. GROSS WEIGHT AND CENTER-OF-
GRAVITY VARIATIONS FLOWN
FOR THE FATIGUE LIFE ANALYSIS

Gross Weight (lb) *	C.G. Station (in.)		
	10,500	12,000	14,000
Forward	-	122	122
Neutral	-	-	129
Aft	136	136	136
Total Time Assumed at Each Gross Weight	20%	60%	20%
*Gross weight was maintained within ± 400 lb during load level survey.			

**TABLE V. DESCRIPTION OF CONDITIONS FLOWN
IN THE LOAD LEVEL SURVEY**

No.	Condition	Remarks	TAS (kn)	Density Altitude (ft)
1, 2	Ground	Start-Stop	-	Ground *
3-9	Hovering	IGE	-	Ground
10-11	Sideward Flt	IGE	30	Ground
12	Rearward Flt	IGE	30	Ground
13	Takeoff	Ground to OGE	Variable	Ground
14	Landing	OGE to Ground	Variable	Ground
15,16	.4 V_L	Level Flight	60	4,000
17,18	.5		75	
19,20	.6		90	
21,22	.7		105	
23,24	.8		120	
25,26	.9		135	
27,28	V_L	Level Flight	150	
29,30	V_{NE} (Dive)	Trans. Cont. Limit	160	4,000
31	Climb	Trans. Cont. Limit	0-60	Ground to 5,000
32	Climb	Trans. T.O. Limit	0-60	Ground to 5,000
33,35	Cyclic Pull-up	1.5-1.7g	50,100,150	4,000
36,38	Left Turn	1.5-1.7g	50,100,150	4,000
39,41	Right Turn	1.5-1.7g	50,100,150	4,000
42,44	Control Reversals	Small Amp High Rate	135	4,000
45,47	Power Transi- tions	0 to Level Flt SHP	Variable	Ground to 5,000
48,58	Autorotation	Level Flt SHP to 0	Variable	Ground to 5,000
TRANSMISSION SHP LIMITS			M/R RPM	
			280	285
	Continuous		1585	1610
	Takeoff		1885	1620
				295
				1670
				1985
*Ground indicates flown at field elevation. Density altitudes from 0 to 1000 feet.				

TABLE VI. SUMMARY OF CALCULATED FATIGUE LIVES FOR
MODEL 609 HINGELESS FLEXBEAM ROTOR SYSTEM

Component	Part Number	Life Hours
<u>Rotor & Mast</u>		
Yoke, Hub	609-010-102	811
Blade Retention Fitting	609-010-105	1,593
Spindle	609-010-140	7,100
Blade	609-010-200	1,334
Mast	609-040-300	Unlimited
<u>Rotating Controls</u>		
Pitch Horn	609-010-104	Unlimited
Pitch Link	609 HES 45-5	22,485
Swashplate Outer	609-010-401	11,557
<u>Nonrotating Controls</u>		
Swashplate Inner	609-010-402	Unlimited
Slider Collective	609-010-404	Unlimited
Slider Lug Bolt	609-010-419	545
Cylinder Housing (Collective)	204-076-317	23,131
Cylinder Housing (F/A Cyclic)	204-076-317	Unlimited
Cylinder Housing (Lat Cyclic)	204-076-317	Unlimited

half were usually higher, but the discrepancies were not resolved, and the use of either blade was arbitrary (see the discussion in the "Technical Problem" section).

The analysis of the life of rotating control system components used measured loads from all four rotor blade pitch links. The components associated with the green blade pitch link had the shortest lives, and are therefore the only ones shown in the summary table.

The life of each of the four critical areas on the nonrotating ring of the swashplate was analyzed. Only the shortest life is shown in the summary table. The lives of all other non-rotating components analyzed are listed.

The results shown in Table VI are conservative in that the peak stresses encountered during a maneuver are assumed to exist for the duration of that maneuver. In reality, the peak stresses exist for only a portion of the time allowed for each maneuver. The effect of stresses occurring during full autorotational landings was analyzed on a cycle-count basis. The method of analysis previously outlined would be overly conservative for this maneuver, due to the small number of damage-generating cycles.

ANALYSIS OF RESULTS

The analyses of these components with low life estimates have been examined to determine if the analytical approach was overly conservative or if, on the other hand, the measured stresses would have been higher with only slight changes in such parameters as gross weight, center of gravity, and airspeed, resulting in an unconservative life determination.

The analysis showed that the slider lug bolt (Appendix III) has the shortest life, but it assumes that oscillatory loads in the cyclic and collective boost cylinder housings peak simultaneously to cause bending in the bolt. Direct measurement of load on this bolt is impractical, and an exact calculation of the load requires a knowledge of the relative phasing of the oscillatory load in the three boost cylinders. Examination of records from one of the conditions causing fatigue damage revealed that the loads peak simultaneously only on one out of every four load cycles. Therefore, the peak stress level used in the analysis occurs only at one per rev of the main rotor, rather than at the four per rev used in the analysis. The remaining three cycles occur at lower stress levels, and it would take a detailed analysis to determine their individual effects on fatigue lives. Thus, this preliminary analysis is conservative.

The short life shown for the main rotor yoke and blades is conservative only in that peak loads are assumed to exist for the duration of all the maneuvers except the autorotational landing.

Stress levels in the yoke (from Table XIII, Appendix III), plotted in Figure 57, illustrate that only nine conditions cause damage. Maneuvers at 14,000 pounds and V_L cause over half of the fatigue damage. The pilot limited maneuvering to 1.3G rather than the 1.7G planned, because the load meter was indicating high oscillatory loads in the rotor. In view of the damage encountered at this low load factor, it would be advisable to exclude maneuvering at 14,000 pounds and 150 knots from the flight envelope. If maneuvering speed at 14,000 pounds is reduced until maneuver loads are equal to those measured at 12,000 pounds, the calculated life of the yoke would be 2016 hours, as opposed to 811 hours, and the blade life would increase from 1334 to 3854 hours. The resulting change in the flight envelope is shown in Figure 58. Lines of constant loading (from the Rotor Loads section of this report) show the speeds at which 12,000-pound maneuver loads would be encountered at higher (and lower) gross weights.

The analysis of the rotor blade retention system includes some conservatism. Damage in this system results from starting and stopping the rotor, and the only assumption which might be questionable is the frequency of start/stop cycles. A frequency of four cycles per hour was used in the analysis. The life of the retention system would double if this number were halved, and conversely, the retention system would have to be redesigned if the frequency were greater than four starts/stops per hour. Reference 15 shows a total of 100 ground-air-ground cycles in 100 hours, but operational experience has shown that many aircraft encounter a higher frequency of occurrence. The frequency used is considered to fit the operational requirements of Army utility helicopters.

CG CODE: F-FORWARD, N-NEUTRAL, A-AFT

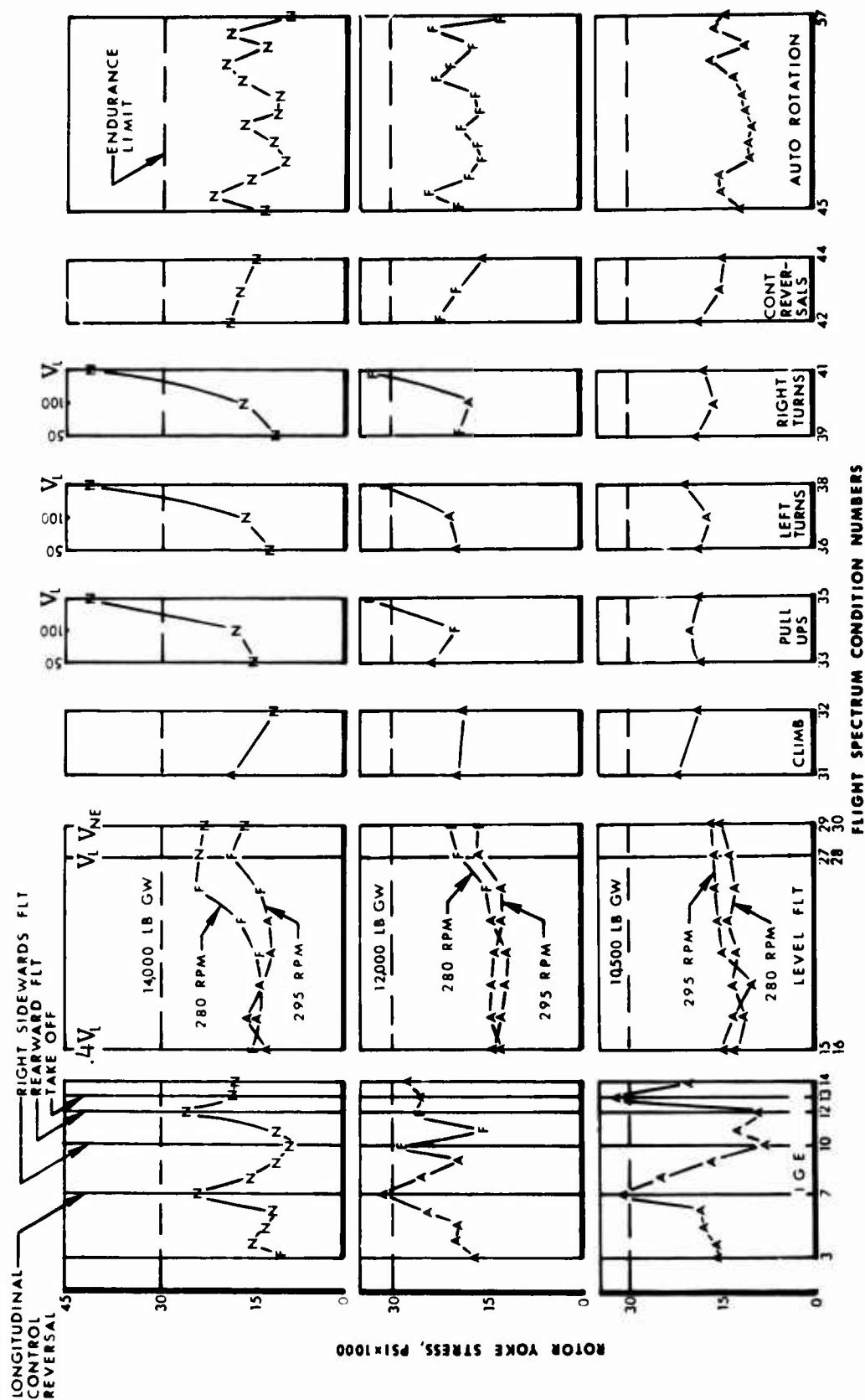


Figure 57. Main Rotor Yoke Stresses for Each Condition in the Flight Spectrum (Data From Table XIII, Appendix III).

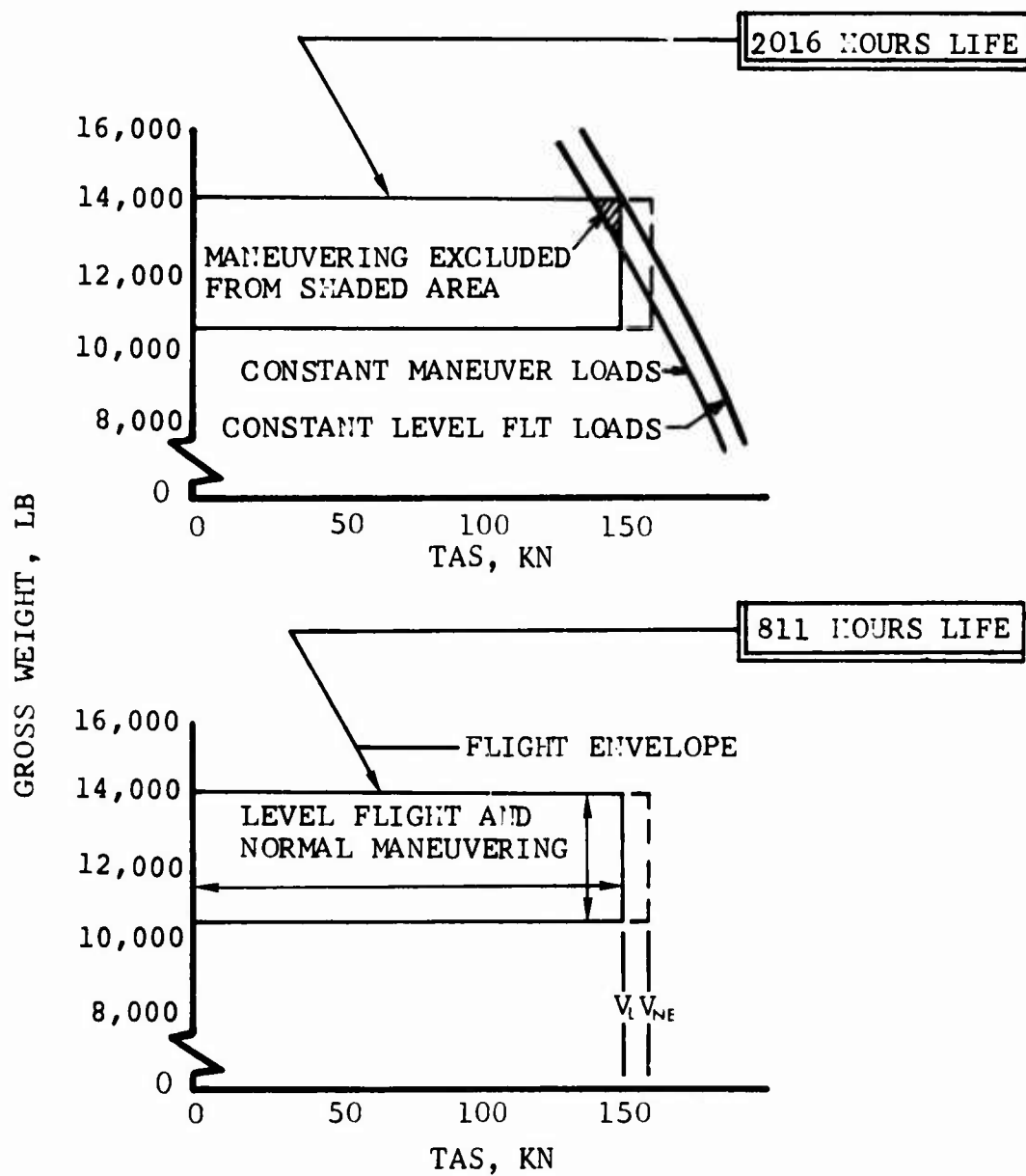


Figure 58. Effect of Maneuvering Restrictions on Rotor Yoke Fatigue Life.

FUSELAGE VIBRATION - RESULTS AND DISCUSSION

Vibrations at the four per rev of the main rotor were the most significant vibrations in the fuselage. Because of this, analyses and investigations of vibration have been confined to four per rev.

FLIGHT TEST RESULTS

Crew and Passenger Vibration Environment

Figures 59 through 61 summarize the vertical four-per-rev vibrations at the pilot's and copilot's station, and center of gravity of the test helicopter, showing the effects of changes in gross weight, center of gravity, main rotor speed, and true airspeed. (The comparison by harmonics in Figure 62 shows that four-per-rev vibration is the most significant.) These summary plots suggest the following comments:

1. Vibration decreases as center of gravity moves aft.
2. Vibration decreases slightly (Figure 61) with increasing main rotor speed.
3. Vibration is below 0.35G.

Overall, the vibration is low at four per rev, and the ride is good in the crew and passenger areas.

Correlation of Fuselage Vibration With Changes in Rotor Loads

Changes in fuselage vibration with airspeed and accompanying changes in rotor system loads have been plotted in Figure 63 in an attempt to establish the excitation source. The four-per-rev fuselage vibration was caused by blade four-per-rev out-of-plane (beam) loads as well as blade three-per-rev in-plane (chord) and out-of-plane loads. Rotor three-per-rev loads build with airspeed in both the beamwise and chordwise directions, and decrease with increasing rpm.

The three per rev in the rotating system is also reflected in the four-per-rev in-plane hub accelerations (fixed system). The similar increase in fuselage roll accelerations is indicated by the difference in pilot and copilot vibrations. Nose vibrations also show an rpm and speed trend.

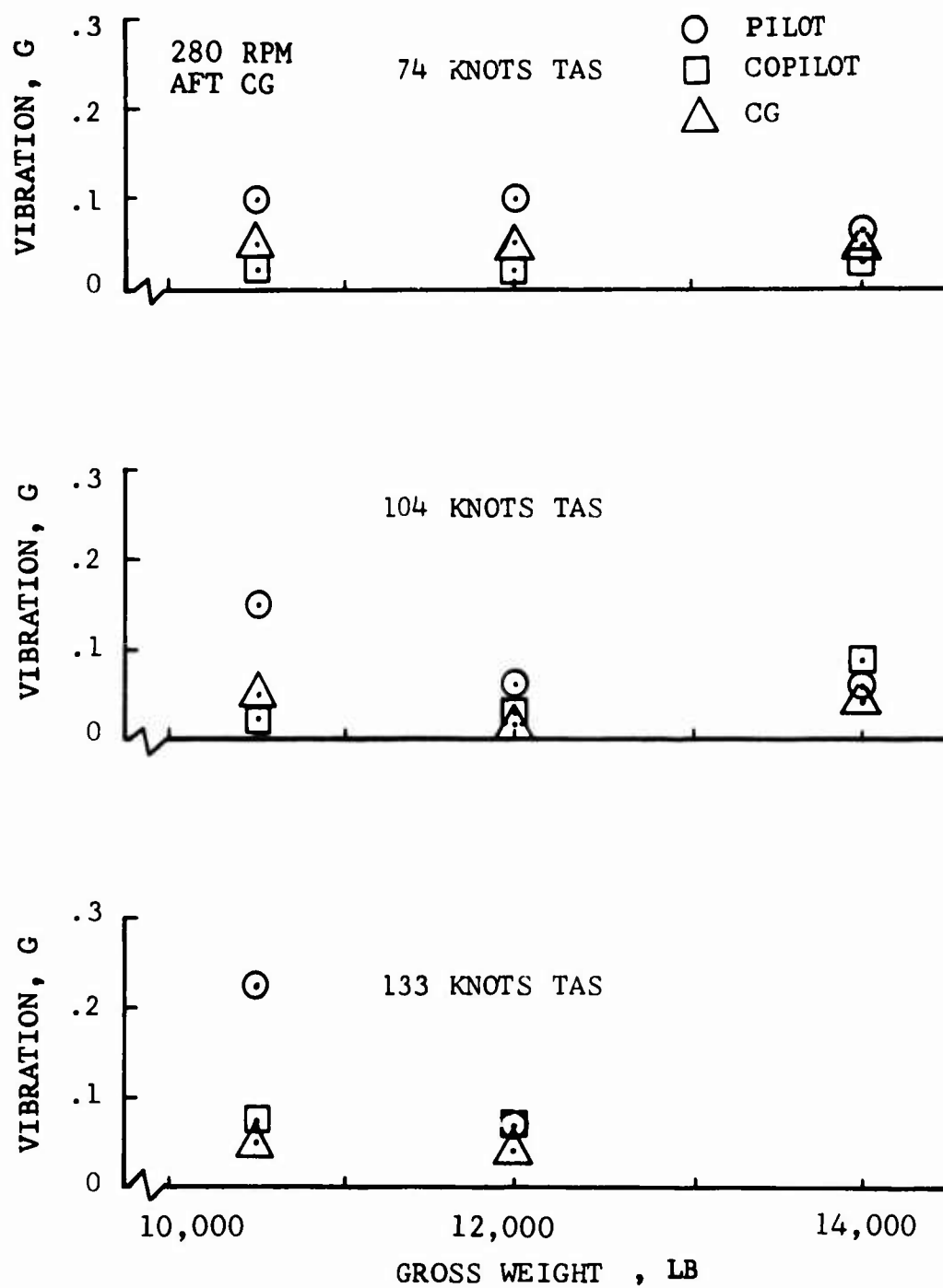


Figure 59. Summary of 4/Rev Vibration Versus Gross Weight, Flight Test Data.

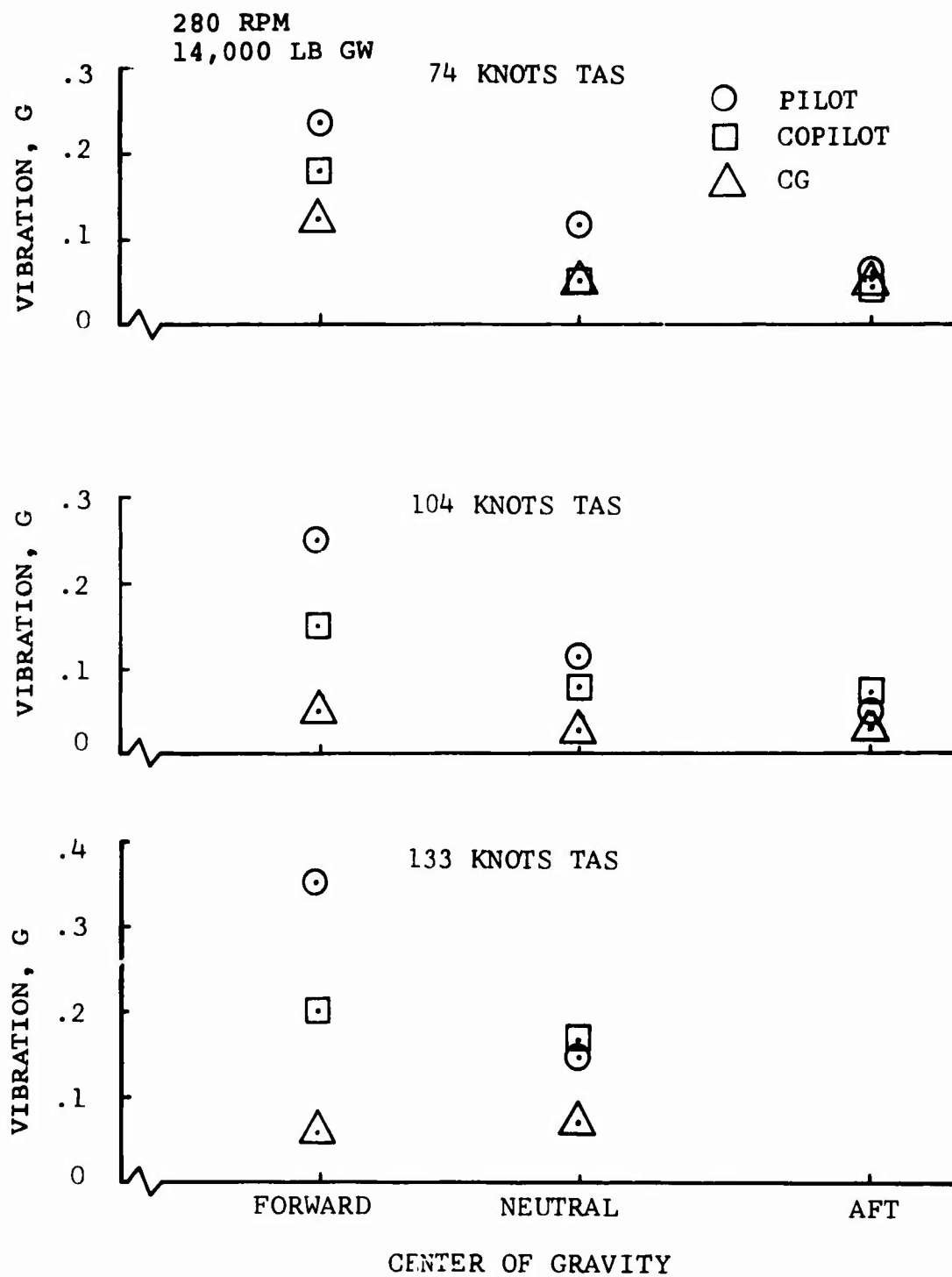


Figure 60. Summary of 4/Rev Vibration Versus Center-of-Gravity Location, Flight Test Data.

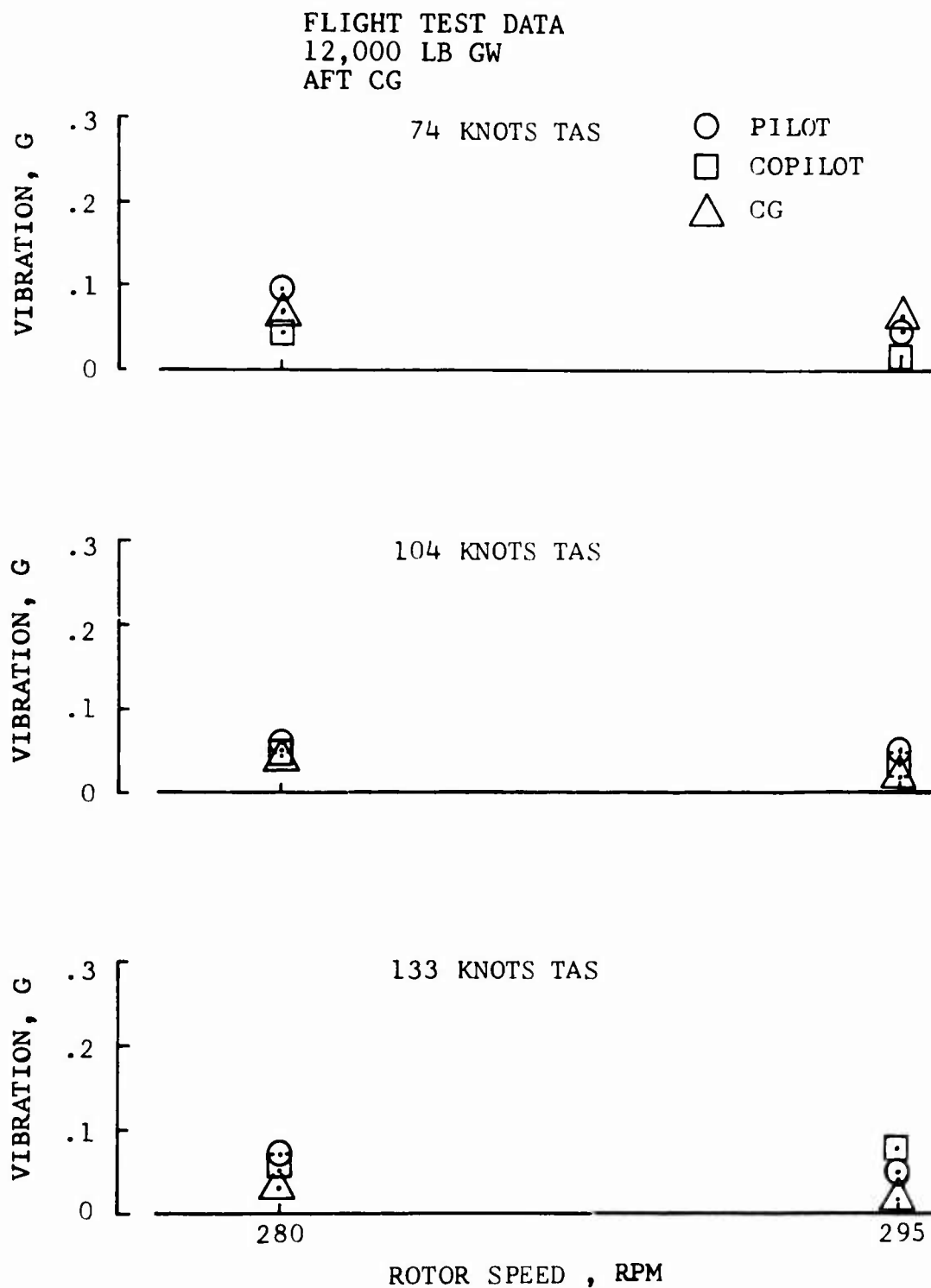


Figure 61. Summary of 4/Rev Vibration Versus Rotor Speed, Flight Test Data.

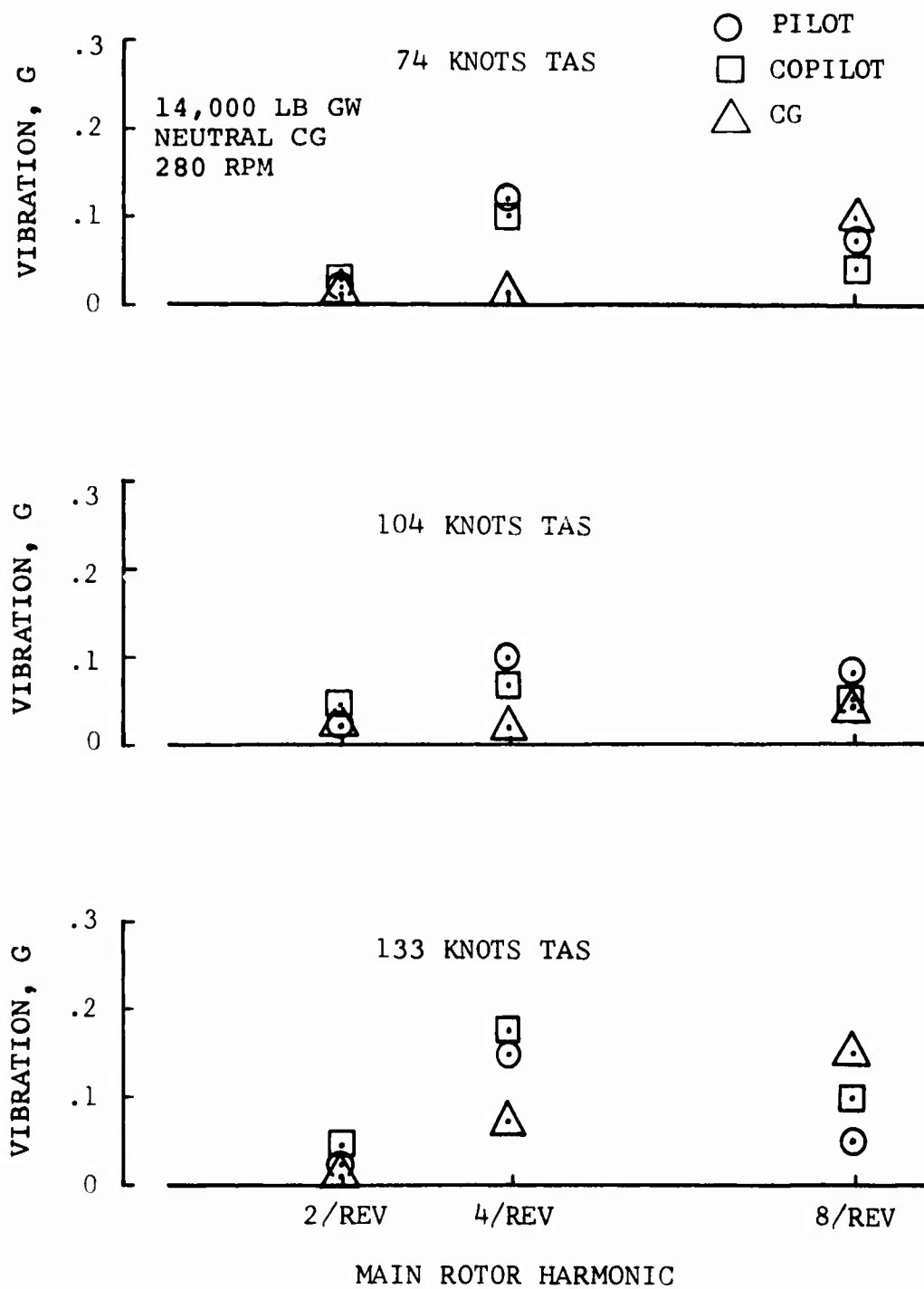


Figure 62. Summary of Vibration Versus Main Rotor Harmonic, Flight Test Data.

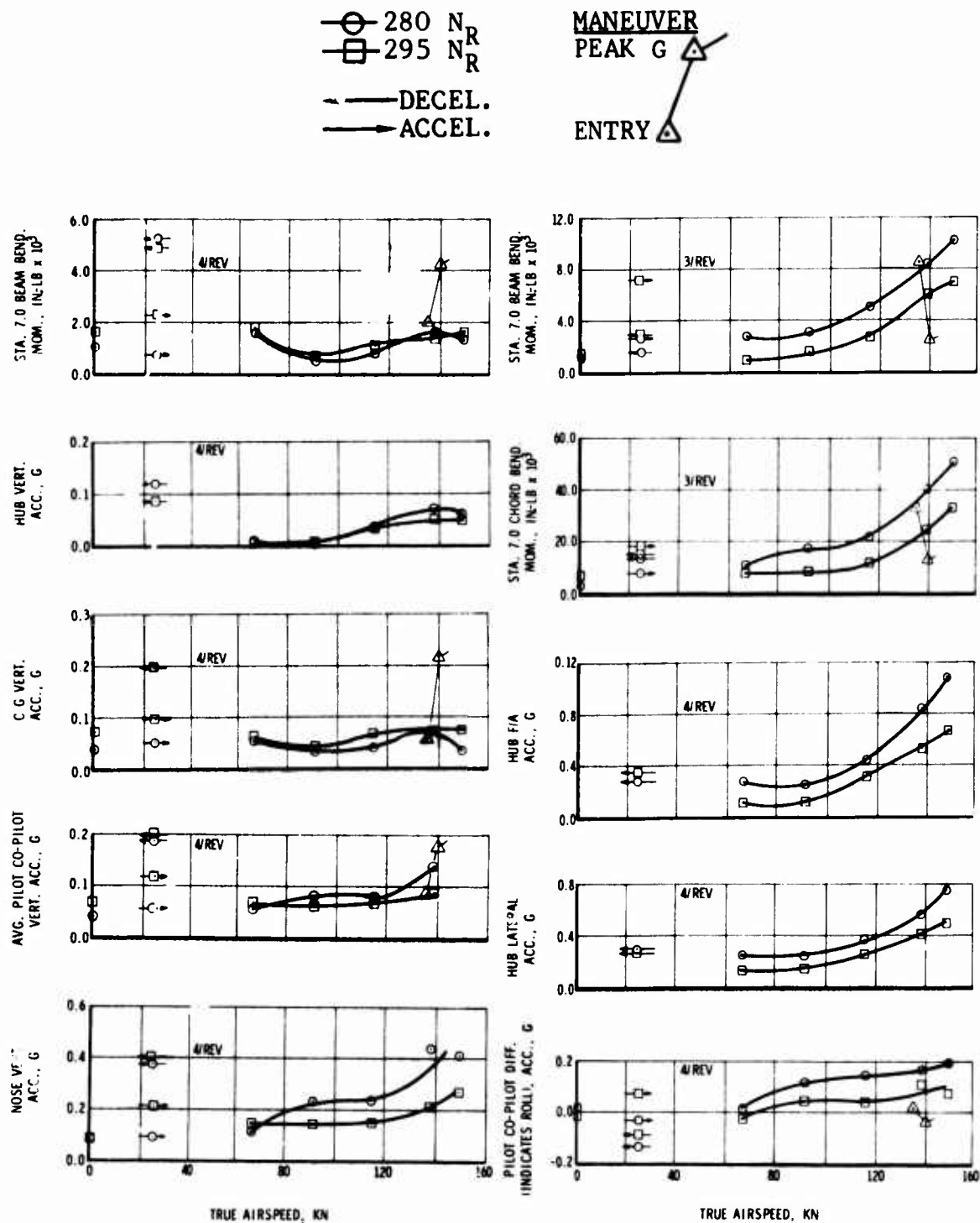


Figure 63. Correlation of 4/Rev Vibrations in the Fuselage With Rotor System Loads and Vibrations, Flight Test Data.

The cg and average of pilot- and copilot-seat vibrations do not show strong rpm and airspeed trends. Vibrations at these stations seem to follow more closely the beamwise four per rev in the rotor, which is transmitted vertically into the fuselage. Thus, superposition of responses to vertical and horizontal excitations is indicated. However, the vertical (beamwise) four per rev is clearly the dominant excitation in the high-speed maneuver.

Vibrations occurring during transitional flight are also presented in Figure 63. The accelerations and decelerations are shown separately with the decelerations having the higher four-per-rev vibrations. The predominant exciting force, as can be seen from Figure 63, is the rotor four-per-rev beamwise load.

COMPUTED HUB MOTIONS

The C-81 flight simulation analysis couples the elastic response of the rotor with the fuselage. The analytical model of the fuselage has three degrees of freedom: pylon roll, pitch of the pylon about its focal point, and vertical rigid body fuselage motions. It generates hub vibrations during the rotor loads computations. Computed fixed-system hub vibrations are compared in Figure 64 with vibrations measured during the pylon evaluation flights. (Hub vibrations were not recorded on subsequent flights.) Since the analytical model has only three degrees of freedom, perfect correlation cannot be expected. The comparison is encouraging, nevertheless, suggesting that the program's aeroelastic treatment of the rotor may be adequate for predicting four-per-rev vibrations when more definitive fuselage modeling is included in the analysis.

NASTRAN ANALYSIS AND MODEL CORRELATION

Fuselage vibration was evaluated analytically with the structural dynamics computer program NASTRAN, which is defined in Reference 11. NASTRAN uses a matrix technique to solve the differential equations of a finite element structural model.

A ground vibration test defined the lower-frequency fuselage modes and the four-per-rev fuselage response. It excited the fuselage in three directions with the helicopter in a basic fuselage configuration weighing 11,594 pounds and a dummy hub weighing 1,900 pounds. The excitation directions were vertical, lateral, and fore and aft. The primary fuselage frequencies determined during the test are listed in Table VII.

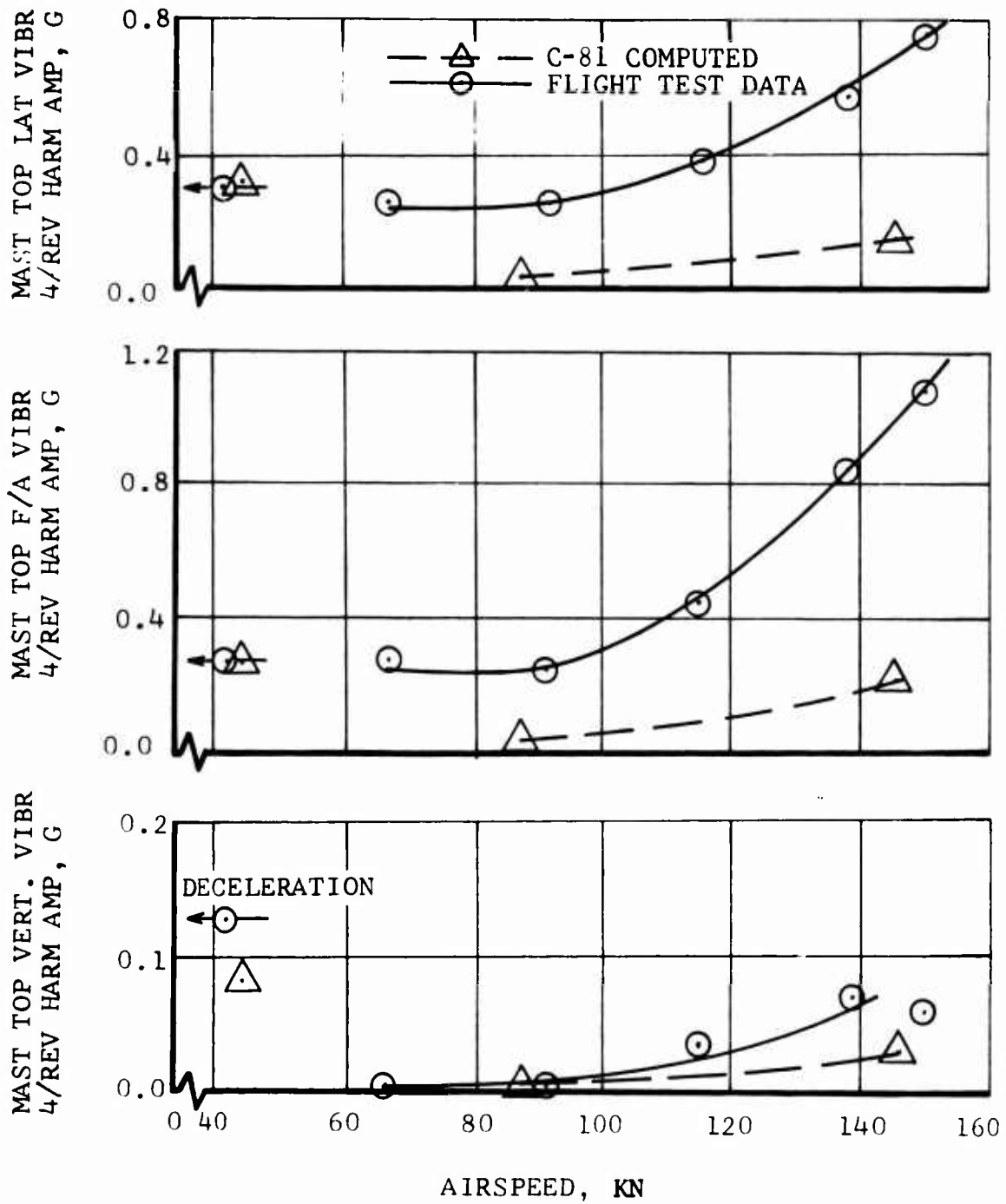


Figure 64. Comparison of Computed and Measured Hub Vibrations, 12,000 Pounds GW, Neutral CG.

TABLE VII. SHAKE TEST CORRELATION		
	FREQUENCIES (Hz)	
	Vibration Test	NASTRAN
1st Fuselage Lateral	6.1 - 6.3	6.9
1st Fuselage Vertical	7.5 - 8.2	7.8
2nd Fuselage Lateral	11.3 - 11.8	11.2
2nd Fuselage Vertical	13.1 - 14.1	13.9

The structural model of the test helicopter was established by determining the approximate inertia of the fuselage in segments along the elastic axis of the fuselage and modeling it on NASTRAN as lumped masses connected with structural elements (Figure 65). The NASTRAN model was tuned by forcing it at the same points that the test vehicle was forced during the ground vibration test and adjusting the location of the lumped masses and stiffness of the model to correlate its response with the measured fuselage mode shapes and frequencies. The results, as seen in Figure 66, show good correlation with the lower fuselage modes.

NASTRAN MODE SHAPE SIMULATION

The NASTRAN structural model was used to analyze the fuselage dynamics. The effective mass of the main rotor was calculated and placed at the main rotor hub of the NASTRAN model. This model was then excited with four-per-rev vertical forces, fore-and-aft forces, and moments at the hub. The excitations were varied to force the model to respond as close as possible to the same four-per-rev mode seen in flight. The results are shown in Figure 67 for 12,000 pounds gross weight and forward, neutral, and aft cg locations. The flight test results are not faired since accelerometer data were not available at the elevator (station 400). The exciting forces used to produce the computed mode shapes are indicated in the figure.

The results of the analysis do not correlate very well with flight test results, possibly for the following reasons:

1. Modeling of the pylon did not include friction damping.
2. The engine mode was not included.

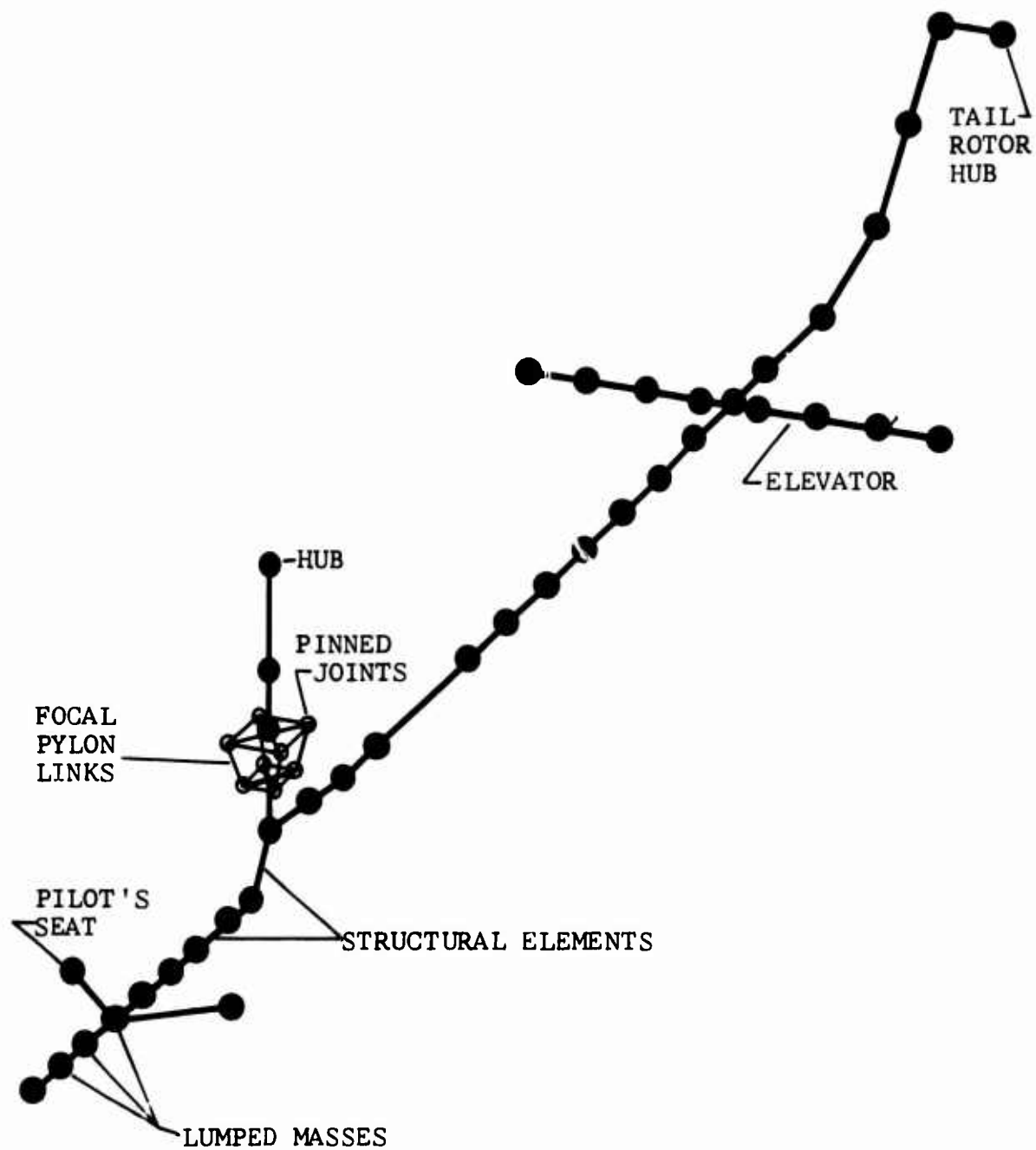


Figure 65. NASTRAN Finite Element Model.

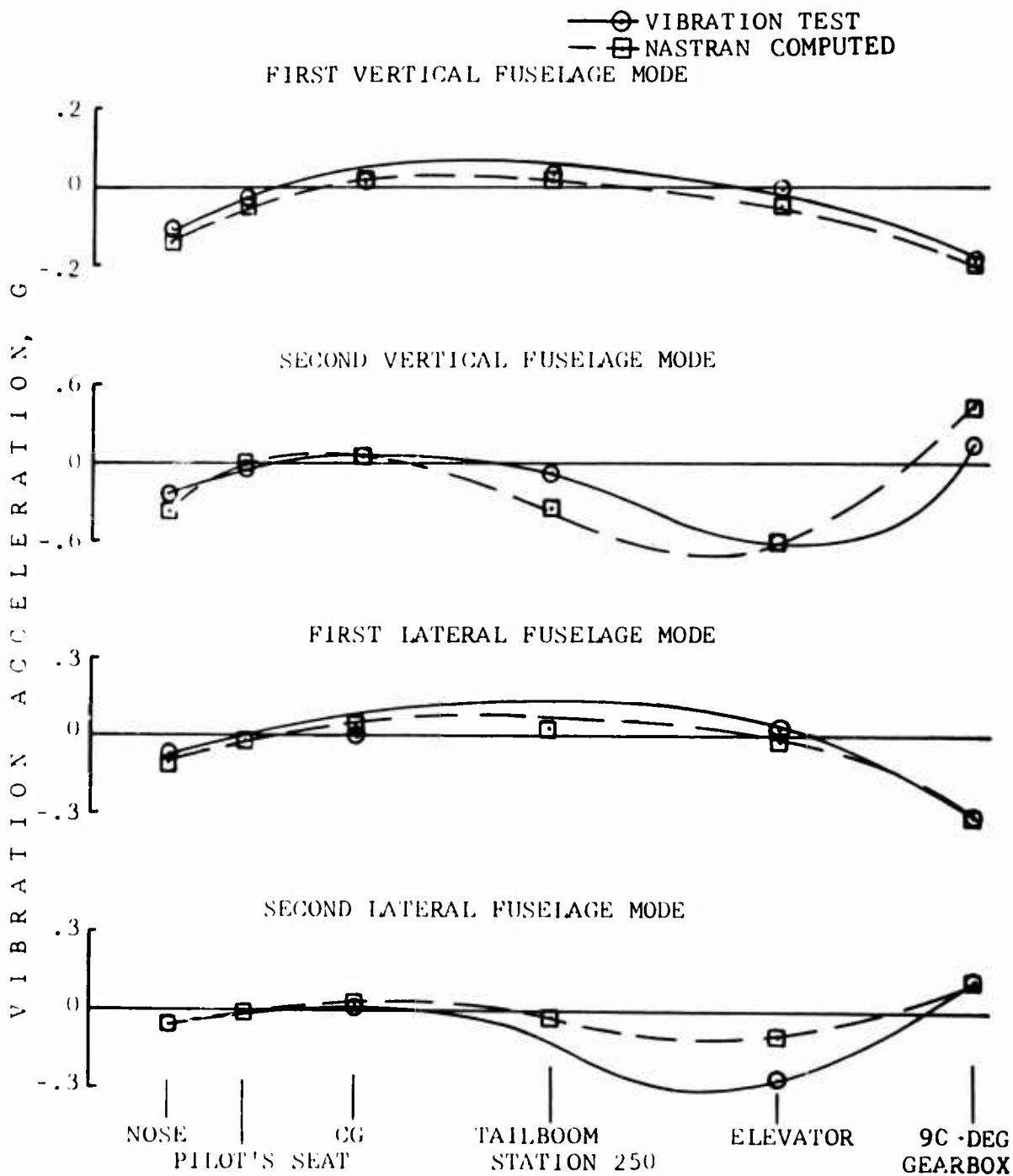


Figure 66. NASTRAN and Vibration Test Mode Shape Correlation.

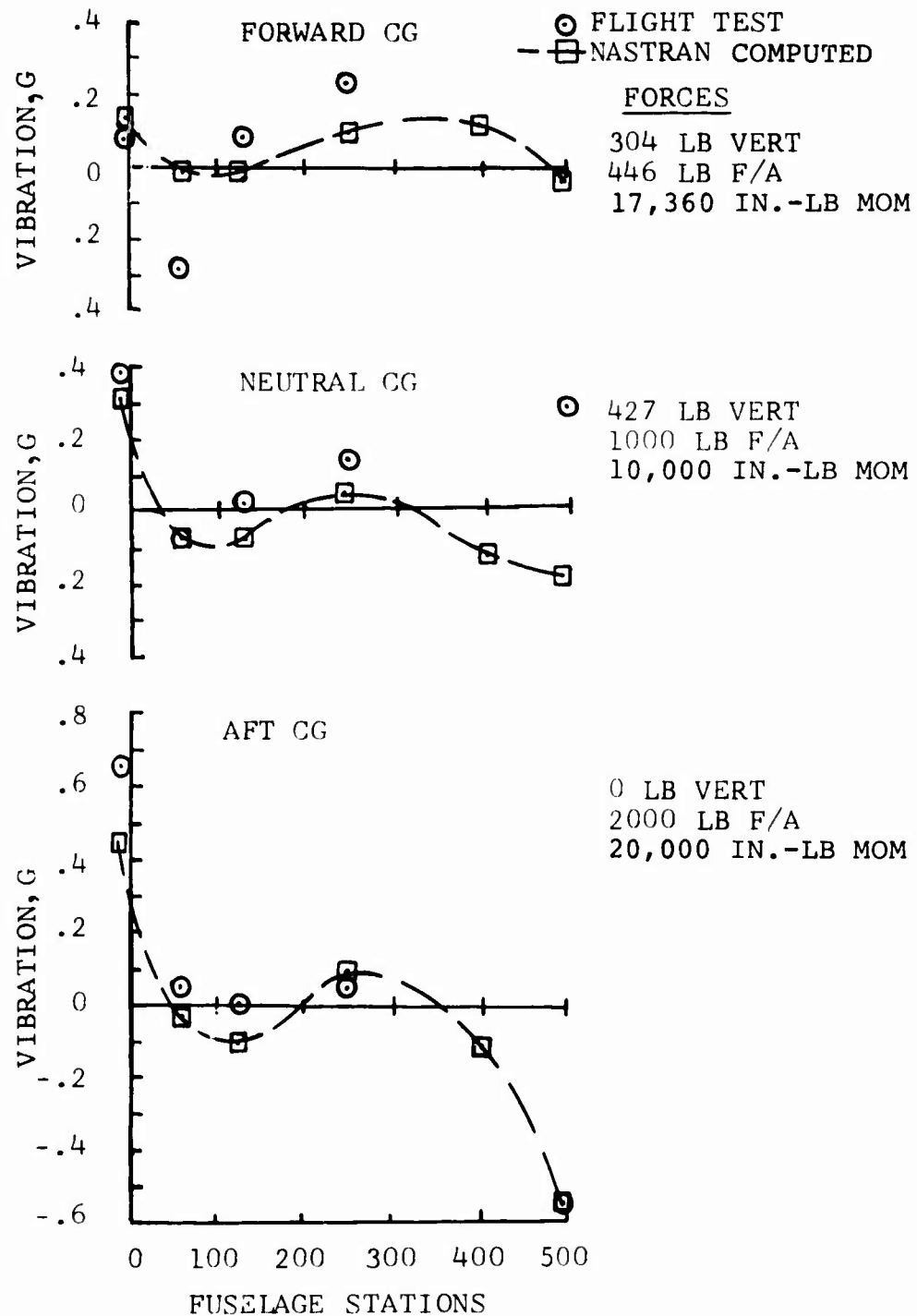


Figure 67. NASTRAN 4/Rev Mode Shape Correlation With Flight Test Data.

3. Second-order aerodynamic excitation was neglected.

Had the helicopter been shake tested in more than one cg ballast configuration, the need for considering some of the above would probably have been recognized.

FOCUSED PYLON EVALUATION

The focused pylon in the test helicopter consisted of four links attaching the transmission to the fuselage and four pylon springs restraining pylon motion and providing a means for tuning the pylon-fuselage dynamic system to isolate rotor hub shears and moments (see schematic, page 4). The four links vary the focal point through changes in the attachments on the fuselage deck (Figure 85, Appendix I). Elastomeric springs on each side of the transmission restrain it laterally. Similar springs (not visible in the figure) restrain it fore and aft through the torque restraint system in front of the pylon.

Analysis

The analysis used in predicting the optimum combination of focal point and spring rate is described in Reference 12. It is based on having two rigid bodies connected through a hinge with a torsional spring restraint about the hinge, as seen in Figure 68. The rotor is treated as a lumped mass. Pylon damping and aerodynamic effects are neglected.

The analysis calculated the loci of minimum fuselage responses to four-per-rev excitations as functions of focal point and torsional spring rate (Figure 69). With this established, the four-per-rev mode shapes of the pylon were calculated for the combinations of focal point and spring rate that were selected for evaluation in flight test. The results will be shown in a later section.

Flight Tests

The eight pylon configurations listed in Table VIII were evaluated in flight. The configurations included three focal points and various pylon-spring combinations at these focal points. The pylon configurations were evaluated at two rotor speeds (280 rpm and 295 rpm) and several flight conditions: hover, acceleration, deceleration, climb, left turn, right turn, and level flight from 60 to 130 knots.

The pylon configurations were evaluated against four criteria: pitch response of the fuselage, roll response of the fuselage, vertical response of the pilots' seats, and helicopter handling characteristics. The results

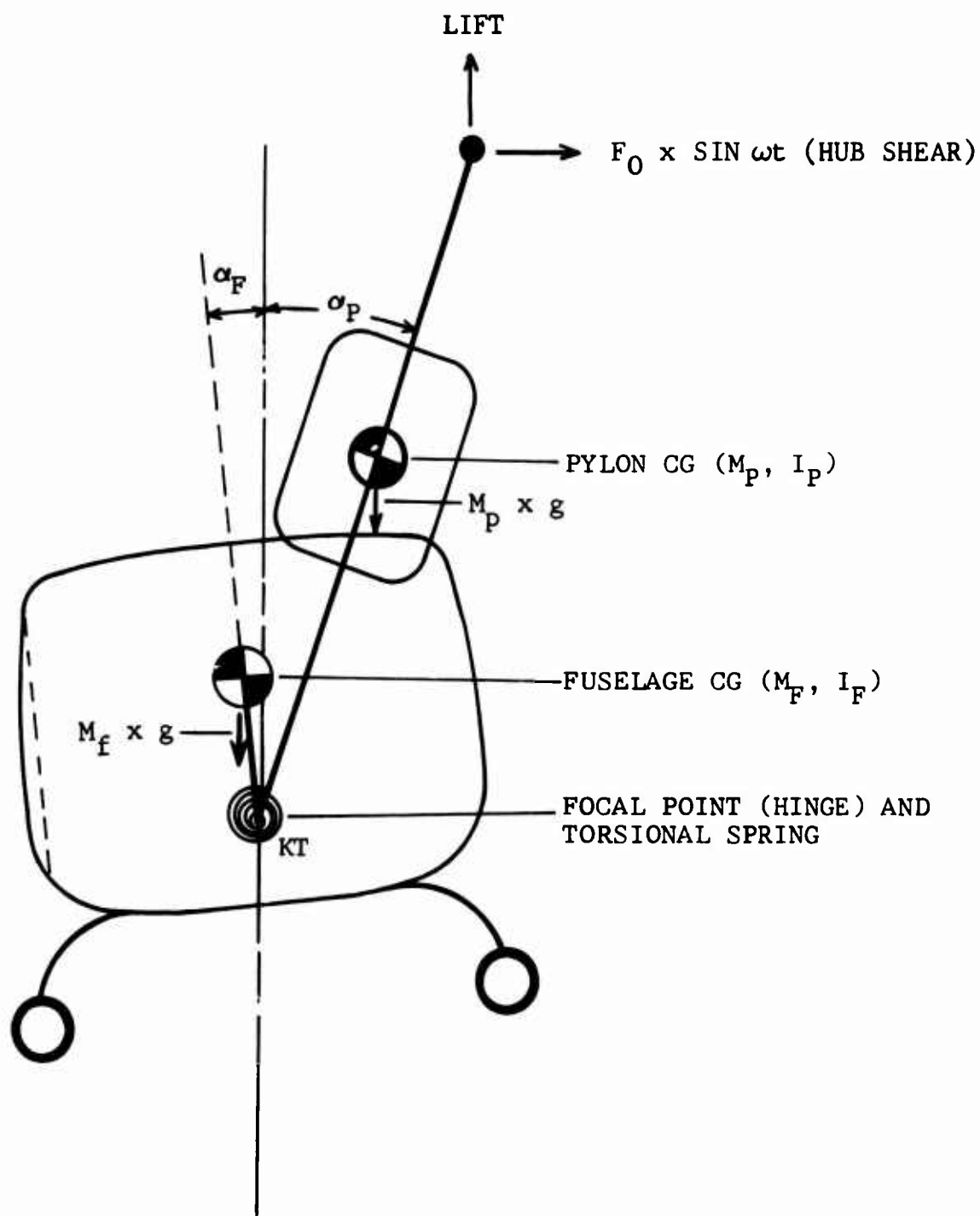


Figure 68. Rigid Body Analysis Model.

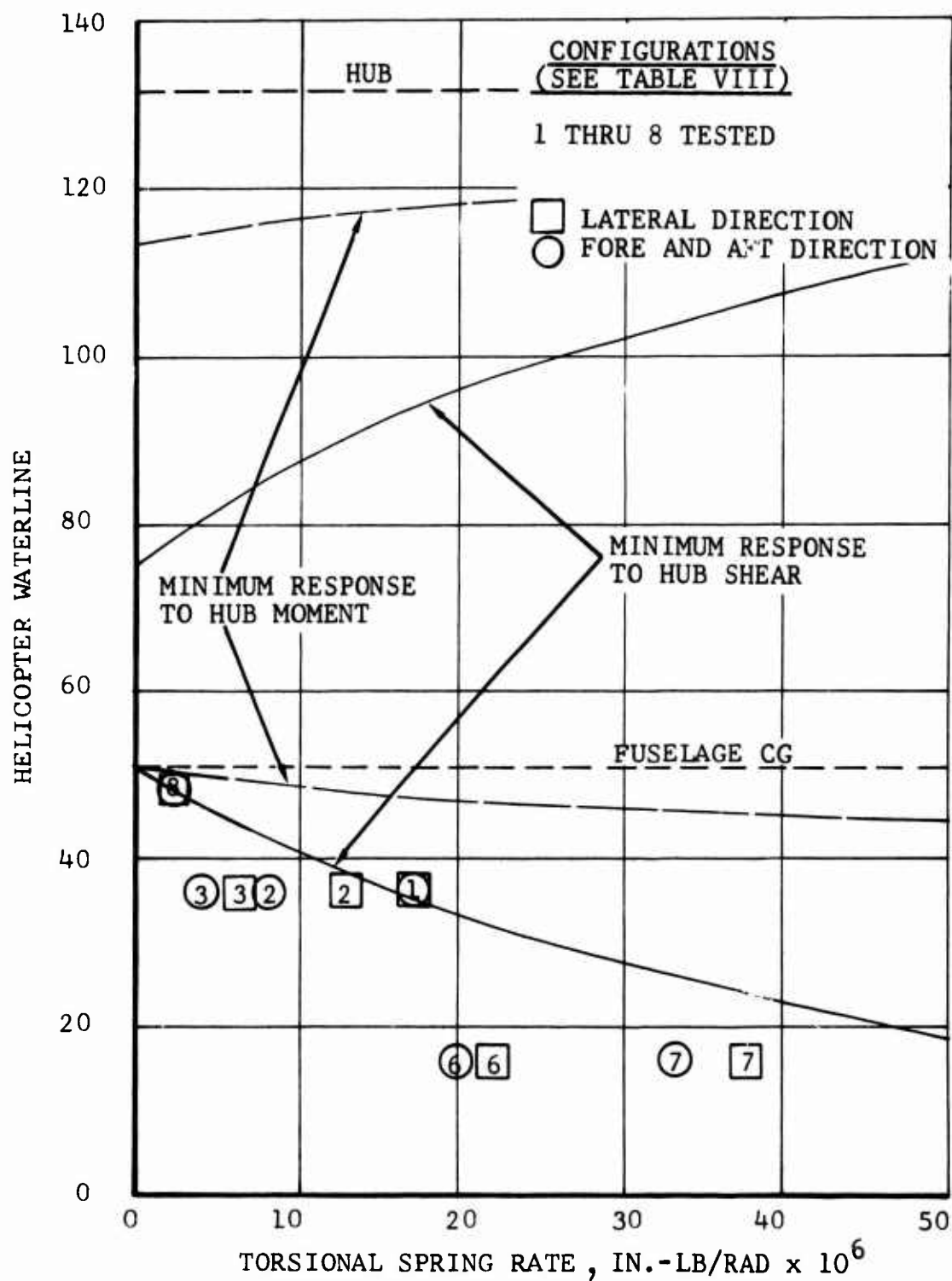


Figure 69. Test Configurations Compared to Theoretical 4/Rev Minimum Fuselage Response Locus.

TABLE VIII. FLIGHT TEST PYLON CONFIGURATIONS				
Configuration	Focal Point Waterline	Direction	Total Elastomer Mount Linear Spring Rate (lb/in.)	Equivalent Pylon Torsional Spring Rate (in.-lb/rad x 10 ⁶)
1	36 36	Fore & Aft Lateral	20000 20000	17.4 17.46
2	36 36	Fore & Aft Lateral	9000 15000	7.83 13.08
3	36 36	Fore & Aft Lateral	4500 7500	3.92 6.54
4	36 36	Fore & Aft Lateral	Rigid 20000	- 17.46
5	36 36	Fore & Aft Lateral	Rigid Rigid	- -
6	16 16	Fore & Aft Lateral	9000 9000	19.92 22.15
7	16 16	Fore & Aft Lateral	15000 15000	33.2 37.5
*8	48 48	Fore & Aft Lateral	20000 20000	7.19 6.19
*Handling characteristic unacceptable to pilot.				

are presented below for 280 main rotor rpm and 120 knots indicated airspeed. As a result of this evaluation, all subsequent contracted flight-test tasks were conducted with the focal point at WL 36, with two linear mounts of 10,000 pounds per inch each in the fore-and-aft direction, and with two linear mounts of 4,500 pounds per inch each in the lateral direction.

Fuselage Pitch Response

The four-per-rev mode shapes measured for the pylon configurations evaluated are shown in Figures 70 and 71 together with the NASTRAN computed rigid body mode shapes. The flight-test mode shapes represent the fore-and-aft responses of three accelerometers focused on the transmission and two accelerometers on the fuselage. The computed mode shapes were determined by applying a hub shear large enough to force the top of the mast of the rigid body model to respond at the same amplitude as the flight test hub responds in flight.

The measured mode shapes show very little fuselage pitching for any of the configurations tested. The effectiveness of the pylon system in isolating fore-and-aft four-per-rev hub motions was not related to the stiffness of the pylon mount or the location of the focal point.

The measured data also show that the angular motion between the pylon and fuselage is not about the intended focal point. Relatively low values of hub shears in the analytical model reproduced the measured hub accelerations. The magnitude of the fore-and-aft rotor forces was probably not large enough to cause the pylon to overcome the friction in the focus link bearings and the torque restraint tube bearings. Mast bending or mast bearing deflections and structural deflections of the transmission supports were apparently sufficient to isolate the relatively low four-per-rev rotor forces acting on the mast.

The system used in these tests would probably have functioned in the fore-and-aft direction if the rotor exciting forces and motions had been larger. A one-G acceleration of the hub at four per rev, which was typical, corresponds to displacements of less than ± 0.030 inch; see Figure 72. A system with bearings and joints is hardly appropriate for such small motions but did function satisfactorily in the lateral direction, which had less friction.

Fuselage Roll Response

The focused pylon had a significant effect on fuselage four-per-rev response in the lateral direction, as seen in

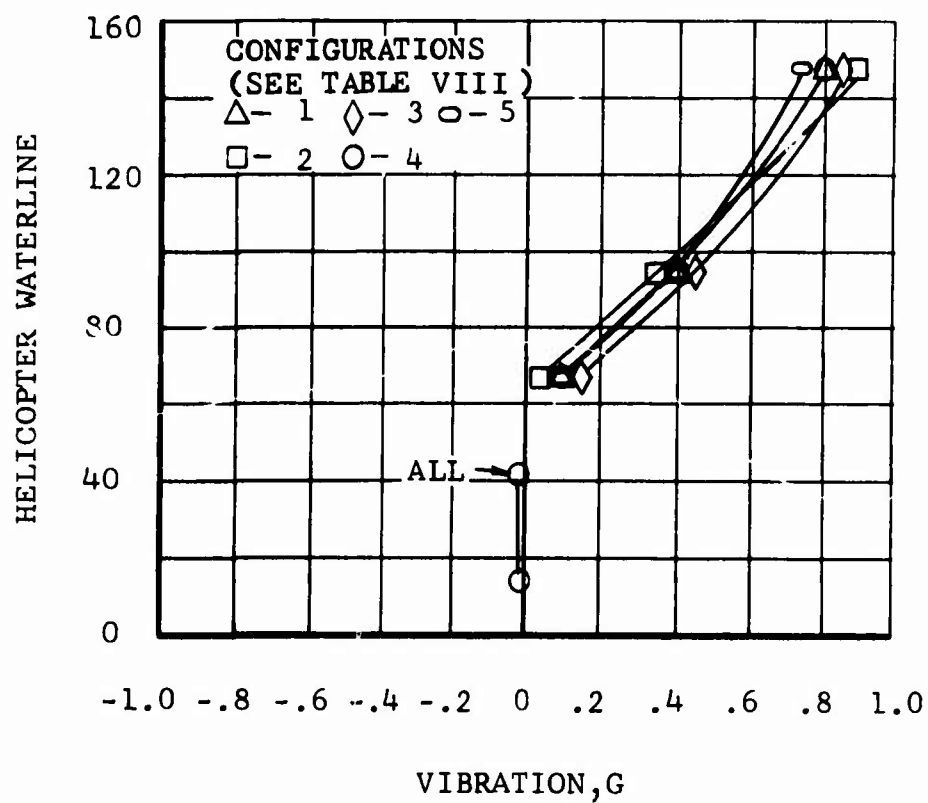


Figure 70. Pylon Fore and Aft 4/Rev Mode Shapes, Focused at WL 36, Flight Test Data.

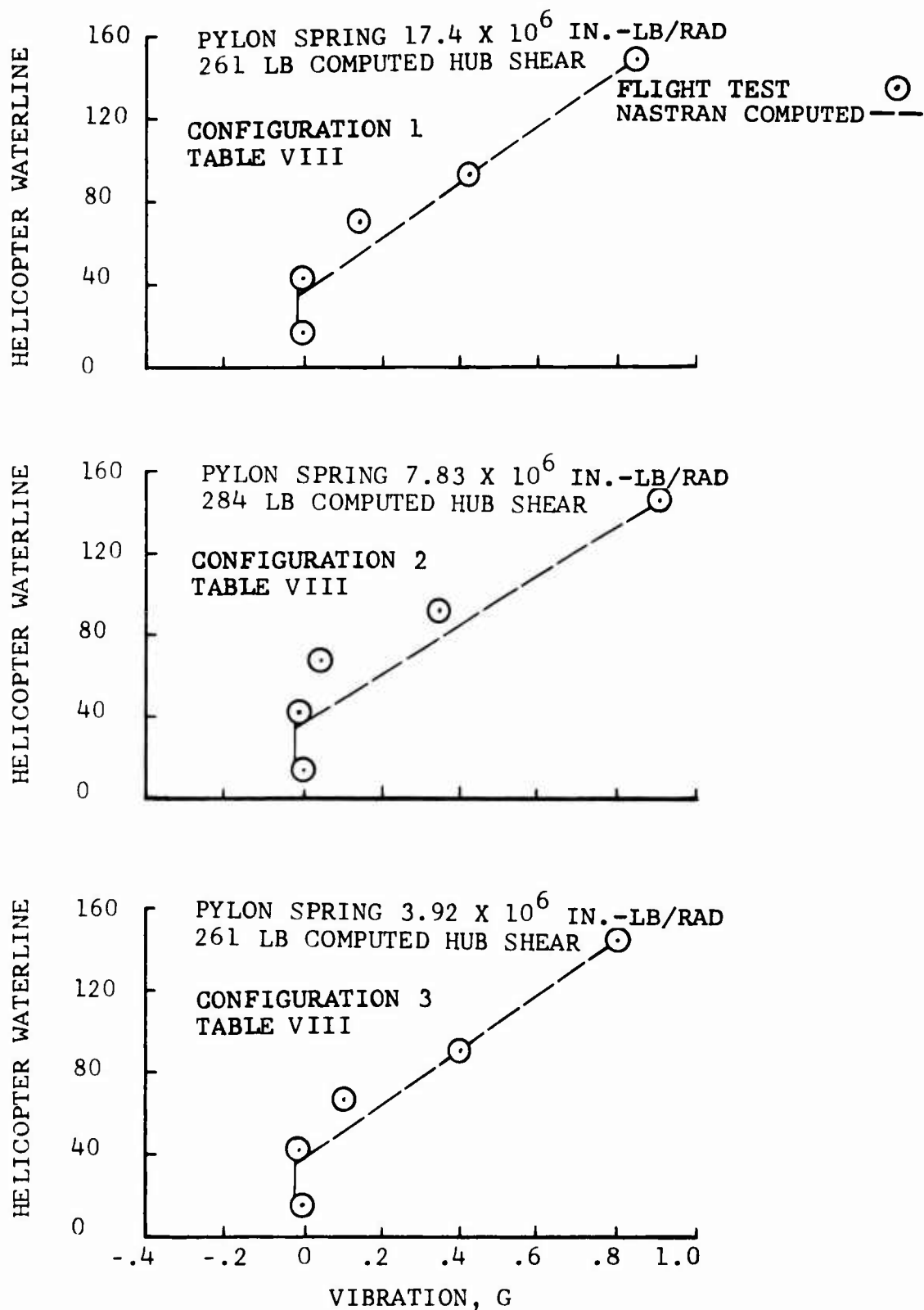
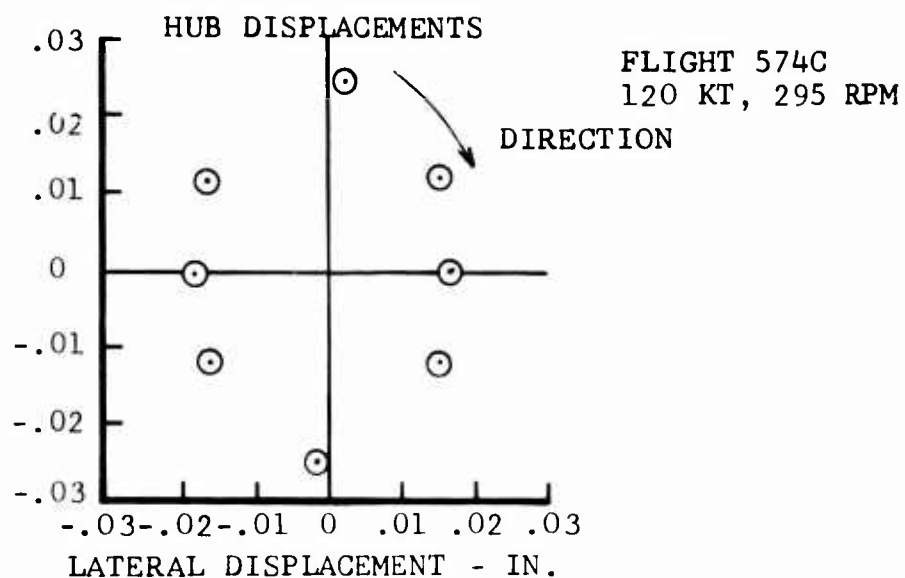


Figure 71. Computed and Measured Pylon Fore and Aft 4/Rev Mode Shapes, Focused at WL 36.

FORE AND AFT DISPLACEMENT, IN.



FORE AND AFT VIBRATION, G

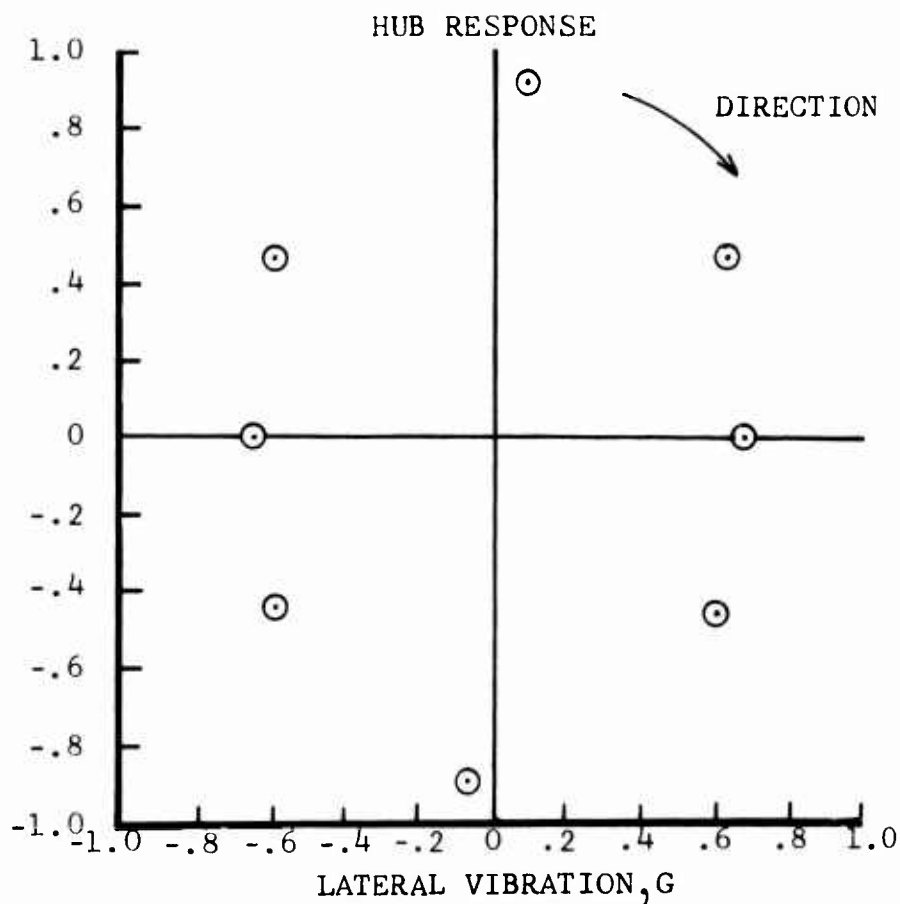


Figure 72. Typical 4/Rev Hub Vibration Displacement and Response in the Fixed System, Flight Test Data.

the lateral pylon mode shapes of Figures 73 and 74. Also presented in these figures are the computed rigid body mode shapes for the same configurations. The NASTRAN computed mode shapes were forced in the same manner as the fore-and-aft mode shapes. Like the fore-and-aft modes, the lateral modes involve some mast bending, but pylon motions in the lateral direction are essentially about the focus point. Changes in spring stiffness altered the fuselage response. As seen in Figure 74, the best roll isolation is achieved with a pylon spring rate range from 6 million to 13 million inch-pounds per radian. The analysis (Figure 69) predicted that optimum isolation for shear would be obtained with a spring rate of 15 million inch-pounds per radian with the focus at WL 36.

Vertical Response of Pilots' Seats

The vertical response of the pilots' seats was evaluated for each of the pylon configurations. These responses are summarized in Figure 75 as functions of the lateral pylon spring, since it appeared to have the greatest effect. As the figure shows, the softer the pylon spring, the lower the vertical response of the pilot's seat; the stiffer the pylon spring, the lower the response of the copilot's seat. The lowest average vertical response of the two seats falls in the center range of pylon springs evaluated with the pylon focused at WL 36. The best compromise between the vertical responses of the two seats occurs at a lateral pylon spring rate between 7 and 14 million inch-pounds per radian.

Helicopter Handling Characteristics

The helicopter handling characteristics were evaluated by considering the pilot's reaction to the various pylon configurations. The pilot noticed significant differences in the response of the helicopter to control inputs for the various pylon configurations, and was more sensitive to fore-and-aft changes in the pylon configuration than to lateral changes. The stiffest fore-and-aft pylon spring gave the best handling characteristics; the pylon configuration focused at WL 48 gave the worst handling characteristics because it felt too soft and was, therefore, considered to be unacceptable by the pilot.

Final Pylon Configuration

The final fore-and-aft pylon configuration was based primarily on handling characteristics. It had the stiffest pylon springs (17.4 million inch-pounds per radian) and was focused at WL 36.

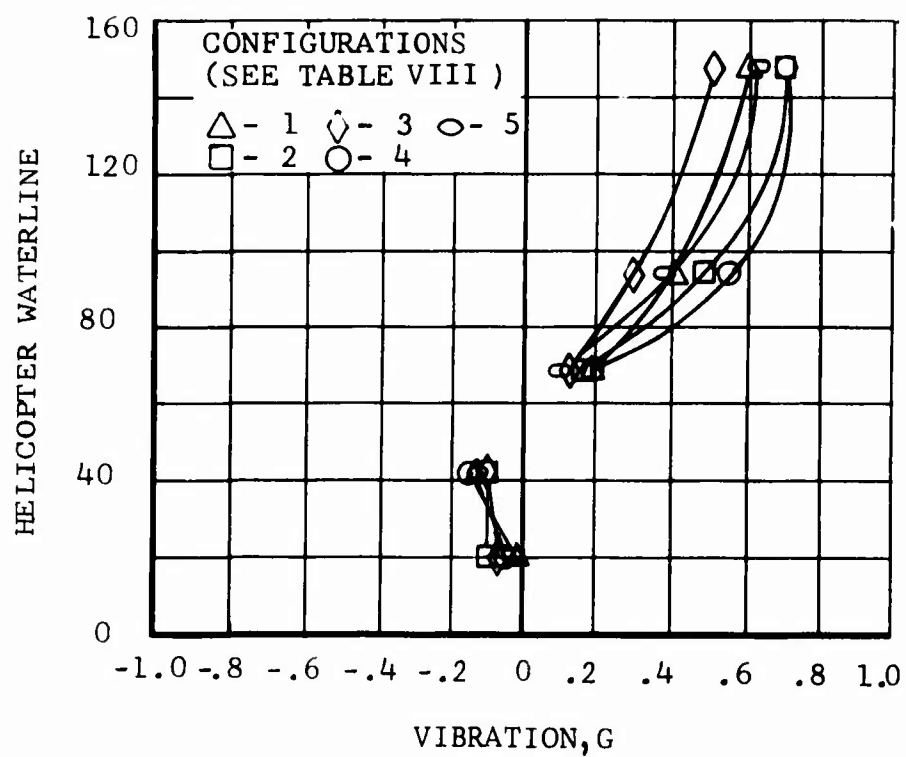


Figure 73. Pylon Lateral 4/Rev Mode Shapes, Focused at WL 36, Flight Test Data.

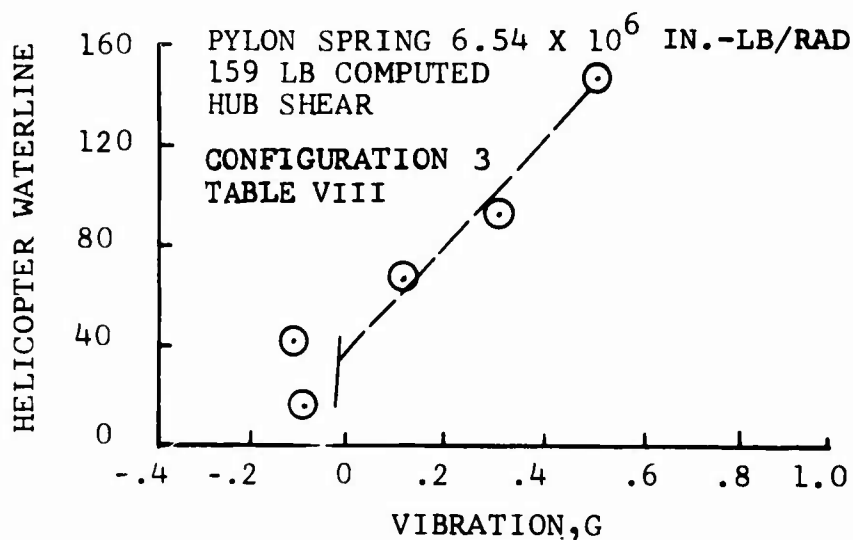
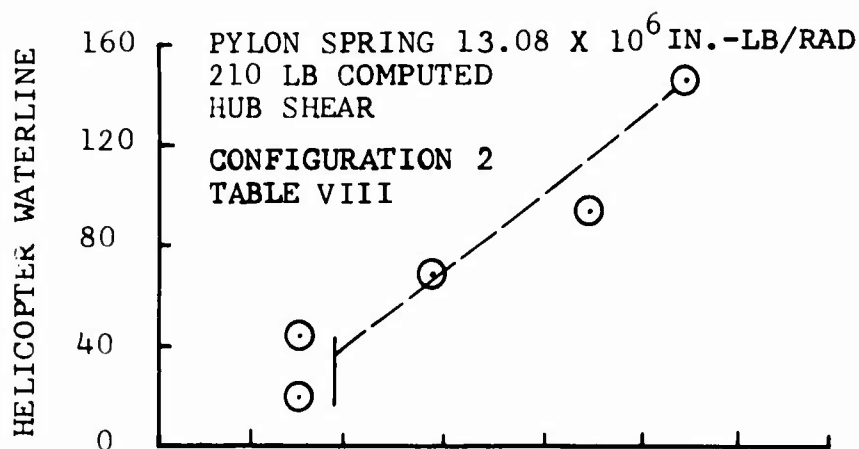
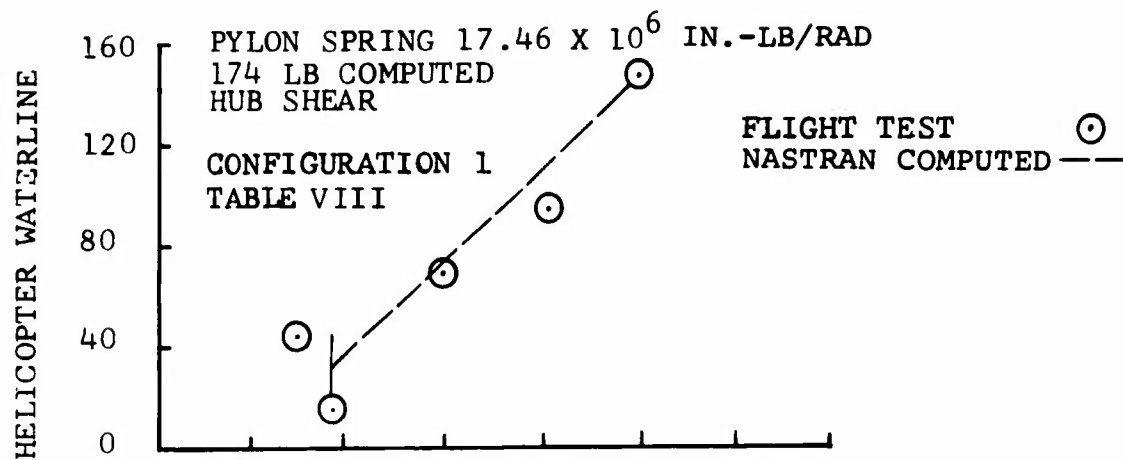


Figure 74. Computed and Measured Lateral 4/Rev Mode Shapes, Focused at WL 36.

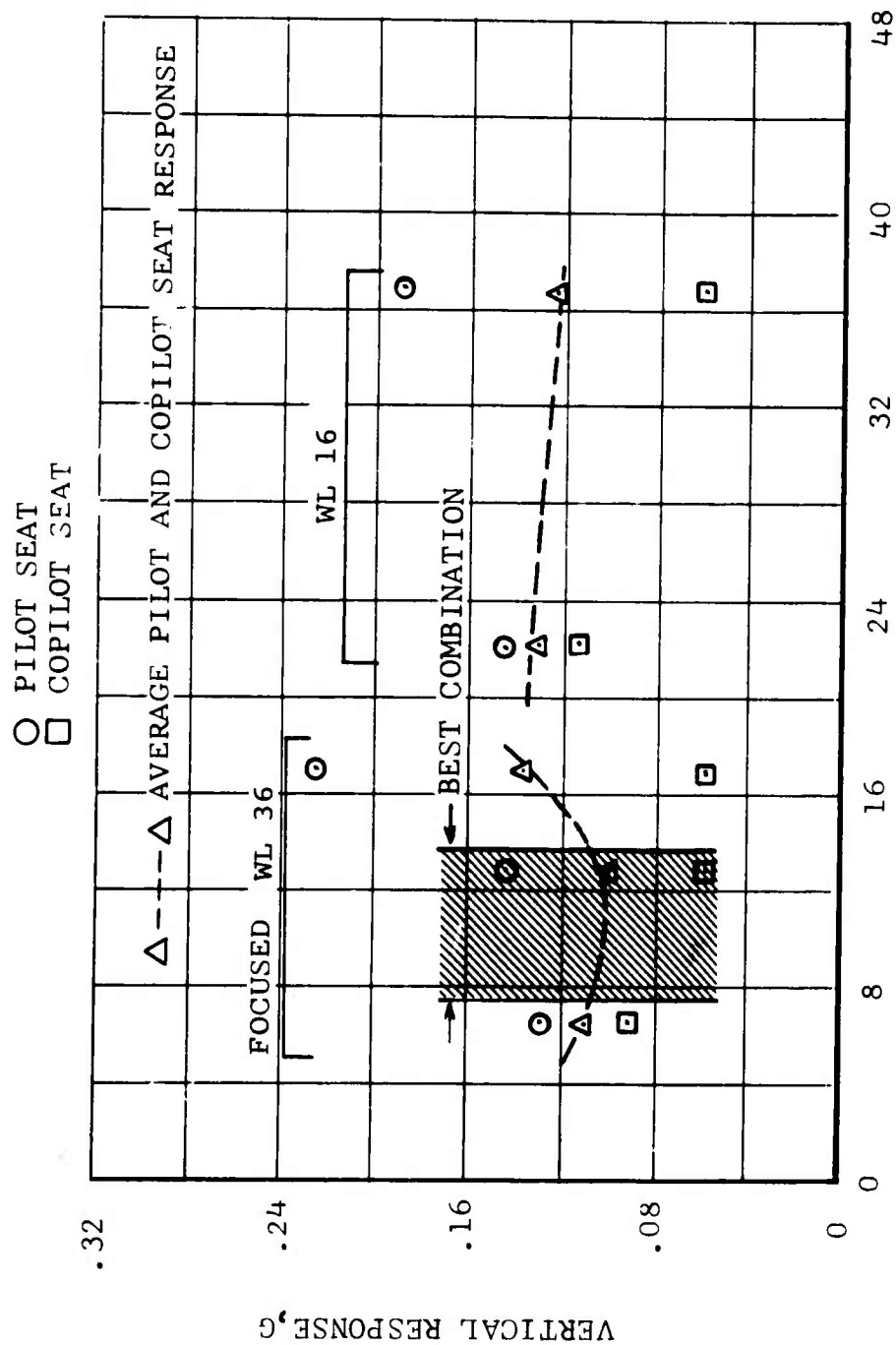


Figure 75. Effect of Pylon Focal Point Location and Spring Rate on Pilot and Copilot Seat Vertical Response at 120 Knots Airspeed, Flight Test Data.

The focused pylon was very effective for isolating lateral (roll) vibration. Therefore, the final lateral pylon configuration was based on all the criteria mentioned. The best tradeoff between the configurations was 7.85 million inch-pounds per radian of spring rate at WL 36.

SUMMARY OF TECHNICAL PROBLEM AREAS

Technical problems encountered during a research task can be of major benefit by identifying risk areas in future programs and/or by indicating the need for additional work. This section discusses difficulties encountered with the Model 609 rotor which are not explained in other sections of the report. Other technical problems encountered during the evaluation, but not rotor-related, are reported in the Flight Test Data Report, Reference 13. Table IX (page 128) contains a brief summary of problems with causes or reasons indicated, if known, and possible solutions offered whenever available.

MAIN ROTOR CLAMP SET

As mentioned in the section entitled Pilot Observations, one-per-rev vibrations sometimes occurred due to shifting of the rotor hub to mast clamp set, necessitating a retorquing. The clamp set replaced (in 1971) an automatic blade-folding device which had a similar but more pronounced problem. The one-per-rev vibrations occurred more frequently on the high-gross-weight and maneuver flights.

Figure 81 (Appendix I) shows the clamp set with its separate yokes and cone sets. The shifting of the rotor clamp set resulted from the many faying surfaces preventing a firm clamp-up and the differential bending or torsion in the separate yokes causing "unseating" or a slight loosening of the system. One way to avoid the problem would be to bolt the yokes together and use one set of splines to drive both pairs of blades. Then differential torsion between the rotor pairs would not transmit back through the clamp set.

LOAD DIFFERENCES BETWEEN UPPER AND LOWER BLADE PAIRS

The load level survey showed differences between the upper and the lower rotor blades. These differences became greater in maneuvers, with the lower blades having 15 percent higher loads than the upper blades. Faulty instrumentation was ruled out as the reason for the differences after a check of the calibrations showed the gages to be functioning properly.

There are two possible explanations for the observed differences in upper and lower rotor loads. One is that the vortex field from the upper rotor caused the higher blade loads in the lower rotor, and further studies using techniques such as schlieren flow visualization with models could check this hypothesis. The other is that air pressure caused the hollow blade (Figure 82, Appendix I) to change contour in flight. (See blade deformation discussion, below.)

POPPING OUT OF TRACK

Popping out of track of one or more blades was first encountered during the IR&D flights in 1971. It occurs at high advancing-tip Mach numbers. In 1971, there was a "deep" encounter producing one-per-rev vibrations of 1G amplitude at the pilot's station. During the 1972 flights, the onset of this phenomenon was mapped, as shown in Figure 76 and found to occur at an advancing-tip Mach number of .89. The pilots perceive the onset as increase in one-per-rev cabin vibrations to the ± 0.1 to $\pm 0.25G$ level. They also see changes in track with the help of an in-flight strobe tracker. Usually, one blade changes its track relative to the other three. Occasionally, changes in track are random, with the relative position of more than one blade changing.

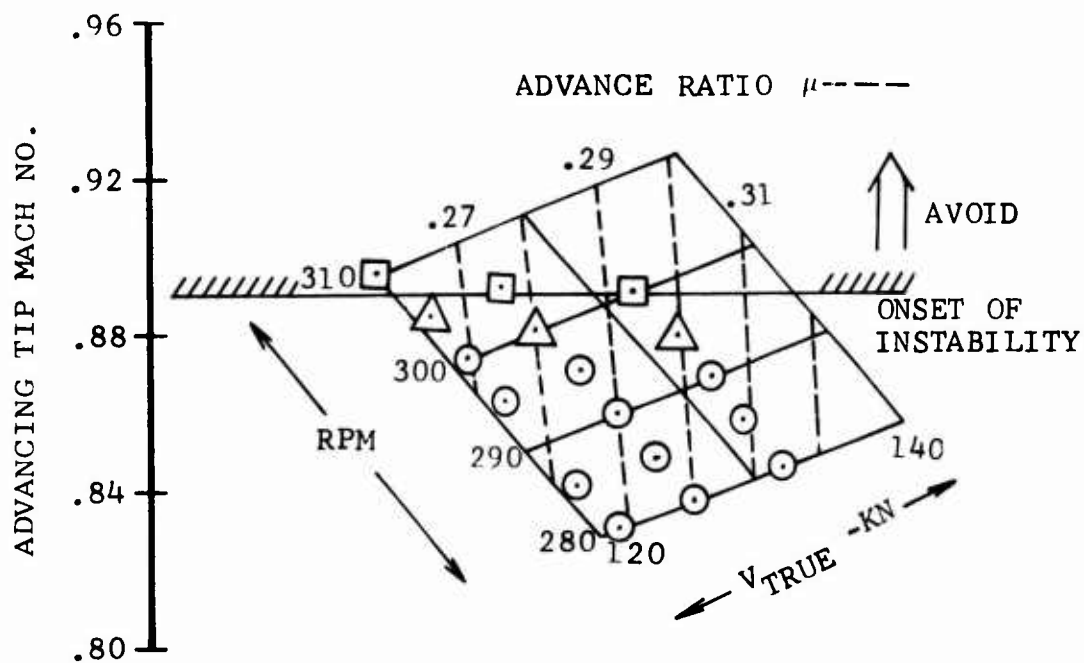
The primary cause of the out-of-track condition has been identified to be Mach number effects, rather than rpm, airspeed, or dynamic pressure. Higher dynamic pressures at the advancing tip were reached on warmer days (higher speed of sound), without any problem, than during the high Mach number flights on colder days. Furthermore, the observed out-of-track boundary shows that the problem is not a direct function of either rpm or airspeed.

The calculated angle-of-attack distribution of the rotor is shown in Figure 77 for the advancing blade at the onset of the out-of-track condition. The drag divergence Mach number is an indicator of the adverse aerodynamic effects associated with high Mach numbers, Reference 14. Figure 78 presents the areas of the rotor disc operating above the blade drag-divergence Mach number as a function of advancing-tip Mach number. The blade angle-of-attack calculations, along with the blade airfoil data, were used in determining these boundaries. The tips of the rotor blades are operating above drag divergence, when the Mach number of the advancing tip is 0.86 or higher.

Figure 79 presents measured blade torsional moments and pilot's seat vertical accelerations. There are large moment excursions on the advancing side of the rotor disc, with noticeable one-per-rev vibration levels. The moments are not the same for each blade; hence, blade dissimilarities coupled with large aerodynamic forces cause the out-of-track condition.

Following the flights in which the onset of the out of track was mapped (Figure 76), the rotor blades were modified to increase torsional stability. The tuning weights at the tips of the blades were replaced with heavier, reshaped weights which moved the cg of the blades forward. The rotor was then flown to an advancing tip Mach number of 0.94 before a change in track was observed. Since air turbulence can cause momentary changes in Mach number and angle of attack, a lower Mach number (0.92) was used as a safe limit. The out-of-track condition could be

- ◻ — OBJECTIONABLE 1/REV
- △ — NOTICEABLE 1/REV
- — LIGHT OR NO 1/REV

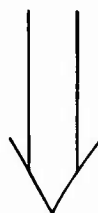


FLIGHT 579

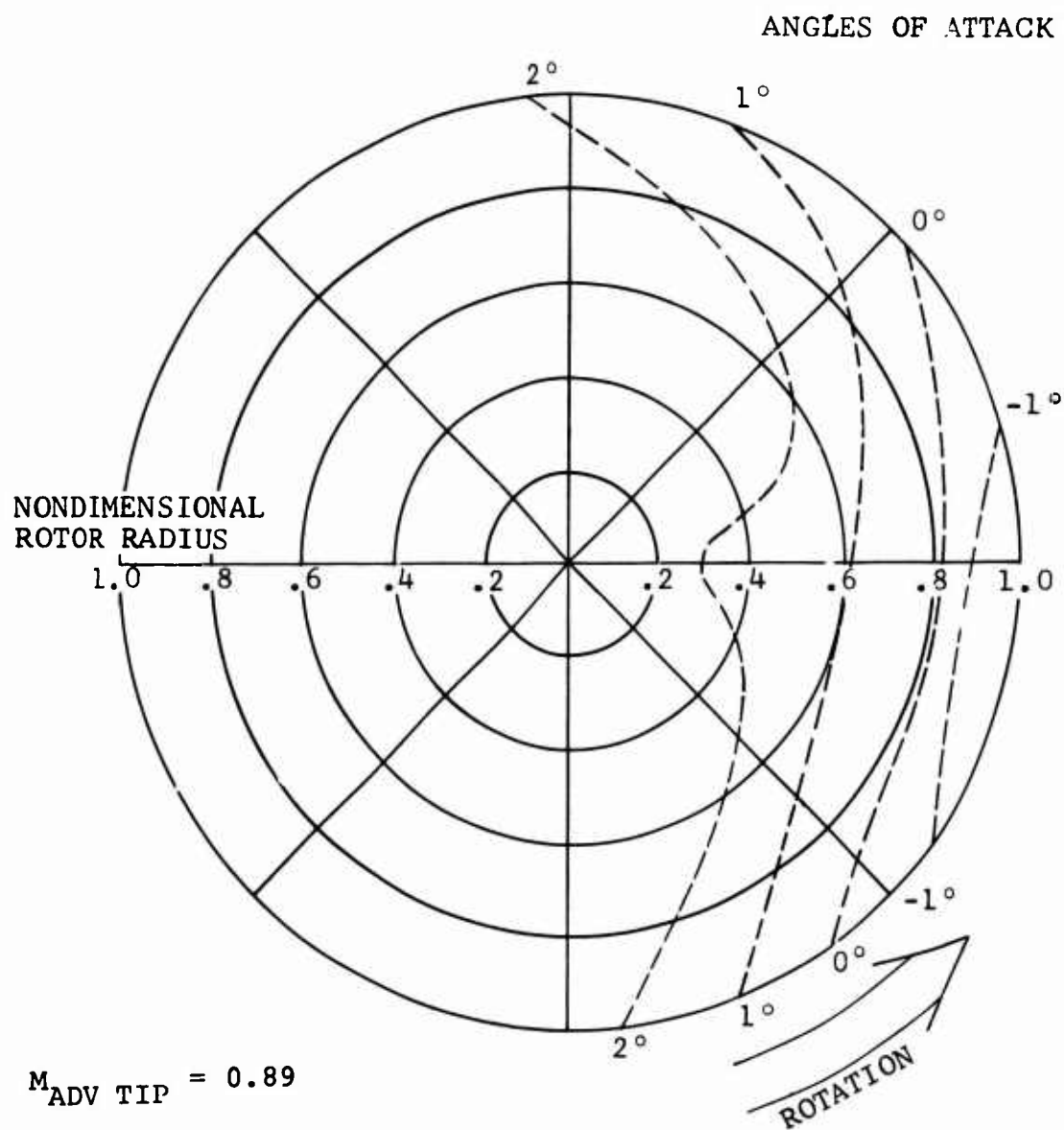
HIGH TIP MACH NO. INVESTIGATION

Figure 76. "Popping-Out-Of-Track" Boundary, Flight Test Data.

609 ROTOR
F-35 COMPUTED DATA



WIND



132 KTAS

Figure 77. Lines of Constant Angle of Attack.

609 ROTOR
F-35 COMPUTED DATA

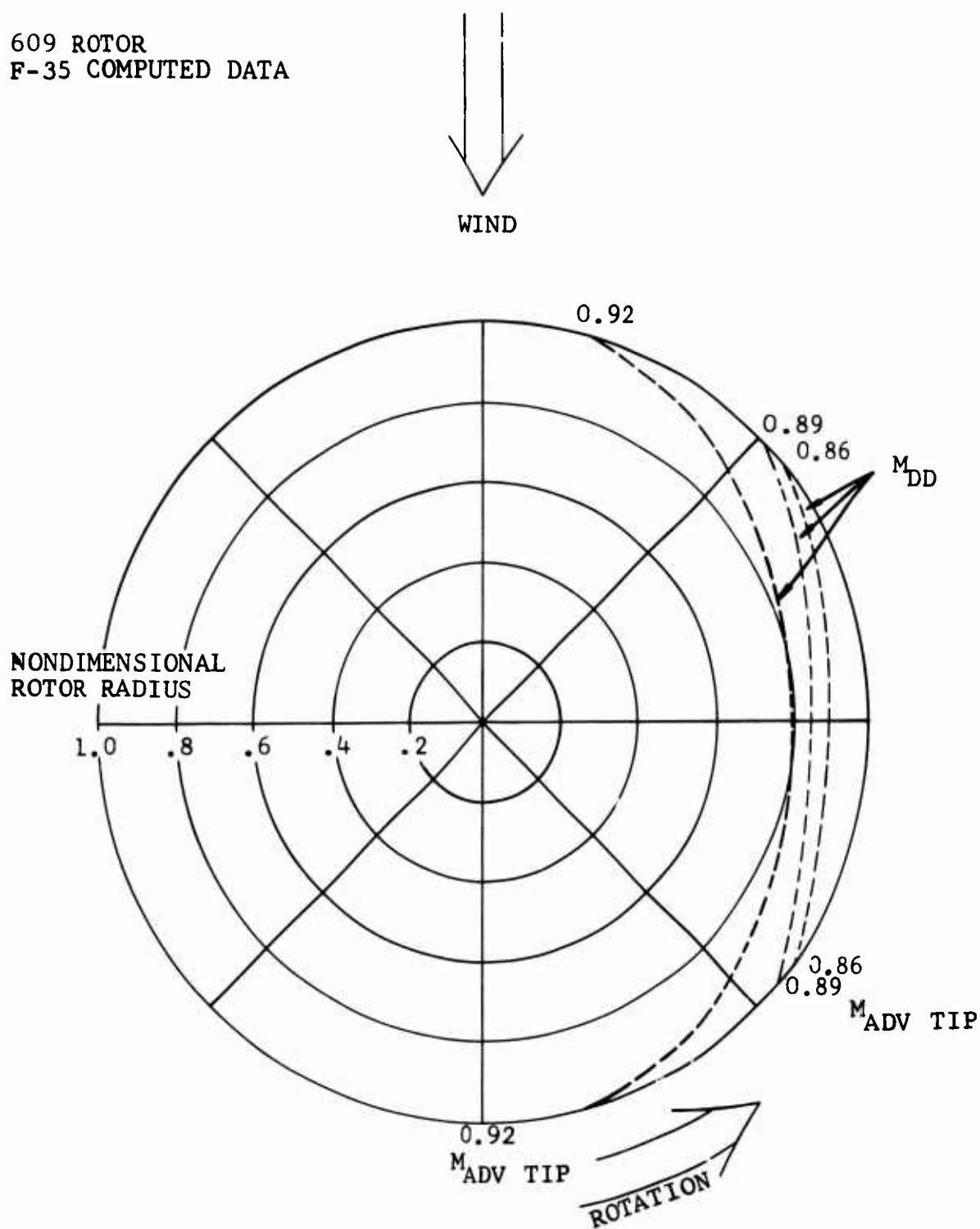
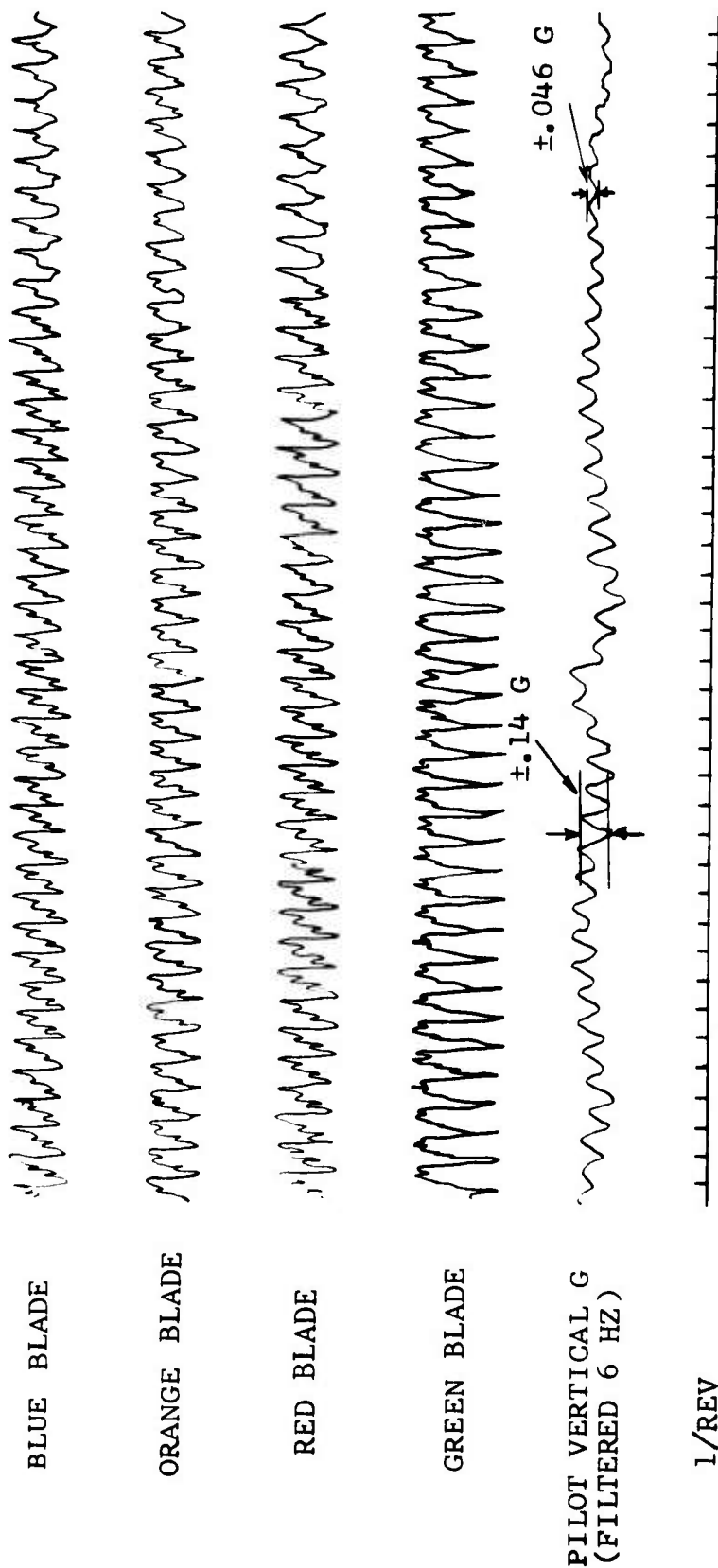


Figure 78. Mach Drag Divergence for Various $M_{Adv Tip}$.

BLADE TORSION GAGES STATION 243



$M_{ADV. TIP} = .87$
RPM = 289

$M_{ADV. TIP} = .89$
RPM = 300

DECREASING RPM →

HIGH TIP MACH NO. INVESTIGATION
FLIGHT TEST (FLIGHT 579A)
GROSS WEIGHT 10,500 LB
CTR. 609

Figure 79. Measured Blade Torsional Moments and Pilot Vertical Acceleration.

alleviated further, and higher advancing tip Mach numbers could be obtained if the torsional stability of the blades were increased and if the tip airfoils were changed to airfoils with better high-Mach-number characteristics.

PERMANENT DEFORMATIONS IN BLADE CONTOURS

Following the contractor evaluation flights and during the Government evaluation tests, the contour at the outboard end of one blade deformed in flight and caused extremely high one-per-rev vibrations. After the helicopter had landed, permanent creases in the upper and lower surfaces of the blade were visible.

An internal examination of the blade revealed that vent holes at the tip had become clogged. The skin panels (Figure 82, Appendix I) were bulged out, and the inner skins had buckled. A stiffening structure between the skin panels in the outboard three feet of the blade had detached from the lower skin panel. The internal pressure at the tip of a blade with plugged vents was calculated to be as much as five psi above ambient. Spread over the outboard two feet of blade, this pressure produces approximately 2500 pounds force, spreading the skins apart. This is apparently what bulged the contour. A positive venting system or nonhollow blade construction would eliminate the problem. The remaining blades were inspected internally with a borescope, and two blades were found to have unbonded stiffening structure.

Either the bulged blade or one of the blades with the unbonded stiffening structure was flown during the contracted tests. These discrepancies could also account for the observed differences, discussed above, between the loads in the upper and lower rotor and for the sensitivity of this rotor to the popped-out-of-track condition.

BLADE TRACKING

The elimination of one-per-rev vertical vibrations from a multi-bladed rotor can be a time-consuming process of making trial and error adjustments to pitch links or blade tabs to equalize all blades aerodynamically throughout the helicopter's velocity envelope. During the Model 609 test program, a Strobex Tracker was used for this process. Reflective coded targets were placed on each blade tip and observed visually when "stopped" by the powerful light that was synchronized with the rotor speed. This relatively small and easily portable unit allows tracking in forward flight as well as on the ground, and works well even in bright sunlight.

During the test program, the behavior of each rotor blade was monitored visually throughout the rpm and speed range. There were significant differences between blades because of small

differences in twist or contour causing blade "crossovers" in certain speed regimes. The visual track mapping technique was used to make up the best combinations (pairings) of individual blades with no time lost to random experimentation.

The 3-inch vertical separation of upper and lower rotors made tracking a little more difficult than it would have been with all four blades in one plane, but 2-per-rev fuselage vibrations were a good indication of mismatches between upper and lower blade sets.

TABLE IX. SUMMARY OF TECHNICAL PROBLEMS ENCOUNTERED DURING THE 609 FLEXBEAM ROTOR PROGRAM

Problem	Cause/Reason	Comment/Solution/ Suggestion	See Page
Calculated hovering performance compares poorly to measurements.	(a) Performance Unequal thrusts of the two blade pairs were not modeled, and use of blade element momentum theory is optimistic.	Use free wake analysis for hover calculation and investigate blade pair separation effects on performance.	16
High gust sensitivity.	(b) Handling Qualities Inherent in rigid type rotors. Sensitivity increases with hub restraint.	SCAS was effective in reducing gust response.	10, 21
High control sensitivity at high speeds.	Same as above.	Force feel system adequately managed the control sensitivity.	9, 43
Blade angles did not correspond to stick inputs for steps or pulses.	Elasticity in control system and pylon coupling.	Measured blade angles at the rotor were used for analysis and correlation when exactness was needed.	-

TABLE IX. Continued		
Problem	Cause/Reason	Comment/Solution/ Suggestion
Permanent blade deformations occurred.	(c) Blade and Rotor Blade vent holes became clogged, and internal pressure loads adding to normal forces and moments caused the deformation.	Positive venting system or nonhollow blade construction.
Blades would "pop" out-of-track at high forward speeds, causing large 1/rev vibrations in the helicopter.	High tip Mach numbers coupled with blade dissimilarities, torsional flexibility, and contour flexibility.	Increase blade torsional stability, solid core instead of shell blade construction for contour stability, and use airfoils at the blade tip that have good moment characteristics at high Mach numbers.
Maneuvers limited by 1/rev beam and chord loads in yoke and 1/rev chord loads in the blade.	High amplification of 1/rev aerodynamic chord loads combined with flapping and Coriolis moments.	Use some type of elevator system feedback during maneuvers to reduce rotor flapping and accompanying Coriolis moments. Conceptual changes in the rotor design are required to reduce the high 1/rev amplification.

126

10, 121

64

TABLE IX. Continued

Problem	Cause/Reason	Comment/Solution/ Suggestion	See Page
(c) Blade and Rotor - Continued			
High yoke stresses in autorotation landings.	High flapping after initial ground contact.	After tail skid contact it is normal to use both cyclic and collective to cushion main gear contact, but the pilot has no indication of when he is using too much cyclic.	92
1/rev vibrations would occur in the ship during high gross weight and/or maneuver flights.	Slight "unseating" of the main rotor retention system.	Bolt the yokes together and use one set of splines to drive both pairs of blades.	11, 120
Load differences between the instrumented blades. The lower rotor (orange blade) loads were up to 15 percent higher than the upper rotor (red blade) loads.	Vortex field from the upper rotor causes the higher loads in the lower rotor or airfoil contour changed in flight and differing aerodynamic forces caused the different loads.	Investigate blade separation effects. Schlieren flow visualization could be used on models.	120
Initial difficulty in blade tracking.	Used "flag," difficult to determine from ground runs whether to adjust blade tab or pitch.	Strobe tracker allowed in-flight observations and thereby allowed relatively quick tracking of all four blades.	126

TABLE IX. Continued

Problem	Cause/Reason	Comment/Solution/ Suggestion	See Page
	(d) Fuselage Vibration		
Increased 4/rev vibration in maneuvers.	Increased out-of-plane blade response in third symmetric beam mode.	Some increase in vibrations with load factor is desirable. Relocation of the third symmetric beam mode might be effective in reducing vibration. However, the increased 4/rev appears to be due to increased aerodynamic excitation.	100, 101
Increased 4/rev vibration in transition.	Increased out-of-plane rotor response at 4/rev and some increased coupled in-plane and out-of-plane response at 3/rev.	Vortex interference is probable cause. More investigation is recommended in this area.	100, 101
Insensitivity to pylon spring rate changes in the fore and aft direction.	Friction in the focus links and pylon torque restraint system prevented the small pylon deflections required at 4/rev.	The use of elastic elements in lieu of bearings would avoid this and the next problem.	111

TABLE IX. Concluded			
Problem	Cause/Reason	Comment/Solution/ Suggestion	See Page
(d) Fuselage Vibration - Concluded			
Increase in 4/rev vibration in all flight regimes midway through the test program.	Bearing became unstaked in the left front pylon focus link.	Fuselage vibrations were lower after the link was replaced. Since angular pylon deflections are so small, any looseness in joints significantly alters dynamic response.	11
Initial fuselage mode shape analyses were inconsistent. Reduced data showed unexplained phase shifts among the accelerometers.	Accelerometer data were recorded on different channels on the magnetic tape system. Different type analog filters were used to reduce the data on the different channels which introduced the phase shifts into the data.	The same filters were used to reduce the accelerometer data when used for mode shape analysis.	-

CONCLUSIONS

The conclusions in this section are in the order in which the topics were first discussed. Conclusions are separated into those pertaining to computer correlation and those resulting from flight test.

PERFORMANCE

C-81 Computer Correlation

- The computed forward flight performance is very sensitive to changes in the blade drag data. After drag input values were adjusted, the performance of the test aircraft correlated well with that predicted by means of computer program C-81.
- Predicted hover performance of the test aircraft correlated poorly with measured data.

HANDLING QUALITIES

Flight Test

- The helicopter was statically and dynamically stable in all flight conditions, with the overall handling qualities good to excellent.
- High control sensitivity at high speeds was managed adequately with the aid of a force feel system.
- The pilots commented on high gust sensitivity but the use of SCAS alleviated the problem.

C-81 Computer Correlation

- Correlation between measured handling qualities and those predicted by computer program C-81 was good.

FUSELAGE VIBRATIONS

Flight Test

- Vibrations were primarily four-per-rev and generally of a low enough amplitude to give the pilot and copilot a comfortable ride.

NASTRAN Computer Correlation

- The focused pylon generally behaved as predicted in the lateral direction. Friction in the system prevented the pylon from making the small deflections it should have made at four-per-rev in the fore-and-aft direction.
- Correlation between measured fuselage vibrations and those resulting from NASTRAN calculations was poor.

ROTOR LOADS IN LEVEL FLIGHT AND MANEUVERS

Flight Test

- Maneuvering above 1.3 G's at high gross weight (14,000 pounds) and high speed (150 knots) was precluded by loads in the yoke and the inboard section of the blade.
- High loads in maneuvers were caused by the high amplification of chordwise one-per-rev aerodynamic forces and by Coriolis moments resulting from flapping and coning.
- At high advancing blade tip Mach numbers, the blade track changed suddenly; this was caused by blade contour flexibility, torsional flexibility, and blade dissimilarities.
- The rotor was stable in all test conditions.
- Level flight blade and yoke loads were within endurance limits. There were no resonant conditions in the blades within the operating envelope.

C-81 Computer Correlation

- Forward flight chord moment correlation is good above $\mu = .15$. Beam moment correlation is good outboard of the flexure. Beam moment correlation in the flexure is poor. Errors in the computations that cause slight differences in flapping (e.g., different trim attitudes) also cause poor beam moment correlation. Additionally, more accurate modeling of the flexure would improve the correlation.
- Prediction of loads in hover is poor.
- The correlation of loads during the maneuver is fair, but further work is needed in this area.

FATIGUE LIFE ANALYSIS

Flight Test

- The rotor system meets the fatigue life requirements of the utility helicopter flight spectrum (defined in Table III) with the following exceptions:
 1. Flight procedures must be developed for avoiding high rotor yoke stresses during autorotation landings.
 2. The high-speed, high-gross-weight maneuvers must be deleted from the flight envelope.
- With the above qualifications, the rotor system would have over 2000 hours fatigue life.

REFERENCES

1. Sonneborn, Walter G. O., HIGH MACH NUMBER/HIGH ADVANCE RATIO FLIGHT TEST PROGRAM WITH THE HIGH-PERFORMANCE UH-1 COMPOUND HELICOPTER, Bell Helicopter Company, Fort Worth, Texas; USAAVLABS Technical Report 71-2, U. S. Army Aviation Materiel Laboratories, Fort Eustis, Virginia, February 1971, AD 881741.
2. Bennett, R. L., ROTOR SYSTEM DESIGN AND EVALUATION USING A GENERAL PURPOSE HELICOPTER FLIGHT SIMULATION PROGRAM, in AGARD Conference Proceedings 122, Specialists Meeting on Helicopter Rotor Loads Prediction Methods, AGARD CPP-122, August 1973.
3. Dooley, L. W., and Van Gaasbeek, J. R., DIGITAL COMPUTER SIMULATION OF A HINGELESS FLEXBEAM ROTOR SYSTEM, Bell Helicopter Company Report No. 299-099-573, Bell Helicopter Company, Fort Worth, Texas, October 1973.
4. Biggers, J. C., McCloud, J. L., III, and Patterakis, P., WIND TUNNEL TESTS OF TWO FULL-SCALE HELICOPTER FUSELAGES, NASA TN D-1548, Ames Research Center, Moffett Field, California, October 1962.
5. Griffin, T. F., and Lamm, R. E., TWO-DIMENSIONAL WIND TUNNEL TESTS OF NINE BELL AIRFOIL SECTIONS AT SUB-SONIC SPEEDS, United Aircraft Research Laboratories; Report F930597-1, United Aircraft Research Laboratories, East Hartford, Connecticut, December 1967.
6. Gustafson, F. B., and Myers, G. C., Jr., STALLING OF HELICOPTER BLADES, NACA TN 1083, Langley Aeronautical Laboratory, Langley Field, Virginia, April 1946.
7. Wells, C. D., and Wood, T. L., MANEUVERABILITY - THEORY AND APPLICATION, Paper presented at the 28th Annual National Forum of the American Helicopter Society, Washington, D. C., May 1972.
8. Jenkins, J. T., Jr., and Deal, P. L., INVESTIGATION OF LEVEL FLIGHT AND MANEUVERING CHARACTERISTICS OF A HINGELESS ROTOR COMPOUND HELICOPTER, NASA TN D-5602, Langley Research Center, Langley Station, Hampton, Virginia, January 1970.
9. Duhon, J. M., Harvey, K. W., and Blankenship, B. L., COMPUTER FLIGHT TESTING OF ROTORCRAFT, Journal of the American Helicopter Society, Vol. 10, No. 4, October 1965.

10. AERONAUTICAL REQUIREMENTS, STRUCTURAL DESIGN REQUIREMENTS (HELICOPTERS) AR-56, Naval Air Systems Command, Department of the Navy, February 1970.
11. McCormick, C. W., NASTRAN USER'S MANUAL, NASA Report SP-222(01), MacNeal-Schwendler Corporation, Los Angeles, California, June 1972.
12. Balke, R. W., ANALYSIS OF THE RIGID BODY PITCH AND ROLL MODES OF THE HELICOPTER IN FLIGHT, Bell Helicopter Company Report No. 599-114-901, Bell Helicopter Company, Fort Worth, Texas, May 1968.
13. Blackman, S., FLIGHT TEST DATA REPORT ON THE MODEL 609 HINGELESS FLEXBEAM ROTOR SYSTEM EVALUATION, Bell Helicopter Company Report No. 299-099-572, Bell Helicopter Company, Fort Worth, Texas, September 1973.
14. Nitzberg, G. E., and Crandall, S., A STUDY OF FLOW CHANGES ASSOCIATED WITH AIRFOIL SECTION DRAG RISE AT SUPERCRITICAL SPEEDS, NACA TN 1813, Ames Aeronautical Laboratory, Moffett Field, California, February 1949.
15. Charles, B. D., and Tanner, W. H., WIND TUNNEL INVESTIGATION OF SEMIRIGID FULL-SCALE ROTORS OPERATING AT HIGH ADVANCE RATIOS, Bell Helicopter Company, Fort Worth, Texas; USAAVLABS Technical Report 69-2, U. S. Army Aviation Materiel Laboratories, Fort Eustis, Virginia, January 1969, AD 684396.
16. Waldrup, H., and Childs, J., FATIGUE DESIGN HANDBOOK, Bell Helicopter Company Report No. 299-099-076, Bell Helicopter Company, Fort Worth, Texas, February 1967.
17. Roark, R. J., FORMULAS FOR STRESS AND STRAIN, New York, McGraw-Hill Book Company, Inc., 1965.
18. Orr, P. M., FATIGUE LIFE SUBSTANTIATION OF THE MAIN ROTOR, TAIL ROTOR, AND CONTROLS COMPONENTS OF THE 204B HELICOPTER, Bell Helicopter Company Report No. 204-099-226, Bell Helicopter Company, Fort Worth, Texas, December 1962.

APPENDIX I TEST VEHICLE AND ROTOR

MAIN ROTOR SYSTEM

The Model 609 is a hingeless flexbeam rotor. Its inboard area is shown in Figure 80. The hub has two titanium flexbeam yokes individually mounted to the mast. (Mounting details are shown in Figure 81.) The steel spindles are mounted in needle bearings for feathering freedom. Wire straps carry the centrifugal load.

The blades are of panel construction, with 301 1/2-hard stainless steel skins (Figure 82). They have inboard doublers for stiffness and strength, and are retained in the grips by two bolts (per blade) arranged in the chordwise direction.

For purposes of simplified mathematical modeling, the 609 flexbeam rotor can be represented as a flapwise articulated rotor with rigid blades. The equivalent hinge offset of such an articulated rotor produces a hub moment per degree flapping equal to the moment produced by the flexbeam rotor. Define flapping in the hingeless rotor as the angle between a line from the centerline of the hub to 75 percent radius and a perpendicular to the mast. Then, the equivalent flapping hinge offset (for the articulated rotor) is located at 5 percent radius. The hub moment is approximately 1920 foot-pounds/degree per blade. For control power calculations, the mast and pylon have to be accounted for separately.

The dimensions of the main rotor, tail rotor, and aircraft are listed in Table X. The dimensions, travels, and riggings of the control system are given in Table XI and Figure 83.

ENGINE AND TRANSMISSION

A Lycoming T55-L-7B or -7C turboshaft engine, with a normal rated power of 2400 shp, drives the main and tail rotors. The engine is fuel-flow limited to 2250 shp.

The transmission is a development model, designated Model 583. It is rated at 1680 hp at 6300 input shaft rpm for continuous operation, and 2000 hp at the same input rpm for five minutes. Table XII gives the speeds of its shafts.

FOCUSED PYLON

An overall view of the rotor and pylon system is shown in Figure 84. The pylon is supported by four links that can be focused at various mast stations and restrained by spring and lever arrangements. The torsional and longitudinal restraints are two forward-facing links which are attached to fulcrums. The fulcrums are connected by a torque tube for the torsional restraint and connect to springs for the longitudinal restraint. Lateral pylon motion is restrained by two lateral links connected to springs. Figure 85 shows a closeup of the pylon and lateral restraint link (also see schematic, page 4).

FLIGHT CONTROL SYSTEMS

The main rotor is controlled by collective and cyclic pitch controls with the travel ranges as given in Table XI. The control sticks and pedals are arranged as in a UH-1 helicopter. The elevator settings can be changed $\pm 2.0^\circ$ about the initial trim position by an electric actuator. A meter displays the trim position to the pilot. The SCAS and force feel system are described in the next sections.

STABILITY AND CONTROL AUGMENTATION SYSTEM (SCAS)

A three-axis SCAS allows the response, sensitivity, and damping to be tailored for the desired handling qualities, as well as decreasing the influence of external disturbances and cross-coupling between axes. SCAS authority is limited to ± 7.5 percent of longitudinal, ± 7.5 percent of lateral, and ± 10 percent of directional control. In the event of an electrical or hydraulic failure, or when the system is turned off, the actuators slowly center and lock.

FORCE-FEEL SYSTEM

The electric-hydraulic cyclic force feel system generates artificial stick feel and trims the stick. It commands lateral stick force gradient as a function of airspeed, and longitudinal stick force gradient as a function of airspeed and pitch rate. Different force gradients can be selected for the lateral and longitudinal axes. These are shown in Figure 86.

Figure 87 shows the pitch rate portion of the longitudinal stick force generated when the pitch rate gain is adjusted to maximum and the airspeed gradient is set to the minimum position. The total longitudinal stick force is a combination of the gradient produced by the pitch rate input and the gradient produced by airspeed.

Also controlled by airspeed are the stick trim rates, as shown in Figure 88. The variation of gradient and trim rate with airspeed allows the helicopter to have a light gradient and fast trim rate at hover and low speed, and a firm, positive maneuvering gradient and slower trim rate at higher speeds.

TABLE X. DIMENSIONAL DATA

Aircraft Weight

Maximum Gross Weight	14,170 lb
Minimum Gross Weight	10,500 lb

Aircraft Inertias

Nominal Gross Weight of 12,000 lb

I _{YY} (Pitch)	18,500 slug-ft ²
I _{XX} (Roll)	4,500 slug-ft ²
I _{ZZ} (Yaw)	12,500 slug-ft ²
I _{XZ}	1,050 slug-ft ²

Engine

Mfg. Number	T55-L7B/-7C
Normal Rated Power	2250 HP

Main Rotor System

Type	Flexbeam Hingeless
Number of Blades	4
Rotor Diameter	48.3 ft
Rotor Disc Area	1833 ft ²
Disc Loading at Minimum Weight	5.73 lb/ft ²
Disc Loading at Maximum Weight	7.73 lb/ft ²
Rotor Solidity	0.092
Airfoil Section	
Inboard	NACA 64 x 18 Mod
Tip	NACA 0008 Drooped Mod
Blade Chord	21.0 IN.
Blade Twist	-8.97 deg
Blade Area (one Blade)	42.27 ft ²
Minus Hub	36.32 ft ²
Location of Center of Hub	
	FS 130.78
	WL 130.82
	BL -3.31
Mast Tilt with Respect to Fuselage Waterline	
	F/A 3 deg fwd
	Lat 2 deg left

TABLE X. - Concluded

Tail Rotor System

Number of Blades	2
Rotor Diameter	9.66 ft
Rotor Disc Area	73.3 ft ²
Rotor Solidity	.132
Airfoil Section	10.5% Symmetrical
Blade Chord	12.0 in.
Gearing Ratio to Main Rotor	5.19
Location of Center of Hub	FS 501.3 WL 126.5 BL -12.
Pitch-Flap Coupling - $\delta 3$ (Flap axis offset 30 deg to avoid feathering due to flapping)	30 deg
Maximum Flapping Freedom	9.5 deg about flapping axis

Horizontal Stabilizer

Area (Total)	38.3 ft ²
Span (Total)	11.5 ft ²
Chord	40.0 in.
Airfoil Section	NACA 0012
Aspect Ratio	3.45
Location of 25% Chord Line	FS 380.0 WL 58.0

Vertical Stabilizer

Area (Total)	26.3 ft ²
Aspect Ratio	1.96
Incidence of Zero Lift Line to Aircraft Centerline	7.0 deg right
Location of Center of Pressure	FS 465.0 WL 88.0

TABLE XI. FLIGHT CONTROL SYSTEMS

CYCLIC CONTROLSLongitudinal Cyclic

Stick Travel	12.50 in.
F/A Swashplate Incidence Angle with Respect to Mast	
- Stick Full Forward	6.8 deg down fwd
- Stick Full Aft	4.8 deg down aft
Ratio of Blade Feathering Angle to Swashplate Angle	17/11
Elevator Incidence at Mid Stick Travel with Respect to Waterline	-3.4 DEG
Elevator Gearing (See Figure 83)	
Pylon Motion Coupling Ratio	
Blade Angle/Fwd Pylon Tilt	1.02 $\frac{\text{deg}}{\text{deg}}$ aft
Blade Angle/Left Pylon Tilt	0.85 $\frac{\text{deg}}{\text{deg}}$ aft

Lateral Cyclic

Stick Travel	12.50 in.
Lateral Swashplate Incidence Angle with Respect to Mast	
- Stick Full Left	4.9 deg left
- Stick Full Right	3.1 deg right
Ratio of Blade Feathering Angle to Swashplate Angle	17/11
Pylon Motion Coupling Ratio	
Blade Angle/Fwd Pylon Tilt	1.02 $\frac{\text{deg}}{\text{deg}}$ left
Blade Angle/Left Pylon Tilt	0.85 $\frac{\text{deg}}{\text{deg}}$ right

COLLECTIVE CONTROLS

Stick Travel	10.45 in.
Collective Blade Angle at Grip	
- Stick Full Down	7.0 deg
- Stick Full Up	25.0 deg
Pylon Motion Coupling Ratio	
Blade Angle/Fwd Pylon Tilt	1.13 $\frac{\text{deg}}{\text{deg}}$ Up
Blade Angle/Left Pylon Tilt	0 Collective

TABLE XI.- Concluded	
<u>DIRECTIONAL CONTROLS</u>	
Pedal Travel	6.50 in.
Blade Pitch Angle with Pedal	
- Full Left	17.4 deg
- Full Right	-3.7 deg

TABLE XII. COMPONENT SPEED RATIOS				
Component	rpm			
Input Shaft	5500	6000	6300	7000
M/R Mast (N_R)	259	283	297	330
T/R Driveshaft	4318	4711	4946	5496
T/R Mast ($N_{T/R}$)	1345	1467	1541	1712

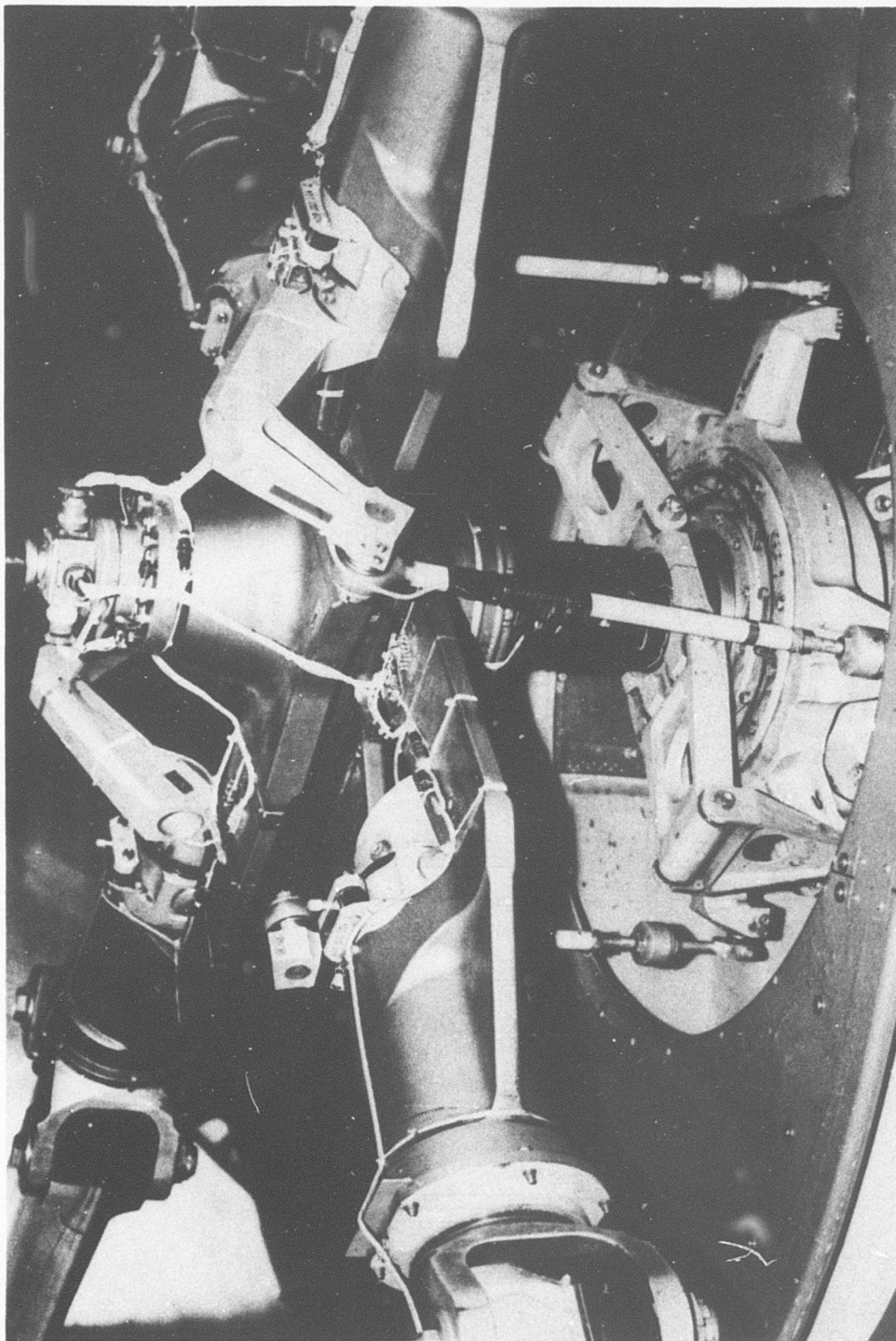


Figure 80. 609 Main Rotor System.

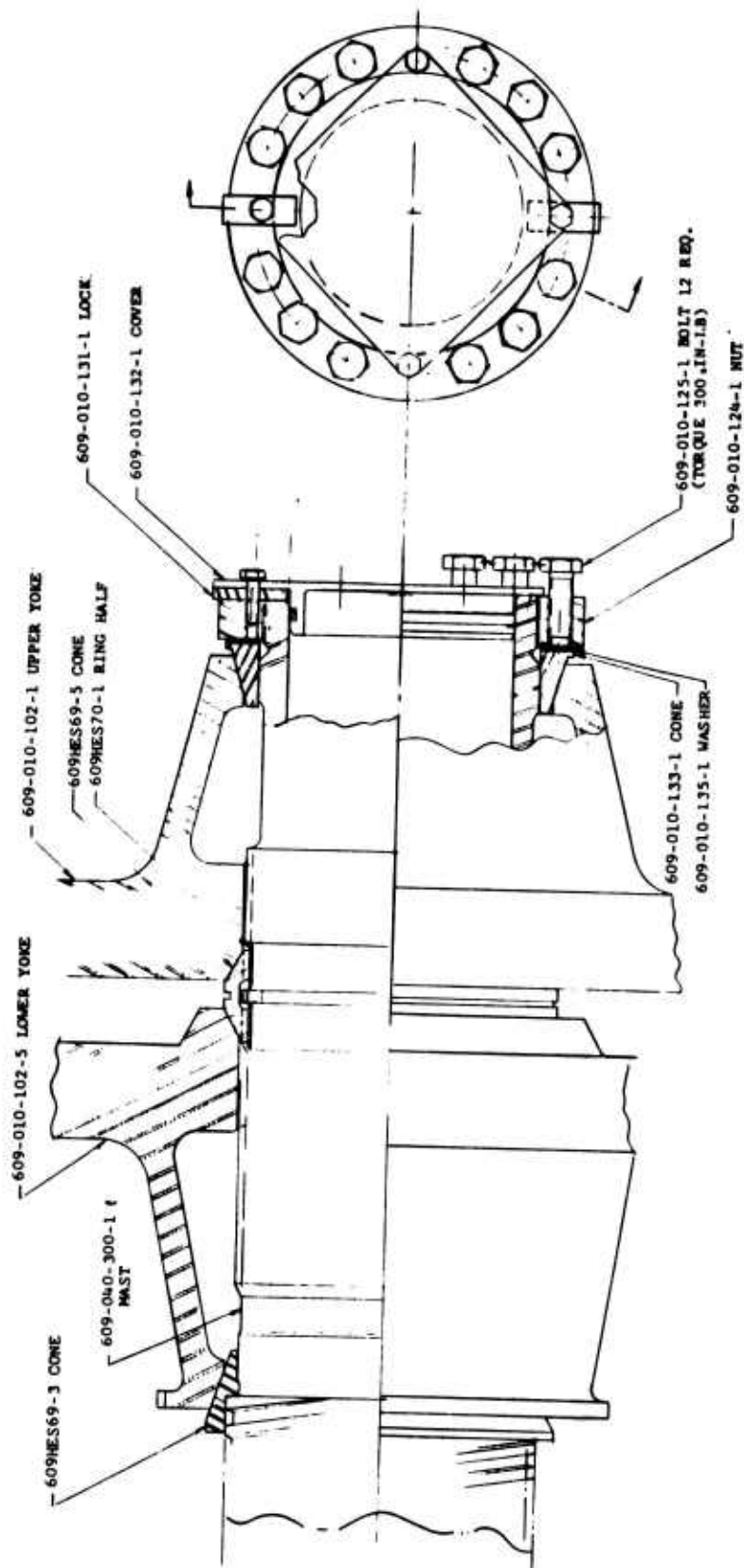


Figure 81. 609 Yoke and Mast Mounting Details.

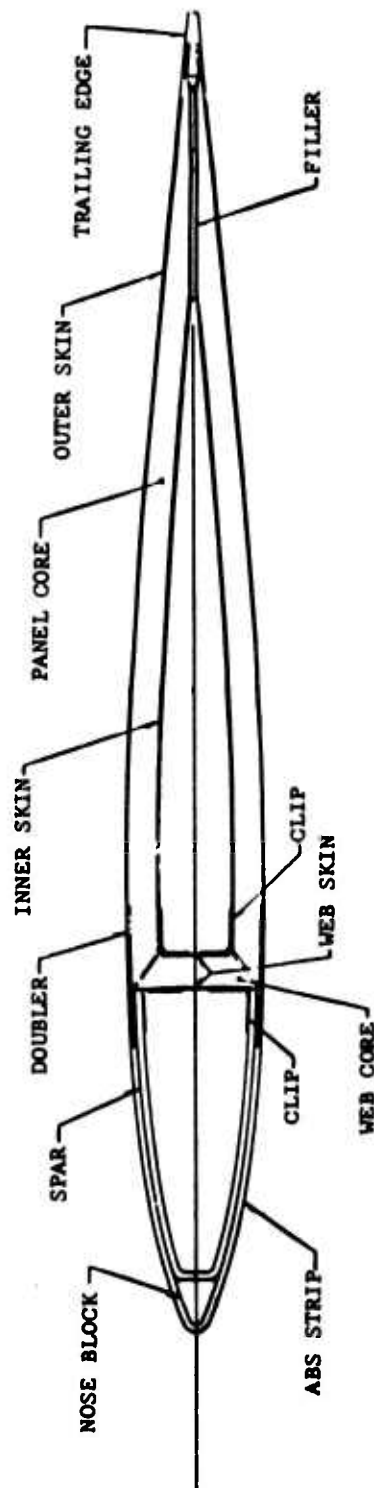
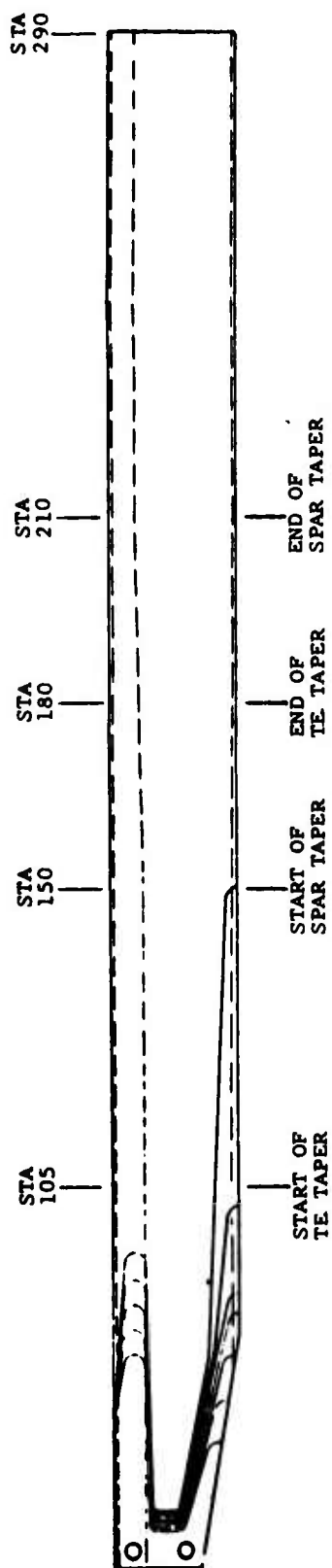
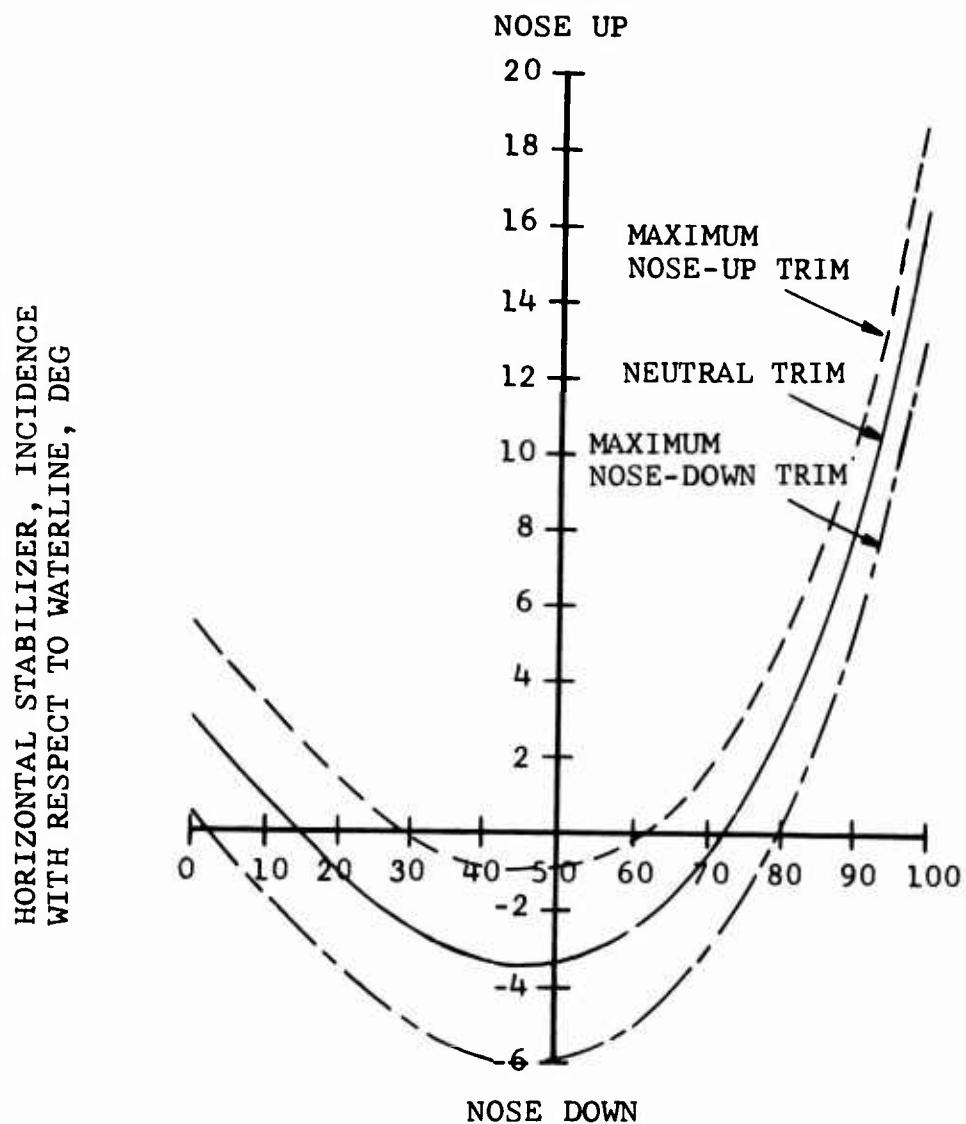


Figure 82. 609 Blade Assembly.



F/A CYCLIC STICK POSITION, 100% FULL FORWARD

Figure 83. Stabilizer and Trim Angle Versus Longitudinal Stick Position.

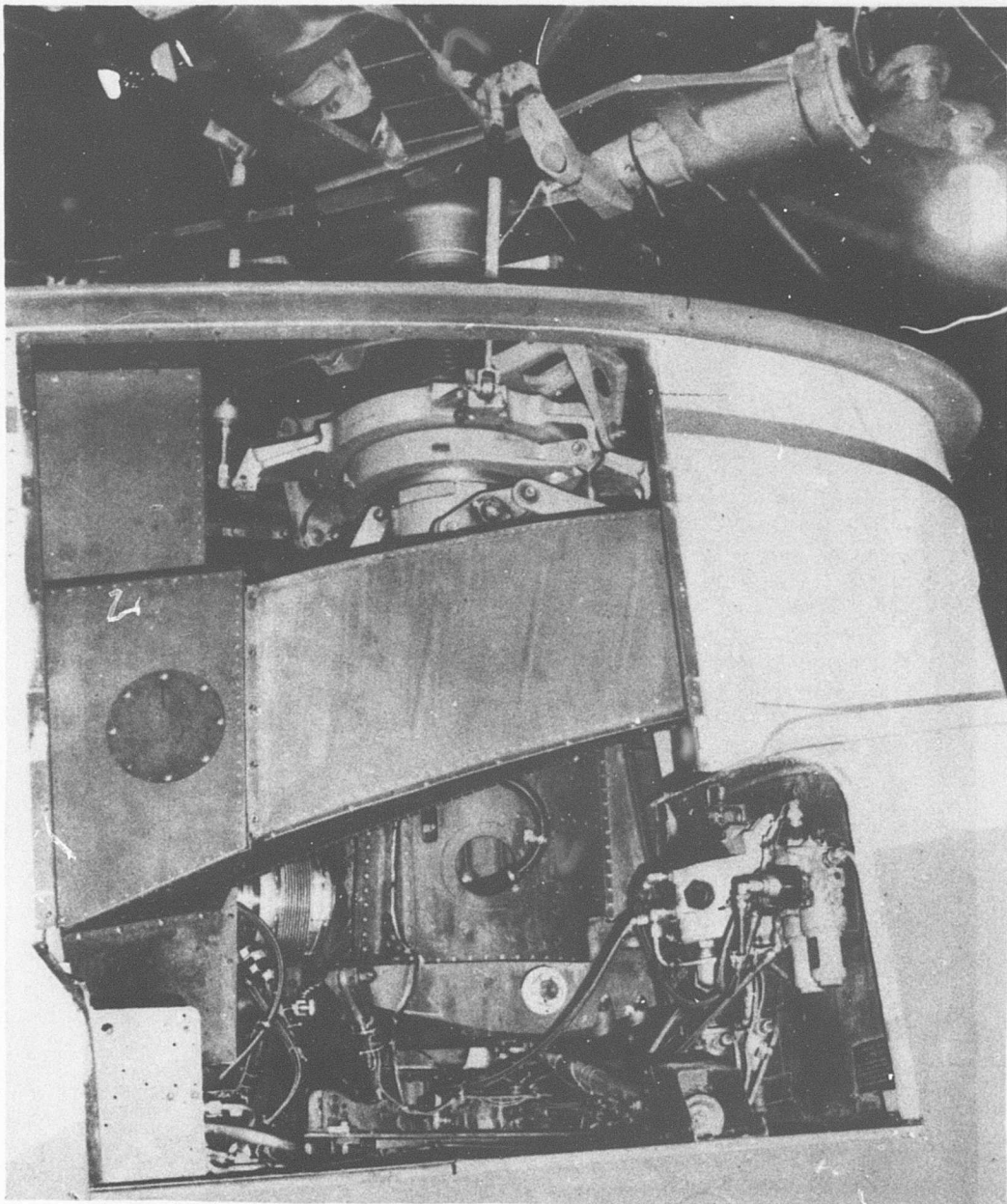


Figure 84. Pylon and 609 Main Rotor Assembly.

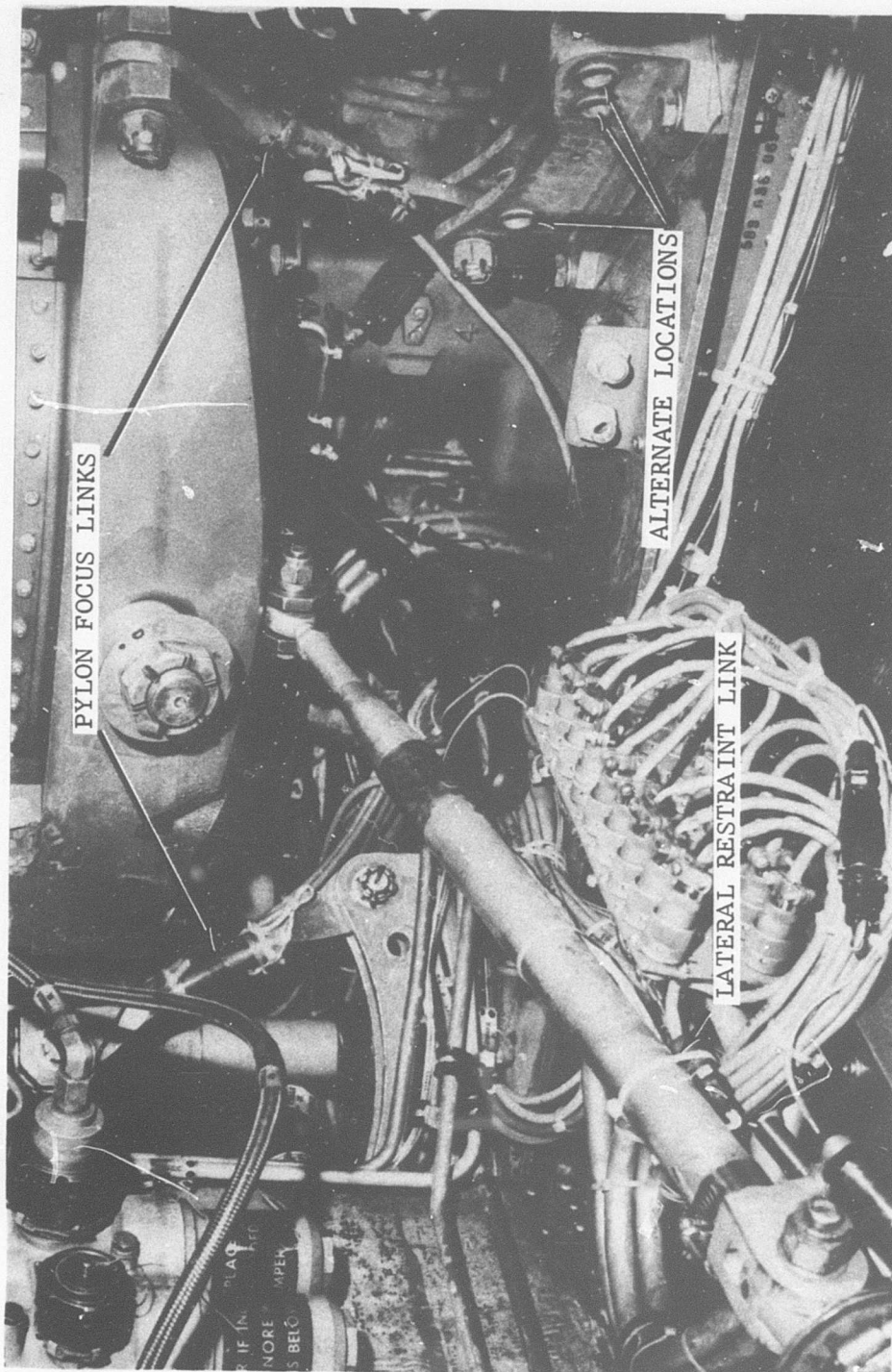


Figure 85. Pylon Base and Lateral Restraint Link.

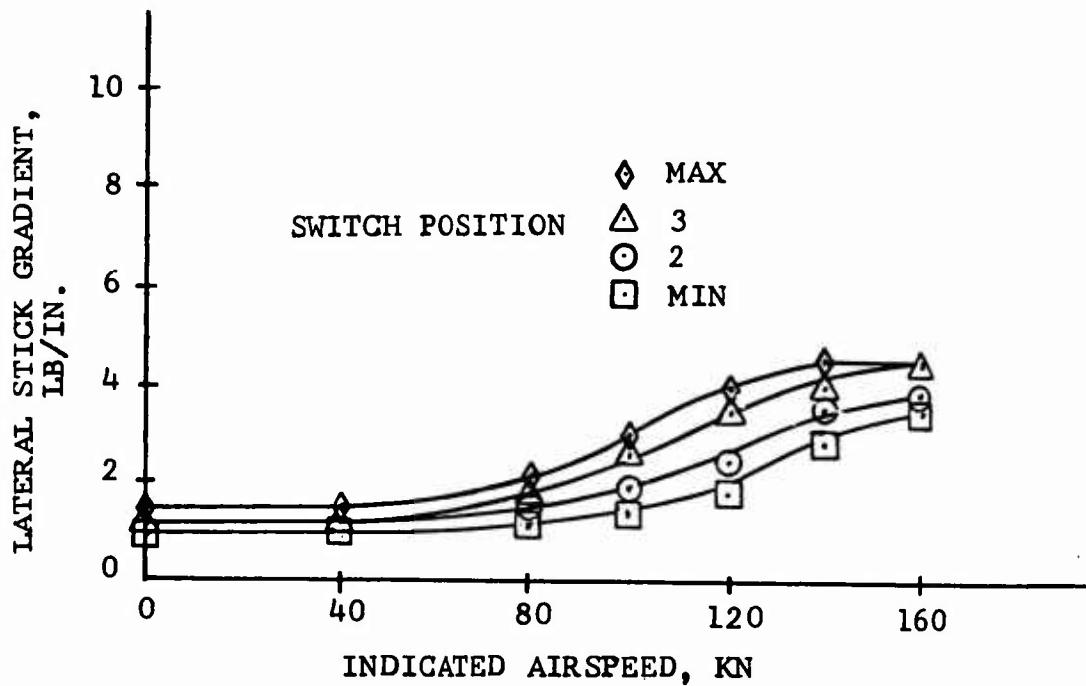
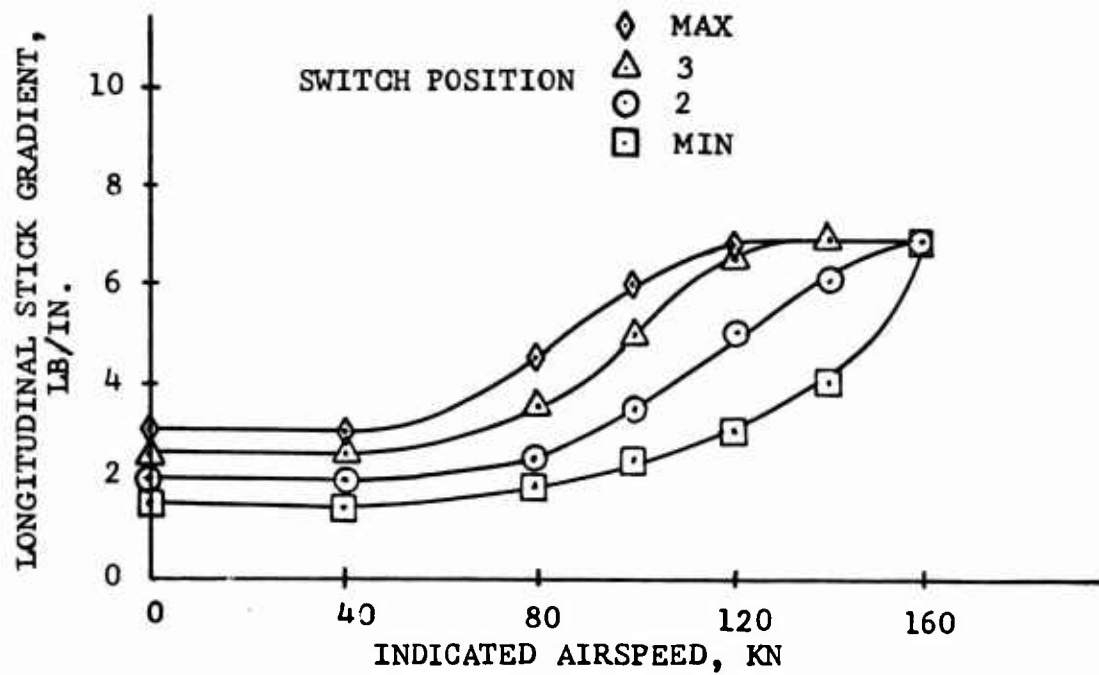


Figure 86. Measured Stick Gradients as a Function of Airspeed and Switch Position.

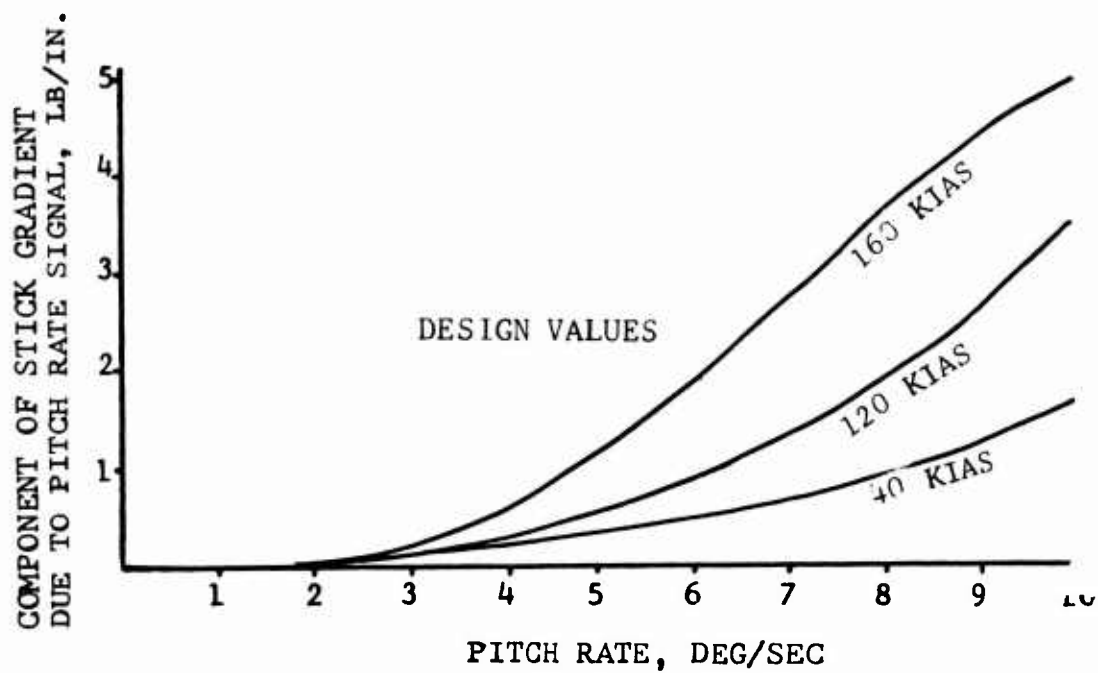


Figure 87. Stick Gradients due to Pitch Rate.

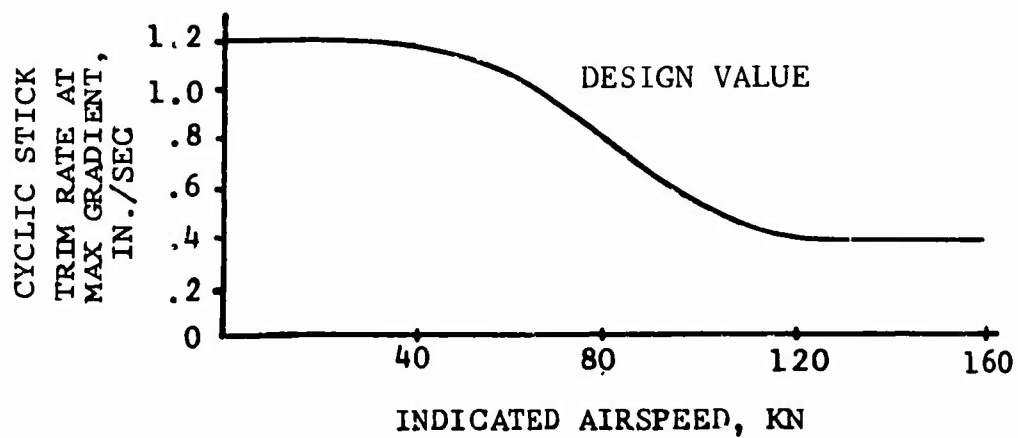


Figure 88. Cyclic Stick Trim Rates Versus Airspeed.

APPENDIX II

WIND-TUNNEL DATA

Full-scale wind-tunnel data from Reference 15 and previously unpublished rotor loads data from the same test are shown in Figures 89, 90, and 91 for different advance ratios. This was a two-bladed semirigid rotor with a diameter of 44 feet and a 21-inch chord. The plots show a very orderly mapping of oscillatory blade chord loads, power coefficients, and collective control positions versus lift and drag coefficients. Intercepts of constant collective and constant moment ($\pm 28,000$) loci have been cross-plotted and were shown earlier in Figure 37 of the main body of the report.

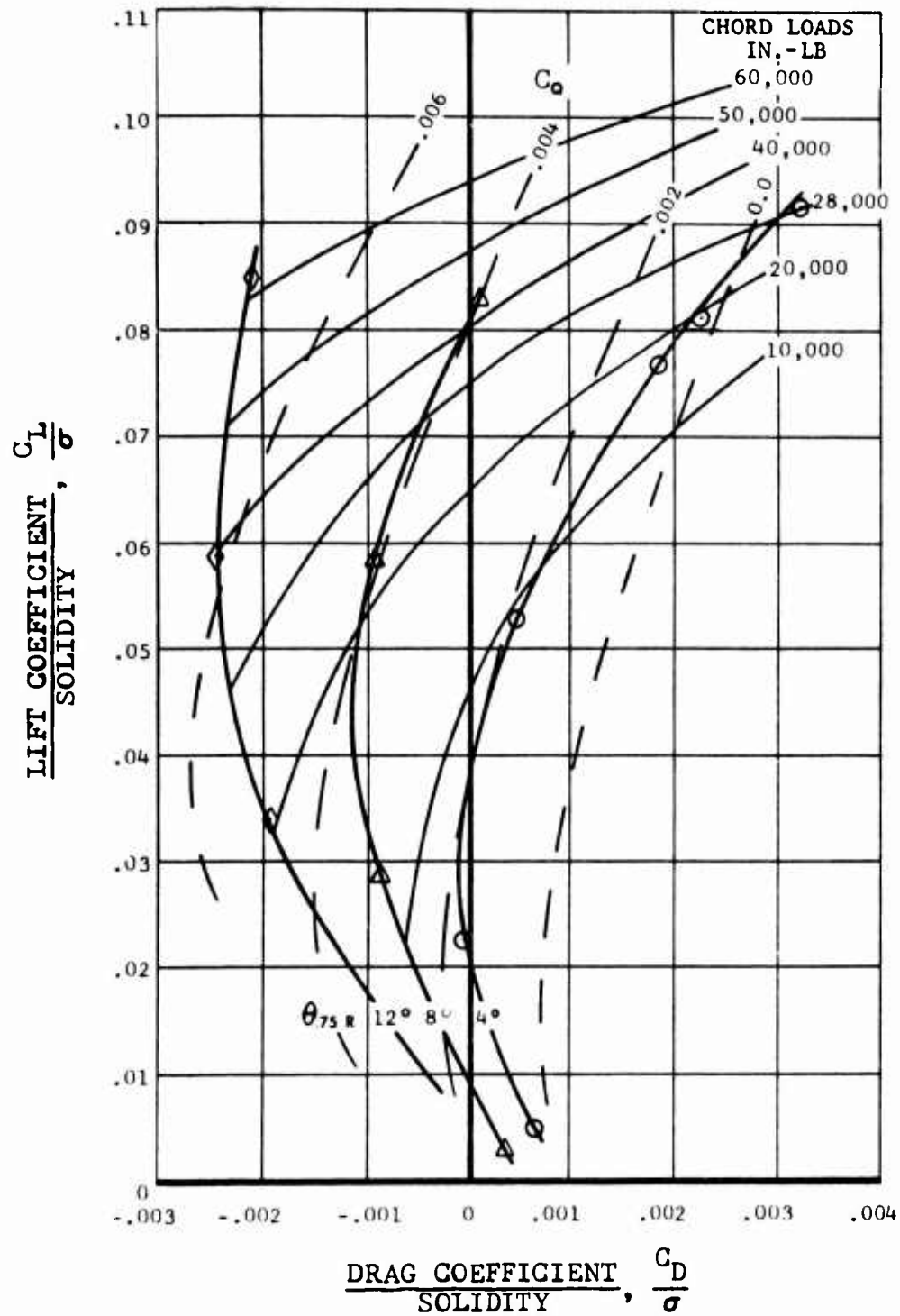


Figure 89. Lift Versus Drag Coefficients for Advance Ratio of .36.

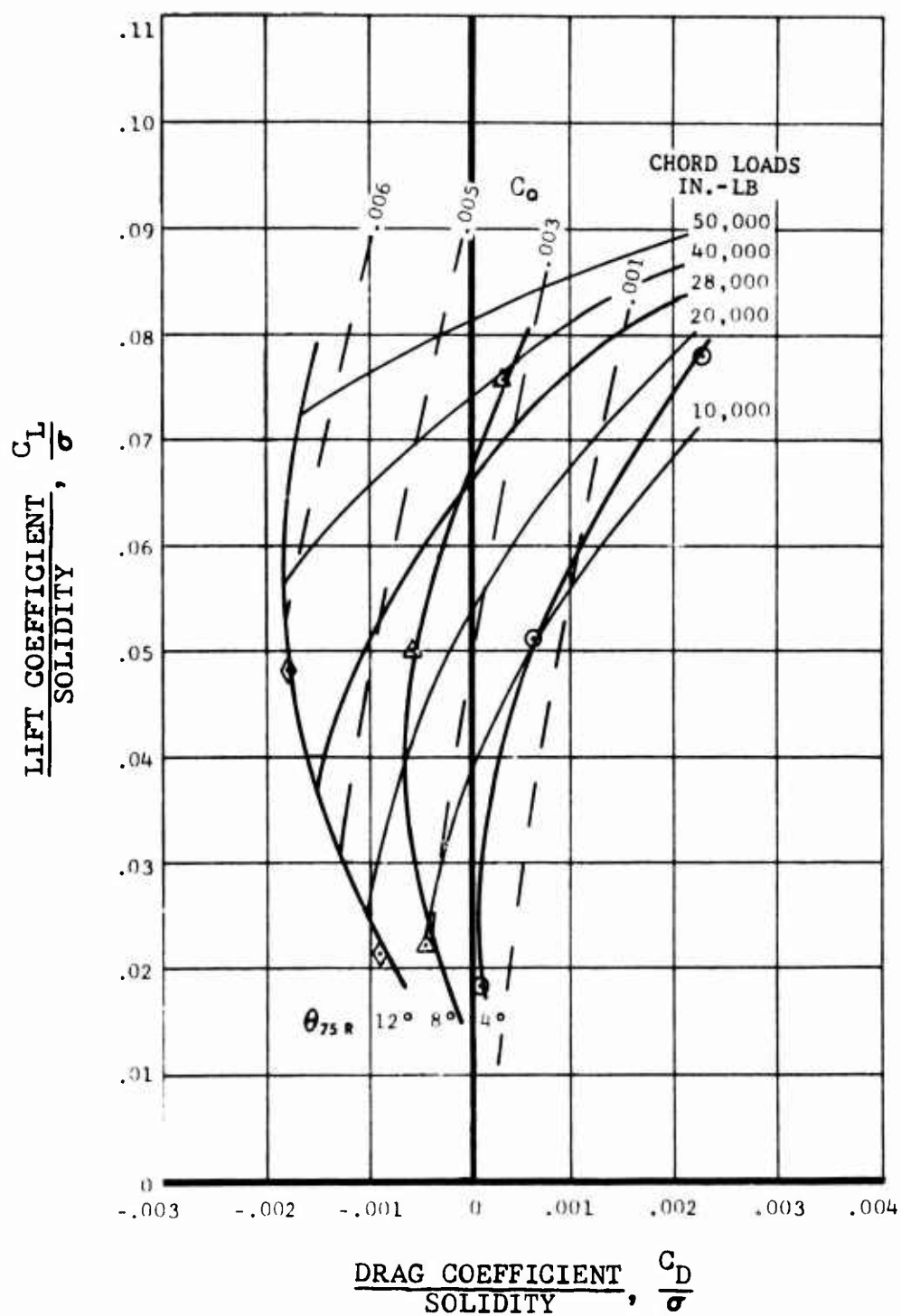


Figure 90. Lift Versus Drag Coefficients for Advance Ratio of .40.

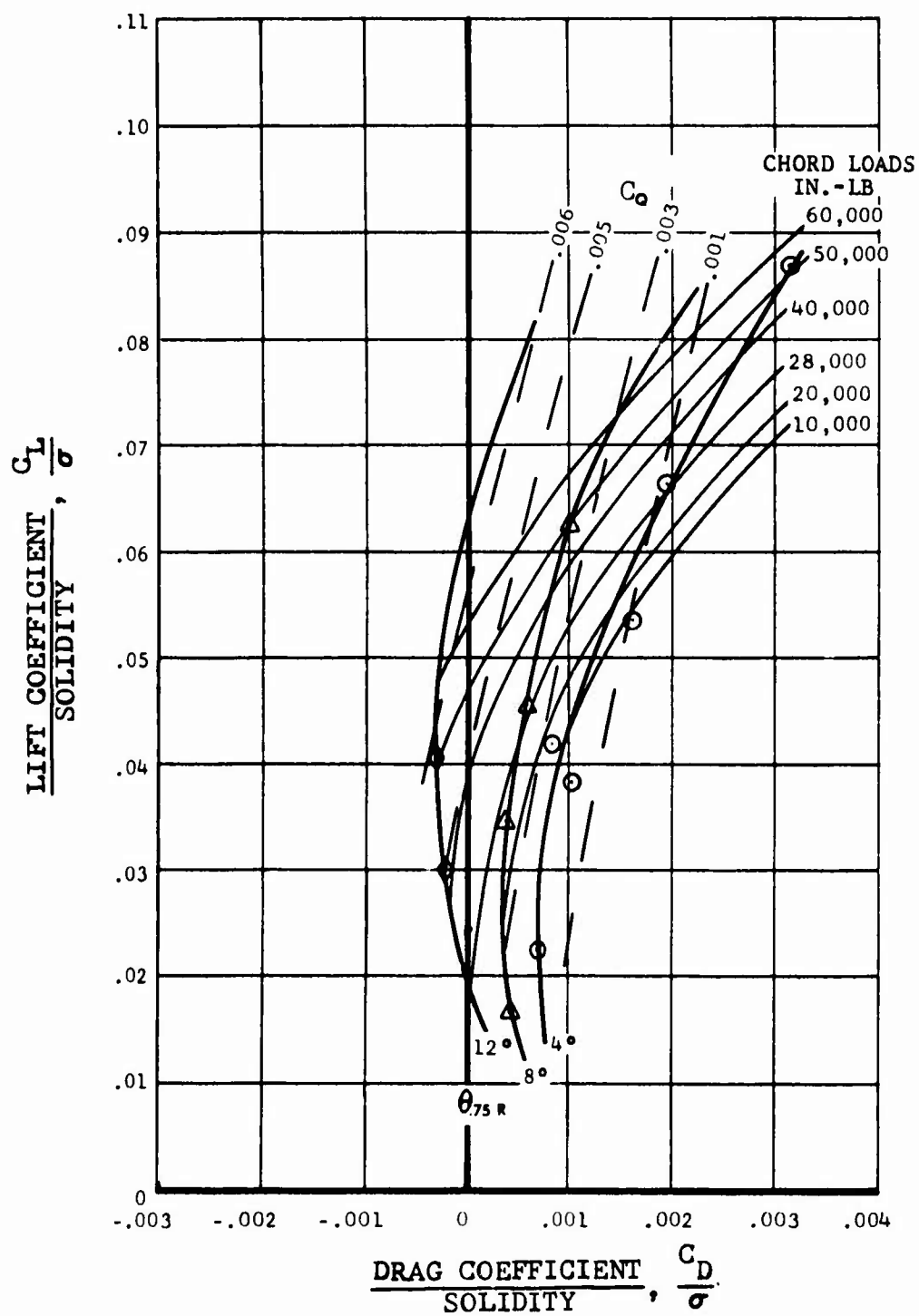


Figure 91. Lift Versus Drag Coefficients
for Advance Ratio of .51.

APPENDIX III FATIGUE LIFE ANALYSIS

The fatigue lives of the Model 609 main rotor and controls are based on loads measured during the flight loads survey. These were used in conjunction with a frequency-of-occurrence spectrum in order to determine the fatigue lives of the various dynamic components. The frequency-of-occurrence spectrum was established as representative of actual helicopter operations in the utility role.

FREQUENCY OF OCCURRENCE

The frequency-of-occurrence spectrum developed for this analysis (shown in Table III) was based on the utility helicopter spectrum presented in Reference 10. The spectrum of Reference 10 was modified to allow for those flight conditions which are allotted a number of occurrences per hundred hours. The occurrences per 100 flight hours were converted to percentage of flight time, and this percentage of time was subtracted from the appropriate flight conditions in order to keep the total flight time at 100 percent.

The load level survey documented the magnitudes and frequencies per revolution of loads, and these loads were then used to calculate fatigue lives of all dynamic components in the rotor system. In order to establish a representative loads spectrum, six gross weight/center-of-gravity configurations were used. These are shown in Table IV. The maximum loads were generated during high-speed maneuvers at the heavy gross weights.

LIFE CALCULATIONS

Fatigue life calculations were based on a comparison between flight stresses and the endurance limit of the component being analyzed. In most cases, only nominal stresses were evaluated. Stress concentration factors were incorporated into the analysis as reductions in the endurance limit. Endurance limits were established by the following methods:

1. Fatigue tests of the specific component.
2. Fatigue tests of a similar component.
3. Published data on material allowables.

Endurance limits were usually obtained for one value of mean stress. The effect of different mean stresses was then evaluated by use of a Goodman diagram similar to that of Figure 92.

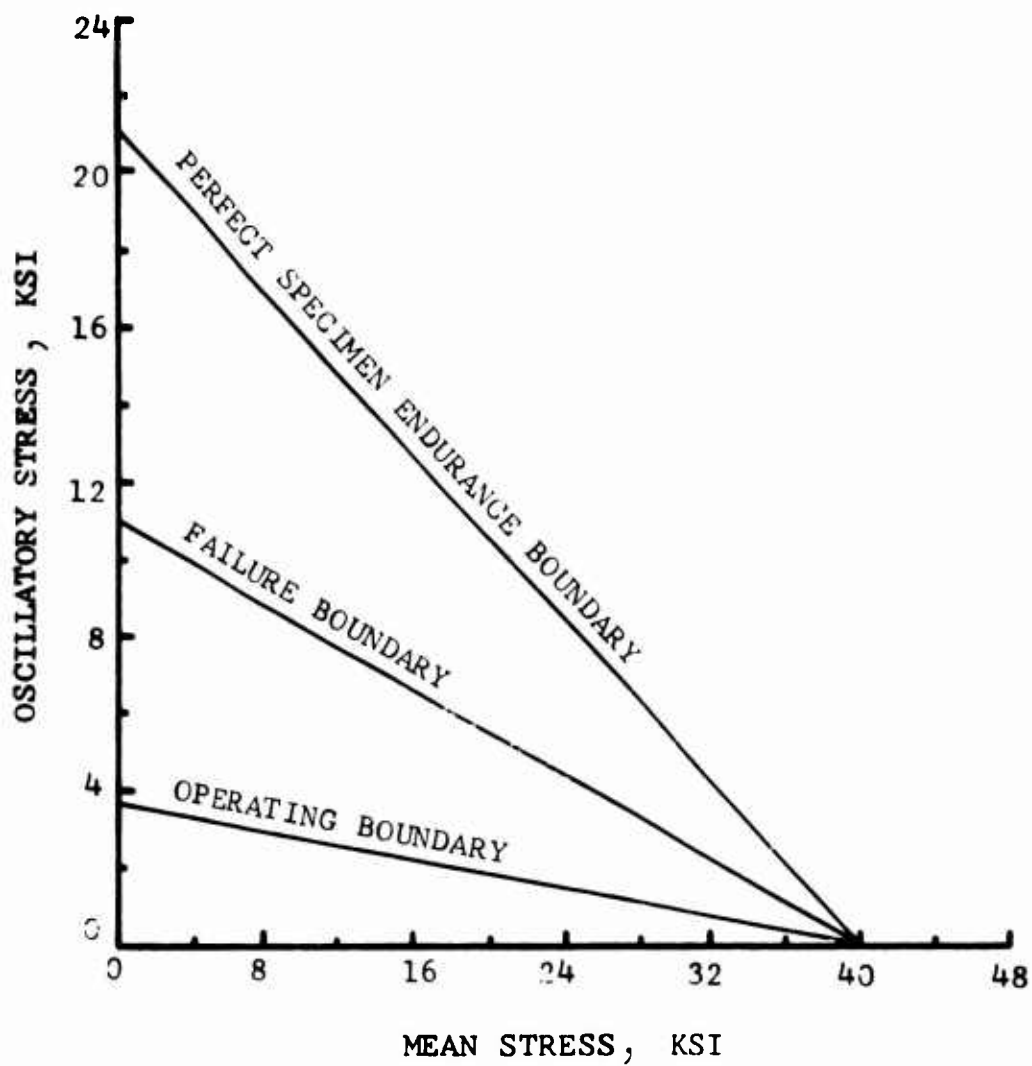


Figure 92. Modified Goodman Diagram for 2024-T4 and/or 2024-T42 Aluminum Alloy.

Once the ratio of operating stress to endurance limit (S/E) was established, those conditions which generate fatigue damage (S/E>1) were evaluated quantitatively by means of the theory of linear cumulative damage as expressed by Miner's Rule:

$$\sum_{i=1}^k n_i/N_i = 1 \quad \text{failure}$$

where n_i = number of cycles at a given (i^{th}) load level

N_i = number of cycles to failure at a given (i^{th}) load level

k = number of conditions

The theory and its application are discussed in detail in Reference 16.

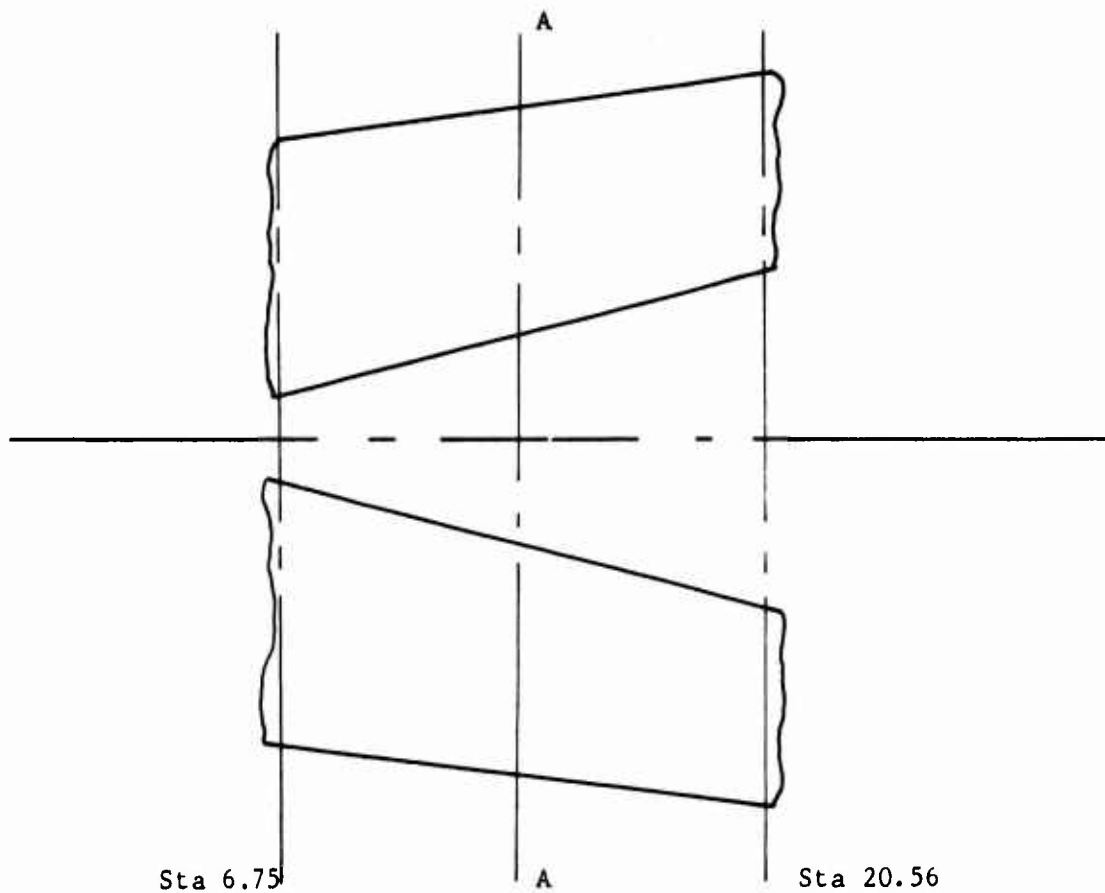
The calculation of S/E ratio was based on the maximum oscillatory load or stress measured during a maneuver, which was assumed to occur during the entire maneuver. This procedure was followed for all conditions except the full autorotation landing. The damage fraction for this condition was calculated on a cycle-by-cycle basis. (This method of fatigue life calculation was used only when the first method had been shown to be overly conservative.) Data for a full autorotation landing are available only for the emergency landing on May 23, 1973, and are not considered representative of loads generated during normal autorotation landings; for this reason, this maneuver is cycle-counted.

MAIN ROTOR HUB AND BLADE

Main Rotor Yoke Part No. 609-010-102-1

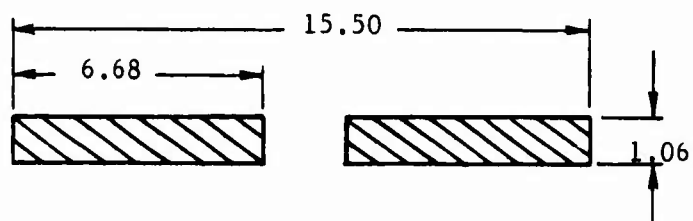
The main rotor yoke is a 6Al-4V titanium flexure subjected to beam and chord bending as well as to centrifugal loading in the axial direction. The two cross-sections at which the yoke was analyzed are shown in Figure 93. Analysis showed the yoke to be critical in fatigue at station 6.75. The flexure was analyzed as a slotted beam by the methods set forth on page 161 of Reference 17. The stress equation used for station 6.75 was:

$$\sigma_b = 0.707(C.F.) + 0.402(M_{B7.0}) + 0.024(M_{C13.65}) + 0.004(M_{C0.0})$$



All Dimensions in Inches

Sta 6.75



Sta 20.56

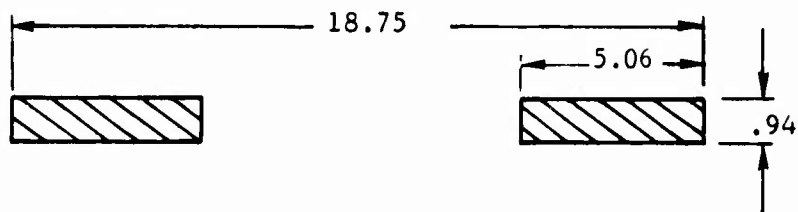


Figure 93. Main Rotor Yoke, Part No. 609-010-102-1.

where C.F. = centrifugal force at station 6.75

$M_{B7.0}$ = beam bending at station 7.0

$M_{C13.65}$ = chord bending at station 13.65

$M_{C0.0}$ = chord bending at station 0.0

An endurance limit of 30,000 psi at zero steady was used as the endurance limit for the yoke, which experiences a loading frequency of one cycle per revolution. On this basis, a fatigue life of 811 hours was substantiated for the Model 609 yoke, and Table XIII shows the calculations.

Main Rotor Spindle Part No. 609-010-140-1

The 609 main rotor spindle is made from 4340 steel, heat treated to an ultimate tensile strength of 180-200 ksi. The spindle acts as a grip for the main rotor blade and is attached to the yoke by means of the retention system (strap, fitting, and retention bolts). The spindle is subjected to beam and chord bending and an axial stress due to the centrifugal force. The loading frequency of the spindle is one cycle per revolution of the main rotor.

The spindle was evaluated at two locations, the main rotor blade attachment tangs at station 41.0 and a cross-section taken at station 34.75 (Section A-A in Figure 94). Section A-A was found to be more critical in fatigue, and therefore life calculations were based on stress at this section.

The cross-section of the spindle at station 34.75 is similar to the 204-011-102-17 yoke at its critical section (station 6.3). Both components are of 4340 steel, heat treated to the same tensile range (see Reference 18 for a comparison). Therefore the endurance limit established for the 204-011-102-17 yoke was used for the 609 spindle. (The S-N curve for the 204 yoke is shown in Figure 95.) An additional Goodman reduction for mean stress was used to obtain the value of 27,500 psi used as the endurance limit for the 609 spindle. Table XIV shows a summary of the fatigue life calculations, which substantiated a fatigue life of 7100 hours for the 609-010-140-1 spindle.

Main Rotor Blade Retention System

The oscillatory loading on the components of the blade retention system differs from that on other components of the main rotor system in that the major oscillatory stress on the retention system arises from start and stop of the main rotor (i.e., the application and removal of centrifugal force). In the

TABLE XIII. FATIGUE LIFE DETERMINATION OF 609
M/R YOKE, PART NO. 609-010-102-1

FLIGHT CONDITION	FREQUENCY OF OCCURRENCE PCT. CYCLES IN TIME 100 HRS.	OSCILLATORY BENDING STR. IN M/R YOKE @ STA. 7.0	CYC. TO FAILURE X 10**(-6)	DAMAGE FRACTION
I. GROUND CONDITIONS				
A. NORMAL START	0.1000	1770	0 AA	0.0
	0.3000	5310	14496 CA	0.0
	0.1000	1770	0 FA	0.0
B. NORMAL SHUTDOWN	0.1000	1770	9219 AA	0.0
	0.3000	5310	8321 BA	0.0
	0.1000	1770	0 FA	0.0
II. POWER-ON ICE				
A. HOVERING				
1. STEADY				
(A) 280 RPM	0.6944	11666	16385 AA	0.0
	2.0832	34998	16867 CA	0.0
	0.6944	11666	11327 DA	0.0
(B) 295 RPM	0.6944	12291	16251 AA	0.0
	2.0832	36873	20166 CA	0.0
	0.6944	12291	15518 EA	0.0
2. LEFT TURN	0.2222	3800	18631 AA	0.0
	0.6666	11399	19693 CA	0.0
	0.2222	3800	13259 EA	0.0
3. RIGHT TURN	0.2222	3800	19019 AA	0.0
	0.6666	11399	24578 CA	0.0
	0.2222	3800	11552 EA	0.0
4. CONTROL REVERSAL				
(A) LONGITUDINAL	0.0556	951	31091 AA	2.022 0.000470
	0.1668	2852	31928 CA	1.022 0.002792
	0.0556	951	24868 EA	0.0
(B) LATERAL	0.0556	951	25151 AA	0.0
	0.1668	2852	25038 CA	0.0
	0.0556	951	15973 EA	0.0
(C) RUDDER	0.0556	951	17903 AA	0.0
	0.1668	2852	19249 CA	0.0
	0.0556	951	11842 EA	0.0
B. MANEUVERS				
1. SIDEWARD FLIGHT				
(A) TO THE RIGHT	0.1000	1710	8064 AA	0.0
	0.3000	5130	29308 BA	0.0
	0.1000	1710	10111 FA	0.0
(B) TO THE LEFT	0.1000	1710	13170 AA	0.0
	0.3000	5130	16098 BA	0.0
	0.1000	1710	11598 EA	0.0
2. REARWARD FLIGHT	0.1000	1710	9099 AA	0.0
	0.3000	5130	26426 BA	0.0
	0.1000	1710	26205 EA	0.0
3. NORMAL TAKE-OFF	0.1778	3040	32581 AA	0.682 0.004460
	0.5334	9121	26354 CA	0.0

TABLE XIII - Continued

FLIGHT CONDITION		FREQUENCY OF OCCURRENCE PCT. CYCLES IN TIME 100 HRS.		OSCILLATORY BENDING STR. IN M/R YOKE @ STA. 7.0		CYC. TO FAILURE X 10**(-6)	DAMAGE FRACTION
4. NORMAL LANDING		0.1778	3040	19034	EA		0.0
		0.4166	7124	20855	AA		0.0
		1.2498	21372	27453	CA		0.0
		0.4166	7124	18452	EA		0.0
III. POWER-ON IGE							
A. LEVEL FLIGHT							
% VL RPM							
1. 40	280	0.1866	3135	13671	AA		0.0
		0.5598	9405	14088	CA		0.0
		0.1866	3135	15536	FA		0.0
		0.1866	3303	13859	AA		0.0
	295	0.5598	9908	13555	CA		0.0
		0.1866	3303	13610	FA		0.0
		0.4917	8261	12568	AA		0.0
		1.4751	24782	13296	CA		0.0
2. 50	280	0.4917	8261	14502	FA		0.0
		0.4917	8703	12964	AA		0.0
		1.4751	26109	13632	CA		0.0
		0.4917	8703	16049	FA		0.0
3. 60	280	0.7838	13168	13020	AA		0.0
		2.3514	39503	12471	CA		0.0
		0.7838	13168	13765	DA		0.0
		0.7838	13873	13870	AA		0.0
	295	2.3514	41620	13327	CA		0.0
		0.7838	13873	14467	FA		0.0
		1.0000	16800	13406	AA		0.0
		3.0000	50400	12799	CA		0.0
4. 70	280	1.0000	16800	14229	DA		0.0
		1.0000	17700	14754	AA		0.0
		3.0000	53100	13411	CA		0.0
		1.0000	17700	13522	FA		0.0
5. 80	280	1.5000	25200	14173	AA		0.0
		4.5000	75600	13849	CA		0.0
		1.5000	25200	17517	DA		0.0
		1.5000	26550	15461	AA		0.0
	295	4.5000	79650	13118	CA		0.0
		1.5000	26550	13650	FA		0.0
		1.7334	29121	13664	AA		0.0
		5.2002	87363	15339	BA		0.0
6. 90	280	1.7334	29121	24648	DA		0.0
		1.7334	30681	16343	AA		0.0
		5.2002	92044	13391	CA		0.0
		1.7334	30681	13793	DA		0.0
7. 100	280	0.9838	16528	13706	AA		0.0
		2.9514	49583	19618	BA		0.0

TABLE XIII - Continued

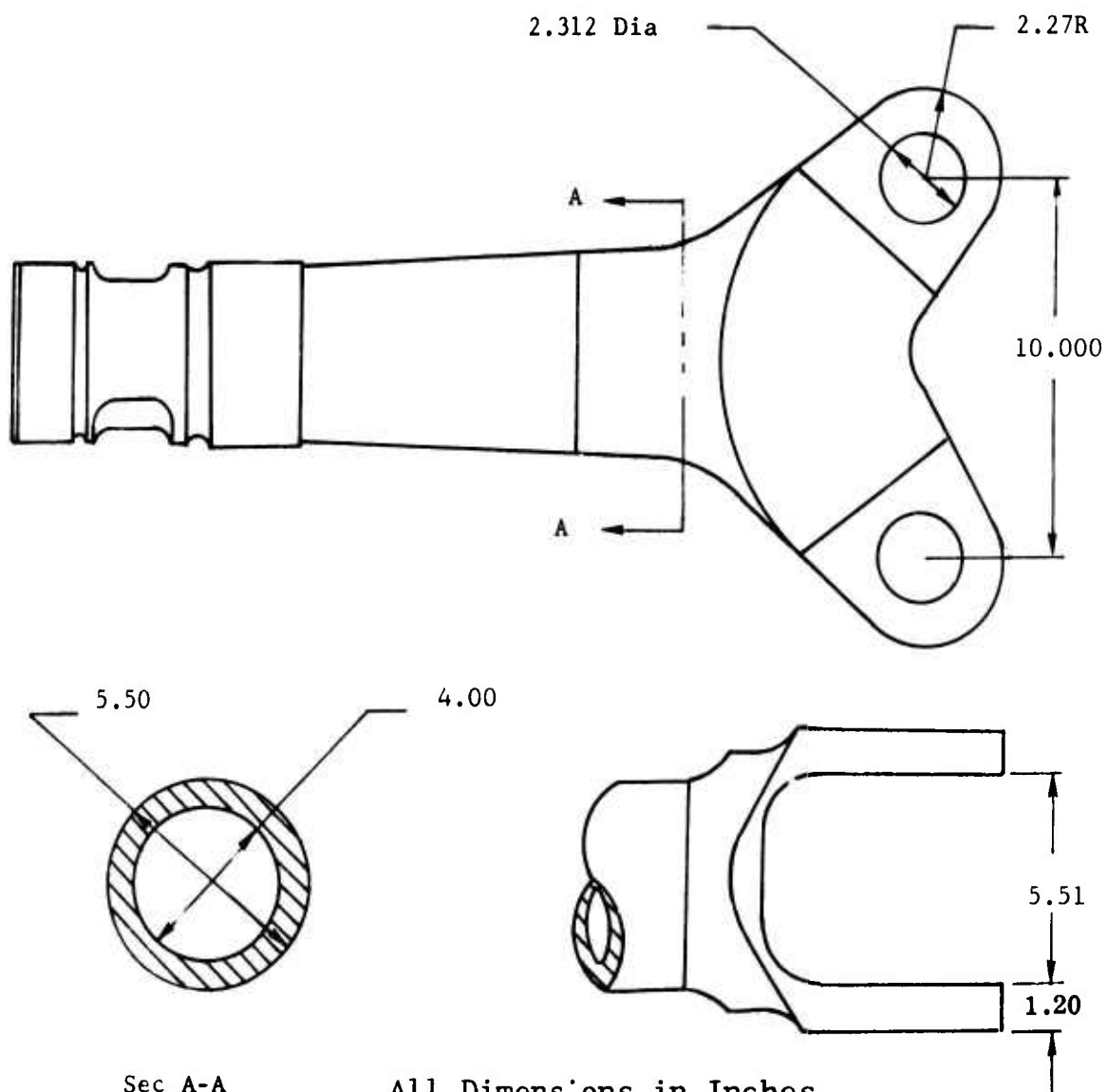
TABLE XIII - Continued						
FLIGHT CONDITION		FREQUENCY OF OCCURRENCE		OSCILLATORY BENDING STR.	CYC. TO FAILURE	DAMAGE FRACTION
		PCT. TIME	CYCLES IN 100 HRS.	IN M/R YOKE STA. 7.0	X 10**(-6)	
9. VNE	295	0.9838	16528	23252 FA		0.0
		0.9838	17413	15972 AA		0.0
		2.9514	52240	16374 CA		0.0
	280	0.9838	17413	18467 DA		0.0
		0.3500	5880	14945 AA		0.0
		1.0500	17640	20805 BA		0.0
	295	0.3500	5880	23787 FA		0.0
		0.3500	6195	15357 AA		0.0
		1.0500	19585	15925 BA		0.0
		0.3500	6195	16419 EA		0.0
		B. MANEUVERS				
1. CLIMB 0-60 KNOTS						
(A) M.C. POWER		0.6000	10260	22135 AA		0.0
		1.8000	30780	19338 CA		0.0
		0.6000	10260	18962 FA		0.0
(B) T.O. POWER		0.2000	3420	19263 AA		0.0
		0.6000	10260	18872 CA		0.0
		0.2000	3420	12103 EA		0.0
2. CYCLIC PULL-UP						
(A) 50 KNOTS		0.0324	554	18446 AA		0.0
		0.0972	1662	23003 CA		0.0
		0.0324	554	15332 EA		0.0
(B) 100 KNOTS		0.0324	554	19897 AA		0.0
		0.0972	1662	19565 CA		0.0
		0.0324	554	18346 EA		0.0
(C) VL		0.0324	554	19203 AA		0.0
		0.0972	1662	34697 BA	0.269	0.006183
		0.0324	554	42521 EA	0.049	0.011401
3. LEFT TURN						
(A) 50 KNOTS		0.2000	3420	18975 AA		0.0
		0.6000	10260	19390 CA		0.0
		0.2000	3420	13370 EA		0.0
(B) 100 KNOTS		0.2000	3420	17765 AA		0.0
		0.6000	10260	20322 CA		0.0
		0.2000	3420	16609 EA		0.0
(C) VL		0.1000	1710	20536 AA		0.0
		0.3000	5130	31613 BA	1.151	0.004457
		0.1000	1710	42621 EA	0.049	0.035189
4. RIGHT TURN						
(A) 50 KNOTS		0.2000	3420	19447 AA		0.0
		0.6000	10260	19541 BA		0.0
		0.2000	3420	11885 EA		0.0
(B) 100 KNOTS		0.2000	3420	16685 AA		0.0
		0.6000	10260	16384 CA		0.0
		0.2000	3420	17198 FA		0.0
(C) VL		0.1000	1710	17998 AA		0.0

TABLE XIII - Continued

FLIGHT CONDITION	FREQUENCY OF OCCURRENCE PCT. CYCLES IN TIME 100 HRS.		OSCILLATORY BENDING STR. IN M/R YOKE @ STA. 7.0	CYC. TO FAILURE X 10**(-6)	DAMAGE FRACTION
	0.3000	5130	33732 BA	0.382	0.013413
	0.1000	1710	42621 EA	0.049	0.035189
5. CONTROL REVERSAL					
(A) LONGITUDINAL	0.0444	759	17863 AA		0.0
	0.1332	2278	22122 BA		0.0
	0.0444	759	18937 EA		0.0
(B) LATERAL	0.0444	759	14689 AA		0.0
	0.1332	2278	19919 CA		0.0
	0.0444	759	17922 EA		0.0
(C) RUDDER	0.0444	759	14301 AA		0.0
	0.1332	2278	14247 CA		0.0
	0.0444	759	14975 EA		0.0
IV. POWER TRANSITIONS					
A. POWER TO AUTO					
1. 40 KNOTS	0.0022	38	11512 AA		0.0
	0.0066	113	19744 BA		0.0
	0.0022	38	13760 EA		0.0
2. VL	0.0022	38	14369 AA		0.0
	0.0066	113	24505 BA		0.0
	0.0022	38	21735 EA		0.0
B. AUTO TO POWER	0.0112	192	14766 AA		0.0
	0.0336	575	16800 BA		0.0
	0.0112	192	15890 EA		0.0
V. AUTOROTATION					
A. STABILIZED FLIGHT					
1. 40 KNOTS	0.0578	988	9750 AA		0.0
	0.1734	2965	16655 BA		0.0
	0.0578	988	10686 EA		0.0
2. 80 KNOTS	0.0776	1327	10132 AA		0.0
	0.2328	3981	16978 BA		0.0
	0.0776	1327	11999 EA		0.0
3. MAX AUTO A/S	0.0378	646	9499 AA		0.0
	0.1134	1939	19408 BA		0.0
	0.0378	646	16320 EA		0.0
B. TURNS. (NORMAL AUTO A/S)					
1. TO THE LEFT	0.0400	684	10925 AA		0.0
	0.1200	2052	16879 BA		0.0
	0.0400	684	11902 EA		0.0
2. TO THE RIGHT	0.0400	684	10859 AA		0.0
	0.1200	2052	17423 BA		0.0
	0.0400	684	11650 EA		0.0
C. CONTROL REVERSAL					
1. LONGITUDINAL	0.0200	342	12655 AA		0.0

TABLE XIII - Concluded

FLIGHT CONDITION	FREQUENCY OF OCCURRENCE PCT. CYCLES IN TIME 100 HRS.	OSCILLATORY BENDING STR. IN M/R YOKE # STA. 7.0	CYC. TO FAILURE X 10**(-6)	DAMAGE FRACTION
2. LATERAL	0.0600	1026	23606 BA	0.0
	0.0200	342	17775 EA	0.0
	0.0200	342	16372 AA	0.0
	0.0600	1026	21151 BA	0.0
3. RUDDER	0.0200	342	19619 EA	0.0
	0.0200	342	10731 AA	0.0
	0.0600	1026	17239 BA	0.0
	0.0200	342	13859 EA	0.0
D. CYCLIC PULL-UP (NORMAL AUTO A/S)	0.0112	192	15668 AA	0.0
	0.0336	575	24080 BA	0.0
	0.0112	192	19326 EA	0.0
	0.4166	7124	13598 AA	0.0
E. PART PWR DSAT, 80KT	1.2498	21372	13189 BA	0.0
	0.4166	7124	9988 EA	0.0
	0.0600	1026	0 AA	0.0
	0.1800	3078	72276 BA	* 0.009818
F. FULL AUTO LANDING	0.0600	1026	0 FA	0.0
ZER. STEADY END. LIMIT = 30000.0				TOTAL DAMAGE (D) = 0.123372
MATERIAL = TIT				
FREQUENCY = 1 / REV OF M/R				FATIGUE LIFE = 100/D = 811 HOURS
* DAMAGE CALCULATED FROM MEASURED LOAD FREQUENCIES.				



Sec A-A

All Dimensions in Inches

$$I = 32.35 \text{ in.}^4$$

$$A = 11.19 \text{ in.}^2$$

$$C = 2.75 \text{ in.}$$

$$\sigma_b = (M_c^2 + M_b^2)^{1/2} (0.085 \text{ in.}^{-3})$$

$$\sigma_{cf} = P/(11.19 \text{ in.}^2)$$

Figure 94. Main Rotor Spindle, Part No. 609-010-140-1.

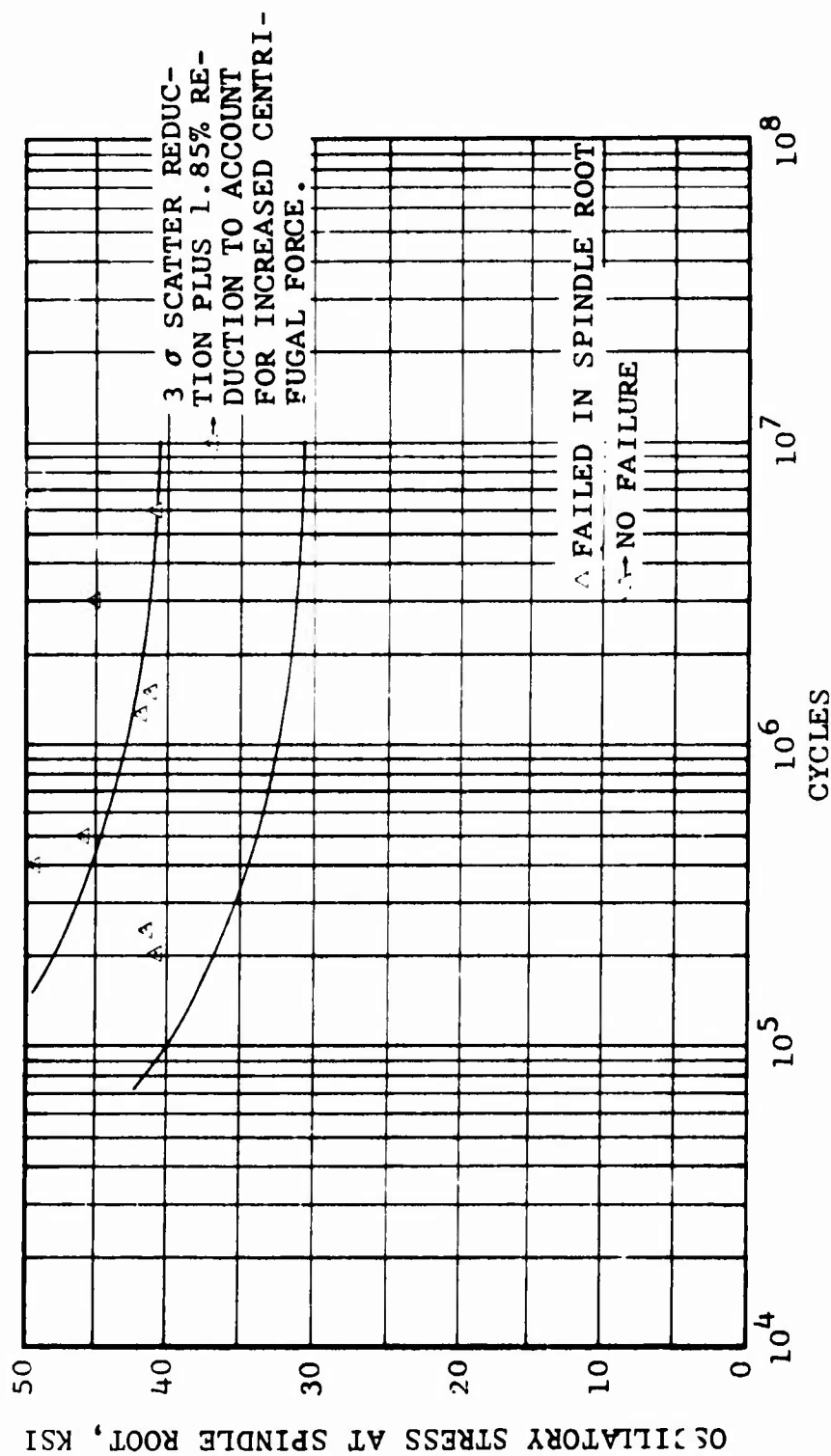


Figure 95. Oscillatory Stress Versus Cycles for the 204-011-102-17 Main Rotor Yoke Used To Substantiate the 609-010-140-1 Spindle.

TABLE XIV. FATIGUE LIFE DETERMINATION OF 609 M/R
SPINDLE, PART NO. 609-010-140-1

FLIGHT CONDITION	FREQUENCY OF OCCURRENCE PCT. CYCLES IN TIME 100 HRS.		Oscillatory bending stress @ STA. 34.75	CYC. TO FAILURE X 10**(-6)	DAMAGE FRACTION
I. GROUND CONDITIONS					
A. NORMAL START	0.1000	1770	0 AA		0.0
	0.3000	5310	2911 CA		0.0
	0.1000	1770	0 FA		0.0
B. NORMAL SHUTDOWN	0.1000	1770	2462 AA		0.0
	0.3000	5310	1217 CA		0.0
	0.1000	1770	0 FA		0.0
II. POWER-ON IGE					
A. HOVERING					
1. STEADY					
(A) 280 RPM	0.6944	11666	3707 AA		0.0
	2.0832	34998	5145 CA		0.0
	0.6944	11666	5906 FA		0.0
(B) 295 RPM	0.6944	12291	3248 AA		0.0
	2.0832	36873	8057 CA		0.0
	0.6944	12291	12041 EA		0.0
2. LEFT TURN	0.2222	3800	5146 AA		0.0
	0.6666	11399	6110 CA		0.0
	0.2222	3800	5267 EA		0.0
3. RIGHT TURN	0.2222	3800	6024 AA		0.0
	0.6666	11399	6701 CA		0.0
	0.2222	3800	5237 EA		0.0
4. CONTROL REVERSAL					
(A) LONGITUDINAL	0.0556	951	8650 AA		0.0
	0.1668	2852	11239 CA		0.0
	0.0556	951	15027 EA		0.0
(B) LATERAL	0.0556	951	9531 AA		0.0
	0.1668	2852	11688 BA		0.0
	0.0556	951	11047 EA		0.0
(C) RUDDER	0.0556	951	5547 AA		0.0
	0.1668	2852	5793 CA		0.0
	0.0556	951	5762 EA		0.0
B. MANEUVERS					
1. SIDEWARD FLIGHT					
(A) TO THE RIGHT	0.1000	1710	6883 AA		0.0
	0.3000	5130	12480 BA		0.0
	0.1000	1710	4064 EA		0.0
(B) TO THE LEFT	0.1000	1710	6771 AA		0.0
	0.3000	5130	7846 CA		0.0
	0.1000	1710	7535 EA		0.0
2. REARWARD FLIGHT	0.1000	1710	5525 AA		0.0
	0.3000	5130	10309 BA		0.0
	0.1000	1710	13343 EA		0.0
3. NORMAL TAKE-OFF	0.1778	3040	12112 AA		0.0
	0.5334	9121	10674 CA		0.0

TABLE XIV- Continued

FLIGHT CONDITION	FREQUENCY OF OCCURRENCE		Oscillatory bend- ing stress @ STA. 34.75		CYC. TO FAILURE X 10**(-6)	DAMAGE FRACTION
	PCT. TIME	CYCLES IN 100 HRS.				
4. NORMAL LANDING		0.1778	3040	13256 EA		0.0
		0.4166	7124	9395 AA		0.0
		1.2498	21372	13611 CA		0.0
		0.4166	7124	15473 EA		0.0
IX. POWER-ON IGF						
A. LEVEL FLIGHT						
	% VL	RPM				
1. 40	230		0.1866	3135	6007 AA	0.0
			0.5598	9405	8118 CA	0.0
			0.1866	3135	10954 FA	0.0
		295	0.1866	3303	5666 AA	0.0
			0.5598	9908	7619 CA	0.0
			0.1866	3303	9562 DA	0.0
		2. 50	0.4917	8261	5347 AA	0.0
			1.4751	24782	7621 CA	0.0
			0.4917	8261	10465 FA	0.0
		295	0.4917	8703	5036 AA	0.0
			1.4751	26109	7893 CA	0.0
			0.4917	8703	10120 FA	0.0
3. 60	280		0.7838	13168	6030 AA	0.0
			2.3514	39503	7970 CA	0.0
			0.7838	13168	10643 DA	0.0
		295	0.7838	13873	5463 AA	0.0
			2.3514	41620	7828 CA	0.0
			0.7838	13873	10711 EA	0.0
		4. 70	1.0000	16800	6662 AA	0.0
			3.0000	50400	8699 BA	0.0
			1.0000	16800	11641 DA	0.0
		295	1.0000	17700	6494 AA	0.0
			3.0000	53100	8271 CA	0.0
			1.0000	17700	11616 EA	0.0
5. 80	280		1.5000	25200	8908 AA	0.0
			4.5000	75600	10920 BA	0.0
			1.5000	25200	14522 DA	0.0
		295	1.5000	26550	7834 AA	0.0
			4.5000	79650	9242 CA	0.0
			1.5000	26550	11847 EA	0.0
		6. 90	1.7334	29121	11298 AA	0.0
			5.2002	87363	13677 BA	0.0
			1.7334	29121	21258 DA	0.0
		295	1.7334	30681	9786 AA	0.0
			5.2002	92044	11286 BA	0.0
			1.7334	30681	14324 DA	0.0
7. 100	280		0.9838	16528	13874 AA	0.0
			2.9514	49583	17010 BA	0.0

TABLE XIV- Continued

FLIGHT CONDITION	FREQUENCY OF OCCURRENCE		Oscillatory bending stress @ STA. FAILURE		DAMAGE FRACTION
	PCT. TIME	CYCLES IN 100 HRS.	34.75	CYC. TO FAILURE X 10**(-6)	
B. VNF 280		0.9838	16528	20587 EA	0.0
		0.9838	17413	11944 AA	0.0
		2.9514	52240	15724 CA	0.0
		0.9838	17413	17466 DA	0.0
		0.3500	5880	15333 AA	0.0
		1.0500	17640	16440 CA	0.0
		0.3500	5880	17922 EA	0.0
	295	0.3500	6195	12098 AA	0.0
		1.0500	18585	14557 CA	0.0
		0.3500	6195	14461 EA	0.0
H. MANEUVERS					
1. CLIMB 3-60 KNOTS					
(A) M.C. POWER		0.6000	10260	9219 AA	0.0
		1.8000	30780	9309 CA	0.0
		0.6000	10260	11490 EA	0.0
(B) T.O. POWER		0.2000	3420	7911 AA	0.0
		0.6000	10260	9342 CA	0.0
		0.2000	3420	10760 EA	0.0
2. CYCLIC PULL-UP					
(A) 50 KNOTS		0.0324	554	7412 AA	0.0
		0.0972	1662	12516 CA	0.0
		0.0324	554	10306 EA	0.0
(B) 100 KNOTS		0.0324	554	10346 AA	0.0
		0.0972	1662	13951 CA	0.0
		0.0324	554	14767 EA	0.0
(C) VL		0.0324	554	16282 AA	0.0
		0.0972	1662	26517 CA	0.0
		0.0324	554	32106 EA	0.282
3. LEFT TURN					
(A) 50 KNOTS		0.2000	3420	7834 AA	0.0
		0.6000	10260	10012 CA	0.0
		0.2000	3420	12316 EA	0.0
(B) 100 KNOTS		0.2000	3420	9880 AA	0.0
		0.6000	10260	12059 CA	0.0
		0.2000	3420	16959 EA	0.0
(C) VL		0.1000	1710	16212 AA	0.0
		0.3000	5130	22266 BA	0.0
		0.1000	1710	32106 EA	0.282
4. RIGHT TURN					
(A) 50 KNOTS		0.2000	3420	8660 AA	0.0
		0.6000	10260	11452 CA	0.0
		0.2000	3420	10750 EA	0.0
(B) 100 KNOTS		0.2000	3420	9840 AA	0.0
		0.6000	10260	13244 CA	0.0
		0.2000	3420	14999 EA	0.0
(C) VL		0.1000	1710	18444 AA	0.0

TABLE XIV- Continued

FLIGHT CONDITION	FREQUENCY OF OCCURRENCE PCT. TIME	CYCLES IN 100 HRS.	Oscillatory bending stress @ STA. 34.75	CYC. TO FAILURE X 10**(-6)	DAMAGE FRACTION
	0.3000	5130	23274 CA		0.0
	0.1000	1710	32106 EA	0.282	0.006057
5. CONTROL REVERSAL					
(A) LONGITUDINAL	0.0444	759	10608 AA		0.0
	0.1332	2278	17203 BA		0.0
	0.0444	759	16692 EA		0.0
(B) LATERAL	0.0444	759	11381 AA		0.0
	0.1332	2278	20014 CA		0.0
	0.0444	759	17842 EA		0.0
(C) RUDDER	0.0444	759	9982 AA		0.0
	0.1332	2278	13364 CA		0.0
	0.0444	759	15804 EA		0.0
IV. POWER TRANSITIONS					
A. POWER TO AUTO					
1. 40 KNOTS	0.0022	38	5412 AA		0.0
	0.0066	113	9002 CA		0.0
	0.0022	38	11419 FA		0.0
2. VL	0.0022	38	12710 AA		0.0
	0.0066	113	14895 BA		0.0
	0.0022	38	16172 FA		0.0
B. AUTO TO POWER	0.0112	192	7664 AA		0.0
	0.0336	575	7121 CA		0.0
	0.0112	192	12963 EA		0.0
V. AUTOROTATION					
A. STABILIZED FLIGHT					
1. 40 KNOTS	0.0578	988	3354 AA		0.0
	0.1734	2965	4983 CA		0.0
	0.0578	988	4474 EA		0.0
2. 80 KNOTS	0.0776	1327	4103 AA		0.0
	0.2328	3981	5800 CA		0.0
	0.0776	1327	5193 EA		0.0
3. MAX AUTO A/S	0.0378	646	4763 AA		0.0
	0.1134	1939	7743 CA		0.0
	0.0378	646	7242 FA		0.0
B. TURNS. (NORMAL AUTO A/S)					
1. TO THE LEFT	0.0400	684	4250 AA		0.0
	0.1200	2052	5213 CA		0.0
	0.0400	684	4882 EA		0.0
2. TO THE RIGHT	0.0400	684	4541 AA		0.0
	0.1200	2052	4547 CA		0.0
	0.0400	684	4481 FA		0.0
C. CONTROL REVERSAL					
1. LONGITUDINAL	0.0200	342	4902 AA		0.0

TABLE XIV- Concluded

TABLE XIV- Concluded					
FLIGHT CONDITION	FREQUENCY OF OCCURRENCE PCT. TIME	CYCLES IN 100 HRS.	Oscillatory bend- ing stress @ STA. 34.75	CYC. TO FAILURE X 10**(-6)	DAMAGE FRACTION
2. LATERAL	0.0600	1026	6445 BA		0.0
	0.0200	342	7081 FA		0.0
	0.0200	342	7088 AA		0.0
	0.0600	1026	11361 CA		0.0
	0.0200	342	8979 EA		0.0
3. ROLLER	0.0200	342	3864 AA		0.0
	0.0600	1026	4974 CA		0.0
	0.0200	342	6195 EA		0.0
D. CYCLIC PULL-UP (NORMAL AUTO 4/S)	0.0112	192	6278 AA		0.0
	0.0336	575	6506 CA		0.0
	0.0112	192	7219 EA		0.0
	E. PART PWR DSNT. 80KT	0.4166	7124	5464 AA	
1.2498		21372	5630 CA		0.0
0.4166		7124	5917 EA		0.0
F. FULL AUTO LANDING	0.0600	1026	0 AA		0.0
	0.1800	3078	28373 BA	*	0.000007
	0.0600	1026	0 FA		0.0
ENDURANCE LIMIT = 27500.0			TOTAL DAMAGE (D) = 0.014084		
MATERIAL = STL2			FATIGUE LIFE = 100/D = 7100 HOURS		
FREQUENCY = 1 / REV OF M/R					
* DAMAGE CALCULATED FROM MEASURED LOAD FREQUENCIES.					

retention system, the most critical component in fatigue is the 609-010-105-3 fitting, Figure 96, which is machined from 2024 aluminum alloy in the T-42 condition. It was analyzed for axial stress at the juncture of barrel and flange. The oscillatory stress calculated for a load of 96,000 pounds applied at the inboard fitting was $\sigma = 16,095$ psi. The number of cycles to failure was calculated to be 6373. This calculation used the Weibull Equation of Reference 16:

$$N = \frac{K}{\left(\frac{S - E^{\infty}}{\bar{E}} \right)^m}$$

where

N = number of cycles to failure at a given oscillatory stress level, S

\bar{E} = 3600 psi, component endurance limit

Material Constants

$$E^{\infty} = 2881$$

$$K = 4.76845 \times 10^5$$

$$m = 3.3184$$

The frequency of occurrence of load cycles on the main rotor retention system was based on four rotor starts and stops per flight hour. Using this spectrum, a life of 1593 hours was substantiated for the main rotor retention system. Calculations for the -105-3 fitting are shown below.

Material: Aluminum

$$A = 5.96 \text{ in.}^2$$

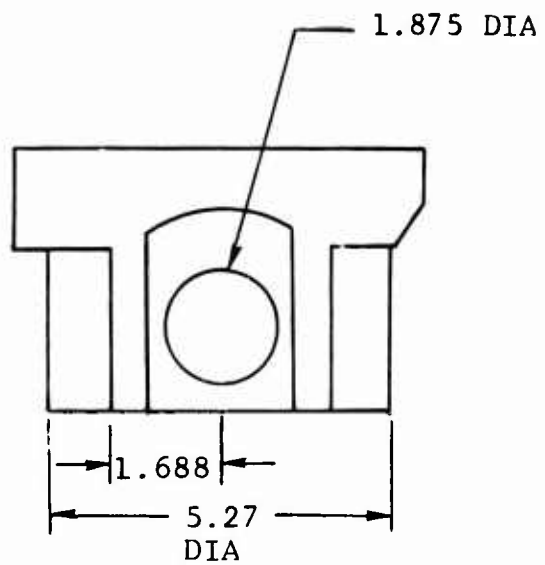
$$\text{C.F.} = 96,000 \text{ lb}$$

$$\sigma = (\text{C.F.})/A = 16,095 \text{ psi}$$

$$N = 6373 \text{ cycles}$$

$$\text{Fatigue life} = N/4 \text{ cycles/hour}$$

$$\text{Fatigue life} = 1593 \text{ hours}$$



All Dimensions in Inches

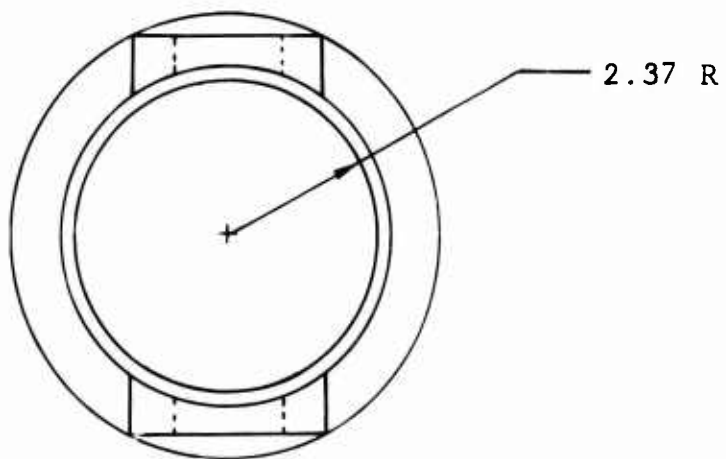


Figure 96. Main Rotor Blade Retention Fitting, Part No. 609-010-105-3.

Main Rotor Blade Part No. 609-010-200-1

Several sections of the blade were analyzed to determine the most critical combination of mean and oscillatory stress. An examination of the loading during various flight conditions showed the blade to be critical in fatigue at station 94.0. The major component of oscillatory stress is due to the chordwise bending moment; the steady stress in the blade is due to the centrifugal loading in addition to chordwise bending. The maximum stress at station 94.0 occurred at the trailing edge for which the stress is given by

$$\begin{aligned}\sigma_{\text{mean}} &= (0.16) (M_C 94.0) + 38422.0 \\ \sigma_{\text{osc}} &= (0.16) (M_C 94.0)\end{aligned}$$

where

$M_C 94.0$ is the chord moment at station 94.0, mean and oscillatory respectively.

For an endurance limit of 22,500 psi, the fatigue life calculated for the main rotor blade was 1334 hours. The fatigue life calculations for this component are shown in Table XV.

ROTATING CONTROLS

The rotating control system of the Model 609 main rotor includes the pitch horns and the outer ring of the swashplate, and all dynamic components in between. Analysis of these components showed the outer ring of the swashplate to be the most critical in fatigue.

The 609-010-401-3 outer ring, of 2014 aluminum alloy, is loaded by the four main rotor pitch links and by the main rotor drive links. Analysis showed the outer ring to be critical in bending at the arm-to-ring juncture (Section A-A of Figure 97). The stress equation for this location is:

$$\sigma_B = 6.86 (\text{pitch link load})$$

In the absence of fatigue test results, an endurance limit of 3600 psi was used for the swashplate outer ring, a value obtained from material allowables given in Reference 16. With these figures, a fatigue life of 11,557 hours was calculated for the 609-010-401-3 swashplate outer ring. All other components in the 609 main rotor rotating control system are at least as good as the swashplate outer ring in fatigue. Table XVI shows the fatigue life calculations for the swashplate outer ring; fatigue lives calculated for other major components of the rotating control system are shown in Table VI.

TABLE XV. FATIGUE LIFE DETERMINATION OF 609 M/R
BLADE, PART NO. 609-010-200-1

FLIGHT CONDITION	FREQUENCY OF OCCURRENCE PCT. CYCLES IN TIME 100 HRS.		OSCILLATORY BENDING STR. IN M/R BLADE @ STA. 94.0	CYC. TO FAILURE X 10**(-6)	DAMAGE FRACTION
I. GROUND CONDITIONS					
A. NORMAL START	0.1000	1770	0 AA		0.0
	0.3000	5310	3265 CA		0.0
	0.1000	1770	0 FA		0.0
B. NORMAL SHUTDOWN	0.1000	1770	2766 AA		0.0
	0.3000	5310	1367 CA		0.0
	0.1000	1770	0 FA		0.0
II. POWER-ON IGF					
A. HOVERING					
1. STEADY					
(A) 280 RPM	0.6944	11666	3437 AA		0.0
	2.0832	34998	5406 CA		0.0
	0.6944	11666	6772 EA		0.0
(B) 295 RPM	0.6944	12291	3097 AA		0.0
	2.0832	36873	8274 CA		0.0
	0.6944	12291	13330 EA		0.0
2. LEFT TURN	0.2222	3800	4830 AA		0.0
	0.6666	11399	6202 CA		0.0
	0.2222	3800	5607 EA		0.0
3. RIGHT TURN	0.2222	3800	5807 AA		0.0
	0.6666	11399	6545 CA		0.0
	0.2222	3800	5873 EA		0.0
4. CONTROL REVERSAL					
(A) LONGITUDINAL	0.0556	951	9728 AA		0.0
	0.1668	2852	11231 CA		0.0
	0.0556	951	16253 EA		0.0
(B) LATERAL	0.0556	951	10281 AA		0.0
	0.1668	2852	12718 BA		0.0
	0.0556	951	11015 EA		0.0
(C) RUDDER	0.0556	951	5443 AA		0.0
	0.1668	2852	6157 CA		0.0
	0.0556	951	6004 EA		0.0
B. MANEUVERS					
1. SIDEWARD FLIGHT					
(A) TO THE RIGHT	0.1000	1710	7267 AA		0.0
	0.3000	5130	13317 BA		0.0
	0.1000	1710	4570 EA		0.0
(B) TO THE LEFT	0.1000	1710	7398 AA		0.0
	0.3000	5130	8050 CA		0.0
	0.1000	1710	8228 EA		0.0
2. REARWARD FLIGHT	0.1000	1710	6210 AA		0.0
	0.3000	5130	10579 BA		0.0
	0.1000	1710	14947 EA		0.0
3. NORMAL TAKE-OFF	0.1778	3040	12347 AA		0.0
	0.5334	9121	11188 CA		0.0

TABLE XV - Continued

FLIGHT CONDITION		FREQUENCY OF OCCURRENCE PCT. CYCLES IN TIME 100 HRS.		OSCILLATORY BENDING STR. IN M/R BLADE @ STA. 94.0	CYC. TO FAILURE X 10**(-6)	DAMAGE FRACTION
4. NORMAL LANDING		0.1778	3040	14501 EA		0.0
		0.4166	7124	14140 AA		0.0
		1.2498	21372	14744 CA		0.0
		0.4166	7124	17618 EA		0.0
III. POWER-ON IGE						
4. LEVEL FLIGHT						
X VL RPM						
1. 40	280	0.1866	3135	6271 AA		0.0
		0.5598	9405	8691 CA		0.0
		0.1866	3135	12345 FA		0.0
		0.1866	3303	5683 AA		0.0
	295	0.5598	9908	8622 CA		0.0
		0.1866	3303	10627 DA		0.0
		0.4917	8261	5387 AA		0.0
		1.4751	24782	8153 CA		0.0
2. 50	280	0.4917	8261	11639 EA		0.0
		0.4917	8703	5346 AA		0.0
		1.4751	26109	8537 CA		0.0
		0.4917	8703	10774 FA		0.0
	295	0.7838	13168	5560 AA		0.0
		2.3514	39503	7938 BA		0.0
		0.7838	13168	10946 DA		0.0
		0.7838	13873	5325 AA		0.0
3. 60	280	2.3514	41620	7738 CA		0.0
		0.7838	13873	10975 EA		0.0
		1.0000	16800	6364 AA		0.0
		3.0000	50400	9293 BA		0.0
	295	1.0000	16800	12375 DA		0.0
		1.0000	17700	6106 AA		0.0
		3.0000	53100	8337 CA		0.0
		1.0000	17700	12146 EA		0.0
5. 80	280	1.5000	25200	8812 AA		0.0
		4.5000	75600	11641 BA		0.0
		1.5000	25200	15048 DA		0.0
		1.5000	26550	8035 AA		0.0
	295	4.5000	79650	9642 CA		0.0
		1.5000	26550	12907 EA		0.0
		1.7334	29121	11446 AA		0.0
		5.2002	87363	14434 BA		0.0
6. 90	280	1.7334	29121	20974 DA		0.0
		1.7334	30681	9906 AA		0.0
		5.2002	92044	12541 BA		0.0
		1.7334	30681	15020 DA		0.0
	295	0.9838	16528	14380 AA		0.0
		2.9514	49583	18250 CA		0.0
7. 100	280					

TABLE XV - Continued

FLIGHT CONDITION		FREQUENCY OF OCCURRENCE PCT. CYCLES IN TIME 100 HRS.		OSCILLATORY BENDING STR. IN M/R BLADE @ STA. 94.0	CYC. TO FAILURE X 10**(-6)	DAMAGE FRACTION
	295	0.9838	16528	21894 EA		0.0
		0.9838	17413	12725 AA		0.0
		2.9514	52240	17257 CA		0.0
		0.9838	17413	19431 DA		0.0
R. VNE	280	0.3500	5880	16051 AA		0.0
		1.0500	17640	17648 CA		0.0
		0.3500	5880	18682 EA		0.0
	295	0.3500	6195	13093 AA		0.0
		1.0500	18585	15778 CA		0.0
		0.3500	6195	15682 EA		0.0
H. MANEUVERS						
1. CLIMB 3-60 KNOTS						
(A) M.C. POWER		0.6000	10260	9218 AA		0.0
		1.8000	30780	9175 CA		0.0
		0.6000	10260	12648 EA		0.0
(B) T.O. POWER		0.2000	3420	7505 AA		0.0
		0.6000	10260	8786 CA		0.0
		0.2000	3420	12151 EA		0.0
2. CYCLIC PULL-UP						
(A) 50 KNOTS		0.0324	554	7418 AA		0.0
		0.0972	1662	13298 CA		0.0
		0.0324	554	11474 EA		0.0
(B) 100 KNOTS		0.0324	554	10236 AA		0.0
		0.0972	1662	14503 CA		0.0
		0.0324	554	16216 EA		0.0
(C) VL		0.0324	554	17520 AA		0.0
		0.0972	1662	27849 CA	0.187	0.008903
		0.0324	554	34315 EA	0.072	0.007712
3. LEFT TURN						
(A) 50 KNOTS		0.2000	3420	7704 AA		0.0
		0.6000	10260	10401 CA		0.0
		0.2000	3420	14001 EA		0.0
(B) 100 KNOTS		0.2000	3420	9702 AA		0.0
		0.6000	10260	12522 CA		0.0
		0.2000	3420	18868 EA		0.0
(C) VL		0.1000	1710	17112 AA		0.0
		0.3000	5130	22363 BA		0.0
		0.1000	1710	34315 EA	0.072	0.003803
4. RIGHT TURN						
(A) 50 KNOTS		0.2000	3420	8390 AA		0.0
		0.6000	10260	12206 CA		0.0
		0.2000	3420	11765 EA		0.0
(B) 100 KNOTS		0.2000	3420	9645 AA		0.0
		0.6000	10260	13660 CA		0.0
		0.2000	3420	15963 EA		0.0
(C) VL		0.1000	1710	19688 AA		0.0

TABLE XV - Continued

FLIGHT CONDITION	FREQUENCY OF OCCURRENCE PCT. TIME	CYCLES IN 100 HRS.	OSCILLATORY BENDING STR. IN M/R BLADE @ STA. 94.0	CYC. TO FAILURE X 10**(-6)	DAMAGE FRACTION
	0.3000	5130	24807 BA	0.497	0.010327
	0.1000	1710	34315 EA	0.072	0.023803
5. CONTROL REVERSAL					
(A) LONGITUDINAL	0.0444	759	10939 AA		0.0
	0.1332	2278	18316 BA		0.0
	0.0444	759	18299 EA		0.0
(B) LATERAL	0.0444	759	11054 AA		0.0
	0.1332	2278	20769 CA		0.0
	0.0444	759	19033 EA		0.0
(C) RUDDER	0.0444	759	9766 AA		0.0
	0.1332	2278	14543 BA		0.0
	0.0444	759	17044 EA		0.0
IV. POWER TRANSITIONS					
A. POWER TO AUTO					
1. 40 KNOTS	0.0022	38	5369 AA		0.0
	0.0066	113	9824 CA		0.0
	0.0022	38	12560 EA		0.0
2. VL	0.0022	38	13660 AA		0.0
	0.0066	113	16671 BA		0.0
	0.0022	38	17396 EA		0.0
B. AUTO TO POWER	0.0112	192	8301 AA		0.0
	0.0336	575	7367 CA		0.0
	0.0112	192	14680 EA		0.0
V. AUTOROTATION					
A. STABILIZED FLIGHT					
1. 40 KNOTS	0.0578	988	3323 AA		0.0
	0.1734	2965	5091 CA		0.0
	0.0578	988	5265 EA		0.0
2. 80 KNOTS	0.0776	1327	3846 AA		0.0
	0.2328	3981	5061 CA		0.0
	0.0776	1327	5912 EA		0.0
3. MAX AUTO A/S	0.0378	646	5314 AA		0.0
	0.1134	1939	8391 CA		0.0
	0.0378	646	23072 EA	2.085	0.000310
B. TURNS. (NORMAL AUTO A/S)					
1. TO THE LEFT	0.0400	684	3964 AA		0.0
	0.1200	2052	4626 CA		0.0
	0.0400	684	5782 EA		0.0
2. TO THE RIGHT	0.0400	684	4430 AA		0.0
	0.1200	2052	4452 CA		0.0
	0.0400	684	5569 EA		0.0
C. CONTROL REVERSAL					
1. LONGITUDINAL	0.0200	342	5274 AA		0.0

TABLE XV - Concluded

FLIGHT CONDITION	FREQUENCY OF OCCURRENCE PCT. CYCLES IN TIME 100 HRS.	OSCILLATORY BENDING STR. IN M/R BLADE @ STA. 94.0	CYC. TO FAILURE X 10**(-6)	DAMAGE FRACTION
2. LATERAL	0.0600	1026	6834 CA	0.0
	0.0200	342	7284 EA	0.0
	0.0200	342	6817 AA	0.0
	0.0600	1026	10836 CA	0.0
3. RUDDER	0.0200	342	10647 EA	0.0
	0.0200	342	3736 AA	0.0
	0.0600	1026	5356 CA	0.0
	0.0200	342	6462 EA	0.0
D. CYCLIC PULL-UP (NORMAL AUTO 4/S)	0.0112	192	6181 AA	0.0
	0.0336	575	5970 CA	0.0
	0.0112	192	7842 EA	0.0
	0.4166	7124	5223 AA	0.0
E. PART PWR DSNT. 80KT	1.2498	21372	5995 CA	0.0
	0.4166	7124	6792 EA	0.0
	0.0600	1026	0 AA	0.0
	0.1800	3078	26395 BA	* 0.000090
F. FULL AUTO LANDING	0.0600	1026	0 FA	0.0
	0.0600	1026	0 FA	0.0
ENDURANCE LIMIT = 22500.0				TOTAL DAMAGE (D) = 0.074948
MATERIAL = ST12				
FREQUENCY = 1 / REV OF M/R				FATIGUE LIFE = 100/D = 1334 HOURS
* DAMAGE CALCULATED FROM MEASURED LOAD FREQUENCIES.				

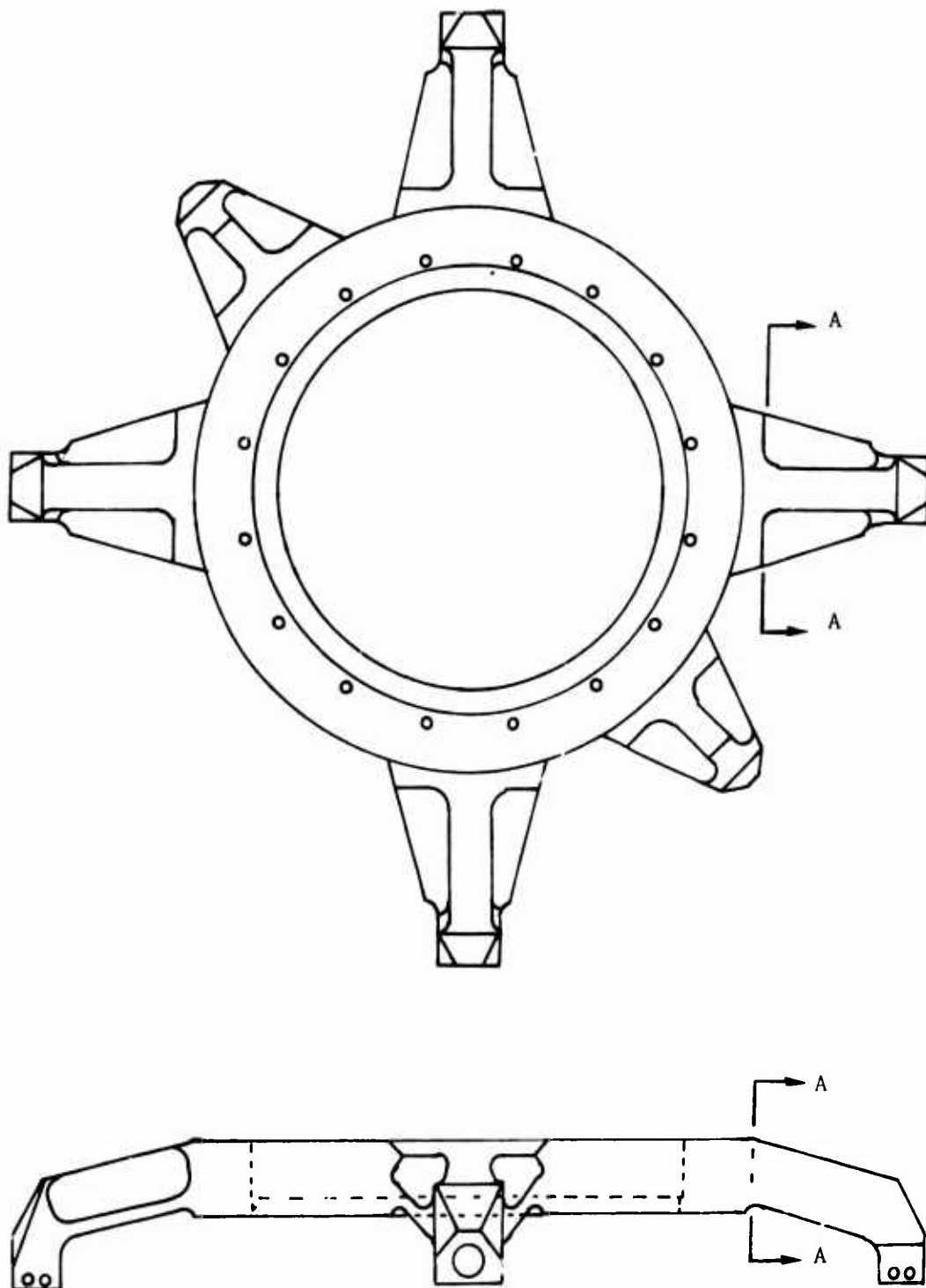
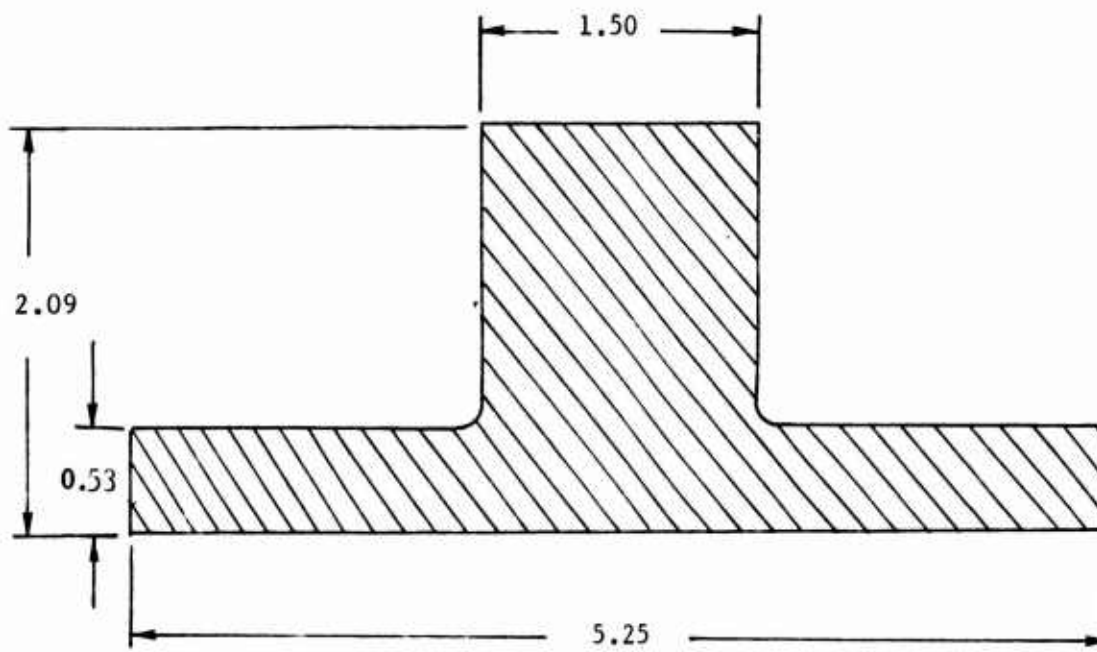


Figure 97. Swashplate Outer Ring, Part No. 609-010-401-3.



All Dimensions in Inches

Sec A-A

$$A = 5.12 \text{ in.}^2$$

$$I_y = 1.81 \text{ in.}^4$$

$$C = 1.30 \text{ in.}$$

$$M = (9.56 \text{ in.})(\text{Pitch Link Load})$$

$$\sigma_b = (6.86/\text{in.}^2)(\text{Pitch Link Load})$$

Figure 97. Concluded.

TABLE XVI. FATIGUE LIFE DETERMINATION OF 609 SWASHPLATE
OUTER RING, PART NO. 609-010-401-3

FLIGHT CONDITION	FREQUENCY OF OCCURRENCE		OSCILLATORY BENDING STR. IN S/P ARM OUTER RING	CYC. TO FAILURE X 10**(-6)	DAMAGE FRACTION
	PCT. TIME	CYCLES IN 100 HRS.			
I. GROUND CONDITIONS					
A. NORMAL START	0.1000	1770	0 AA		0.0
	0.3000	5310	782 CA		0.0
	0.1000	1770	0 FA		0.0
B. NORMAL SHUTDOWN	0.1000	1770	700 AA		0.0
	0.3000	5310	453 CA		0.0
	0.1000	1770	0 FA		0.0
II. POWER-ON ICE					
A. HOVERING					
1. STEADY					
(A) 280 RPM	0.6944	11666	761 AA		0.0
	2.0832	34998	1104 CA		0.0
	0.6944	11666	1564 EA		0.0
(B) 295 RPM	0.6944	12291	782 AA		0.0
	2.0832	36873	1276 CA		0.0
	0.6944	12291	1948 EA		0.0
2. LEFT TURN	0.2222	3800	885 AA		0.0
	0.6666	11399	885 CA		0.0
	0.2222	3800	1166 EA		0.0
3. RIGHT TURN	0.2222	3800	954 AA		0.0
	0.6666	11399	1111 CA		0.0
	0.2222	3800	1015 EA		0.0
4. CONTROL REVERSAL					
(A) LONGITUDINAL	0.0556	951	1255 AA		0.0
	0.1668	2852	1468 CA		0.0
	0.0556	951	1269 EA		0.0
(B) LATERAL	0.0556	951	1221 AA		0.0
	0.1668	2852	1269 CA		0.0
	0.0556	951	1194 EA		0.0
(C) RUDDER	0.0556	951	816 AA		0.0
	0.1668	2852	857 CA		0.0
	0.0556	951	947 EA		0.0
B. MANEUVERS					
1. SIDEWARD FLIGHT					
(A) TO THE RIGHT	0.1000	1710	1091 AA		0.0
	0.3000	5130	1667 BA		0.0
	0.1000	1710	748 EA		0.0
(B) TO THE LEFT	0.1000	1710	906 AA		0.0
	0.3000	5130	1091 CA		0.0
	0.1000	1710	1255 EA		0.0
2. REARWARD FLIGHT	0.1000	1710	1235 AA		0.0
	0.3000	5130	1626 BA		0.0
	0.1000	1710	2092 EA		0.0
3. NORMAL TAKE-OFF	0.1778	3040	2003 AA		0.0
	0.5334	9121	1811 BA		0.0

TABLE XVI- Continued

FLIGHT CONDITION	FREQUENCY OF OCCURRENCE		OSCILLATORY BENDING STR. IN S/P ARM OUTER RING	CYC. TO FAILURE X 10**(-6)	DAMAGE FRACTION	
	PCT. TIME	CYCLES IN 100 HRS.				
4. NORMAL LANDING		0.1778	3040	1900 EA	0.0	
		0.4166	7124	1832 AA	0.0	
		1.2498	21372	2367 CA	0.0	
		0.4166	7124	2627 EA	0.0	
III. POWER-ON IGF						
A. LEVEL FLIGHT						
% VL	RPM					
1. 40	280	0.1866	3135	1098 AA	0.0	
		0.5598	9405	1098 CA	0.0	
		0.1866	3135	1585 FA	0.0	
		295	0.1866	3303	1125 AA	0.0
		0.5598	9908	1077 CA	0.0	
		0.1866	3303	1461 FA	0.0	
		280	0.4917	8261	1056 AA	0.0
			1.4751	24782	1132 CA	0.0
		0.4917	8261	1605 FA	0.0	
		295	0.4917	8703	1050 AA	0.0
			1.4751	26109	1098 CA	0.0
			0.4917	8703	1598 FA	0.0
3. 60	280	0.7838	13168	1180 AA	0.0	
		2.3514	39503	1303 CA	0.0	
		0.7838	13168	1784 FA	0.0	
		295	0.7838	13873	1228 AA	0.0
		2.3514	41620	1200 CA	0.0	
		0.7838	13873	1749 FA	0.0	
		280	1.0000	16800	1249 AA	0.0
			3.0000	50400	1303 CA	0.0
		1.0000	16800	2223 FA	0.0	
		295	1.0000	17700	1406 AA	0.0
			3.0000	53100	1290 CA	0.0
			1.0000	17700	1907 FA	0.0
5. 80	280	1.5000	25200	1489 AA	0.0	
		4.5000	75600	1509 BA	0.0	
		1.5000	25200	2291 DA	0.0	
		295	1.5000	26550	1646 AA	0.0
		4.5000	79650	1358 BA	0.0	
		1.5000	26550	2017 FA	0.0	
		280	1.7334	29121	1859 AA	0.0
			5.2002	87463	1976 BA	0.0
		1.7334	29121	3307 DA	0.0	
		295	1.7334	30681	2188 AA	0.0
			5.2002	92044	1996 CA	0.0
			1.7334	30681	2579 FA	0.0
7. 100	280	0.9838	16528	2326 AA	0.0	
		2.9514	49583	2614 CA	0.0	

TABLE XVI- Continued

FLIGHT CONDITION		FREQUENCY OF OCCURRENCE PCT. CYCLES IN TIME 100 HRS.		OSCILLATORY BENDING STR. IN S/P ARM OUTER RING	CYC. TO FAILURE X 10**(-6)	DAMAGE FRACTION	
R. VNE	295	0.9838	16528	3114 EA		0.0	
		0.9838	17413	2559 AA		0.0	
		2.9514	52240	3293 CA		0.0	
	280	0.9838	17413	3361 EA		0.0	
		0.3500	5880	2346 AA		0.0	
		1.0500	17640	2792 CA		0.0	
		0.3500	5880	2785 EA		0.0	
		295	0.3500	6195	3190 AA		0.0
		1.0500	18585	3533 CA		0.0	
		0.3500	6195	3499 EA		0.0	
R. MANEUVERS							
1. CLIMB 0-60 KNOTS							
(A) M.C. POWER	0.6000	10260	1417 AA		0.0		
	1.8000	30780	1276 CA		0.0		
	0.6000	10260	1886 EA		0.0		
	(B) T.O. POWER	0.2000	3420	1626 AA		0.0	
		0.6000	10260	1447 CA		0.0	
		0.2000	3420	1886 EA		0.0	
2. CYCLIC PULL-UP							
(A) 50 KNOTS	0.0324	554	1441 AA		0.0		
	0.0972	1662	1681 CA		0.0		
	0.0324	554	1585 EA		0.0		
	(B) 100 KNOTS	0.0324	554	1777 AA		0.0	
		0.0972	1662	1976 CA		0.0	
		0.0324	554	2291 EA		0.0	
(C) VL	0.0324	554	2374 AA		0.0		
	0.0972	1662	5083 CA	2.436	0.000682		
	0.0324	554	6270 EA	0.583	0.000951		
3. LEFT TURN							
(A) 50 KNOTS	0.2000	3420	1249 AA		0.0		
	0.6000	10260	1331 CA		0.0		
	0.2000	3420	1777 EA		0.0		
	(B) 100 KNOTS	0.2000	3420	1454 AA		0.0	
		0.6000	10260	1866 BA		0.0	
		0.2000	3420	2380 EA		0.0	
(C) VL	0.1000	1710	2675 AA		0.0		
	0.3000	5130	3821 BA	41.084	0.000125		
	0.1000	1710	6270 EA	0.583	0.002935		
4. RIGHT TURN							
(A) 50 KNOTS	0.2000	3420	1310 AA		0.0		
	0.6000	10260	1550 CA		0.0		
	0.2000	3420	1482 EA		0.0		
	(B) 100 KNOTS	0.2000	3420	1571 AA		0.0	
		0.6000	10260	1688 CA		0.0	
		0.2000	3420	2051 EA		0.0	
(C) VL	0.1000	1710	2895 AA		0.0		

TABLE XVI- Continued

FLIGHT CONDITION	FREQUENCY OF OCCURRENCE		OSCILLATORY BENDING STR. IN S/P ARM OUTER RING	CYC. TO FAILURE X 10**(-6)	DAMAGE FRACTION
	PCT. TIME	CYCLES IN 100 HRS.			
	0.3000	5130	4637 CA	5.161	0.000994
	0.1000	1710	6270 EA	0.583	0.002935
5. CONTROL REVERSAL					
(A) LONGITUDINAL	0.0444	759	2175 AA		0.0
	0.1332	2278	2223 BA		0.0
	0.0444	759	2655 EA		0.0
(B) LATERAL	0.0444	759	1996 AA		0.0
	0.1332	2278	2531 CA		0.0
	0.0444	759	2867 EA		0.0
(C) RUDDER	0.0444	759	1886 AA		0.0
	0.1332	2278	1996 BA		0.0
	0.0444	759	2497 EA		0.0
IV. POWER TRANSITIONS					
A. POWER TO AUTO					
1. 40 KNOTS	0.0022	38	1022 AA		0.0
	0.0066	113	1159 CA		0.0
	0.0022	38	1578 EA		0.0
2. VL	0.0022	38	1893 AA		0.0
	0.0066	113	2326 BA		0.0
	0.0022	38	2689 EA		0.0
B. AUTO TO POWER	0.0112	192	1228 AA		0.0
	0.0336	575	1056 CA		0.0
	0.0112	192	1605 EA		0.0
V. AUTOROTATION					
A. STABILIZED FLIGHT					
1. 40 KNOTS	0.0578	988	837 AA		0.0
	0.1734	2965	637 CA		0.0
	0.0578	988	857 EA		0.0
2. 80 KNOTS	0.0776	1327	960 AA		0.0
	0.2328	3981	1043 CA		0.0
	0.0776	1327	919 EA		0.0
3. MAX AUTO A/S	0.0378	646	1043 AA		0.0
	0.1134	1939	1255 CA		0.0
	0.0378	646	1166 EA		0.0
B. TURNS. (NORMAL AUTO A/S)					
1. TO THE LEFT	0.0400	684	974 AA		0.0
	0.1200	2052	1111 CA		0.0
	0.0400	684	988 EA		0.0
2. TO THE RIGHT	0.0400	684	809 AA		0.0
	0.1200	2052	809 CA		0.0
	0.0400	684	851 EA		0.0
C. CONTROL REVERSAL					
1. LONGITUDINAL	0.0200	342	1132 AA		0.0

TABLE XVI- Concluded

FLIGHT CONDITION	FREQUENCY OF OCCURRENCE PCT. CYCLES IN TIME 100 HRS.	OSCILLATORY BENDING STR. IN S/P ARM OUTER RING	CYC. TO FAILURE X 10**(-6)	DAMAGE FRACTION
	0.0600	1026	1125 CA	0.0
	0.0200	342	1043 EA	0.0
2. LATERAL	0.0200	342	1036 AA	0.0
	0.0600	1026	1063 CA	0.0
	0.0200	342	1029 EA	0.0
3. RUDDER	0.0200	342	906 AA	0.0
	0.0600	1026	933 CA	0.0
	0.0200	342	974 EA	0.0
D. CYCLIC PULL-UP (NORMAL AUTO A/S)	0.0112	192	1084 AA	0.0
	0.0336	575	1022 CA	0.0
	0.0112	192	1104 EA	0.0
F. PART PWR DSNT. ROKT	0.4166	7124	1050 AA	0.0
	1.2498	21372	1022 CA	0.0
	0.4166	7124	974 EA	0.0
F. FULL AUTO LANDING	0.0600	1026	0 AA	0.0
	0.1800	3078	5941 BA	*
	0.0600	1026	0 FA	0.0
ENDURANCE LIMIT = 3600.0				TOTAL DAMAGE (D) = 0.008652
MATERIAL = ALUM				
FREQUENCY = 1 / REV OF M/R				FATIGUE LIFE = 100/D = 11557 HOURS
* DAMAGE CALCULATED FROM MEASURED LOAD FREQUENCIES.				

NONROTATING CONTROLS

The nonrotating control system of the Model 609 main rotor includes all dynamic components below the outer ring of the swashplate, to and including the three boost cylinder housings. Analysis of these components showed the 609-010-419-5 slider lug attachment bolt to be the most critical in fatigue.

This bolt, of H-11 steel heat treated to an ultimate tensile strength of 256-284 ksi, is critical in bending. The bending stress equation at the point of maximum stress is:

$$\sigma_B = 16.2 \text{ (collective boost tube load)} \\ +44.4 \text{ (cyclic boost tube load)}$$

An endurance limit of 38,079 psi in bending was established for the 540-011-478-1 and -416-1 pins during tests of the 540-011-404-1 and -5 swashplate outer rings. These pins, of the same material as the -419-5 bolt and loaded in the same manner, have the S-N curve shown in Figure 98. Their characteristics were used to calculate a fatigue life of 545 hours for the -419-5 bolt. Table XVII shows the fatigue life calculations. They were based on a loading frequency of four cycles per main rotor revolution, which is a conservative estimate. Analysis of the flight test data showed that the phasing relationship between the collective and cyclic boost tubes is such that the stress calculated by the above equation occurs only once every rotor revolution. It is because the other three cycles are at a lower stress level that the above analysis is conservative. A detailed analysis of the loading on this component would result in a higher life estimate. A summary of fatigue lives calculated for some of the major components of the nonrotating control system is included in Table VI.

CONCLUSIONS

Fatigue lives have been calculated for the dynamic components of the Model 609 main rotor system, and are summarized in Table VI. They establish as the minimum fatigue life of the entire system the 545 hours of helicopter operation which is the fatigue life of the 609-010-419-5 slider lug attachment bolt.

These lives were based on the frequency-of-occurrence spectrum shown in Table III and should not be considered applicable in cases where the spectrum of operation differs radically from it. Spectrums consisting mainly of operations at high gross weights and aft cg locations cause substantial reductions in fatigue life, whereas low gross weights and forward or neutral

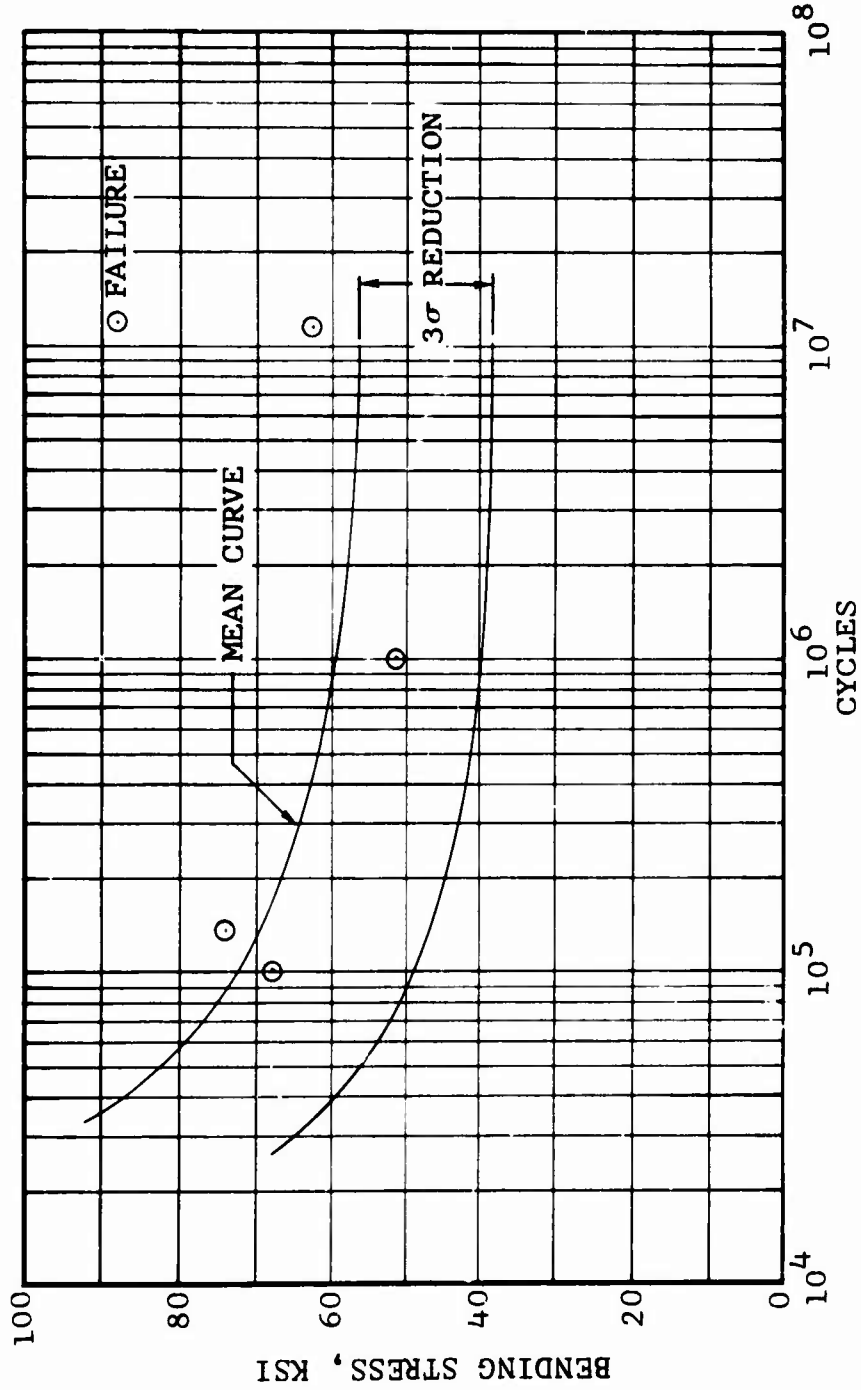


Figure 98. Oscillatory Stress Versus Cycles for the 540-011-478-1 Swashplate Outer Ring Pin Used To Substantiate the 609-010-419-5 Slider Lug Bolt.

TABLE XVII. FATIGUE LIFE DETERMINATION OF 609 SLIDER
LUG BOLT, PART NO. 609-010-419-5

FLIGHT CONDITION	FREQUENCY OF OCCURRENCE PCT. CYCLES IN TIME 100 HRS.		OSCILLATORY BENDING STR. FAILURE IN SLIDER LUG BOLT	CYC. TO FAILURE X 10**(-6)	DAMAGE FRACTION
I. GROUND CONDITIONS					
A. NORMAL START	0.1000	7080	0 AA		0.0
	0.3000	21240	5391 CA		0.0
	0.1000	7080	0 FA		0.0
B. NORMAL SHUTDOWN	0.1000	7080	6493 AA		0.0
	0.3000	21240	5788 CA		0.0
	0.1000	7080	0 FA		0.0
II. POWER-ON IGF					
A. HOVERING					
1. STEADY					
(A) 280 RPM	0.6944	46664	4877 AA		0.0
	2.0832	139991	7588 CA		0.0
	0.6944	46664	15892 EA		0.0
(B) 255 RPM	0.6944	49164	5196 AA		0.0
	2.0832	147490	7706 CA		0.0
	0.6944	49164	10168 EA		0.0
2. LEFT TURN	0.2222	15198	7330 AA		0.0
	0.6666	45595	7429 CA		0.0
	0.2222	15198	10460 EA		0.0
3. RIGHT TURN	0.2222	15198	7647 AA		0.0
	0.6666	45595	9832 BA		0.0
	0.2222	15198	8558 EA		0.0
4. CONTROL REVERSAL					
(A) LONGITUDINAL	0.0556	3803	12436 AA		0.0
	0.1668	11409	12107 CA		0.0
	0.0556	3803	14705 EA		0.0
(B) LATERAL	0.0556	3803	11308 AA		0.0
	0.1668	11409	6782 BA		0.0
	0.0556	3803	9648 EA		0.0
(C) RUDDER	0.0556	3803	6141 AA		0.0
	0.1668	11409	6495 CA		0.0
	0.0556	3803	7816 EA		0.0
B. MANEUVERS					
1. SIDEWARD FLIGHT					
(A) TO THE RIGHT	0.1000	6840	6797 AA		0.0
	0.3000	20520	10310 BA		0.0
	0.1000	6840	6081 EA		0.0
(B) TO THE LEFT	0.1000	6840	5376 AA		0.0
	0.3000	20520	5281 CA		0.0
	0.1000	6840	7683 EA		0.0
2. REARWARD FLIGHT	0.1000	6840	5363 AA		0.0
	0.3000	20520	10276 CA		0.0
	0.1000	6840	13159 EA		0.0
3. NORMAL TAKE-OFF	0.1778	12162	10255 AA		0.0
	0.5334	36485	13343 BA		0.0

TABLE XVII - Continued

FLIGHT CONDITION		FREQUENCY OF OCCURRENCE PCT. CYCLES IN TIME 100 HRS.	OSCILLATORY BENDING STR. IN SLIDER LUG BOLT	CYC. TO FAILURE X 10**(-6)	DAMAGE FRACTION
4. NORMAL LANDING		0.1778	12162	10955 EA	0.0
		0.4166	28495	13016 AA	0.0
		1.2498	85486	15809 CA	0.0
		0.4166	28495	23929 EA	0.0
III. POWER-ON IGF					
A. LEVEL FLIGHT					
% VL	RPM				
1. 40	230	0.1866	12540	6071 AA	0.0
		0.5598	37619	6892 BA	0.0
		0.1866	12540	9182 DA	0.0
		0.1866	13211	5472 AA	0.0
	295	0.5598	39634	7300 CA	0.0
		0.1866	13211	8363 FA	0.0
2. 50	230	0.4917	33042	6226 AA	0.0
		1.4751	99127	6688 CA	0.0
		0.4917	33042	8498 DA	0.0
		0.4917	34812	6517 AA	0.0
	295	1.4751	104437	7446 CA	0.0
		0.4917	34812	7854 DA	0.0
3. 60	230	0.7838	52671	7567 AA	0.0
		2.3514	158014	7216 BA	0.0
		0.7838	52671	10114 DA	0.0
		0.7838	55493	8468 AA	0.0
	295	2.3514	166479	7766 BA	0.0
		0.7838	55493	9777 DA	0.0
4. 70	230	1.0000	67200	8181 AA	0.0
		3.0000	201600	7924 BA	0.0
		1.0000	67200	11584 FA	0.0
		1.0000	70800	8766 AA	0.0
	295	3.0000	212400	9025 CA	0.0
		1.0000	70800	10847 DA	0.0
5. 80	230	1.5000	100800	8459 AA	0.0
		4.5000	302400	8320 BA	0.0
		1.5000	100800	11392 CA	0.0
		1.5000	105200	4923 AA	0.0
	295	4.5000	318600	9098 BA	0.0
		1.5000	106200	10770 DA	0.0
6. 90	230	1.7334	116484	9589 AA	0.0
		5.2002	349453	9039 CA	0.0
		1.7334	116484	14037 DA	0.0
		1.7334	122725	12605 AA	0.0
	295	5.2002	368174	12181 CA	0.0
		1.7334	122725	12749 FA	0.0
7. 100	230	0.9833	66111	11261 AA	0.0
		2.9514	198334	13035 CA	0.0

TABLE XVII - Continued

FLIGHT CONDITION	FREQUENCY OF OCCURRENCE PCT. CYCLES IN TIME 100 HRS.	OSCILLATORY BENDING STR. IN SLIDER LUG BOLT	CYC. TO FAILURE X 10 ⁴ (-6)	DAMAGE FRACTION
	0.9838	66111	12994 EA	0.0
295	0.9838	69653	13941 AA	0.0
	2.9514	208959	19603 CA	0.0
	0.9838	69653	16702 EA	0.0
8. VNE 280	0.3500	23520	11670 AA	0.0
	1.0500	70560	15839 CA	0.0
	0.3500	23520	14948 EA	0.0
295	0.3500	24780	17750 AA	0.0
	1.3500	74340	21910 CA	0.0
	0.3500	24780	18915 EA	0.0
H. MANEUVERS				
1. CLIMB 0-60 KNOTS				
(A) M.C. POWER	0.6000	41040	7966 AA	0.0
	1.8000	123120	6857 CA	0.0
	0.6000	41040	8221 DA	0.0
(B) T.O. POWER	0.2000	13680	6221 AA	0.0
	0.6000	41040	6872 BA	0.0
	0.2000	13680	7898 EA	0.0
2. CYCLIC PULL-UP				
(A) 50 KNOTS	0.0324	2216	9115 AA	0.0
	0.0972	6648	10586 CA	0.0
	0.0324	2216	11717 EA	0.0
(B) 100 KNOTS	0.0324	2216	10793 AA	0.0
	0.0972	6648	12582 CA	0.0
	0.0324	2216	13116 EA	0.0
(C) VL	0.0324	2216	11579 AA	0.0
	0.0972	6648	30856 CA	0.0
	0.0324	2216	49872 EA	0.087 0.025533
3. LEFT TURN				
(A) 50 KNOTS	0.2000	13680	8710 AA	0.0
	0.6000	41040	9839 BA	0.0
	0.2000	13680	11773 EA	0.0
(B) 100 KNOTS	0.2000	13680	10181 AA	0.0
	0.6000	41040	10860 BA	0.0
	0.2000	13680	14716 EA	0.0
(C) VL	0.1000	6840	17888 AA	0.0
	0.3000	20520	21047 BA	0.0
	0.1000	6840	49872 EA	0.087 0.078804
4. RIGHT TURN				
(A) 50 KNOTS	0.2000	13680	7408 AA	0.0
	0.6000	41040	9038 BA	0.0
	0.2000	13680	8920 EA	0.0
(B) 100 KNOTS	0.2000	13680	9845 AA	0.0
	0.6000	41040	10555 CA	0.0
	0.2000	13680	12365 EA	0.0
(C) VL	0.1000	6840	10497 AA	0.0

TABLE XVII - Continued

FLIGHT CONDITION	FREQUENCY OF PCT. OCCURRENCE TIME	CYCLES IN 100 HRS.	OSCILLATORY BENDING STR. FAILURE IN SLIDER LUG BOLT	CYC. TO FAILURE X 10**(-6)	DAMAGE FRACTION
	0.3000	20520	22489 CA		0.0
	0.1000	6840	49872 EA	0.087	0.078804
5. CONTROL REVERSAL					
(A) LONGITUDINAL	0.0444	3037	12676 AA		0.0
	0.1332	9111	14950 CA		0.0
	0.0444	3037	12639 FA		0.0
(B) LATERAL	0.0444	3037	10284 AA		0.0
	0.1332	9111	11827 CA		0.0
	0.0444	3037	11789 FA		0.0
(C) RUDDER	0.0444	3037	9258 AA		0.0
	0.1332	9111	10040 BA		0.0
	0.0444	3037	10372 FA		0.0
IV. POWER TRANSITIONS					
A. POWER TO AUTO					
1. 40 KNOTS	0.0022	150	7655 AA		0.0
	0.0066	451	8826 CA		0.0
	0.0022	150	9286 EA		0.0
2. VL	0.0022	150	12692 AA		0.0
	0.0066	451	16835 CA		0.0
	0.0022	150	16482 EA		0.0
B. AUTO TO POWER	0.0112	766	10081 AA		0.0
	0.0336	2298	10030 CA		0.0
	0.0112	766	10980 EA		0.0
V. AUTOROTATION					
A. STABILIZED FLIGHT					
1. 40 KNOTS	0.0578	3954	5504 AA		0.0
	0.1734	11861	5428 BA		0.0
	0.0578	3954	5672 EA		0.0
2. 30 KNOTS	0.0776	5308	6658 AA		0.0
	0.2328	15924	7214 BA		0.0
	0.0776	5308	5924 EA		0.0
3. MAX AUTO A/S	0.0378	2586	10912 AA		0.0
	0.1134	7757	10171 BA		0.0
	0.0378	2586	9860 EA		0.0
B. TURNS. (NORMAL AUTO A/S)					
1. TO THE LEFT	0.0400	2736	7538 AA		0.0
	0.1200	8208	8933 BA		0.0
	0.0400	2736	5983 EA		0.0
2. TO THE RIGHT	0.0400	2736	6919 AA		0.0
	0.1200	8208	6922 CA		0.0
	0.0400	2736	6736 EA		0.0
C. CONTROL REVERSAL					
1. LONGITUDINAL	0.0200	1368	13736 AA		0.0

TABLE XVII - Concluded

FLIGHT CONDITION	FREQUENCY OF OCCURRENCE		OSCILLATORY BENDING STR. IN SLIDER LUG BOLT	CYC. TO FAILURE X 10**(-6)	DAMAGE FRACTION
	PCT. TIME	CYCLES IN 100 HRS.			
2. LATERAL	0.0600	4104	13190 BA		0.0
	0.0200	1368	10942 FA		0.0
	0.0200	1368	9679 AA		0.0
	0.0600	4104	11093 CA		0.0
3. RUDDER	0.0200	1368	6668 EA		0.0
	0.0200	1368	7019 AA		0.0
	0.0600	4104	6191 BA		0.0
	0.0200	1368	6203 EA		0.0
D. CYCLIC PULL-UP (NORMAL AUTO A/S)	0.0112	766	9983 AA		0.0
	0.0336	2298	7635 BA		0.0
	0.0112	766	7517 EA		0.0
E. PART PWR DSNT. HOKT	0.416	28495	7409 AA		0.0
	1.2498	85486	5960 BA		0.0
	0.4166	28495	6545 EA		0.0
F. FULL AUTO LANDING	0.0600	4104	0 AA		0.0
	0.1800	12312	42635 BA	*	0.000147
	0.0600	4104	0 FA		0.0
ENDURANCE LIMIT = 38079.0			TOTAL DAMAGE (D) = 0.183288		
MATERIAL = STL1					
FREQUENCY = 4 / REV OF M/R			FATIGUE LIFE = 100/D = 545 HOURS		
* DAMAGE CALCULATED FROM MEASURED LOAD FREQUENCIES.					

cg locations increase it. The fatigue analysis also shows that the weight could be reduced significantly if the various components were redesigned. Furthermore, more extensive fatigue testing would allow the use of analytical methods which are less conservative than those used for this analysis.

LIST OF SYMBOLS

a	speed of sound, fps
b	number of blades
c	blade chord, ft
C_D	rotor drag coefficient $C_D = \frac{D}{\rho \pi R^2 (\Omega R)^2}$
C_{do}	average minimum blade section profile drag coefficient
C_L	rotor lift coefficient $C_L = \frac{L}{\rho \pi R^2 (\Omega R)^2}$
C_P	rotor-shaft power coefficient $C_P = \frac{\text{horsepower} \times 550}{\rho \pi R^2 (\Omega R)^3}$
C_Q	rotor torque coefficient $C_Q = \frac{Q}{\rho \pi R^2 (\Omega R)^2 R}$
C_T	rotor thrust coefficient $C_T = \frac{T}{\rho \pi R^2 (\Omega R)^2}$
cg	center of gravity
D	drag, lb
f	equivalent drag area, ft ²
F_O	hub shear force, lb
g	acceleration of gravity, in./sec ²
G	acceleration divided by acceleration of gravity, nondimensional

LIST OF SYMBOLS (Continued)

I_F	inertia of the fuselage about the fuselage cg, in.-lb-sec ²
I_P	inertia of the pylon about the pylon cg, in.-lb-sec ²
KT	effective torsional spring rate about hinge, in.-lb/rad
L	lift, lb
M_{DD}	drag divergence Mach number (Mach number at which slope of curve of drag coefficient versus Mach number attains a value of 0.10)
$M_{Adv\ Tip}$	advancing blade tip Mach number $M_{Adv\ Tip} = \frac{1.688V + \Omega R}{a}$
M_F	mass of the fuselage, lb-sec ² /in.
M_P	mass of the pylon, lb-sec ² /in.
N_R	main rotor speed, rpm
Q	rotor shaft torque, ft-lb
R	rotor radius, ft
T	rotor thrust, lb
t	time, sec
V	velocity, kn
α_F	angular motion of the fuselage, rad
α_P	angular motion of the pylon, rad
β	1/rev rotor flapping
$\theta_{.75}$	blade collective pitch angle at the 75% radial blade station, deg

LIST OF SYMBOLS (Concluded)

θ'	ratio of temperature to sea level standard temperature in deg Kelvin
μ	advance ratio, $\mu = V/(\Omega R)$
ρ	density of air, lb-sec ² /ft ⁴
ρ_0	density of air at sea level standard day $\rho_0 = .002377$ lb-sec ² /ft ⁴
σ	rotor solidity, $\sigma = bc/\pi R$
σ'	air density ratio, $\sigma' = \rho/\rho_0$
ψ	rotor azimuth angle, zero when the red blade is over the tailboom, deg
Ω	rotor shaft angular velocity, rad/sec
ω	excitation frequency, rad/sec